3-16-2021 1:00 PM

NNeMo (Neonatal NeuroMonitor) - a hybrid optical system to characterize perfusion and metabolism in the newborn brain

Ajay Rajaram, *The University of Western Ontario*

Supervisor: Keith St. Lawrence, *The University of Western Ontario*
Co-Supervisor: Mamadou Diop, *The University of Western Ontario*
A thesis submitted in partial fulfillment of the requirements for the Doctor of Philosophy degree in Medical Biophysics

Abstract

Premature birth, defined as a gestational period less than 37 weeks, occurs in 8% of infants born in Canada. These births are associated with a higher risk of developing neurological complications. Infants born with very low birth weights (VLBW, < 1500 g) experience cognitive or behavioural deficits at a rate of 40-50%, while a further 5-10% develop major disorders such as cerebral palsy. The likelihood of injury increases with a shorter gestational period and/or a lower birthweight. Intraventricular hemorrhaging (IVH) occurs in 20-25% of VLBW infants, characterized by bleeding in the germinal matrix and surrounding white matter. This highly vascularized region is particularly susceptible to bleeds due to underdeveloped cerebrovascular structures. Severe IVH causes an inflammatory response and subsequent obstruction of cerebrospinal fluid (CSF) drainage, resulting in enlargement of the brain's ventricles, referred to as post-hemorrhagic ventricular dilatation (PHVD). PHVD increases intracranial pressure and can result in compression/damage of brain tissue.

Diagnosis of IVH and PHVD is regularly performed using cranial ultrasound. Clinicians can visually assess and grade hemorrhaging/ventricle dilatation. Ultrasound, however, is limited in its ability to continuously monitor and only detects irreversible damage. NNeMo (Neonatal NeuroMonitor) is a hybrid optical device combining diffuse correlation (DCS) and near-infrared spectroscopy (NIRS) to simultaneous monitor cerebral blood flow (CBF) and metabolism at the bedside. DCS analyzes light scatter from red blood cells to infer their motion and calculate CBF while NIRS exploits light absorption properties to quantify changes in oxidized cytochrome c oxidase (oxCCO), a direct marker of energy metabolism. System validation was presented in a piglet model of neonatal hypoxia-ischemia. Clinical translation of NNeMo was demonstrated in PHVD infants during ventricular taps (i.e., CSF drainage). Changes in perfusion and metabolism are presented in premature infants at high risk of IVH within the first 72 hours of life. Lastly, NNeMo was translated to the cardiac operating room, in patients undergoing surgery with cardiopulmonary bypass, to observe metabolic response to large intraoperative changes in CBF. Optical measures of perfusion and metabolism show potential to act as prognostic markers of injury and could aid clinicians in patient management before significant damage persists.

Keywords

Premature brain injury, Optical brain monitoring, Near-infrared spectroscopy, Diffuse correlation spectroscopy, Cerebral hemodynamics, Cerebral metabolism, Intraventricular hemorrhaging, Post-hemorrhagic ventricular dilatation.

Summary for Lay Audience

A full-term pregnancy is approximately 40 weeks in duration. Infants born within 37 weeks are defined as premature and often experience inadequate brain growth and underdeveloped cerebrovascular structures, which are necessary to maintain an adequate supply of blood and oxygen to the brain. As a result, premature infants are at a higher risk of developing a brain injury, which further increases with a shorter gestational period or a lower weight at birth. A common injury is intraventricular hemorrhaging (IVH), which describes bleeding in and around the ventricles of the brain. IVH has been found to occur in up to 25% of infants weighing less than 1500 g at birth and 45% in those less than 1000 g, with most cases appearing within the first 48 hours of life. Furthermore, severe cases of IVH can result in improper draining of cerebrospinal fluid (CSF) from the brain's ventricles. This leads to increased intracranial pressure and ventricle volume, described as post-hemorrhagic ventricular dilatation (PHVD), which can compress brain tissue and result in long-term cognitive deficit.

In today's neonatal intensive care unit (NICU), brain monitoring is limited to infrequent imaging using cranial ultrasound. While ultrasound can accurately diagnose bleeding/ventricle enlargement, it cannot continuously monitor and can only image damage that has already occurred. This dissertation explores the use of biomedical optics to monitor potential physiological markers of brain injury before significant damage occurs. NNeMo (Neonatal NeuroMonitor) is a non-invasive optical device developed to continuously monitor cerebral blood flow (CBF) and metabolism at the bedside. This was achieved by combining diffuse correlation spectroscopy to characterize CBF with broadband near-infrared spectroscopy to monitor cerebral metabolism. NNeMo demonstrated changes in CBF and metabolism prior to the onset of brain injury in an animal model. The system was translated to the NICU to monitor PHVD infants during CSF drainage and preterms at risk of IVH soon after birth. Lastly, the relationship between CBF and metabolism as indicators of potential injury was investigated in patients undergoing cardiac surgery with cardiopulmonary bypass. Real-time monitoring of cerebral perfusion and metabolism has potential to aid in patient management and improve clinical outcome.

Co-Authorship Statement

Chapters 2, 3, and 5 of this dissertation were adapted from published journal articles. As the first author of these manuscripts, I spearheaded all aspects of the work presented, contributing significantly to technological development, experimental design, subject recruitment, data acquisition & analysis, interpretation of results, and manuscript preparation. NNeMo, the optical system featured in this work, was developed in collaboration with Lawrence Yip while under the supervision of Dr. Keith St. Lawrence and Dr. Mamadou Diop. Dr. Diop provided supervision and support in developing the device and in its validation within animal studies. Dr. St. Lawrence secured funding for all work presented and supervised all projects from conception to completion, while greatly assisting in the clinical translation of NNeMo. Dr. Daniel Milej provided additional support and guidance in data analysis and interpretation of results. Each of the co-authors listed contributed significantly to the work presented and approved manuscript submission. Individual contributions are listed below by chapter.

Chapter 2 was adapted from the publication titled "Simultaneous monitoring of cerebral perfusion and cytochrome c oxidase by combining broadband near-infrared spectroscopy and diffuse correlation spectroscopy," published in *Biomedical Optics Express* in 2018 by Ajay Rajaram, Gemma Bale, Matthew Kewin, Laura B. Morrison, Ilias Tachtsidis, Keith St. Lawrence, and Mamadou Diop. Matthew Kewin and Laura Morrison assisted in data acquisition, Gemma Bale and Ilias Tachtsidis aided with data analysis, interpretation, and manuscript preparation.

Chapter 3 was adapted from the publication titled "Perfusion and metabolic neuromonitoring during ventricular taps in infants with post-hemorrhagic ventricular dilatation," published in *Brain Sciences* in 2020 by Ajay Rajaram, Lawrence C. M. Yip, Daniel Milej, Marianne Suwalski, Matthew Kewin, Marcus Lo, Jeffrey J. L. Carson, Victor Han, Soume Bhattacharya, Mamadou Diop, Sandrine de Ribaupierre, and Keith St. Lawrence. Matthew Kewin, Marcus Lo, Victor Han, Soume Bhattacharya, and Sandrine de Ribaupierre aided with patient recruitment and data acquisition, while the latter two also assisted in data interpretation. Marianne Suwalski contributed to data interpretation and manuscript preparation. Jeffrey Carson provided technical support in system development.

Chapter 4 is unpublished work titled “Monitoring cerebral hemodynamic and metabolic stability in premature infants following birth using NNeMo (Neonatal NeuroMonitor) a hybrid broadband NIRS/DCS optical brain monitor,” which is in preparation for submission by Ajay Rajaram, Daniel Milej, Lilian Kebaya, Matthew Kewin, Lawrence C. M. Yip, Marianne Suwalski, Sandrine de Ribaupierre, Mamadou Diop, Soume Bhattacharya, and Keith St. Lawrence. Lilian Kebaya and Matthew Kewin contributed to patient recruitment and data acquisition. Marianne Suwalski, Sandrine de Ribaupierre, and Soume Bhattacharya assisted with data interpretation. Daniel Milej contributed to data analysis.

Chapter 5 was adapted from the publication titled “Optical monitoring of cerebral perfusion and metabolism in adults during cardiac surgery with cardiopulmonary bypass,” published in *Biomedical Optics Express* in 2020 by Ajay Rajaram, Daniel Milej, Marianne Suwalski, Lawrence C. M. Yip, Linrui R. Guo, Michael W. A. Chu, Jason Chui, Mamadou Diop, John M. Murkin, and Keith St. Lawrence. Patient recruitment was completed with the assistance of Linrui Duo, Michael Chu, Jason Chui, and John M. Murkin, while the latter two also aided in data interpretation. Marianne Suwalski and Daniel Milej contributed to data acquisition, analysis, and manuscript preparation.

Dedication

I would like to dedicate this work firstly to family for their unwavering love and support. To my Mom and Dad, thank you for providing me with everything at your disposal and teaching me to, above all else, be kind and do good. To my sister Sheila and brother-in-law Dan, thank you for your friendship and for always having my back. To my Thatha (grandfather), thank you for teaching me about C.V. Raman and saving every newspaper clipping about brain injury and neuromonitoring. To my Amama (grandmother), thank you for inspiring me through your poems with your beautiful words and imagery.

To my partner and best friend, Krisin. You have been by my side through every single aspect of the past five years. Your thoughtful and empathic perspective has guided my motivations and helped me become a better person. Thank you for sharing every burden and celebration with me. This work is as much yours as it is mine. I could not have done this without you.

To Krisin's Mom and Laolao (grandmother), thank you for welcoming me into your home and creating wonderful and lasting memories together. I am excited for the next time we can all sit together and share a meal.

To my friend Wonton (rabbit), thank you for hanging out with me while I wrote this entire dissertation. You're an endless source of smiles and your ability to relax is inspiring.

Finally, to my many friends and family with whom I've shared countless laughs, experiences, and memories. Thank you for the support and friendship, I dedicate this work to you all.

Acknowledgments

During my time at Western there have been a number of individuals who have significantly contributed to my research and personal growth. The work presented in this dissertation was only made possible through their support.

Firstly, my academic/research accolades, scientific writing, and ability to critically analyze work are all a direct result of the supervision from Dr. Keith St. Lawrence. Your enthusiasm for research and open-door policy allowed for an unrivaled learning experience. You provided me with the tools, encouragement, and support to be a successful graduate student. Thank you for dedicating countless hours, including many late nights and weekends, to helping me achieve my goals and grow as an independent scientist.

To my co-supervisor Dr. Mamadou Diop, I entered the lab with no prior experience in optics and you took on the huge task of teaching me the fundamentals. Through your guidance and support I learned how to approach a problem, design an experiment, and most importantly how to ask the right questions. You helped me become a better programmer and taught me to work with my hands in the lab. Thank you for the great conversations and the years of advice that have helped me get to this point in my career.

My good friend and forever office-mate Lawrence Yip was instrumental in developing NNeMo, the optical system presented in this body of work. Over the last 6-years we have worked together closely on numerous projects, prepared for countless presentations, and problem solved more than I would have thought possible. None of this work would have been completed if not for your advanced troubleshooting abilities and years of contributions. Similarly, Dr. Daniel Milej was a consistent form of support for much of the work presented. Through his mentoring in data analysis I learned how to problem-solve efficiently and present data in a meaningful way. His enthusiasm for research and excitement to explore new perspectives is inspiring.

This work was supported by amazing clinical collaborators in the neonatal intensive care unit (NICU) at Victoria Hospital and the cardiac operating room at University Hospital in London, Ontario. Thank you to Dr. David Lee, Dr. Victor Han, Dr. Soume Bhattacharya, Dr. Sandrine de Ribaupierre, and Dr. Lilian Kebaya for welcoming me into the NICU and addressing my

endless stream of questions. I am very grateful for your feedback and direction. Thank you to Dr. John Murkin and Jason Chui for supporting our work in the cardiac OR and helping us transition to monitoring adults intraoperatively, it was no small task.

I also have to acknowledge the many graduate students, past and present, who have helped me along the way. Matthew Kewin, Marianne Suwalski, and Marcus Lo were a huge help in translating our work to the clinic. Androu Abdalmalak, Peter McLachlan, Kyle Verdecchia, and Jessica Kishimoto taught me their perspectives on biomedical optics and its applications. To my many other lab-mates and peers in Medical Biophysics thank you for the friendship and support in this long journey.

My coworkers and friends at the Lawson Health Research Institute made countless hours of benchtop experiments a complete joy. Thank you to Jennifer Hadway, Laura Morrison, and Lise Desjardins for sharing your in-depth knowledge, huge smiles, and extreme enthusiasm. Lynn Keenliside was a major asset in modifying NNeMo for the clinic and providing technical and hardware assistance. Michele Avon assisted me significantly in all administrative matters. I would also like to thank the department of Medical Biophysics for supporting my graduate career. Dr. Aaron Ward provided invaluable direction and career advice and Dr. Matthew Teeter guided me in becoming a better public speaker and instructor. Wendy Hough and Kathleen Petts helped me navigate numerous examinations and scholarship applications with ease.

I am forever thankful for the following sources of funding that have supported me and my research over the past six years: Natural Sciences and Engineering Council (NSERC), Canadian Institutes of Health Research (CIHR), Ontario Graduate Scholarship (OGS), Queen Elizabeth II Graduate Scholarship in Science and Technology (QEII-GSST), Schulich School of Medicine and Dentistry, Western University, and the department of Medical Biophysics. Thank you for providing me with the opportunity to undertake and present this work.

Finally, I would like to thank the patients and families who enrolled in our clinical studies. Your contribution to this work helps us further the field as we move towards improved clinical outcomes.

Table of Contents

List of Tables

List of Figures

List of Abbreviations

ANOVA	Analysis of variance
APD	Avalanche photodiode
ASL-MRI	Arterial spin labelling magnetic resonance imaging
AVR	Aortic valve replacement
B-NIRS	Broadband near infrared spectroscopy
BFI	Blood flow index
CA	Cerebral autoregulation
CAPG	Coronary artery bypass graft
CBF	Cerebral blood flow
CBV	Cerebral blood volume
CCD	Charged couple device
CCO	Cytochrome c oxidase
CDE	Correlation diffusion equation
$CMRO_2$	Cerebral metabolic rate of oxygen
CPAP	Continuous positive airway pressure
CPB	Cardiopulmonary bypass
CSF	Cerebrospinal fluid
cUS	Cranial ultrasound
CW	Continuous wave

DA	Diffusion approximation
DCE	Dynamic contrast enhanced
DCS	Diffuse correlation spectroscopy
DP	Differential pathlength
EEG	Electroencephalography
ELBW	Extremely low birth weight
ETC	Electron transport chain
EVD	External ventricular drain
FD	Frequency domain
FR	Flow rate
GA	Gestational age
Hb	Deoxyhemoglobin
HbO_2	Oxyhemoglobin
HI	Hypoxia-ischemia
HIE	Hypoxic ischemic
ICG	Indocyanine green
ICP	Intracranial pressure
IVH	Intraventricular hemorrhaging
LED	Light emitting diode
LLA	Lower limit of autoregulation

LP	Lumbar puncture
MAP	Mean arterial pressure
MRI	Magnetic resonance imaging
MRS	Magnetic resonance spectroscopy
MVR	Mitral valve replacement
NA	Numerical aperture
NICU	Neonatal intensive care unit
NIR	Near-infrared
NIRS	Near-infrared spectroscopy
NNeMo	Neonatal NeuroMonitor
OEF	Oxygen extraction fraction
oxCCO	Oxidation state of cytochrome c oxidase
$PaCO_2$	Partial pressure of CO_2
PE	Photoelectric effect
PET	Positron emission tomography
PHVD	Post-hemorrhagic ventricular dilatation
PMA	Post menstrual age
PMT	Photomultiplier tube
PNA	Post-natal age
PVL	Periventricular leukomalacia

RBC	Red blood cells
RTE	Radiative transfer equation
SaO_2	Arterial oxygen saturation
SDD	Source-detector distance
SNR	Signal-to-noise ratio
SPAD	Single-photon avalanche diode
SRS	Spatially resolved spectroscopy
StO_2	Cerebral tissue oxygen saturation
SvO_2	Venous oxygen saturation
TCD	Transcranial doppler ultrasound
TD	Time domain
tHb	Total hemoglobin
TPSF	Temporal point spread function
VLBW	Very low birth weight
VT	Ventricular tap
WF	Water fraction

Chapter 1

1 Introduction

Advancements in the modern neonatal intensive care unit (NICU) have greatly improved outcomes of premature infants and those with complications at birth. With increasing survival rates across NICU patients, clinical efforts have shifted to quality of life following patient discharge. A notable area of focus is in neurodevelopment and prevention/mitigation of long-term cognitive deficit. This dissertation explores development of optical technologies to aid in the diagnosis and management of premature brain injury with the goal of improving clinical outcomes.

1.1 Clinical Rationale

1.1.1 Premature Brain Injury

Premature birth, defined as a gestational period lasting fewer than 37 weeks, is a common occurrence with 8% of infants in Canada born prematurely [1]. The shorter the gestational age (GA) at birth and the less these infants weigh, the higher the risk of neurological complications. Very low birth weight (VLBW; < 1500 g) infants experience behavioural or cognitive deficits at a rate of 25-50%, with a further 5-10% developing major motor disorders such as cerebral palsy [2]. These rates are more severe in extremely low birth weight (ELBW; < 1000 g) infants, with apparent and significant long-term deficits [3,4]. Intraventricular hemorrhaging (IVH), is a common injury following premature birth and is characterized by bleeding in the germinal matrix and surrounding white matter. The germinal matrix is a highly vascularized region in the brain, comprised of glial and neuronal precursor cells, and is particularly susceptible to hemorrhaging within the first 48 hours following birth [5]. Substantial bleeding in this area can cause a rupture of the ependyma (ventricle lining) and result in blood entering the ventricles. IVH has been found to occur in 20-25% of VLBW infants [6] and in 45% of ELBW infants [7]. Periventricular leukomalacia (PVL) is another common injury characterized by ischemic damage to periventricular white matter. PVL has been found in up to 50% of VLBW infants and can take the form of a focal cystic injury embodying tissue necrosis or a diffuse non-cystic

injury vulnerable to ischemia, with the latter being far more prevalent in preterms [2,8]. In severe cases of cerebral hemorrhaging, an inflammatory response, followed by fibrosis, can obstruct the drainage of cerebrospinal fluid (CSF) in the brain's ventricles and lead to post-hemorrhagic ventricular dilatation (PHVD) [9,10]. PHVD is a common complication of high-grade IVH and can result in CSF accumulation, increased intracranial pressure, and compression/damage of brain tissue.

The pathogenesis of IVH and PVL is multifaceted. The shortened gestation of a premature birth prevents adequate development of cerebrovascular structures (i.e., vascularization of the germinal matrix). In addition to an immature cerebrovascular system, poor regulation of cerebral blood flow (CBF) is believed to contribute to injury as evident by the prevalence of impaired cerebral autoregulation (CA; i.e., the ability to maintain CBF despite changes in blood pressure) in this population [5,11,12]. In addition, preterms have a significantly lower basal CBF compared to adults (<10 ml/100 g/min in preterms versus 50 ml/100 g/min in adults), and are therefore less tolerant of any disturbance in flow [13].

1.1.2 Clinical Diagnosis and Neuromonitoring

Considering the incidence of IVH and PVL following birth increases the risk of long-term neurological complications, early characterization of injury is paramount [4]. Many infants with brain injury are asymptomatic. Diagnosis is based on screening, most commonly with cranial ultrasound (cUS). Cranial US is a non-invasive, bedside imaging technique that can detect and grade IVH, identify PVL, and gauge ventricular dilatation [10,14]. Routine monitoring with cUS is employed in standard practice in most centers with all infants admitted to the NICU receiving a scan within the first week of life and a second at 36-40 weeks postmenstrual age (PMA) [15]. Imaging with ultrasound has two notable limitations. Firstly, cUS cannot provide continuous monitoring, as it only captures a single snapshot of the brain. Timely diagnosis, therefore, relies on frequency of imaging. In addition, brain injury as observed by cUS is based on structural damage that has already occurred. It is of note that magnetic resonance imaging (MRI) can also provide high resolution imaging to accurately diagnose injury but, in addition to similar limitations as ultrasound, is costly and not deployable at the bedside [16]. At the point of imaging, in both techniques, any damage

identified is irreversible and clinical decision making seeks to manage the injury and prevent further damage.

Recent work has looked into physiological precursors of brain injury. More specifically, CBF has been measured as a potential marker of damage. The approaches and technologies implemented to make this measurement have varied greatly over the years. Early work by Volpe et al. in 1983 used positron emission tomography (PET), with oxygen-15 labelled water as a radiotracer, to measure CBF in premature infants with IVH [17]. In this study, significant reductions in CBF were found in areas of the brain impacted by hemorrhaging. The study concluded that a drop in flow was principally responsible for successive neurological deficits. In 1986, Greisen implemented a 133-Xenon clearance method to measure CBF in premature infants soon after birth [18]. In this study, an arterial injection of 133-Xenon was used while monitoring activity over the brain with a sodium-iodide crystal detector. A lower-than-expected CBF was found in infants requiring ventilation. While PET and 133-Xenon clearance approaches provide a fairly robust measure of CBF, the radiation exposure required is a significant drawback.

Several studies have implemented transcranial Doppler ultrasound (TCD) to measure CBF non-invasively. TCD operates by emitting an acoustic wave and monitoring changes in frequency of reflected waves scattered from red blood cells (RBC). The difference in frequency between incident and reflected wave is referred to as the Doppler shift and is directly proportional to RBC velocity [19]. In premature infants, some studies have shown strong correlations between TCD-measured CBF and the development of cerebral hemorrhages [20]. However, a recent systematic review by Camfferman et al. reports a high variability across studies, speculating that measurement frequency may be a limitation in correlating flow measurements to the onset of injury [21]. While a continuous measure of CBF by TCD is possible, ultrasound equipment is bulky, requiring a transducer immediately above the site of interest, and impractical for longitudinal monitoring. Similar doppler ultrasound-based techniques have also been implemented to measure CBF indirectly via extracerebral feeding arteries. Studies have investigated early changes in cerebral blood volume (calculated from CBF) in preterms during the first weeks of life [22] and have found strong relationships between superior vena cava flow (measured as a

reflection of CBF) and the onset of IVH [23,24]. Additional limitations of TCD include its operator dependence, requiring substantial understanding of the underlying cerebrovascular structures in order to obtain an adequate measure, and its ability to measure only large basal arteries, which describes global changes in flow [19].

A further consideration when relying on perfusion monitoring is to understand that CBF is not a wholistic marker of cerebral health. Dynamic changes in CBF are generally managed by brain homeostasis. So, when do changes in CBF become clinically significant? This question can be addressed through a measure of oxygen utilization (i.e., cerebral metabolism) as a biomarker of potential injury [25]. When the brain has a limited oxygen supply, or is inefficient in metabolizing the oxygen available, there is an impact on energy production which can lead to cell death. In the healthy brain, fluctuations in CBF are compensated for by changes in the amount of oxygen extracted from the blood, known as the oxygen extraction fraction (OEF). Only with extreme changes in flow, at which point this compensatory mechanism fails, do changes in metabolism persist (Figure 1.1). Metabolism has therefore proven a more direct marker of tissue viability [26]. Approaches for monitoring cerebral metabolism in the newborn are limited; disregarding techniques that require radiation exposure, magnetic resonance spectroscopy (MRS) is the most notable. MRS is capable of directly measuring the concentrations of metabolites in brain tissue, which have been shown to correlate with injury in infants with asphyxia [27] and hypoxia-ischemia [28]. However, MRS is inconvenient for routine monitoring and poses a practical challenge for use on premature infants.

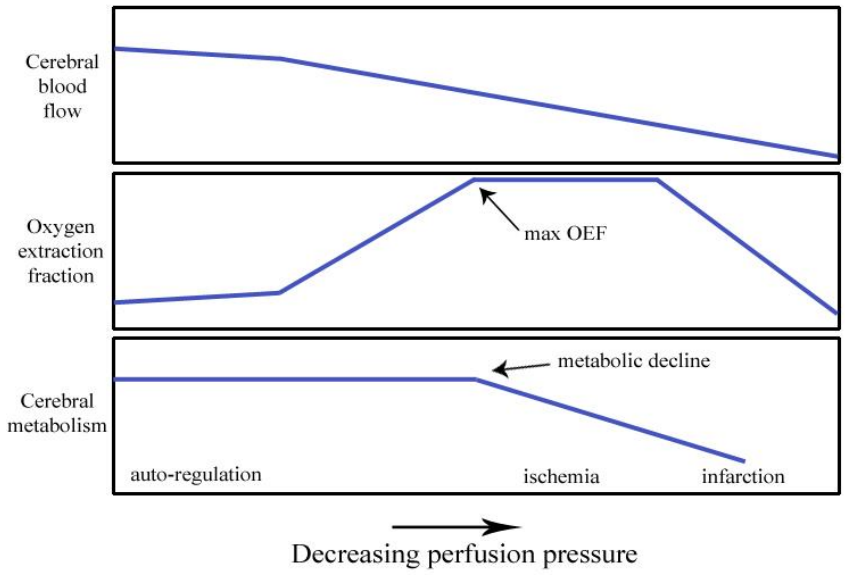

Figure 1.1: Oxygen extraction and metabolic response to changes in CBF.

Limited availability of robust and convenient bedside technologies has sparked the development of optical techniques to provide a safe, non-invasive approach to neuromonitoring. This dissertation describes the technology and clinical translation of optical techniques to monitor cerebral tissue saturation, blood flow, and metabolism at the bedside. Continuous bedside monitoring of physiological precursors has potential to alter patient management and improve clinical outcomes associated with premature brain injury.

1.2 Near-Infrared Spectroscopy

Near-infrared spectroscopy (NIRS) is a non-invasive optical technique used to measure the concentrations of light-absorbing molecules, termed chromophores, in living tissue. By interrogating tissue with non-ionizing light within the near-infrared spectral range, light absorption can be characterized and related to the *in* vivo concentration of chromophores. NIRS was introduced by Frans Jöbsis in 1977 who discovered that NIR light could penetrate the skull, providing a promising in-situ technique to monitor hemoglobin content and oxygen utilization through photo-transmission [29]. Jöbsis observed an optical window from 650-950 nm where light absorption from endogenous tissue chromophores is relatively small, allowing for deeper photon penetration [30]. The most prevalent

chromophores in tissue within this range are oxy-hemoglobin (HbO_2), deoxy-hemoglobin (Hb), and water. Wavelengths immediately above and below this region are highly absorbed by water and Hb, respectively. Similar optical windows of lower absorption also exist between 1100–1350 nm and 1600–1870 nm [31]; however, light sources in these ranges have traditionally been power inefficient or not cost-effective for bedside monitoring. Figure 1.1 shows the absorption spectra of HbO_2, Hb, and water in the NIR optical window where distinct spectral features between chromophores are apparent.

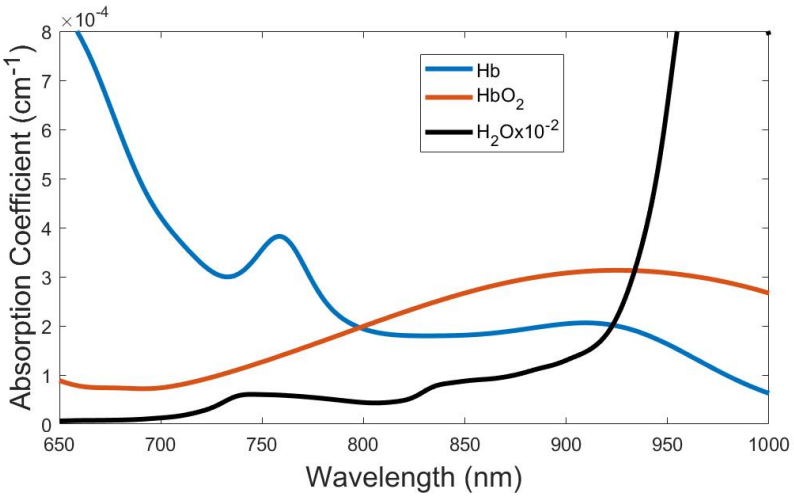

Figure 1.2: Optical window in the near-infrared.

By interrogating tissue with light at various wavelengths, the proportion absorbed by each chromophore can be determined and related to their respective concentrations. A measure of tissue oxygen saturation (StO_2) can be calculated as follows:

$$StO_2 = \frac{[HbO_2]}{[HbO_2] + [Hb]} \tag{1.1}$$

This section will elaborate on the analytical basis of NIRS and the principles of converting light absorption into chromophore concentrations.

1.2.1 Physical Principles of NIRS

Light incident on any media will be attenuated by two primary interactions: absorption and scattering. When a photon strikes a medium it is absorbed if the frequency of the incoming light is equivalent to the energy required to excite the molecule to a higher energy state.

The loss of intensity as light travels through a non-scattering medium was first described as absorption by Pierre Bouguer in 1729. Johann Heinrich Lambert, in 1760, expanded this idea to describe absorption (*A*) in a homogenous material as proportional to the length of sample through which the light passes:

$$A = -\log\left(\frac{I}{I_0}\right) = \mu_a l \tag{1.2}$$

where I/I_0 is the proportion of light absorbed, μ_a is the absorption coefficient representing the inverse of the average distance that a photon is likely to travel before an absorption event, and l is the thickness of a sample. August Beer, in 1852, determined that light absorption is proportional to the concentration of the solution in which light is travelling. This relationship between absorption and concentration is commonly referred to as the Beer-Lambert law:

$$A = \varepsilon c l \tag{1.3}$$

where ε is the molar extinction coefficient, an intrinsic property specific to each species, and c is the concentration of the solution. In a sample consisting of numerous absorbers, this law can be expanded to account for all constituents:

$$A = \sum_i \varepsilon_i c_i l \tag{1.4}$$

The Beer-Lambert law, however, is only satisfied in a non-scattering medium. Within the NIR window, light scatter is the most dominant interaction in tissue [32,33]. Rayleigh scattering can occur when light interacts with particles smaller than the incident wavelength, and Mie scattering when particles are much larger; the latter is more common in tissues with the abundance of larger bodies such as nuclei and mitochondria. Scattering via Fresnel Reflections is also common, occurring at an index of refraction. To account for the influence of scatter, a modified Beer-Lambert law was introduced by Delpy et al. in 1988 [34]. Firstly, equation 1.3 can be adapted to describe intensity loss due to light scattering as follows:

$$I = I_0 e^{-\mu_s l} \tag{1.5}$$

where μ_s represents the inverse distance that a photon is likely to travel before it is scattered. Similar to absorption, the behaviour of light scatter varies across different media.

The Henyey-Greenstein Phase Function, described in 1941, is a probability density function which describes the likelihood of light scattering at an angle θ given the scattering anisotropy factor, g [35],

$$p(\theta) = \frac{1}{4\pi} \frac{1-g^2}{(1+g^2-2g\cos\theta)^{\frac{3}{2}}} \tag{1.6}$$

where g is intrinsic to the media and describes the likely direction of a scattered photon. This metric can range from -1 to 1 as the mean cosine of the scatter angle; a value of 0 represents isometric scattering. Most tissue types have a g of approximately 0.9, which means that light is mostly forward scattered. However, due to the high prevalence of scattering events relative to absorption, directionality is quickly lost in tissue and photon propagation resembles a photon cloud. As a result, scatter is assumed to be isotropic and non-directional. In highly diffuse media such as tissue, scattering is commonly characterized by the reduced scattering coefficient, μ_s':

$$\mu_s' = \mu_s(1-g) \tag{1.7}$$

where $1/\mu_s'$ describes the average distance that a photon travels before its movement can be modelled as a random walk or diffusion-like process. The change in μ_s' with respect to wavelength can be modelled using a power law:

$$\mu_s'(\lambda) = \mathrm{A}\left(\frac{\lambda}{\lambda_0}\right)^{-\alpha} \tag{1.8}$$

where α is the scattering power and A is the μ_s' value at λ_0, both of which can be determined experimentally. For biological tissue, scattering is a combination of Mie and Rayleigh effects with α between 3 and 5.5 [36]. The Beer-Lambert law can be modified to account for the effects of scattering:

$$A(\lambda) = DP(\lambda)\sum_i \varepsilon_i c_i + G(\lambda) \tag{1.9}$$

where G is wavelength dependent scalar term, describing the proportion of light not detected due to scatter, and the *DP* is the differential pathlength characterizing the distance that light travels following multiple scattering events. In order to quantify chromophore concentrations, these scattering dependent metrics must be determined in addition to absorption information. Section 1.2.2 elaborates on modelling light propagation in a highly scattering media.

1.2.2 Light Propagation in Tissue

The behaviour of electromagnetic radiation is governed by Maxwell's equations; however, modelling this becomes exceedingly complex within a highly scattering and heterogeneous medium such as tissue. Instead, the radiative transfer equation (RTE) can be used as a simplification, describing light as discrete photons which undergo absorption and elastic scattering events while conserving energy.

$$\left[\frac{1}{v}\frac{\delta}{\delta t} + \hat{s}\cdot\nabla + \mu_a + \mu_s\right] L(r,t,\hat{s}) = \mu_s \int_{4\pi} L(r,t,\hat{s}) P(\hat{s},\hat{s}')\, d\Omega' + S(r,t,\hat{s}) \quad (1.10)$$

where $L(r,t,\hat{s})$ is the radiance at position r in the direction defined by the vector $\hat{s}$ at time t. $P(\hat{s},\hat{s}')$ is the scattering phase function which describes the probability of scattering to from direction $\hat{s}$ to $\hat{s}'$, $S(r,t,\hat{s})$ is the source term and v is the speed of light in the medium. The RTE can be greatly simplified for light propagation through a diffuse medium considering the directionality of light quickly becomes isotropic due to the far greater number of scattering events compared to absorption. For a source-detector distance (SDD) significantly larger than μ_s', the radiance becomes equivalent to the isotropic fluence and a directional flux.

$$\frac{1}{v}\frac{\partial \Phi(r,t)}{\partial t} + \nabla\cdot\vec{J}(r,t) + \mu_a\phi(r,t) = S(r,t) \quad (1.11)$$

where fluence, $\Phi = \int L(r,t,\Omega)d\Omega$ and the flux, $\vec{J}(r,t) = -D\nabla\Phi(r,t)$. This can be further simplified to the diffusion approximation (DA) as follows,

$$\left(\frac{1}{v}\frac{\delta}{\delta t} - D\nabla^2 + \mu_a\right)\phi(r,t) = S(r,t) \quad (1.12)$$

where D is the diffusion coefficient defined as follows:

$$D = \frac{1}{3[(1-g)\mu_s + \mu_a]} = \frac{1}{3[\mu_s' + \mu_a]} \quad (1.13)$$

Given certain boundary conditions and geometries, analytical solutions to the diffusion approximation can be derived, which can be used to determine tissue optical properties (i.e., μ_a and μ_s'). Section 1.3 elaborates on NIRS techniques that have been developed for brain monitoring and approaches used to separate the effects of light scattering from absorption.

1.3 In vivo NIRS Techniques

The fundamental understanding of light interaction with tissue described above is utilized in various approaches to quantify chromophore concentrations *in vivo* for a wide range of clinical applications. These methods characterize absorption and scattering effects through interrogating an area of interest with NIR light and analyzing changes in light intensity, frequency, wavelength, time, and location. This section will describe the different NIRS approaches investigated, the technology involved, and touch upon several applications of these techniques in neuromonitoring with particular focus on the premature brain. Studies involving hybrid/multi-modal devices will be discussed in section 1.5.

1.3.1 Continuous-wave NIRS

Continuous-wave (CW) NIRS systems utilize light sources that are constant in intensity and implement a minimum of two wavelengths to characterize absorption changes related to the concentrations of HbO_2 and Hb. These devices are advantageous due to their high temporal resolution, cost-effectiveness, and portability [37]. System components include light sources, often either laser diodes or light-emitting diodes (LED), optical fibers to direct and capture light, and photon detectors which vary across different optical techniques. Most detectors rely on the photoelectric effect (PE) where a photon generates a charge carrier and electrical current. This can occur ‘externally’, such as in photo-multiplier tubes (PMT), where an incident photon liberates an electron, is accelerated in an electric field, and causes a cascade of electrons ejections resulting in a signal amplification [38]. The PE can also occur ‘internally’ as an absorbed photon creates an electron-hole pair, produces a photocurrent, and is detected as an electrical signal. An example of the internal PE is in the common photodiode, prevalent within CW-NIRS systems, where the output voltage is proportional to the power of incident light. Further advances have led to the avalanche photodiode (APD) which utilizes the internal PE, as in photodiodes, but generates electron cascades to improve signal amplification similar to PMTs [38,39]. The portability of sources and detectors, and their ability to effectively shield from ambient light, have allowed for bedside monitoring and even wireless/wearable devices [37,40].

CW-NIRS operates under the assumption that scattering is unchanged over the course of a measurement. By analyzing only changes in intensity, without characterizing the optical properties, only relative values of hemoglobin and StO_2 can be acquired. While relative measures can be valuable for tracking longitudinal changes, they are limited for establishing clinical thresholds or comparing measures between subjects. Another set-back of many CW-NIRS system is depth sensitivity, as they are unable to differentiate between brain tissue and extra-cerebral layers (scalp and skull) [41]. This is less of an issue within neonatal applications due to the thin skull thickness in the newborn [42].

1.3.1.1 Spatially Resolved Spectroscopy

Spatially resolved spectroscopy traditionally utilizes CW-NIRS techniques while quantifying optical properties by implementing multiple light source-detector distances (SDD). In 1989 Patterson et al. proposed that the effective attenuation coefficient (μ_{eff}) could be measured by acquiring intensity information as a function of distance from the light source [43]. Equation 1.15 defines μ_{eff}, and simplifies it given that $\mu_s >> \mu_a$:

$$\mu_{eff} = \sqrt{3\mu_a(\mu_a + \mu_s')} \cong \sqrt{3\mu_a\mu_s'} \qquad (1.14)$$

Through modelling the diffusion approximation (described in section 1.2.2) for a semi-infinite geometry, while assuming the SDD, $\rho >> 1/\mu_s'$, light reflectance can be described as follows:

$$R(\rho) \propto \frac{\exp -\mu_{eff}}{\rho^2} \qquad (1.15)$$

Taking a natural logarithm, the reflectance can be modelled as a linear equation with μ_{eff} as the slope:

$$\ln\left(\rho^2 R(\rho)\right) = -\mu_{eff}\rho + intercept \qquad (1.16)$$

By acquiring data at multiple distances, μ_{eff} can be determined. To quantify μ_a, an estimate of μ_s' is required [44]. Some work has utilized calibrated reflectance measurements to solve for the intercept of the linear equation and estimate μ_s' [45]. SRS was first demonstrated by Matcher et al. in 1995 to provide absolute hemoglobin concentrations and saturation values comparable to blood-gas analysis [46]. This technique is the basis for most

commercially available NIRS devices. Section 1.3.1.2 elaborates on the clinical application of commercial CW-NIRS systems implementing SRS technology.

1.3.1.2 Commercial CW-NIRS Devices

CW-NIRS has proven extremely useful in brain monitoring studies involving premature infants, a very fragile patient population, due to its safe and non-invasive approach. Compared to other techniques for examining the brain (described in section 1.1.2), NIRS allows for continuous monitoring, requires minimal handling, and can be implemented without disrupting clinical care (i.e., x-ray imaging, ventilation equipment, electroencephalography (EEG) monitoring, etc.). NIRS was first implemented on newborns to monitor cerebral oxygen levels *in vivo* in 1985 by Brazy et al. [47]. Since these preliminary reports, optical neuromonitoring with NIRS has been implemented around the world to investigate the developing brain. Numerous commercial systems using SRS technology have been developed for neonatal brain monitoring. Several groups have compared the robustness of systems available and the clinical relevance of their measures [48–52]. Generally, NIRS monitoring of StO_2 has proven robust in characterizing trends but absolute values have varied depending on the device and sensors used. Saturation differences as large as 14% have been reported with neonatal sensors [53]. Notably, work by Kleiser et al. compared measurements with five commercially available oximeters on a phantom model of a neonatal head. Both system brand and sensor type were determined to influence StO_2 measures but values were found to be linearly related, allowing for comparison across devices [54].

Despite these differences, the SafeBoosC Phase II randomized clinical trial was implemented to determine the benefit of CW-NIRS measures of StO_2 in extremely preterm infants by developing a treatment guideline to manage deviations from an expected range (55–85%) [55]. This study accepted a handful of NIRS devices that produced absolute StO_2 values, allowing only a 5% deviation from the INVOS oximeter (Medtronic) and an absolute repeatability of at least than 6% [56]. With these criteria, across 166 preterm infants, the trial found that NIRS monitoring resulted in a significantly reduced burden of hypoxia within the first 72 hours of life [57]. Without a gold-standard technique to provide a robust absolute measure, establishing clinical guidelines for StO_2 to gauge brain

development or indicate injury remains a challenge. The following sections elaborate on advanced NIRS techniques that have been investigated to provide more robust measurements or more sensitive biomarkers of development/injury.

1.3.1.3 Broadband NIRS

Broadband NIRS (B-NIRS) is a CW-NIRS technique which analyzes absorption as a function of wavelength across the entire optical window. An estimate of DP can be derived using the absorption spectrum of water, which has distinct spectral features. This approach was first reported by Matcher et al. in 1993 who calculated DP as the quotient of the apparent water concentration, determined using the measured amplitude at 970 nm, divided by an assumed water concentration for brain tissue [58]. Light attenuation is also influenced by a DC scattering component (the G term from the modified Beer-Lambert law, equation 1.9). By taking the second derivative of the reflectance spectrum, the influence of scattering can be considered negligible due to its weak wavelength dependence. Derivatives of G can therefore be omitted by assuming wavelength independence over this range. The second derivative of the attenuation is modelled as follows:

$$\frac{\partial^2 A(\lambda)}{\partial \lambda^2} = DP \sum_i \frac{\partial^2 \varepsilon_i(\lambda)}{\partial \lambda^2} C_i \tag{1.17}$$

where terms are defined as in equation 1.9. The water feature can be characterized by performing a least-squares fit between the second derivatives of the measured and ground truth water absorption spectra. The DP can be determined by scaling this factor by an assumed brain water concentration [58].

Derivative spectroscopy has since been extended to solve for absolute concentrations of hemoglobin by fitting the first and second derivatives of solutions for the diffusion approximation to the first and second derivatives of the measured reflectance data (Figure 1.3) [59–61].

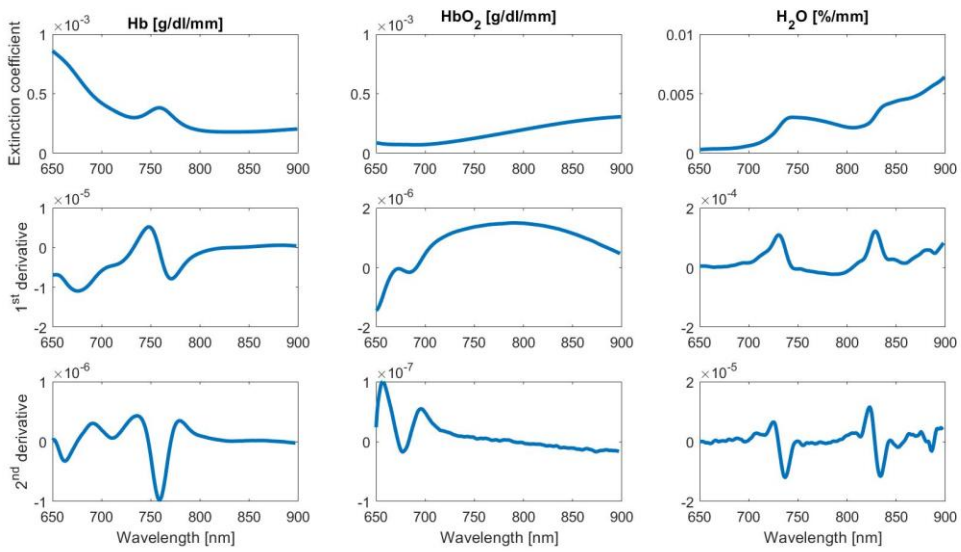

Figure 1.3: Extinction coefficient, 1st, and 2nd derivatives for HbO_2, Hb, and water.

In this approach, light propagation is modelled via a steady-state solution to the diffusion approximation with reflectance given by [62]:

$$R(\rho) = \frac{1}{4\pi}\left[z_0\left(\mu_{eff} + \frac{1}{r_1}\right)\right]\frac{e^{(-\mu_{eff}r_1)}}{r_1^2} + (z_0 + 2z_b)\left(\mu_{eff} + \frac{1}{r_2}\right)\frac{e^{(-\mu_{eff}r_2)}}{r_2^2} \quad (1.18)$$

where $r_1 = [\rho^2 + z_0^2]^{1/2}$ and $r_2 = [\rho^2 + (z_0 + 2z_b)^2]^{1/2}$. The effective depth is represented by $z_0 = 1/\mu_s'$, while $z_b = 2D(1+R_{eff})(1-R_{eff})^{-1}$ is the extrapolated boundary [63] with $R_{eff} = 0.493$ as the effective reflection coefficient for tissue and air refractive indices [64].

The impact of scatter (described by equation 1.8) is characterized by solving for the scattering terms A and α using a least-square minimization algorithm. The introduction of a derivative analysis has the added benefit of minimizing the influence of DC noise from ambient light sources. However, the fitting algorithms involved have proven to be computationally heavy and require too much time to allow for real-time monitoring. Recent work has combined the derivative approach to quantify chromophores at baseline with relative models using the Beer-lambert Law to provide continuous absolute monitoring at high temporal resolutions:

$$S_tO_2 = \frac{(HbO_2^b + \Delta HbO_2)}{(Hb^b + \Delta Hb) + (HbO_2^b + \Delta HbO_2)} \quad (1.19)$$

where the superscript '*b*' indicated absolute values measured at baseline and variables preceded by Δ indicate relative changes [65].

In addition to measuring StO_2, B-NIRS is capable of monitoring cerebral metabolism. This is achieved through the metabolic marker cytochrome c oxidase (CCO), an enzyme in the mitochondria's electron transport chain vital to oxidative phosphorylation. CCO is the final electron accepter that becomes oxidized, reducing oxygen to water. This exchange builds on an electrochemical gradient which ultimately drives ATP synthesis. A reduction in CCO may signal subsequent damage; significant reductions in energy production can lead to cell death and tissue damage [66]. To meet high energy demands, the brain has a relatively higher concentration of mitochondria compared to the skin and muscle that comprises the extra-cerebral layers, making CCO a more brain-sensitive marker of metabolism. Similar to hemoglobin, oxygenated and deoxygenated CCO have distinct absorption spectrum in the NIR (Figure 1.4).

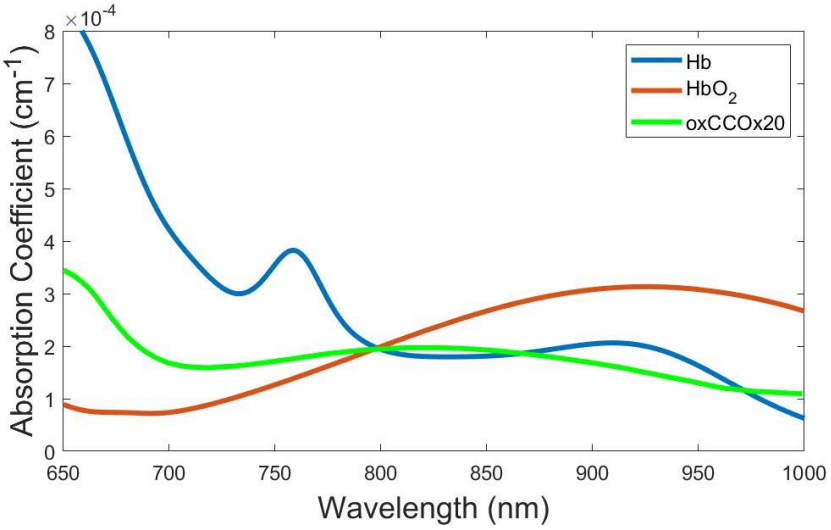

Figure 1.4: Absorption spectra of oxCCO

The total concentration of CCO in the brain is stable; however, its oxidization is dynamic [67]. A relative change in metabolism can therefore be determined by comparing the interchange between oxidation states. This is achieved using B-NIRS by analyzing the oxidized-reduced difference spectrum to indicate changes in the oxidized state of CCO

(oxCCO). Analytically, a modified Beer-Lambert law (similar to equation 1.9), developed by researchers at University College London, includes oxCCO as a chromophore [68]:

$$\begin{bmatrix} \Delta HbO_2 \\ \Delta Hb \\ \Delta oxCCO \end{bmatrix} = \frac{1}{DP} \begin{bmatrix} \varepsilon_{HbO_2}(\lambda_1) & \varepsilon_{Hb}(\lambda_1) & \varepsilon_{oxCCO}(\lambda_1) \\ \vdots & \vdots & \vdots \\ \varepsilon_{HbO_2}(\lambda_n) & \varepsilon_{Hb}(\lambda_n) & \varepsilon_{oxCCO}(\lambda_n) \end{bmatrix}^{-1} \times \begin{bmatrix} \Delta A(\lambda_1) \\ \vdots \\ \Delta A(\lambda_n) \end{bmatrix} \quad (1.20)$$

An *in vivo* measurement of CCO has been sought since the conception of NIRS [29]. With a concentration less than 10% of hemoglobin's, accurate measures of CCO have proven challenging and controversial with traditional NIRS technology [68–71]. The more recent use of spectral analysis has allowed for robust measures, characterizing oxCCO's broad absorption feature [72,73]. Optical measurements of oxCCO were found consistent with metabolic measures from cerebral microdialysis [74] and MRS [75]. To confirm signal contribution from cytochrome, equation 1.20 can be solved both with (3-component model) and without (2-component model) the inclusion of ΔoxCCO. The resulting concentrations can then be used to back-calculate the attenuation from which a residual difference between calculated and measured attenuation can be determined. The incorporation of oxCCO as a chromophore can be justified by noting that the 2-component residual resembles the absorption spectra of oxCCO, suggesting a missing chromophore in the fit, while the 3-component residual is approximately zero across all wavelengths [67].

B-NIRS achieves hyperspectral analysis by implementing a 'white-light' halogen bulb as a source, which emits throughout the NIR, and a spectrometer employing a diffraction grating to separate incoming light as a function of wavelength. In the spectrometer, light is detected by a charged couple device (CCD) which operates using the internal PE (described in section 1.3.1). In comparison to APD or PMT technology, CCDs collect spatial information along an array of pixels. B-NIRS systems, in comparison to other advanced NIRS approaches (discussed in sections 1.3.2 and 1.3.3), are simple in their design and are cost-effective [76]. While B-NIRS is able to acquire metabolic information, it is limited in depth sensitivity, similar to traditional CW-NIRS approaches.

B-NIRS measures of StO_2 and oxCCO have been acquired in several relevant animal models and neonatal studies. Early work investigating cytochrome using discrete

wavelength CW-NIRS systems have reported conflicting and inconsistent measures. Given these discrepancies, only recent applications utilizing B-NIRS systems will be discussed (for a detailed history of CCO measures see the recent review by Bale et al. [67]). Within a piglet model of neonatal hypoxia-ischemia (achieved through reducing inspired oxygen and occluding carotid arteries), Bainbridge et al. reported a correlation between oxCCO and clinical outcome at 48 hours post-injury [75]. In a similar animal model, measures of oxCCO were able to gauge injury severity [77]. In this study, controlled anoxia events prior to and following injury were monitored while injury severity was confirmed using MRS. In 2014, Bale et al. monitored cerebral saturation and metabolism in six infants with neonatal encephalopathy for over 200 hours in the NICU [73]. This work demonstrated the feasibility for longitudinal optical monitoring while observing 236 desaturation events. A significant similarity between oxCCO and MRS biomarkers of injury severity was reported. McLachlan et al. utilized a B-NIRS system to monitor StO_2 nine infants with PHVD receiving a ventricular tap and demonstrated the potential of optical monitoring in gauging intervention efficacy. A significant increase in post-operative StO_2 was found compared to a control group. In addition, preliminary work in a neonatal piglet model manipulated cerebral metabolism through inducing ischemia and using an anaesthetic to reduce oxygen demand. This work compared oxCCO and calculated measures of metabolism based on oxygen utilization, finding a temporal delay in the latter [78]. Further work is required to elucidate the difference between the two metabolic measures.

1.3.2 Time-resolved NIRS

Time-resolved NIRS was first introduced in 1988 by Chance et al. and Delpy et al. to characterize the DP using time-of-flight information as photons traverse tissue [34,79]. TR-NIRS utilizes a light source with extremely short laser pulses, on the order of picoseconds. High temporal resolution detectors and electronics generate histograms of incoming photons as a function of arrival time, referred to as temporal point spread functions (TPSF, Figure 4).

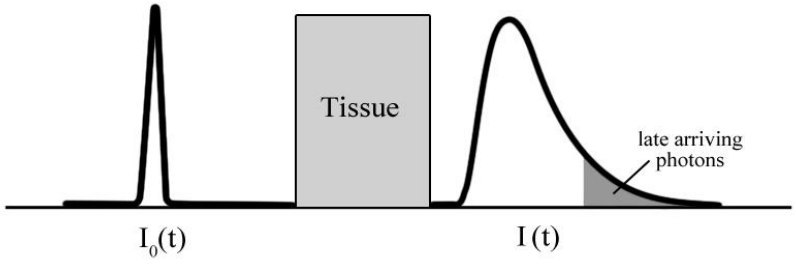

Figure 1.5: Time-resolved NIRS with pulse of intensity $I_0(t)$ is incident on tissue, producing a TPSF with intensity I(t).

By modelling the TPSF by the DA, the optical properties can be quantified and, in turn, used to determine absolute chromophore concentrations. The time dependent solution of the DA for semi-infinite geometry can be given as follows [80]:

$$R_d(\rho, t) = \frac{1}{2}(4\pi Dc)^{-\frac{3}{2}} t^{-\frac{5}{2}} e^{(-\mu_a ct)} \left[z_0 e^{-\frac{r_1^2}{4Dct}} + (z_0 + 2z_b) e^{-\frac{r_2^2}{4Dct}} \right] \qquad (1.21)$$

Time-of-flight information provides the added benefit of increased depth sensitivity. Later arriving photons, depicted by the tail-end of each TPSF, can be separately binned to isolate light that has travelled deeper within tissue [81]. Recent studies have demonstrated the impact of analyzing these photons to differentiate between signal contribution from the brain versus extra-cerebral layers [82]. Depth sensitivity can also be achieved through calculating the statistical moments, with higher moments more sensitive to the latter end of the histogram representing later arriving photons [83,84].

To achieve high temporal resolution measures, TR-NIRS systems utilize pulsed lasers operating on the order 80 MHz and quick detectors such as PMTs coupled to a photon counting module to generate TPSFs. These components are costly and bulky compared to other NIRS approaches, making TR-NIRS challenging for bedside monitoring with few commercial TR-NIRS systems available, most notably is the TRS device by Hamamatsu Photonics, Japan. Many recent studies have worked to minimize the size of TR-NIRS equipment and develop portable systems [85,86]. Multi-channel devices have also been developed for complete brain mapping and optical tomography [87,88]. The UCL group

has utilized their 32-channel system, dubbed MONSTIR, to generate three-dimensional images of the premature brain with IVH. Measured absorption and cerebral blood volume (CBV) was consistent with the asymmetry expected from the hemorrhaged area [89]. In neonatal animal models, TR-NIRS measurements of venous oxygenation (calculated from StO_2) were shown to agree with values obtained from directly from sagittal sinus blood [90]. However, in a neonatal piglet model of hyper/hypoxia, measures of StO_2 with TR- and B-NIRS devices produced strong a correlation but discrepancies between absolute values persisted, with B-NIRS reporting significantly higher measures [91]. Experiments in phantom and animal models have also demonstrated the ability of TR-NIRS to monitor deep brain temperature by analyzing shifts in the water absorption peak [92].

TR-NIRS was first used on newborn infants by Van der Zee et al. in 1992 to characterize the DP as a function of depth [93] and similar devices have since been translated to the clinic in a number of exploratory studies. In 2005, Ijichi et al. measured optical properties, StO_2, and CBV as a function of GA in term infants admitted to the NICU [94]. This study demonstrated the feasibility for bedside neuromonitoring in the NICU while reporting a positive correlation of μ_s' and CBV and a negative correlation of StO_2 with increasing GA. Following this, a number of clinical studies have implemented Hamamatsu's TRS devices in neonatal populations. Using the TRS-10 system, Koyano et al. found significant increases in CBV and decreases in StO_2 in infants with high Hb levels prior to blood transfusion. This work demonstrated the potential of TR-NIRS monitoring to guide the decision to transfuse in VLBW infants [95]. Using the TRS-20 system, Ishii et al. reported significantly higher StO_2 and lower OEF in infants small for their GA compared to infants of an appropriate size [96]. In similar measurements, Fujioka et al. compared premature infants to those born at term, within the first three days of life, and found similar StO_2 values but significantly increased CBV in the full-term group [97].

1.3.3 Frequency-domain NIRS

Frequency domain NIRS (FD-NIRS) was proposed in 1990 as an alternative approach for quantifying tissue optical properties using a radiofrequency modulated light source [98–100]. By altering the emission-source intensity, light interrogating tissue will reach the detector with a change in phase proportional to the distance travelled (Figure 7). By

acquiring both the light attenuation and phase shift, the DP and optical properties can be determined and used to quantify chromophore concentrations [32].

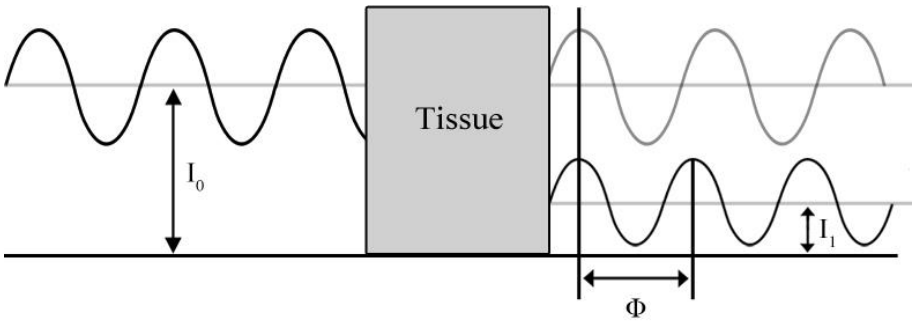

Figure 1.6: Frequency domain NIRS, phase modulated light source with intensity I_0 is incident on tissue resulting in an intensity change (I_1) and change in phase (Φ).

The intensity collected at the detector can be represented by [101]:

$$I = I_{DC} + I_{AC}\, sin(2\pi vt - \phi) \tag{1.22}$$

where I_{DC} is the average detected intensity, I_{AC} is the amplitude of the frequency dependent intensity, v is the modulating frequency, and Φ is the phase shift. The DP can then be calculated as $DP = \Phi c_v / 2\pi v n_t$ [101]. By assuming the modulating frequency is significantly smaller than frequency of scattering events, a solution to the diffusion approximation exists for a semi-infinite homogeneous medium. In 1993, Fishkin and Gratton [102] derived expressions for the measured phase (F Φ), AC (F_{AC}), and DC (F_{DC}) signals which can be summarized as follows [103]:

$$F_{\varphi}(\varphi, \rho, \omega, \mu_a, \mu_s') = S_{\varphi}(\omega, \mu_a, \mu_s')\rho + K_{\varphi-Source} + K_{\varphi-Detector} \tag{1.23}$$

$$F_{AC}(DC, \rho, \omega, \mu_a, \mu_s') = S_{AC}(\omega, \mu_a, \mu_s')\rho + K_{AC-Source} + K_{AC-Detector} \tag{1.24}$$

$$F_{DC}(DC, \rho, \mu_a, \mu_s') = S_{DC}(\mu_a, \mu_s')\rho + K_{DC-Source} + K_{DC-Detector} \tag{1.25}$$

where ρ represents the SDD and ω is the angular modulation frequency of the source. S_{DC}, S_{AC}, and Sφ represent the slopes of these linear functions and the K terms embody instrumental factors intrinsic to the source and detector [103]. While the latter terms are

unknown, SRS techniques can be used to acquire measurements at multiple distances and determine the optical properties from a calculated slope as follows:

$$\mu_a = \frac{\bar{\omega}}{2v}\frac{S_{dc}}{S_\phi}\left(\frac{S_\phi^2}{S_{dc}^2}+1\right)^{-\frac{1}{2}} \tag{1.26}$$

$$\mu'_s = \frac{S_{dc}^2}{3\mu_a} - \mu_a \tag{1.27}$$

where S denotes the slope for equations 1.24-1.26. With data acquired from a minimum of two wavelengths, absolute concentrations of Hb and HbO_2 can be determined [101]. Single-distance approaches to quantify FD-NIRS measures has also been achieved by using a calibration phantom with known optical properties to determine K terms (in equations 1.23-1.25) or by using a multi-frequency measurement with the modulation frequency (ω) as the independent variable opposed to the SDD (ρ) [103].

While FD-NIRS systems are more complex than CW-NIRS techniques, they are simpler and more cost-effective compared to TR-NIRS. Sources often exist as laser diodes alternately driven at frequencies on the order of 100 MHz and fast detectors, such as PMTs, operating in heterodyne mode. Compared to TR-NIRS devices, FD-NIRS requires multi-distance or multi-frequency measurements to quantify tissue chromophores. Alternatively, FD-NIRS requires the inclusion of a calibration measurement, prior to monitoring, in order to characterize the power of different sources and gains of detectors [104]. Despite the ability of FD-NIRS to characterize the DP, a study by Binzoni et al. compared the depth sensitivity between FD and CW-NIRS approaches and reported a similarity when modulation frequencies were < 200 MHz [105]. A study by Dehaes et al. found a major source of error with FD-NIRS measures, determined through Monte Carlo simulations, to be the significant curvature of the neonatal head relative to the typical source-detector distance since FD-NIRS are typically calibrated assuming a planar geometry. In this study optical absorption in the neonatal brain was retrieved with an error of 8–24% [106].

FD-NIRS was first implemented on newborn infants in 1995 by Duncan et al. to characterize optical pathlength [107], and in 1998 ISS Inc. (Champaign, IL) developed Oxiplex, the first commercial FD-NIRS system. Today it remains as one of the few

commercially available devices. In 2007, Franceschini et al. implemented FD-NIRS to monitor early brain development [108]. Here, StO_2, CBV, and $CMRO_2$ were calculated from measurements of hemoglobin concentrations and agreed with previously described developmental milestones from PET and EEG studies. A strong correlation was also found between changes in CBV/$CMRO_2$ measures and neonatal brain injury [109]. Recent work by van Essen et al. compared StO_2 measurements acquired using the Oxiplex FD-NIRS and the INVOS CW-NIRS (Medtronic) systems in premature infants within the first 15-minutes of life [110]. Significantly higher saturation values resulted using the Oxiplex system, suggesting persistent inconsistencies between optical techniques. Comparing preterm to term infants, Arri et al. found no significant difference between mean StO_2 values, similar to the study by Fujioka et al. using TR-NIRS [97], but reported measurement precision greater in infants at term due to changes in tissue homogeneity with development [33]. Roche-Labarbe et al. acquired optical measures of CBV and StO_2 using FD-NIRS in combination with CBF from TCD to calculate $CMRO_2$ in premature infants within six weeks following birth [111]. CBV was found to increase with GA, similar to reports using TR-NIRS [94]; however, no change in StO_2 was noted. This study found a significant discrepancy between $CMRO_2$ calculated using estimated and direct measures of CBF and emphasized the benefit of combining NIRS approaches with CBF monitoring. Section 1.4 describes optical techniques to measure CBF and section 1.5 elaborates on the development of hybrid systems.

1.4 Optical Blood Flow Monitoring

NIRS measurements of StO_2 have been used to describe oxygen content in the newborn brain during various stages and abnormalities. This metric has acted as a surrogate marker of cerebral hemodynamics and metabolism, due to a lack of adequate technology to provide more direct measures, but has proven limited in indicating adverse cerebral events or in predicting clinical outcomes [49,50,112]. Emerging optical techniques have proven capable of measuring blood flow in cerebral macro and microvasculature. This section will elaborate on approaches to directly measure CBF in the premature brain and their clinical applications.

1.4.1 Dynamic Contrast-Enhanced NIRS

NIRS is capable of quantifying blood flow using both endogenous [113,114] and exogenous [115–117] contrast agents. The former approach is based on the Fick principle and work by Kety and Schmidt who, in 1945, utilized nitrous oxide gas inhalation and brain uptake to provide the first quantitative measure of cerebral perfusion in humans [118]. NIRS can similarly use light absorption from HbO_2 as a flow tracer and has demonstrated comparable CBF measures with ^{133}Xe clearance techniques in premature infants [119,120]. Dynamic contrast-enhanced (DCE) NIRS instead utilizes an intravenous injection of the light absorbing dye indocyanine green (ICG) to act as an intravascular contrast agent. This exogenous tracer has a stronger and more distinct absorption peak in the NIR. DCE-NIRS can quantify CBF through a tracer kinetics model [121–123]:

$$C_b(t) = CBF \cdot R(t) * C_a(t) \tag{1.28}$$

where C_b is the ICG concentration in brain tissue measured using NIRS and C_a is the arterial concentration acquired using a dye densitometer. $R(t)$ is the impulse residue function which describes the fraction of dye in the tissue at time t following a bolus injection at $t = 0$. CBF can be solved by deconvolution since $R(0) \equiv 1$. Absolute measures of CBF have been validated in piglets against measurements obtained with computed tomography (CT) perfusion [115,124] and in adults against arterial spin labelling (ASL) MRI [125]. DCE-NIRS has shown strong agreement when using both CW- and TR-NIRS techniques [116]. In addition, multi-distance NIRS has allowed for depth-resolved flow measurements [126,127]. The use of ICG to monitor CBF was demonstrated in infants by Patel et al. in 1998 who found good agreement with NIRS measures of flow using HbO_2 as an endogenous marker [128]. DCE-NIRS measures of CBF have been combined with StO_2 from standalone NIRS to calculate $CMRO_2$ in piglet models of neonatal hypoxia ischemia [129,130] and in infants with patent ductus arteriosus [131] and post-hemorrhagic hydrocephalus [132]. The development and clinical translation of hybrid systems to acquire metabolic information is the focus of section 1.5. Due to the need for a contrast agent, DCE-NIRS is a minimally invasive technique but is only able to provide discrete measurements of CBF. More recent advancements in optical technology have provided a means of continuous non-invasive monitoring of CBF at the bedside.

1.4.2 Diffuse Correlation Spectroscopy

Diffuse correlation spectroscopy (DCS) is a technique gaining significant popularity in recent literature which can continuously acquire microvascular CBF without the use of contrast. DCS, similarly to NIRS, utilizes light in the NIR range, but focuses on characterizing scattering events caused by red blood cells (RBC). When interrogating a region with light, constructive and destructive interference of light electric fields will be apparent at the site of the detection fiber as dynamic bright and dark spots; this is referred to as a speckle pattern. Speckle intensity analysis was originally investigated to determine the size and structure of large molecules [133] and, under various names, has shown potential in flow monitoring [134,135]. More recently, Boas et al. set the ground work in developing DCS as a potential tool for measuring cerebral perfusion [136,137]. Since RBC are the primary moving light scatterers in tissue [138], the faster they move in vasculature the quicker the speckle intensity will fluctuate. By analyzing these temporal fluctuations with an autocorrelation, RBC motion can be related to correlation decay and, in turn, to blood flow. For an electromagnetic field in a highly scattering medium, the field autocorrelation function G1(ρ,t) can be given by:

$$G_1(\rho,\tau) = \langle E(\rho,\tau)\cdot E(\rho,t+\tau)\rangle \tag{1.29}$$

where E(ρ,t) is the electric field at SSD (ρ) and time (t), τ is the delay time, and angle brackets denote temporal averages. The normalized field autocorrelation function can then be represented as:

$$g_1(\rho,\tau) = \frac{\langle E(\rho,\tau)\cdot E^*(\rho,t+\tau)\rangle}{\langle |E(\rho,t)|^2\rangle} \tag{1.30}$$

DCS monitors speckle light intensity at high temporal resolutions, from which a normalized intensity autocorrelation function can be determined:

$$g_2(\rho,\tau) = \frac{\langle I(\rho,\tau)\cdot I(\rho,t+\tau)\rangle}{\langle |I(\rho,t)|^2\rangle} \tag{1.31}$$

where I(ρ,t) is the detected light intensity at an SDD ρ and time t. The normalized intensity and electric field autocorrelation function are related via the Siegert relationship [139]:

$$g_2(\rho,\tau) = 1 + \beta|g_1(\rho,\tau)|^2 \tag{1.32}$$

where β is the coherence factor dictated by the number of speckles detected and laser properties (i.e., coherence length and stability). G1 satisfies the diffusion equation and, assuming a point source and semi-infinite homogenous geometry, can be solved for using the correlation diffusion equation (CDE) [137]. Similar to the RTE (Equation 1.10) which assumes energy conservation with photon scatter, the CDE describes a transfer of correlation, in that it accumulates a correlation decay with scattering events. The DA (equation 1.12), simplified from the RTE, can instead be modelled as the CDE [136]:

$$[D(r,t)\nabla^2 - v\mu_a(r,t) - k_D^2(\tau)] \cdot G_1(r,t) = -vS(r) \tag{1.33}$$

where D is the diffusion coefficient (equation 1.13) and k_D^2 represents a correlation decay caused by the motion of scatterers.

$$k_D^2(\tau) = 3\mu'_s\mu_a + \alpha\mu'^2_s k_0^2\langle r^2(\tau)\rangle \tag{1.34}$$

where alpha is the ratio of moving scatterers to all scatterers, $k_0 = 2\pi n/\lambda$ is the light wavenumber (with λ as the wavelength and n as the refractive index), and $<\Delta r^2(\tau)>$ is the mean-square displacement of the scatterers over delay time τ. To model flow in vasculature, the Brownian diffusion model assumes incoherent motion and is given by:

$$\langle \Delta r^2(\tau)\rangle = 6D_B\tau \tag{1.35}$$

where D_B is the effective diffusion coefficient. Applying Brownian motion to the equation k_D^2 gives:

$$k_D^2 = 3\mu'_s\mu_a + 6\mu'^2_s k_0^2 \alpha D_B \tau \tag{1.36}$$

where the collective term αD_B (in units cm^2/s) represents an index of blood flow (BFI) [140,141]. To solve for aD_B, G_1 must first be calculated, which is achieved through an analytical solution to the CDE (equation 1.33) [62,142]:

$$G_1(\rho,\tau) = \frac{3\mu'_s}{4\pi}\left[\frac{e^{-k_D(\tau)r_1}}{r_1} - \frac{e^{-k_D(\tau)r_2}}{r_2}\right] \tag{1.37}$$

where $r_1 = [\rho^2 + z_0^2]^{1/2}$ and $r_2 = [\rho^2 + (z_0 + 2z_b)^2]^{1/2}$.. The effective depth is represented by $z_0 = 1/\mu_s'$, while $z_b = 2D(1+R_{eff})(1-R_{eff})^{-1}$ is the extrapolated boundary [63] with $R_{eff} = 0.493$ as the effective reflection coefficient for tissue and air refractive indices [64].

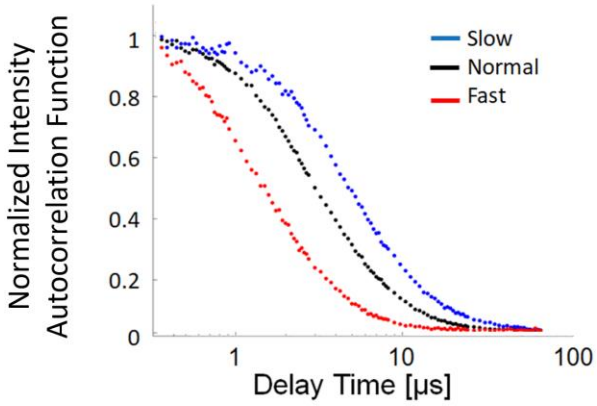

Figure 1.7: Normalized intensity autocorrelation function showing correlation decay at varying flowrates

To isolate speckle intensity fluctuations from RBC motion, DCS employs a continuous-wave long-coherence laser. A coherence length (>5 m) significantly larger than the photon pathlength (<1 m) is required to ensure that the light interrogating tissue remains in-phase despite the large pathlength travelled. Any decay in the correlation can then be attributed to the movement of scatterers opposed to fluctuations from the source itself. Most commonly, DCS utilizes a laser within the first optical window (e.g. 785 nm). Recent work has shown that longer wavelengths (>1000 nm) have SNR advantages [143]. When collecting light, implementing a single-mode detection fiber (core radius ~2-8 μm) improves speckle contrast by allowing only a single scattered electric field component. However, the small amount of light collected from the small core greatly reduces SNR. The use of few-mode fibers has been shown to improve upon this by increasing the number of photons collected while suffering only a slight decrease in speckle contrast [144–146]. To monitor CBF at high temporal resolutions, single-photon avalanche photodiode (SPAD) detectors are utilized. Coupled with a counting board, these detectors can achieve a high SNR. To calculate an autocorrelation curve, incoming photons are binned as a function of time. Traditionally, this is achieved using a multi-tau hardware correlator board with set delay times, ranging from μs to s. Improving upon this, Baker et al. found a selection of delay times to increase temporal resolution and SNR [147]. Modifying delay times also has potential to improve depth sensitivity, as fitting earlier delay times represents longer photon

pathlengths and increased brain signal contribution [148]. Further, Wang et al. showed the development of a software correlator to digitally bin photons for calculation of the autocorrelation curve, allowing increased selectivity of the delay time range [149]. High temporal resolution flow measurements achieved using software correlators have proven capable of monitoring CBF pulsatility [149,150]. In comparison to NIRS, DCS has improved depth sensitivity, showing a three-fold increase in brain-to-scalp signal contribution, making it ideal for bedside neuromonitoring [148]. Multi-layer models have been implemented to differentiate between scalp and brain flow in both animals and humans [147,151]. Signal contribution from the brain has been further investigated with the development of time-domain (TD) DCS systems. Similar to TR-NIRS approaches, TD-DCS acquires a temporal point spread function, while simultaneously measuring the autocorrelation function, and through time-gating can differentiate photon pathlengths and ultimately depth penetration [152].

A large number of studies in animal models, adults, and neonates have reported strong correlations of BFI (measured in cm^2/s) with CBF (measured in traditional units of mL/min/100 g) using numerous techniques including Doppler ultrasound [153], DCE-ultrasound [154], TCD [155], Xenon-CT [156], DCE-NIRS [60,157], phase-contrast MRI [158], and ASL-MRI [140,159–162]. DCS has generally been used to track relative measures of CBF, as quantification requires measuring the optical properties [157,163,164]. BFI's relative measure of flow has been implemented alongside DCE-NIRS techniques to quantify CBF [157,165]. Recently, a stand-alone DCS system was shown to capable of providing absolute CBF through multi-distance DCE measurements, finding a strong correlation with DCE-NIRS measures of flow [141].

DCS systems have been implemented to monitor the premature brain in a number of studies and are often combined with other NIRS techniques to provide both perfusion and metabolic information. Section 1.5 outlines the benefits of hybrid optical systems in acquiring these metrics and elaborates on the clinical applications of both CBF and metabolic neuromonitoring in the NICU.

1.5 Hybrid Optical Systems

Limitations in the clinical relevance of StO_2 alone, and the more recent emergence of DCS measures of flow, has prompted the development of hybrid NIRS/DCS devices to acquire both cerebral perfusion and metabolism concurrently [25]. A bedside measure of metabolism has potential in providing a more direct marker of injury. It can provide context to fluctuations in CBF and indicate when changes are significant enough to impact oxygen utilization. When cells are not sufficiently metabolizing oxygen to create energy, it can result in cell death and subsequent brain damage. Metabolism is most commonly calculated as $CMRO_2$, a conservation equation based on the Fick principle, which determines oxygen consumption in units of O_2/100 g/min by measuring cerebral blood flow and the arteriovenous oxygen difference [90,118,140]:

$$CMRO_2 = K \times tHb \times CBF \times (SaO_2 - SvO_2) \tag{1.38}$$

where K is the oxygen carrying capacity of hemoglobin (1.39 mL of O_2 per g of Hb [166]), tHb is the total hemoglobin concentration, SaO_2 is the arterial oxygen saturation, and SvO_2 is the venous oxygen saturation. When applied to NIRS, SvO_2 is determined from StO_2 by assuming a fixed ratio of arterial-to-venous blood:

$$SvO_2 = \frac{StO_2 - SaO_2(1-f_v)}{f_v} \tag{1.39}$$

where f_v is the venous volume fraction (0.75) [167]. Equation 1.38 can then be simplified as follows:

$$CMRO_2 = \frac{K \times tHb \times CBF}{f_v} \times (SaO_2 - StO_2) \tag{1.40}$$

By combining NIRS measures of StO_2 and DCS measures of CBF, $CMRO_2$ can be determined. This combination was first demonstrated by Cheung et al. in 2001 and has since evolved in highly sophisticated and commercially available devices [142]. This section elaborates on the development of systems combining the NIRS techniques described in section 1.3 with DCS to monitor the newborn brain.

1.5.1 Frequency-domain NIRS and DCS

The first hybrid system presented by Cheung et al. utilized multi-distance FD-NIRS and DCS technology to collect optical data from four different positions on a rat's brain [142]. The system was adapted to monitor CBF and $CMRO_2$ during ischemia in a similar animal model [168] and soon after in the adult brain [169]. This device acquired FD-NIRS and DCS information in succession and reported a 2.5-minute temporal resolution for a full data set. Since this work, significant improvements have been made to system SNR, temporal resolution, and depth sensitivity. Advancements have allowed for robust monitoring and translation of technology to the NICU to monitor perfusion and metabolism at the bedside [104]. A notable milestone was the development of the MetaOx described by Carp et al. in 2017, the first commercially available FD-NIRS/DCS device [170]. This system can acquire data at 10 Hz, enabling pulsatile measurements, and can analyze collected data in real-time. By implementing a short-pass filter to block DCS light from FD-NIRS PMT detectors, it allows for a truly simultaneous measure of perfusion and metabolism. Validation of the system demonstrated similar results to stand-alone devices. Recent work has also introduced motion correction algorithms for CBF and $CMRO_2$ measures [171].

Both research and commercial FD-NIRS/DCS systems have been translated to the NICU to investigate perfusion and metabolic change during early stages of brain development. In 2010, Roche-Labarbe et al. monitored CBF and $CMRO_2$ in preterm infants during the first six weeks of life. In this study StO_2 measures steadily decreased during this period, while CBF and $CMRO_2$ increased, with the latter increasing 40% [111]. This group also observed changes in CBF and $CMRO_2$ as a function of brain development, finding both to positively correlate with post-menstrual age [172]. Recent work has also found correlations between CBF and malnutrition impeding adequate development [173]. Significantly reduced CBF and $CMRO_2$ values have been reported in extremely low GA (24-28 weeks gestation) infants with IVH compared to those without hemorrhages [174]. Regional changes in CBF and $CMRO_2$ in both preterm and term infants have also been investigated, finding significantly increased values in the right hemisphere [175,176]. In age-matched groups, males were found to have higher CBF in most regions, a higher $CMRO_2$ in the frontal

region, and more prominent hemispheric asymmetry [104,176]. Such a discrepancy was expected since newborn males are generally more susceptible to white matter injury, hypoxic-ischemic injury, and cerebral palsy than females [177,178].

Similar FD-NIRS/DCS systems have been utilized to investigate a wide range of neonatal brain injuries. Several studies have monitored CBF and $CMRO_2$ in infants with complex congenital heart disease (CHD). Durduran et al. investigated cerebrovascular reactivity (i.e., changes in CBF in response to change in partial pressure of CO_2), which has been associated with adverse neurodevelopment, finding minimal influence of hypercapnia on flow/metabolic measures in term infants [179] while differences in CBF and $CMRO_2$ were found in CHD patients compared with controls [180]. Severe forms of CHD were found to produce CBF and $CMRO_2$ values similar to expected values for preterms and showed a strong correlation to MRI-measured values when infants were at rest and hypercapnic [161]. In infants with ventricle lesions undergoing neonatal cardiac surgery, no correlation was found between changes in CBF/$CMRO_2$ and duration of deep hypothermic circulatory arrest [181]. In infants with hypoxic-ischemic encephalopathy decreases in both metrics were found when undergoing therapeutic hypothermia [182]. Optical measures of perfusion and metabolism have also been used as a marker of functional activation in preterm infants [183].

1.5.2 Time-resolved NIRS and DCS

Similar to devices described in section 1.5.1, hybrid systems combining TR-NIRS and DCS techniques offer continuous and robust measurements of CBF and $CMRO_2$. Due to the complexity of TR-NIRS devices (as described in section 1.3.2) studies combining these approaches are limited. In 2010, Diop et al. first utilized TR-NIRS in conjunction with DCS to quantify the relative measures of CBF using a DCE-NIRS approach [157]. The device's ability to monitor flow and metabolic information was demonstrated in a neonatal piglet model of brain injury by manipulating metabolism using anaesthetics and sodium cyanide [90]. The system's ability to accurately monitor optical properties and CBF was demonstrated in a phantom model along with the depth sensitivity of acquired measures [184]. Recent iterations of this device employed optical filters to allow NIRS and DCS technique to run truly simultaneously [185].

More recent work by Giovannella et al. presented a commercial-grade hybrid TR-NIRS/DCS device called the BabyLux [186]. This system also utilizes optical filters to acquire simultaneous NIRS and DCS data at a temporal resolution of 1 s, while avoiding crosstalk between signals. System stability was demonstrated, and in-vivo measurements were conducted on the adult brain. The accuracy and precision of this device was described using phantoms and piglet models in comparison to expected values from simulated data [187]. Concurrent measures of cerebral oxygenation and blood flow were demonstrated in healthy term infants, reporting an improved intra-subject variability in oxygenation values compared to commercial NIRS devices [188].

1.5.3 Broadband NIRS and DCS

While hybrid systems using FD- and TR-NIRS can provide concurrent measures of CBF and $CMRO_2$, the latter is a calculated metric based on the former. As such, any error in the CBF measure is also reflected in $CMRO_2$. As discussed in section 1.3.1.3, B-NIRS has the advantage of acquiring a measure of oxCCO, a direct marker of cerebral metabolism, in addition to $CMRO_2$. While a comparison between oxCCO and $CMRO_2$ is limited, preliminary work reports a slight discrepancy [78]. Compared to other NIRS approaches, B-NIRS devices have the added benefit of simplicity and cost, requiring only a halogen bulb and spectrometer. A study utilizing both B-NIRS and DCS was presented, but continuous measurements of both techniques had not been achieved. In premature infants receiving an indomethacin infusion (a vasoconstrictor) as treatment for patent ductus arteriosus, Diop et al. monitored CBF and $CMRO_2$ surrounding the intervention using B-NIRS and DCS [60]. This study reported a significant reduction in StO_2 and CBF, with no change in $CMRO_2$. Measurements in this work were non-continuous, and simultaneous acquisitions of oxCCO and CBF had yet to be reported.

1.6 Research Objectives

The goals of my doctoral research were to develop a hybrid optical system to provide a continuous measure of cerebral perfusion and metabolism, via the marker oxCCO, in infants at risk of brain injury. A non-invasive technique to characterize these metrics has

potential to aid in early detection and clinical management of IVH and PHVD. These goals have been addressed through the following aims:

1. Develop and validate a hybrid B-NIRS and DCS neuromonitor to simultaneously acquire CBF and oxCCO at the bedside.

2. Assess system feasibility in PHVD infants in the neonatal intensive care unit.

3. Investigate cerebral perfusion and metabolic stability during early brain development in premature infants soon after following birth.

4. Investigate the impact of significant changes in CBF on cerebral energy metabolism.

Chapters two through five address these goals in order.

1.7 Thesis Outline

This dissertation includes six chapters. Chapters two to four were adapted from published work. Chapter five presents the first application of CBF and oxCCO measures in premature infants immediately following birth. Chapter 7 summarizes the advancements presented in this body of work.

1.7.1 Development of a hybrid broadband NIRS and DCS device for concurrent measurements of cerebral perfusion and cytochrome c oxidase (Chapter 2)

The development of a novel system combining B-NIRS and DCS is described. The system's ability to acquire oxCCO and CBF is demonstrated in a piglet model of neonatal hypoxia-ischemia. This chapter is based on a publication titled "Simultaneous monitoring of cerebral perfusion and cytochrome c oxidase by combining broadband near-infrared spectroscopy and diffuse correlation spectroscopy," published in *Biomedical Optics Express* in 2018 by Ajay Rajaram, Gemma Bale, Matthew Kewin, Laura B. Morrison, Ilias Tachtsidis, Keith St. Lawrence, and Mamadou Diop [65].

1.7.2 Monitoring changes in cerebral blood flow and metabolism in infants with post-hemorrhagic ventricular dilatation during ventricular taps (Chapter 3)

NNeMo (Neonatal Neuromonitor) a clinical B-NIRS/DCS system is presented. System feasibility is demonstrated in infants with post-hemorrhagic ventricular dilatation (PHVD) to monitor hemodynamics and metabolism during the surgical removal of cerebrospinal fluid. This chapter is based on a publication titled "Perfusion and metabolic neuromonitoring during ventricular taps in infants with post-hemorrhagic ventricular dilatation," published in *Brain Sciences* in 2020 by Ajay Rajaram, Lawrence C. M. Yip, Daniel Milej, Marianne Suwalski, Matthew Kewin, Marcus Lo, Jeffrey J. L. Carson, Victor Han, Soume Bhattacharya, Mamadou Diop, Sandrine de Ribaupierre, and Keith St. Lawrence [189].

1.7.3 Monitoring cerebral hemodynamic, oxygenation and metabolic stability in premature infants following birth using a hybrid broadband NIRS/DCS optical brain monitor (Chapter 4)

NNeMo was utilized to monitor premature infants with the first 72 hours of life, starting soon after birth. Spontaneous and dynamic changes in CBF and metabolism are reported during this early period. A publication titled "Monitoring cerebral hemodynamic and metabolic stability in premature infants following birth using NNeMo (Neonatal NeuroMonitor) a hybrid broadband NIRS/DCS optical brain monitor," which elaborates on the data presented in this section is in preparation by Ajay Rajaram, Daniel Milej, Lilian Kebaya, Matthew Kewin, Lawrence C. M. Yip, Marianne Suwalski, Sandrine de Ribaupierre, Soume Bhattacharya, Mamadou Diop, and Keith St. Lawrence.

1.7.4 Changes in cerebral blood flow and metabolism in response to hypoperfusion events in adults during surgery with cardiopulmonary bypass (Chapter 5)

Successful preliminary results in the NICU prompted translation of NNeMo to monitor CBF and metabolism in adults undergoing surgery with cardiopulmonary bypass. While this study investigates a very different patient population, the underlying pathophysiology

and development of brain injury is similar. The relationship between cerebral perfusion and metabolism is demonstrated during extreme hypoperfusion events and transitions on/off cardiopulmonary bypass. This chapter is based on a publication titled “Optical monitoring of cerebral perfusion and metabolism in adults during cardiac surgery with cardiopulmonary bypass,” published in *Biomedical Optics Express* in 2020 by Ajay Rajaram, Daniel Milej, Marianne Suwalski, Lawrence C. M. Yip, Linrui R. Guo, Michael W. A. Chu, Jason Chui, Mamadou Diop, John M. Murkin, and Keith St. Lawrence [150].

1.7.5 Conclusion and Future Directions (Chapter 6)

This section summarizes the main findings of all work presented and elaborates on future directions for optical neuromonitoring in the newborn. Final conclusions and closing remarks are discussed.

1.8 References

1. Candian Institute for Health Information, "Highlights of 2010 – 2011 Selected Indicators Describing the Birthing Process in Canada," Heal. Indic. Reports (2012).

2. J. J. Volpe, "Brain injury in premature infants: a complex amalgam of destructive and developmental disturbances," Lancet **8**(1), 110–124 (2009).

3. N. Marlow, E. M. Hennessy, M. A. Bracewell, and D. Wolke, "Motor and executive function at 6 years of age after extremely preterm birth," Pediatrics **120**(4), 793–804 (2007).

4. N. Marlow, D. Wolke, M. A. Bracewell, M. Samara, and EPICureStudyGroup, "Neurologic and developmental disability at six years of age after extremely preterm birth," N. Engl. J. Med. **352**(1), 9–19 (2005).

5. P. Ballabh, "Intraventricular hemorrhage in premature infants: Mechanism of disease," Pediatr. Res. **67**(1), 1–8 (2010).

6. H. Bassan, "Intracranial Hemorrhage in the Preterm Infant: Understanding It, Preventing It," Clin. Perinatol. **36**(4), 737–762 (2009).

7. D. Wilson-Costello, H. Friedman, N. Minich, A. A. Fanaroff, and M. Hack, "Improved survival rates with increased neurodevelopmental disability for extremely low birth weight infants in the 1990s," Pediatrics **115**(4), 997–1003 (2005).

8. O. Khwaja and J. J. Volpe, "Pathogenesis of cerebral white matter injury of prematurity," Arch Dis Child Fetal Neonatal Ed. **93**(2), (2008).

9. S. Cherian, A. Whitelaw, M. Thoresen, and S. Love, "The pathogenesis of neonatal post-hemorrhagic hydrocephalus," Brain Pathol. **14**(3), 305–311 (2004).

10. A. Whitelaw, "Intraventricular haemorrhage and posthaemorrhagic hydrocephalus:

Pathogenesis, prevention and future interventions," Semin. Neonatol. **6**(2), 135–146 (2001).

11. J. S. Soul, P. E. Hammer, M. Tsuji, J. P. Saul, H. Bassan, C. Limperopoulos, D. N. Disalvo, M. Moore, P. Akins, S. Ringer, J. J. Volpe, F. Trachtenberg, and A. J. Du Plessis, "Fluctuating Pressure-Passivity Is Common in the Cerebral Circulation of Sick Premature Infants," Pediatr. Res. **61**(4), (2007).

12. O. Pryds, "Control of cerebral circulation in the high-risk neonate," Ann. Neurol. **30**(3), 321–329 (1991).

13. D. I. Altman, W. J. Powers, J. M. Perlman, P. Herscovitch, S. L. Volpe, and J. J. Volpe, "Cerebral blood flow requirement for brain viability in newborn infants is lower than in adults," Ann. Neurol. **24**(2), 218–226 (1988).

14. M. Hinojosa-Rodríguez, T. Harmony, C. Carrillo-Prado, J. D. Van Horn, A. Irimia, C. Torgerson, and Z. Jacokes, "Clinical neuroimaging in the preterm infant: Diagnosis and prognosis," NeuroImage Clin. **16**(August), 355–368 (2017).

15. H. J. McCrea and L. R. Ment, "The Diagnosis, Management and Postnatal Prevention of IVH in the Preterm neonate," Clin Perinatol **35**(4), (2010).

16. D. M. Ferriero, "Neonatal brain injury," N. Engl. J. Med. **351**(19), 1985–1995 (2004).

17. J. J. Volpe, P. Herscovitch, J. M. Penman, and M. E. Raichie, "Positron emission tomography in the newborn: extensive impairment of regional cerebral blood flow with intraventricular hemorrhage and hemorrhagic intracerebral involvement," Pediatrcs **72**(5), 1983 (1983).

18. G. Greisen, "Cerebral blood flow in preterm infants during the first week of life," Acta Paediatr Scand **75**(1), 43–51 (1986).

19. S. Purkayastha and F. Sorond, "Transcranial doppler ultrasound: Technique and application," Semin. Neurol. **32**(4), 411–420 (2012).

20. M. L. Gabriel, V. B. Piatto, and A. S. Souza, "Clinical application of transcranial doppler ultrasonography in premature, very-low-birth-weight neonates," Radiol. Bras. **43**(4), 213–218 (2010).

21. F. A. Camfferman, R. de Goederen, P. Govaert, J. Dudink, F. van Bel, A. Pellicer, F. Cools, T. Agut, A. Alarcon, R. Arena, M. Bartocci, M. Bravo, F. Cabañas, N. Carreras, O. Claris, J. Dudink, M. Fumagalli, P. Govaert, S. Horsch, A. Parodi, A. Pellicer, L. Ramenghi, C. C. Roehr, S. Steggerda, and E. Valverde, "Diagnostic and predictive value of Doppler ultrasound for evaluation of the brain circulation in preterm infants: a systematic review," Pediatr. Res. **87**, 50–58 (2020).

22. M. Kehrer, G. Blumenstock, S. Ehehalt, R. Goelz, C. Poets, and M. Schöning, "Development of cerebral blood flow volume in preterm neonates during the first two weeks of life," Pediatr. Res. **58**(5), 927–930 (2005).

23. N. Evans, M. Kluckow, M. Simmons, and D. Osborn, "Which to measure, systemic or organ blood flow? Middle cerebral artery and superior vena cava flow in very preterm infants," Arch. Dis. Child. Fetal Neonatal Ed. **87**(3), 181–184 (2002).

24. M. Kluckow and N. Evans, "Superior vena cava flow and intraventricular haemorrhage in extremely preterm infants," J. Matern. Neonatal Med. **82**(3), 188–194 (2000).

25. D. A. Boas and M. A. Franceschini, "Haemoglobin oxygen saturation as a biomarker: the problem and a solution," Philos. Trans. R. Soc. A Math. Phys. Eng. Sci. **369**, 4407–4424 (2011).

26. W. J. Powers, R. L. Grubb, D. Darriet, and M. E. Raichle, "Cerebral blood flow and cerebral metabolic rate of oxygen requirements for cerebral function and viability in humans," J. Cereb. Blood Flow Metab. **5**(4), 600–608 (1985).

27. A. J. Barkovich, K. Baranski, D. Vigneron, J. C. Partridge, D. K. Hallam, B. L. Hajnal, and D. M. Ferriero, "Proton MR spectroscopy for the evaluation of brain

injury in asphyxiated, term neonates," Am. J. Neuroradiol. **20**(8), 1399–1405 (1999).

28. J. L. Y. Cheong, E. B. Cady, J. Penrice, J. S. Wyatt, I. J. Cox, and N. J. Robertson, "Proton MR spectroscopy in neonates with perinatal cerebral hypoxic-ischemic injury: Metabolite peak-area ratios, relaxation times, and absolute concentrations," Am. J. Neuroradiol. **27**(7), 1546–1554 (2006).

29. F. F. Jöbsis, "Noninvasive , Infrared Monitoring of Cerebral and Myocardial Oxygen Sufficiency and Circulatory Parameters," Science (80). **198**(4323), 1264–1267 (1997).

30. F. F. Jöbsis-vanderVliet, "Discovery of the near-infrared window into the body and the early development of near-infrared spectroscopy," J. Biomed. Opt. **4**(4), 392–396 (1999).

31. L. A. Sordillo, Y. Pu, S. Pratavieira, Y. Budansky, and R. R. Alfano, "Deep optical imaging of tissue using the second and third near-infrared spectral windows," J. Biomed. Opt. **19**(5), (2014).

32. S. R. Arridge, M. Cope, and D. T. Delpy, "The theoretical basis for the determination of optical pathlengths in tissue: Temporal and frequency analysis," Phys. Med. Biol. **37**(7), 1531–1560 (1992).

33. S. J. Arri, T. Muehlemann, M. Biallas, H. U. Bucher, and M. Wolf, "Precision of cerebral oxygenation and hemoglobin concentration measurements in neonates measured by near-infrared spectroscopy," J. Biomed. Opt. **16**(4), 047005 (2011).

34. D. T. Delpy, M. Cope, P. Van Der Zee, S. Arridge, S. Wray, and J. Wyatt, "Estimation of optical pathlength through tissue from direct time of flight measurement," Phys. Med. Biol. **33**(12), 1433–1442 (1988).

35. L. C. Henyey and J. L. Greenstein, "Diffuse radiation in the galaxy," Astrophys **93**, 70–83 (1941).

36. R. K. Wang, "Modelling optical properties of soft tissue by fractal distribution of scatterers," J. Mod. Opt. **47**(1), 103–120 (2000).

37. M. Wolf and M. Ferrari, "Progress of near-infrared spectroscopy and topography for brain and muscle clinical applications," J. Biomed. Opt. **12**(6), (2007).

38. J. Lui, "Photonic Devices," Cambridge Univ. Press (2005).

39. F. Scholkmann, S. Kleiser, A. J. Metz, R. Zimmermann, J. Mata Pavia, U. Wolf, and M. Wolf, "A review on continuous wave functional near-infrared spectroscopy and imaging instrumentation and methodology," Neuroimage **85**, 6–27 (2014).

40. P. Pinti, C. Aichelburg, S. Gilbert, A. Hamilton, J. Hirsch, P. Burgess, and I. Tachtsidis, "A Review on the Use of Wearable Functional Near-Infrared Spectroscopy in Naturalistic Environments," Jpn. Psychol. Res. **60**(4), 347–373 (2018).

41. G. E. Strangman, Q. Zhang, and Z. Li, "Scalp and skull influence on near infrared photon propagation in the Colin27 brain template," Neuroimage **85**, 136–149 (2013).

42. Z. Li, B. K. Park, W. Liu, J. Zhang, M. P. Reed, J. D. Rupp, C. N. Hoff, and J. Hu, "A statistical skull geometry model for children 0-3 years old," PLoS One **10**(5), 1–13 (2015).

43. M. S. Patterson, E. Schwartz, and B. C. Wilson, "Quantitative Reflectance Spectrophotometry For The Noninvasive Measurement Of Photosensitizer Concentration In Tissue During Photodynamic Therapy," SPIE Proceeidings Photodyn. Ther. Mech. **1065**, 115 (1989).

44. S. L. Jacques, "Optical properties of biological tissues: a review," Phys. Med. Biol. **58**(11), R37–R61 (2013).

45. H. Liu, D. A. Boas, Y. Zhang, A. G. Yodh, and B. Chance, "Determination of optical properties and blood oxygenation in tissue using continuous NIR light,"

Phys. Med. Biol. **40**(11), 1983–1993 (1995).

46. S. J. Matcher, P. J. Kirkpatrick, K. Nahid, M. Cope, and D. T. Delpy, "Absolute quantification methods in tissue near-infrared spectroscopy," Proc. SPIE 2389 (May 1995), 486–495 (1995).

47. J. E. Brazy, V. Lewis, H. Mitnick, and Frans F. Jobsis, "Noninvasive Monitoring of Cerebral Oxygenation in Preterm Infants: Preliminary Observations," Pediatrics **75**(2), 217–225 (1985).

48. G. Greisen, B. Andresen, A. M. Plomgaard, and S. Hyttel-Sørensen, "Cerebral oximetry in preterm infants: an agenda for research with a clear clinical goal," Neurophotonics **3**(3), 031407 (2016).

49. M. Wolf and G. Greisen, "Advances in Near-Infrared Spectroscopy to Study the Brain of the Preterm and Term Neonate," Clin. Perinatol. **36**(4), 807–834 (2009).

50. S. Hyttel-Sorensen, G. Greisen, B. Als-Nielsen, and C. Gluud, "Cerebral near-infrared spectroscopy monitoring for prevention of brain injury in very preterm infants," Cochrane Database Syst. Rev. **2017**(9), (2017).

51. H. Hummler, "Near-Infrared spectroscopy for perfusion assessment and neonatal management," Semin. Fetal Neonatal Med. **25**(5), (2020).

52. L. M. L. Dix, F. van Bel, and P. M. A. Lemmers, "Monitoring cerebral oxygenation in neonates: An update," Front. Pediatr. **5**(46), (2017).

53. L. M. L. Dix, F. Van Bel, W. Baerts, and P. M. A. Lemmers, "Comparing near-infrared spectroscopy devices and their sensors for monitoring regional cerebral oxygen saturation in the neonate," Pediatr. Res. **74**(5), 557–563 (2013).

54. S. Kleiser, D. Ostojic, B. Andresen, N. Nasseri, H. Isler, F. Scholkmann, T. Karen, G. Greisen, and M. Wolf, "Comparison of tissue oximeters on a liquid phantom with adjustable optical properties: an extension," Biomed. Opt. Express **9**(1), 86–101 (2018).

55. A. Pellicer, G. Greisen, M. Benders, O. Claris, E. Dempsey, M. Fumagalli, C. Gluud, C. Hagmann, L. Hellström-Westas, S. Hyttel-Sorensen, P. Lemmers, G. Naulaers, G. Pichler, C. Roll, F. Van Bel, W. Van Oeveren, M. Skoog, M. Wolf, and T. Austin, "The SafeBoosC phase II randomised clinical trial: A treatment guideline for targeted near-infrared-derived cerebral tissue oxygenation versus standard treatment in extremely preterm infants," Neonatology **104**(3), 171–178 (2013).

56. S. Hyttel-Sorensen, A. Pellicer, T. Alderliesten, T. Austin, F. Van Bel, M. Benders, O. Claris, E. Dempsey, A. R. Franz, M. Fumagalli, C. Gluud, B. Grevstad, C. Hagmann, P. Lemmers, W. Van Oeveren, G. Pichler, A. M. Plomgaard, J. Riera, L. Sanchez, P. Winkel, M. Wolf, and G. Greisen, "Cerebral near infrared spectroscopy oximetry in extremely preterm infants: Phase II randomised clinical trial," BMJ **350**(January), 1–11 (2015).

57. A. M. Plomgaard, W. Van Oeveren, T. H. Petersen, T. Alderliesten, T. Austin, F. Van Bel, M. Benders, O. Claris, E. Dempsey, A. Franz, M. Fumagalli, C. Gluud, C. Hagmann, S. Hyttel-Sorensen, P. Lemmers, A. Pellicer, G. Pichler, P. Winkel, and G. Greisen, "The SafeBoosC II randomized trial: Treatment guided by near-infrared spectroscopy reduces cerebral hypoxia without changing early biomarkers of brain injury," Pediatr. Res. **79**(4), 528–535 (2016).

58. S. J. Matcher, M. Cope, and D. T. Delpy, "Use of the water absorption spectrum to quantify tissue chromophore concentration changes in near-infrared spectroscopy.," Phys. Med. Biol. **39**(1), 177–96 (1993).

59. H. Z. Yeganeh, V. Toronov, J. T. Elliott, M. Diop, T.-Y. Lee, and K. St Lawrence, "Broadband continuous-wave technique to measure baseline values and changes in the tissue chromophore concentrations.," Biomed. Opt. Express **3**(11), 2761–70 (2012).

60. M. Diop, J. Kishimoto, V. Toronov, D. S. C. Lee, and K. S. Lawrence, "Development of a combined broadband near-infrared and diffusion correlation

system for monitoring cerebral blood flow and oxidative metabolism in preterm infants," Biomed. Opt. Express **6**(10), 3907–3918 (2015).

61. Z. Kovacsova, G. Bale, S. Mitra, F. Lange, and I. Tachtsidis, "Absolute quantification of cerebral tissueoxygen saturation with multidistancebroadband NIRS in newborn brain," Biomed. Opt. Express **12**(2), 907–925 (2020).

62. A. Kienle and M. S. Patterson, "Improved solutions of the steady-state and the time-resolved diffusion equations for reflectance from a semi-infinite turbid medium," J. Opt. Soc. Am. A **14**(1), 246–254 (1997).

63. A. Kienle and T. Glanzmann, "In vivo determination of the optical properties of muscle with time- resolved reflectance using a layered model," Phys. Med. Biol. **44**(11), 2689–2702 (1999).

64. R. C. Haskell, L. O. Svaasand, T.-T. Tsay, T.-C. Feng, B. J. Tromberg, and M. S. McAdams, "Boundary conditions for the diffusion equation in radiative transfer," J. Opt. Soc. Am. A **11**(10), 2727 (1994).

65. A. Rajaram, G. Bale, M. Kewin, L. B. Morrison, I. Tachtsidis, K. St. Lawrence, and M. Diop, "Simultaneous monitoring of cerebral perfusion and cytochrome c oxidase by combining broadband near-infrared spectroscopy and diffuse correlation spectroscopy," Biomed. Opt. Express **9**(6), 2588–2603 (2018).

66. C. E. Cooper, S. J. Matcher, J. S. Wyatt, M. Cope, G. C. Brown, E. M. Nemoto, and D. T. Delpy, "Near-infrared spectroscopy of the brain: Relevance to cytochrome oxidase bioenergetics," Biochem. Soc. Trans. **22**(4), 974–980 (1994).

67. G. Bale, C. E. Elwell, and I. Tachtsidis, "From Jöbsis to the present day : a review of clinical near-infrared spectroscopy measurements of cerebral cytochrome-c-oxidase," J. Biomed. Opt. **21**(9), (2016).

68. S. J. Matcher, C. E. Elwell, C. E. Cooper, M. Cope, and D. T. Delpy, "Performance comparison of several published tissue near-infrared spectroscopy algorithms," Anal. Biochem. **227**(1), 54–68 (1995).

69. C. E. Cooper and R. Springett, "Measurement of cytochrome oxidase and mitochondrial energetics by near-infrared spectroscopy," Philos. Trans. R. Soc. B Biol. Sci. **352**, 669–676 (1997).

70. K. Uludağ, J. Steinbrink, M. Kohl-Bareis, R. Ü. Wenzel, A. Villringer, and H. Obrig, "Cytochrome-c-oxidase redox changes during visual stimulation measured by near-infrared spectroscopy cannot be explained by a mere cross talk artefact," Neuroimage **22**(1), 109–119 (2004).

71. Y. A. B. D. Wickramasinghe, P. Rolfe, K. Palmer, and S. A. Spencer, "Investigation of neonatal brain cytochrome redox by NIRS," Dev. Brain Res. **89**(2), 307–308 (1995).

72. R. Springett, J. Newman, M. Cope, and D. T. Delpy, "Oxygen dependency and precision of cytochrome oxidase signal from full spectral NIRS of the piglet brain.," Am. J. Physiol. - Hear. Circ. Physiol. **279**(5), H2202–H2209 (2000).

73. G. Bale, S. Mitra, J. Meek, N. Robertson, and I. Tachtsidis, "A new broadband near-infrared spectroscopy system for in-vivo measurements of cerebral cytochrome-c-oxidase changes in neonatal brain injury," Biomed. Opt. Express **5**(10), 3450 (2014).

74. M. M. Tisdall, I. Tachtsidis, T. S. Leung, C. E. Elwell, and M. Smith, "Increase in cerebral aerobic metabolism by normobaric hyperoxia after traumatic brain injury," J. Neurosurg. **109**(3), 424–432 (2008).

75. A. Bainbridge, I. Tachtsidis, S. D. Faulkner, D. Price, T. Zhu, E. Baer, K. D. Broad, D. L. Thomas, E. B. Cady, N. J. Robertson, and X. Golay, "Brain mitochondrial oxidative metabolism during and after cerebral hypoxia-ischemia studied by simultaneous phosphorus magnetic-resonance and broadband near-infrared spectroscopy," Neuroimage **102**(P1), 173–183 (2014).

76. M. Diop, E. Wright, V. Toronov, T.-Y. Lee, and K. St Lawrence, "Improved light collection and wavelet de-noising enable quantification of cerebral blood flow and

oxygen metabolism by a low-cost, off-the-shelf spectrometer.," J. Biomed. Opt. **19**(5), 057007 (2014).

77. G. Bale, A. Rajaram, M. Kewin, L. Morrison, A. Bainbridge, M. Diop, K. S. Lawrence, and I. Tachtsidis, "Broadband NIRS Cerebral Cytochrome-C-Oxidase Response to Anoxia Before and After Hypoxic-Ischaemic Injury in Piglets," Oxyg. Transp. to Tissue XL **1072**, 151–156 (2018).

78. A. Rajaram, L. Yip, M. Kewin, L. Morrison, M. Diop, and K. St. Lawrence, "Development of a neonatal neuromonitor for concurrent measurements of cytochrome c oxidase and CMRO2," Brain Brain PET Conf. Proc. PB01-D04 **39**, 183 (2019).

79. B. Chance, J. S. Leigh, H. Miyake, D. S. Smith, S. Nioka, R. Greenfeld, M. Finander, K. Kaufmann, W. Levy, and M. Young, "Comparison of time-resolved and -unresolved measurements of deoxyhemoglobin in brain.," Proc. Natl. Acad. Sci. U. S. A. **85**(14), 4971–4975 (1988).

80. M. S. Patterson, B. Chance, and B. C. Wilson, "Time resolved reflectance and transmittance for the non-invasive Measurement of Tissue Optical Properties," Appl. Opt. **28**(12), 2331–2336 (1989).

81. J. Selb, J. J. Stott, M. A. Franceschini, A. G. Sorensen, and D. A. Boas, "Improved sensitivity to cerebral hemodynamics during brain activation with a time-gated optical system: analytical model and experimental validation," J. Biomed. Opt. **10**(1), 011013 (2005).

82. D. Milej, A. Abdalmalak, A. Rajaram, and K. St. Lawrence, "Direct assessment of extracerebral signal contamination on optical measurements of cerebral blood flow, oxygenation, and metabolism," Neurophotonics **7**(04), 1–17 (2020).

83. A. Liebert, H. Wabnitz, J. Steinbrink, H. Obrig, and M. Mo, "Time-resolved multidistance near-infrared spectroscopy of the adult head: intracerebral and extracerebral absorption changes from moments of distribution of times of flight of

photons," Appl. Opt. **43**(15), 3037–3047 (2004).

84. D. Milej, A. Abdalmalak, P. McLachlan, M. Diop, A. Liebert, and K. St. Lawrence, "Subtraction-based approach for enhancing the depth sensitivity of time-resolved NIRS," Biomed. Opt. Express **7**(11), 4514 (2016).

85. M. Buttafava, E. Martinenghi, D. Tamborini, D. Contini, A. D. Mora, M. Renna, A. Torricelli, A. Pifferi, F. Zappa, and A. Tosi, "A Compact Two-Wavelength Time-Domain NIRS System Based on SiPM and Pulsed Diode Lasers," IEEE Photonics J. **9**(1), 1–14 (2017).

86. A. Abdalmalak, D. Milej, L. C. M. Yip, A. R. Khan, M. Diop, A. M. Owen, and K. St. Lawrence, "Assessing Time-Resolved fNIRS for Brain-Computer Interface Applications of Mental Communication," Front. Neurosci. **14**(February), 1–10 (2020).

87. F. E. W. Schmidt, M. E. Fry, E. M. C. Hillman, J. C. Hebden, and D. T. Delpy, "A 32-channel time-resolved instrument for medical optical tomography," Rev. Sci. Instrum. **71**(1), 256–265 (2000).

88. R. J. Cooper, E. Magee, N. Everdell, S. Magazov, M. Varela, D. Airantzis, A. P. Gibson, and J. C. Hebden, "MONSTIR II: A 32-channel, multispectral, time-resolved optical tomography system for neonatal brain imaging," Rev. Sci. Instrum. **85**(5), (2014).

89. J. C. Hebden, A. Gibson, R. M. Yusof, N. Everdell, E. M. C. Hillman, D. T. Delpy, S. R. Arridge, T. Austin, J. H. Meek, and J. S. Wyatt, "Three-dimensional optical tomography of the premature infant brain," Phys. Med. Biol. **47**(23), 4155–4166 (2002).

90. K. Verdecchia, M. Diop, T.-Y. Lee, and K. St Lawrence, "Quantifying the cerebral metabolic rate of oxygen by combining diffuse correlation spectroscopy and time-resolved near-infrared spectroscopy.," J. Biomed. Opt. **18**(2), 27007 (2013).

91. M. Kewin, A. Rajaram, D. Milej, A. Abdalmalak, L. Morrison, M. Diop, and K. St

Lawrence, "Evaluation of hyperspectral NIRS for quantitative measurements of tissue oxygen saturation by comparison to time-resolved NIRS," Biomed. Opt. Express **10**(9), 4789–4802 (2019).

92. M. F. Bakhsheshi, M. Diop, K. St. Lawrence, and T.-Y. Lee, "Monitoring brain temperature by time-resolved near-infrared spectroscopy: pilot study," J. Biomed. Opt. **19**(5), (2003).

93. P. Van der Zee, M. Cope, S. R. Arridge, M. Essenpreis, L. A. Potter, A. D. Edwards, J. S. Wyatt, D. C. McCormick, S. C. Roth, E. O. R. Reynolds, and D. T. Delpy, "Experimentally measured optical pathlengths for the adult head, calf and forearm and the head of the newborn infant as a function of inter optode spacing," Adv. Exp. Med. Biol. **316**, 143–153 (1992).

94. S. Ijichi, T. Kusaka, K. Isobe, K. Okubo, K. Kawada, M. Namba, H. Okada, T. Nishida, T. Imai, and S. Itoh, "Developmental changes of optical properties in neonates determined by near-infrared time-resolved spectroscopy," Pediatr. Res. **58**(3), 568–573 (2005).

95. K. Koyano, T. Kusaka, S. Nakamura, M. Nakamura, Y. Konishi, T. Miki, M. Ueno, S. Yasuda, H. Okada, T. Nishida, K. Isobe, and S. Itoh, "The effect of blood transfusion on cerebral hemodynamics in preterm infants," Transfusion **53**(7), 1459–1467 (2013).

96. H. Ishii, T. Takami, T. Fujioka, N. Mizukaki, A. Kondo, D. Sunohara, A. Hoshika, O. Akutagawa, and K. Isaka, "Comparison of changes in cerebral and systemic perfusion between appropriate- and small-for-gestational-age infants during the first three days after birth," Brain Dev. **36**(5), 380–387 (2014).

97. T. Fujioka, T. Takami, H. Ishii, A. Kondo, D. Sunohara, and H. Kawashima, "Difference in Cerebral and Peripheral Hemodynamics among Term and Preterm Infants during the First Three Days of Life Title," Neonatology **106**, 181–187 (2014).

98. J. R. Lakowicz and K. Berndt, "Frequency-domain measurements of photon migration in tissues," Chem. Phys. Lett. **166**(3), 246–252 (1990).

99. M. S. Patterson, J. D. Moulton, B. C. Wilson, and B. Chance, "Applications of time-resolved light scattering measurements to photodynamic therapy dosimetry," SPIE Proc. Photodyn. Ther. Mech. II **1203**, 62–75 (1990).

100. B. Chance, M. B. Maris, J. Sorge, and M. Z. Zhang, "Phase modulation system for dual wavelength difference spectroscopy of hemoglobin deoxygenation in tissues," SPIE Proc. Time-Resolved Laser Spectrosc. Biochem. II **1204**(May 1990), 481 (1990).

101. P. Rolfe, "In vivo near-infrared spectroscopy," Annu. Rev. Biomed. Eng **2**(1), 715–754 (2000).

102. J. B. Fishkin and E. Gratton, "Propagation of photon-density waves in strongly scattering media containing an absorbing semi-infinite plane bounded by a straight edge," J. Opt. Soc. Am. A **10**(1), 127 (1993).

103. S. Fantini and A. Sassaroli, "Frequency-Domain Techniques for Cerebral and Functional Near-Infrared Spectroscopy," Front. Neurosci. **14**(April), 1–18 (2020).

104. P.-Y. Lin, N. Roche-Labarbe, M. Dehaes, S. Carp, A. Fenoglio, B. Barbieri, K. Hagan, P. E. Grant, and M. A. Franceschini, "Non-invasive optical measurement of cerebral metabolism and hemodynamics in infants.," J. Vis. Exp. (73), e4379 (2013).

105. T. Binzoni, A. Sassaroli, A. Torricelli, L. Spinelli, A. Farina, T. Durduran, S. Cavalieri, A. Pifferi, and F. Martelli, "Depth sensitivity of frequency domain optical measurements in diffusive media," Biomed. Opt. Express **8**(6), 2990 (2017).

106. M. Dehaes, P. E. Grant, D. D. Sliva, N. Roche-Labarbe, R. Pienaar, D. A. Boas, M. A. Franceschini, and J. Selb, "Assessment of the frequency-domain multi-distance method to evaluate the brain optical properties: Monte Carlo simulations

from neonate to adult," Biomed. Opt. Express **2**(3), 552 (2011).

107. A. Duncan, J. H. Meek, M. Clemence, C. E. Elwell, L. Tyszczuk, M. Cope, and D. Delpy, "Optical pathlength measurements on adult head, calf and forearm and the head of the newborn infant using phase resolved optical spectroscopy," Phys. Med. Biol. **40**(2), 295–304 (1995).

108. M. A. Franceschini, S. Thaker, G. Themelis, K. K. Krishnamoorthy, H. Bortfeld, S. G. Diamond, D. A. Boas, K. Arvin, and P. E. Grant, "Assessment of Infant Brain Development With Frequency-Domain Near-Infrared Spectroscopy," Pediatr. Res. **61**(5), 546–551 (2007).

109. P. E. Grant, N. Roche-Labarbe, A. Surova, G. Themelis, J. Selb, E. K. Warren, K. S. Krishnamoorthy, D. A. Boas, and M. A. Franceschini, "Increased cerebral blood volume and oxygen consumption in neonatal brain injury," J. Cereb. Blood Flow Metab. **29**(10), 1704–1713 (2009).

110. T. van Essen, T. G. Goos, L. van Ballegooijen, G. Pichler, B. Urlesberger, I. K. M. Reiss, and R. C. J. De Jonge, "Comparison of frequency-domain and continuous-wave near-infrared spectroscopy devices during the immediate transition," BMC Pediatr. **20**(1), 1–9 (2020).

111. N. Roche-labarbe, S. A. Carp, A. Surova, M. Patel, A. David, P. E. Grant, and M. A. Franceschini, "Noninvasive Optical Measures of CBV, StO2, CBF Index, and rCMRO2 in Human Premature Neonates' Brains in the First Six Weeks of Life," **31**(3), 341–352 (2010).

112. G. Greisen, T. Leung, and M. Wolf, "Has the time come to use near-infrared spectroscopy as a routine clinical tool in preterm infants undergoing intensive care?," Philos. Trans. R. Soc. A Math. Phys. Eng. Sci. **369**(1955), 4440–4451 (2011).

113. C. E. Elwell, M. Cope, A. D. Edwards, J. S. Wyatt, D. T. Delpy, and E. O. R. Reynolds, "Quantification of adult cerebral hemodynamics by near-infrared

spectroscopy," J. Appl. Physiol. **77**(6), 2753–2760 (1994).

114. A. D. Edwards, J. S. Wyatt, C. Richardson, D. T. Delpy, M. Cope, and E. O. Reynolds, "Cotside measurement of cerebral blood flow in ill newborn infants by near infrared spectroscopy," Lancet **332**(8614), 770–771 (1988).

115. J. T. Elliott, M. Diop, K. M. Tichauer, T.-Y. Lee, and K. St. Lawrence, "Quantitative measurement of cerebral blood flow in a juvenile porcine model by depth-resolved near-infrared spectroscopy," J. Biomed. Opt. **15**(3), 037014 (2010).

116. M. Diop, K. M. Tichauer, J. T. Elliott, M. Migueis, T.-Y. Lee, and K. St Lawrence, "Comparison of time-resolved and continuous-wave near-infrared techniques for measuring cerebral blood flow in piglets.," J. Biomed. Opt. **15**(5), (2010).

117. M. Diop, K. M. Tichauer, J. T. Elliott, M. Migueis, T.-Y. Lee, and K. St. Lawrence, "Time-resolved near-infrared technique for bedside monitoring of absolute cerebral blood flow," Proc. SPIE **7555**, (2010).

118. S. S. Kety and C. F. Schmidt, "The Nitrous Oxide Method for the Quantitative Determination of Cerebral Blood Flow in Man: Theory, Procedure and Normal Values," J. Clin. Invest. **27**(4), 476–483 (1948).

119. L. Skov, O. Pryds, and G. Greisen, "Estimating cerebral blood flow in newborn infants: Comparison of near infrared spectroscopy and 133xe clearance," Pediatr. Res. **30**(6), 570–573 (1991).

120. H. U. Bucher, A. D. Edwards, A. E. Lipp, and G. Duc, "Comparison between near infrared spectroscopy and 133xenon clearance for estimation of cerebral blood flow in critically III preterm infants," Pediatr. Res. **33**(1), 56–60 (1993).

121. D. W. Brown, P. a Picot, J. G. Naeini, R. Springett, D. T. Delpy, and T.-Y. Lee, "Quantitative near infrared spectroscopy measurement of cerebral hemodynamics in newborn piglets.," Pediatr. Res. **51**(5), 564–570 (2002).

122. K. St Lawrence, K. Verdecchia, J. Elliott, K. Tichauer, M. Diop, L. Hoffman, and

T. Y. Lee, "Kinetic model optimization for characterizing tumour physiology by dynamic contrast-enhanced near-infrared spectroscopy.," Phys. Med. Biol. **58**(5), 1591–1604 (2013).

123. A. Rajaram, S. Ioussoufovitch, L. B. Morrison, K. St Lawrence, T.-Y. Lee, Y. Bureau, and M. Diop, "Joint blood flow is more sensitive to inflammatory arthritis than oxyhemoglobin, deoxyhemoglobin, and oxygen saturation," Biomed. Opt. Express **7**(10), 3843–3854 (2016).

124. M. Diop, J. T. Elliott, K. M. Tichauer, T.-Y. Lee, and K. St Lawrence, "A broadband continuous-wave multichannel near-infrared system for measuring regional cerebral blood flow and oxygen consumption in newborn piglets.," Rev. Sci. Instrum. **80**(5), 054302 (2009).

125. D. Milej, L. He, A. Abdalmalak, W. B. Baker, U. C. Anazodo, M. Diop, S. Dolui, V. C. Kavuri, W. Pavlosky, L. Wang, R. Balu, J. A. Detre, O. Amendolia, F. Quattrone, W. A. Kofke, A. G. Yodh, and K. St Lawrence, "Quantification of cerebral blood flow in adults by contrast-enhanced near-infrared spectroscopy: Validation against MRI," J. Cereb. Blood Flow Metab. **40**(8), (2020).

126. J. T. Elliott, M. Diop, L. B. Morrison, C. D. d'Esterre, T. Y. Lee, and K. St. Lawrence, "Quantifying cerebral blood flow in an adult pig ischemia model by a depth-resolved dynamic contrast-enhanced optical method," Neuroimage **94**, 303–311 (2014).

127. D. Milej, D. Janusek, A. Gerega, S. Wojtkiewicz, P. Sawosz, J. Treszczanowicz, W. Weigl, and A. Liebert, "Optimization of the method for assessment of brain perfusion in humans using contrast-enhanced reflectometry: multidistance time-resolved measurements," J. Biomed. Opt. **20**(10), (2015).

128. J. Patel, K. Marks, I. Roberts, D. Azzopardi, and A. D. Edwards, "Measurement of Cerebral Blood Flow in Newborn Infants Using Near Infrared Spectroscopy with Indocyanine Green," Pediatr. Res. **43**, 34–39 (1998).

129. K. M. Tichauer, D. W. Brown, J. Hadway, T.-Y. Lee, K. St Lawrence, K. S. Lawrence, M. Kenneth, Y. Lee, K. St, and L. Near-infrared, "Near-infrared spectroscopy measurements of cerebral blood flow and oxygen consumption following hypoxia-ischemia in newborn piglets.," J. Appl. Physiol. **100**, 850–857 (2006).

130. K. M. Tichauer, J. T. Elliott, J. a Hadway, D. S. Lee, T.-Y. Lee, and K. St Lawrence, "Using near-infrared spectroscopy to measure cerebral metabolic rate of oxygen under multiple levels of arterial oxygenation in piglets.," J. Appl. Physiol. **109**(3), 878–85 (2010).

131. R. Arora, M. Ridha, D. S. C. Lee, J. Elliott, H. C. Rosenberg, M. Diop, T.-Y. Lee, and K. St Lawrence, "Preservation of the metabolic rate of oxygen in preterm infants during indomethacin therapy for closure of the ductus arteriosus.," Pediatr. Res. **73**(6), 713–8 (2013).

132. P. J. McLachlan, J. Kishimoto, M. Diop, D. Milej, D. S. C. Lee, S. De Ribaupierre, and K. S. Lawrence, "Investigating the effects of cerebrospinal fluid removal on cerebral blood flow and oxidative metabolism in infants with post-hemorrhagic ventricular dilatation," Pediatr. Res. **82**(4), 634–641 (2017).

133. R. Pecora, "Quasi-Elastic Light Scattering from Macromolecules," Annu. Rev. Biophys. Bioeng. **1**, 257–276 (1972).

134. F. C. MacKintosh and S. John, "Diffusing-wave spectroscopy and multiple scattering of light in correlated random media," Phys. Rev. B **40**(4), 2383–2406 (1989).

135. D. J. Pine, D. A. Weitz, P. M. Chaikin, and E. Herbolzherimer, "Diffusion-Wave Spectroscopy," Phys. Rev. Lett. **60**(12), 1134–1137 (1988).

136. D. A. Boas, L. E. Campbell, and A. G. Yodh, "Scattering and Imaging with Diffusing Temporal Field Correlations," Phys. Rev. Lett. **75**(9), 1855–1859 (1995).

137. D. A. Boas and A. G. Yodh, "Spatially varying dynamical properties of turbid media probed with diffusing temporal light correlation," J. Opt. Soc. Am. A **14**(1), 192–215 (1997).

138. R. Bonner and R. Nossal, "Model for laser Doppler measurements of blood flow in tissue," Appl. Opt. **20**(12), 2097–2107 (1981).

139. P.-A. Lemieux and D. J. Durian, "Investigating non-Gaussian scattering processes by using nth -order intensity correlation functions," J. Opt. Soc. Am. **16**(7), 1651–1664 (1999).

140. T. Durduran, R. Choe, W. B. Baker, and A. G. Yodh, "Diffuse optics for tissue monitoring and tomography," Reports Prog. Phys. **73**(7), (2010).

141. M. Khalid, D. Milej, A. Rajaram, A. Abdalmalak, L. Morrison, M. Diop, and K. St. Lawrence, "Development of a stand-alone DCS system for monitoring absolute cerebral blood flow," Biomed. Opt. Express **10**(9), 4607–4620 (2019).

142. C. Cheung, J. P. Culver, K. Takahashi, J. H. Greenberg, and A. G. Yodh, "In vivo cerebrovascular measurement combining diffuse near-infrared absorption and correlation spectroscopies," Phys. Med. Biol. **46**(8), 2053–2065 (2001).

143. S. A. Carp, D. Tamborini, D. Mazumder, K.-C. (Tony) Wu, M. R. Robinson, K. A. Stephens, O. Shatrovoy, N. Lue, N. Ozana, M. H. Blackwell, and M. A. Franceschini, "Diffuse correlation spectroscopy measurements of blood flow using 1064 nm light," J. Biomed. Opt. **25**(09), 1–15 (2020).

144. G. Dietsche, M. Ninck, C. Ortolf, J. Li, F. Jaillon, and T. Gisler, "Fiber-based multispeckle detection for time-resolved diffusing-wave spectroscopy: Characterization and application to blood flow detection in deep tissue," Appl. Opt. **46**(35), 8506–8514 (2007).

145. T. Gisler, H. Rüger, S. U. Egelhaaf, J. Tschumi, P. Schurtenberger, and J. Rička, "Mode-selective dynamic light scattering: theory versus experimental realization," Appl. Opt. **34**(18), 3546 (1995).

146. L. He, Y. Lin, Y. Shang, B. J. Shelton, and G. Yu, "Using optical fibers with different modes to improve the signal-to-noise ratio of diffuse correlation spectroscopy flowoximeter measurements," J. Biomed. Opt. **18**(3), (2003).

147. W. B. Baker, A. B. Parthasarathy, D. R. Busch, R. C. Mesquita, J. H. Greenberg, and A. G. Yodh, "Modified Beer-Lambert law for blood flow," Biomed. Opt. Express **5**(11), 4053 (2014).

148. J. Selb, D. a. Boas, S.-T. Chan, K. C. Evans, E. M. Buckley, and S. a. Carp, "Sensitivity of near-infrared spectroscopy and diffuse correlation spectroscopy to brain hemodynamics: simulations and experimental findings during hypercapnia.," Neurophotonics **1**(1), 015005 (2014).

149. D. Wang, A. B. Parthasarathy, W. B. Baker, K. Gannon, V. Kavuri, T. Ko, S. Schenkel, Z. Li, Z. Li, M. T. Mullen, J. A. Detre, and A. G. Yodh, "Fast blood flow monitoring in deep tissues with real-time software correlators," Biomed. Opt. Express **7**(3), 776–797 (2016).

150. A. Rajaram, D. Milej, M. Suwalski, L. C. M. Yip, L. R. Guo, M. W. A. Chu, J. Chui, M. Diop, J. M. Murkin, and K. St. Lawrence, "Optical monitoring of cerebral perfusion and metabolism in adults during cardiac surgery with cardiopulmonary bypass," Biomed. Opt. Express **11**(10), 5967–5981 (2020).

151. K. Verdecchia, M. Diop, A. Lee, L. B. Morrison, T.-Y. Lee, and K. St. Lawrence, "Assessment of a multi-layered diffuse correlation spectroscopy method for monitoring cerebral blood flow in adults," Biomed. Opt. Express **7**(9), 3659–3674 (2016).

152. J. Sutin, B. Zimmerman, D. Tyulmankov, D. Tamborini, K. C. Wu, J. Selb, A. Gulinatti, I. Rech, A. Tosi, D. A. Boas, and M. A. Franceschini, "Time-domain diffuse correlation spectroscopy," Optica **3**(9), 1006 (2016).

153. G. Yu, T. Durduran, C. Zhou, H. W. Wang, M. E. Putt, H. M. Saunders, C. M. Sehgal, E. Glatstein, A. G. Yodh, and T. M. Busch, "Noninvasive monitoring of

murine tumor blood flow during and after photodynamic therapy provides early assessment of therapeutic efficacy," Clin. cancer Res. **11**(9), 3543 (2005).

154. U. Sunar, S. Makonnen, C. Zhou, T. Durduran, G. Yu, H.-W. Wang, W. M. Lee, and A. G. Yodh, "Hemodynamic responses to antivascular therapy and ionizing radiation assessed by diffuse optical spectroscopies," Opt. Express **15**(23), 15507–15516 (2007).

155. E. M. Buckley, N. M. Cook, T. Durduran, M. N. Kim, C. Zhou, R. Choe, G. Yu, S. Schultz, C. M. Sehgal, D. J. Licht, P. H. Arger, M. E. Putt, H. H. Hurt, and A. G. Yodh, "Cerebral hemodynamics in preterm infants during positional intervention measured with diffuse correlation spectroscopy and transcranial Doppler ultrasound.," Opt. Express **17**(15), 12571–12581 (2009).

156. M. N. Kim, T. Durduran, S. Frangos, B. L. Edlow, E. M. Buckley, H. E. Moss, C. Zhou, G. Yu, R. Choe, E. Maloney-Wilensky, R. L. Wolf, M. S. Grady, J. H. Greenberg, J. M. Levine, A. G. Yodh, J. A. Detre, and W. A. Kofke, "Noninvasive measurement of cerebral blood flow and blood oxygenation using near-infrared and diffuse correlation spectroscopies in 44 critically brain-injured adults," Neurocrit Care **12**(2), 173–180 (2010).

157. M. Diop, K. Verdecchia, T.-Y. Lee, and K. St Lawrence, "Calibration of diffuse correlation spectroscopy with a time-resolved near-infrared technique to yield absolute cerebral blood flow measurements.," Biomed. Opt. Express **2**(7), 2068–2081 (2011).

158. E. M. Buckley, D. Hance, T. Pawlowski, J. Lynch, F. B. Wilson, R. C. Mesquita, T. Durduran, L. K. Diaz, M. E. Putt, D. J. Licht, M. A. Fogel, and A. G. Yodh, "Validation of diffuse correlation spectroscopic measurement of cerebral blood flow using phase-encoded velocity mapping magnetic resonance imaging," J. Biomed. Opt. **17**(3), (2012).

159. S. A. Carp, G. P. Dai, D. A. Boas, M. A. Franceschini, and Y. R. Kim, "Validation of diffuse correlation spectroscopy measurements of rodent cerebral blood flow

with simultaneous arterial spin labeling MRI; towards MRI-optical continuous cerebral metabolic monitoring," Biomed. Opt. Express **1**(2), 553 (2010).

160. G. Yu, T. F. Floyd, T. Durduran, C. Zhou, J. Wang, J. A. Detre, and A. G. Yodh, "Validation of diffuse correlation spectroscopy for muscle blood flow with concurrent arterial spin labeled perfusion MRI," Opt. Express **15**(3), 1064–1075 (2007).

161. V. Jain, E. M. Buckley, D. J. Licht, J. M. Lynch, P. J. Schwab, M. Y. Naim, N. A. Lavin, S. C. Nicolson, L. M. Montenegro, A. G. Yodh, and F. W. Wehrli, "Cerebral oxygen metabolism in neonates with congenital heart disease quantified by MRI and optics," J. Cereb. Blood Flow Metab. **34**(3), 380–388 (2014).

162. D. A. Goff, E. M. Buckley, T. Durduran, J. Wang, and D. J. Licht, "Noninvasive cerebral perfusion imaging in high-risk neonates," Semin Perinatol. **34**(1), 46–56 (2010).

163. D. Irwin, L. Dong, Y. Shang, R. Cheng, M. Kudrimoti, S. D. Stevens, and G. Yu, "Influences of tissue optical properties on diffuse correlation spectroscopy blood flow measurements," Biomed. Opt. Express **2**(7), 1969–1985 (2011).

164. Z. Li, W. B. Baker, A. B. Parthasarathy, T. S. Ko, D. Wang, S. Schenkel, T. Durduran, G. Li, and A. G. Yodh, "Calibration of diffuse correlation spectroscopy blood flow index with venous-occlusion diffuse optical spectroscopy in skeletal muscle," J. Biomed. Opt. **20**(12), (2015).

165. L. He, W. B. Baker, D. R. Busch, J. Y. Jiang, K. S. Lawrence, W. A. Kofke, A. G. Yodh, L. He, W. B. Baker, D. Milej, V. C. Kavuri, R. C. Mesquita, D. R. Busch, K. Abramson, J. Y. Jiang, M. Diop, K. S. Lawrence, O. Amendolia, F. Quattrone, R. Balu, W. A. Kofke, and A. G. Yodh, "Noninvasive continuous optical monitoring of absolute cerebral blood flow in critically ill adults," Neurophotonics **5**(4), (2018).

166. E. D. De Villota, M. T. G. Carmona, J. J. Rubio, and S. R. De Andrés, "Equality of

the In vivo and In vitro oxygen-binding capacity of haemoglobin in patients with severe respiratory disease," Br. J. Anaesth. **53**(12), 1325–1328 (1981).

167. H. M. Watzman, C. D. Kurth, L. M. Montenegro, J. Rome, J. M. Steven, and S. C. Nicolson, "Arterial and venous contributions to near-infrared cerebral oximetry," Anesthesiology **93**(4), 947–953 (2000).

168. J. P. Culver, T. Durduran, D. Furuya, C. Cheung, J. H. Greenberg, and A. G. Yodh, "Diffuse optical tomography of cerebral blood flow, oxygenation, and metabolism in rat during focal ischemia," J. Cereb. Blood Flow Metab. **23**(8), 911–924 (2003).

169. T. Durduran, G. Yu, M. G. Burnett, J. A. Detre, J. H. Greenberg, J. Wang, C. Zhou, and A. G. Yodh, "Diffuse optical measurement of blood flow, blood oxygenation, and metabolism in a human brain during sensorimotor cortex activation," Opt. Lett. **29**(15), 1766 (2004).

170. S. A. Carp, P. Farzam, N. Redes, D. M. Hueber, and M. A. Franceschini, "Combined multi-distance frequency domain and diffuse correlation spectroscopy system with simultaneous data acquisition and real-time analysis," Biomed. Opt. Express **8**(9), 3993–4006 (2017).

171. V. Quaresima, P. Farzam, P. Anderson, P. Y. Farzam, D. Wiese, S. A. Carp, M. Ferrari, and M. A. Franceschini, "Diffuse correlation spectroscopy and frequency-domain near-infrared spectroscopy for measuring microvascular blood flow in dynamically exercising human muscles," J. Appl. Physiol. **127**(5), 1328–1337 (2019).

172. N. Roche-Labarbe, A. Fenoglio, A. Aggarwal, M. Dehaes, S. a. Carp, M. A. Franceschini, and P. E. Grant, "Near-infrared spectroscopy assessment of cerebral oxygen metabolism in the developing premature brain," J. Cereb. Blood Flow Metab. **32**(3), 481–488 (2012).

173. S. B. Roberts, M. A. Franceschini, R. E. Silver, S. F. Taylor, A. B. De Sa, R. Có,

A. Sonco, A. Krauss, A. Taetzsch, P. Webb, S. K. Das, C. Y. Chen, B. L. Rogers, E. Saltzman, P. Y. Lin, N. Schlossman, W. Pruzensky, C. Balé, K. K. H. Chui, and P. C. T. Muentener, "Effects of food supplementation on cognitive function, cerebral blood flow, and nutritional status in young children at risk of undernutrition: Randomized controlled trial," BMJ **370**, (2020).

174. P. Lin, K. Hagan, A. Fenoglio, P. E. Grant, and M. A. Franceschini, "Reduced cerebral blood flow and oxygen metabolism in extremely preterm neonates with low-grade germinal matrix- intraventricular hemorrhage," Sci. Rep. **6**, (2016).

175. P. Y. Lin, N. Roche-Labarbe, M. Dehaes, A. Fenoglio, P. E. Grant, and M. A. Franceschini, "Regional and hemispheric asymmetries of cerebral hemodynamic and oxygen metabolism in newborns," Cereb. Cortex **23**(2), 339–348 (2013).

176. P. Farzam, E. M. Buckley, P. Y. Lin, K. Hagan, P. E. Grant, T. E. Inder, S. A. Carp, and M. A. Franceschini, "Shedding light on the neonatal brain: Probing cerebral hemodynamics by diffuse optical spectroscopic methods," Sci. Rep. **7**(1), 1–10 (2017).

177. M. V. Johnston and H. Hagberg, "Sex and the pathogenesis of cerebral palsy," Dev. Med. Child Neurol. **49**(1), 74–78 (2007).

178. G. C. Di Renzo, A. Rosati, R. D. Sarti, L. Cruciani, and A. M. Cutuli, "Does fetal sex affect pregnancy outcome?," Gend. Med. **4**(1), 19–30 (2007).

179. T. Durduran, C. Zhou, E. M. Buckley, M. N. Kim, G. Yu, R. Choe, J. W. Gaynor, T. L. Spray, S. M. Durning, S. E. Mason, L. M. Montenegro, S. C. Nicolson, R. A. Zimmerman, M. E. Putt, J. Wang, J. H. Greenberg, J. A. Detre, A. G. Yodh, and D. J. Licht, "Optical measurement of cerebral hemodynamics and oxygen metabolism in neonates with congenital heart defects," J. Biomed. Opt. **15**(3), 037004 (2010).

180. H. H. Cheng, S. L. Ferradal, R. Vyas, D. Wigmore, E. McDavitt, J. S. Soul, M. A. Franceschini, J. W. Newburger, and P. E. Grant, "Abnormalities in cerebral hemodynamics and changes with surgical intervention in neonates with congenital

heart disease," J. Thorac. Cardiovasc. Surg. **159**(5), 2012–2021 (2020).

181. E. M. Buckley, J. M. Lynch, D. a. Goff, P. J. Schwab, W. B. Baker, T. Durduran, D. R. Busch, S. C. Nicolson, L. M. Montenegro, M. Y. Naim, R. Xiao, T. L. Spray, A. G. Yodh, J. W. Gaynor, and D. J. Licht, "Early postoperative changes in cerebral oxygen metabolism following neonatal cardiac surgery," J Thorac Cardiovasc Surg **145**(1), 196–205 (2013).

182. M. Dehaes, A. Aggarwal, P.-Y. Lin, C. Rosa Fortuno, A. Fenoglio, N. Roche-Labarbe, J. S. Soul, M. A. Franceschini, and P. E. Grant, "Cerebral oxygen metabolism in neonatal hypoxic ischemic encephalopathy during and after therapeutic hypothermia," J. Cereb. Blood Flow Metab. **34**(1), 87–94 (2014).

183. N. Roche-Labarbe, A. Fenoglio, H. Radhakrishnan, M. Kocienski-Filip, S. A. Carp, J. Dubb, D. A. Boas, P. E. Grant, and M. A. Franceschini, "Somatosensory evoked changes in cerebral oxygen consumption measured non-invasively in premature neonates," Neuroimage **85**(0 1), 279–286 (2014).

184. K. Verdecchia, M. Diop, A. Lee, and K. St. Lawrence, "Characterization of a hybrid diffuse correlation spectroscopy and time-resolved near-infrared spectroscopy system for real-time monitoring of cerebral blood flow and oxygenation," SPIE BiOS Conf. Proc. Adv. Biomed. Clin. Diagnostic Surg. Guid. Syst. XIII **9313**(13), (2015).

185. D. Milej, M. Shahid, A. Abdalmalak, A. Rajaram, M. Diop, and K. St. Lawrence, "Characterizing dynamic cerebral vascular reactivity using a hybrid system combining time-resolved near-infrared and diffuse correlation spectroscopy," Biomed. Opt. Express **11**(8), 4571–4585 (2020).

186. M. Giovannella, D. Contini, M. Pagliazzi, A. Pifferi, L. Spinelli, R. Erdmann, R. Donat, I. Rocchetti, M. Rehberger, N. König, R. Schmitt, A. Torricelli, T. Durduran, and U. M. Weigel, "BabyLux device: a diffuse optical system integrating diffuse correlation spectroscopy and time-resolved near-infrared spectroscopy for the neuromonitoring of the premature newborn brain,"

Neurophotonics **6**(2), (2019).

187. M. Giovannella, L. Spinelli, M. Pagliazzi, D. Contini, G. Greisen, U. M. Weigel, A. Torricelli, and T. Durduran, "Accuracy and precision of tissue optical properties and hemodynamic parameters estimated by the BabyLux device: a hybrid time-resolved near-infrared and diffuse correlation spectroscopy neuro-monitor," Biomed. Opt. Express **10**(5), 2556 (2019).

188. B. Andresen, A. De Carli, M. Fumagalli, M. Giovannella, T. Durduran, U. Michael Weigel, D. Contini, L. Spinelli, A. Torricelli, and G. Greisen, "Cerebral oxygenation and blood flow in normal term infants at rest measured by a hybrid near-infrared device (BabyLux)," Pediatr. Res. **86**(4), 515–521 (2019).

189. A. Rajaram, L. C. M. Yip, D. Milej, M. Suwalski, M. Kewin, M. Lo, J. J. L. Carson, V. Han, S. Bhattacharya, M. Diop, S. de Ribaupierre, and K. St. Lawrence, "Perfusion and Metabolic Neuromonitoring during Ventricular Taps in Infants with Post-Hemorrhagic Ventricular Dilatation," Brain Sci. **10**(7), (2020).

Chapter 2

2 Simultaneous monitoring of cerebral perfusion and cytochrome c oxidase by combining broadband near-infrared spectroscopy and diffuse correlation spectroscopy

This chapter has been adapted from the publication titled "Simultaneous monitoring of cerebral perfusion and cytochrome c oxidase by combining broadband near-infrared spectroscopy and diffuse correlation spectroscopy" published in the journal *Biomedical Optics Express* in 2018 by Ajay Rajaram, Gemma Bale, Matthew Kewin, Laura B. Morrison, Ilias Tachtsidis, Keith St. Lawrence, and Mamadou Diop, volume 9, issue 6.

2.1 Abstract

Preterm infants born with very low birth weights are at a high risk of brain injury, in part because the premature brain is believed to be prone to periods of low cerebral blood flow (CBF). Tissue damage is likely to occur if reduction in CBF is sufficient to impair cerebral energy metabolism for extended periods. Therefore, a neuromonitoring method that can detect reductions in CBF, large enough to affect metabolism, could alert the neonatal intensive care team before injury occurs. In this report, we present the development of an optical system that combines diffuse correlation spectroscopy (DCS) for monitoring CBF and broadband near-infrared spectroscopy (B-NIRS) for monitoring the oxidation state of cytochrome c oxidase (oxCCO) – a key biomarker of oxidative metabolism. The hybrid instrument includes a multiplexing system to enable concomitant DCS and B-NIRS measurements while avoiding crosstalk between the two subsystems. The ability of the instrument to monitor dynamic changes in CBF and oxCCO was demonstrated in a piglet model of neonatal hypoxia-ischemia (HI). Experiments conducted in eight animals, including two controls, showed that oxCCO exhibited a delayed response to ischemia while CBF and tissue oxygenation (StO_2) responses were instantaneous. These findings suggest that simultaneous neuromonitoring of perfusion and metabolism could provide critical information regarding clinically significant hemodynamic events prior to the onset of brain injury.

2.2 Introduction

An estimated 15 million babies are born prematurely each year and those with very low birth weights (VLBW < 1500 g) are at a high risk of neurodevelopmental impairment [1]. Among the 63,000 VLBW infants born annually in the United States, 5-10% develop major disabilities such as cerebral palsy and 25-50% show other cognitive and behavioural deficits [2,3]. Although other factors contribute to perinatal brain injury, alterations in cerebral blood flow (CBF) are believed to play a significant role due to the immaturity of the cerebral vascular system and complications associated with premature birth, such as poor cardiac and lung function, which can impede blood flow and oxygenation [4]. In addition, changes in brain tissue metabolism are likely to precede structural abnormalities associated with injury [5]. In term infants, metabolite ratios measured by magnetic resonance (MR) spectroscopy have shown high accuracy in predicting adverse neurodevelopmental outcome [6,7] and have potential in guiding clinical management. Despite this, applications of MR methods for routine brain monitoring are clearly impractical. Cranial ultrasound remains the first-line option in the neonatal intensive care unit (NICU), particularly for monitoring intraventricular haemorrhage. However, ultrasound is used to detect brain damage that has already occurred, rather than detecting pathophysiological events that are indicative of oncoming injury. This speaks to the need for bedside methods capable of detecting CBF and metabolic fluctuations which could act as prognostic markers of brain injury.

Advancements in biomedical optics have provided cost-effective alternatives for monitoring the brain with the aim of detecting hemodynamic/metabolic events that may precede brain injury. In particular, near-infrared spectroscopy (NIRS) – a safe, quantitative, and portable technology – is widely used to obtain estimates of cerebral oxygen saturation (StO_2), which has been used as a surrogate marker of CBF in the clinic [8]. NIRS can also directly measure CBF, either by dynamic contrast-enhanced (DCE) methods [9,10], or by diffuse correlation spectroscopy (DCS). DCS has been extensively validated against other perfusion techniques and it has the advantage of providing continuous monitoring [11].

The combination of NIRS and DCS has the potential to further enhance brain monitoring by combining flow and oxygenation measurements to determine the cerebral metabolic

rate of oxygen ($CMRO_2$) [8,12–15], which is a more sensitive marker of tissue viability [16]. Consequently, monitoring $CMRO_2$ could help identify clinically significant changes in CBF considering the fact that only flow reductions large enough to exhaust the compensatory increase in oxygen extraction will have an impact on energy metabolism [9]. However, a potential challenge with continuous monitoring of $CMRO_2$ is that it requires the combination of a number of parameters: CBF, StO_2, and arterial oxygen saturation (SaO_2) – which have proven challenging to measure during asphyxia [16]. Furthermore, $CMRO_2$ computation relies on assuming a fixed arteriovenous blood volume ratio, which may vary under pathological conditions [17–19].

A direct measure of cerebral energy metabolism can be obtained by measuring changes in the oxidation state of cytochrome c oxidase (CCO) – a key element in oxidative metabolism – which is directly related to mitochondrial ATP production [20]. CCO is the terminal electron acceptor in the electron transport chain (ETC): the final stage of oxidative metabolism. A unique copper dimer (Copper A) in the enzyme has an absorption peak around 835 nm in its oxidized form (oxCCO), but not in its reduced state. A change in the redox state represents a change in oxidative cellular metabolism. To accurately resolve changes in oxCCO, many wavelengths (broadband) are required as the concentration of CCO is 10% of the in vivo hemoglobin concentration. Previous studies have shown that broadband NIRS (B-NIRS) measured oxCCO changes are associated with acute changes in metabolism following hypoxia-ischemia (see Bale et al. for a detailed review [20]). As well, changes in oxCCO measured by B-NIRS showed strong correlation with measures of cellular metabolism from magnetic resonance spectroscopy [21] and microdialysis [22]. Simultaneous monitoring of perfusion and oxygen metabolism, through combining DCS and B-NIRS, could therefore provide a valuable tool for neuromonitoring in the NICU. This report presents the development a hybrid B-NIRS/DCS system for real-time monitoring of StO_2, CBF, and ΔoxCCO. The ability of the instrument to capture dynamic oxygenation, blood flow, and metabolic changes was demonstrated in an animal model of neonatal hypoxia-ischemia that has been shown to cause rapid reductions in cerebral blood flow and oxygenation [15].

2.3 Methods

2.3.1 Instrumentation

The light source of the B-NIRS subsystem, a 20 W halogen lamp (Ocean Optics Hl-2000-HP), was high-pass filtered at 500 nm to remove ultraviolet light and directed towards the tissue by an optical fiber bundle (3.5 mm active diameter, 30-μm core, 0.55 numerical aperture). Light diffusely reflected from the tissue was collected with an identical fiber bundle, placed at 30 mm away from the emission probe (see Fig. 1), and directed to a custom-made spectrometer (iDus Andor camera, Oxford Instruments; 548-1085 nm bandwidth; 1.65 nm resolution; P&P Optica, ON, Canada). The light source of the DCS was a long coherence length, continuous-wave laser emitting at 785 nm (DL785-100s, CrystaLaser, NV) and was coupled into a 400-μm diameter fiber. Light from the tissue was collected with a few-mode fiber (SMF-28e+, 8 μm core; few-mode at 785 nm) placed 20 mm from the DCS emission probe and coupled to a single-photon counting module (SPCM-AQR4C, Excelitas, QC, Canada). The output of the SPCM was fed into a correlator board (Flex033LQ-1, Correlator.com, NJ) to generate normalized intensity autocorrelation curves. Note that in some of the phantom experiments, a single-mode fiber (S630 Nufern, 6 μm core) was used instead of the few-mode fiber.

Operating the two subsystems simultaneously would result in significant crosstalk since the DCS laser is powerful enough to saturate the spectrometer's CCD detector. As well, the presence of incoherent light from the broadband light source alters the autocorrelation curves acquired while the B-NIRS light is on. To avoid crosstalk, a shutter-based multiplexing approach was used to alternatively collect measurements from each subsystem (i.e., B-NIRS and DCS). Fig. 2.1 shows a schematic of the hybrid B-NIRS/DCS device.

Optical fibers were discontinuous on the NIRS emission and detection ends, with shutters placed at these junctions. Signal loss was minimized by securing the probes in close proximity to the shutter, using an optical breadboard. A shutter was also placed in front of the DCS laser, and another in front of the single-photon counting module. The latter was equipped with a light collimator and a coupling lens to maximize the signal-to-noise ratio

(SNR). A dual DC power supply was used to operate the multiplexer: a high voltage (24 V) was sent to rapidly open the shutter, immediately followed by a lower voltage (10 V) to maintain the open state. These voltage values were chosen to minimize shutter blade transition time and digital modules (NI 9477, National Instruments, TX) were utilized to cycle between the voltage outputs. Opening and closing of the shutters were alternated to allow for sequential acquisition and were controlled using a field programmable gate array (FPGA) card (PCI-7811R, National Instruments). Digital modules (NI 9401, NI) were also used to control and monitor shutter states, which were synchronized by in-house software written in LabVIEW FPGA, as detailed in [23]. B-NIRS and DCS measurements were analyzed using a customized MATLAB script to yield cerebral oxygen saturation, perfusion, and metabolism.

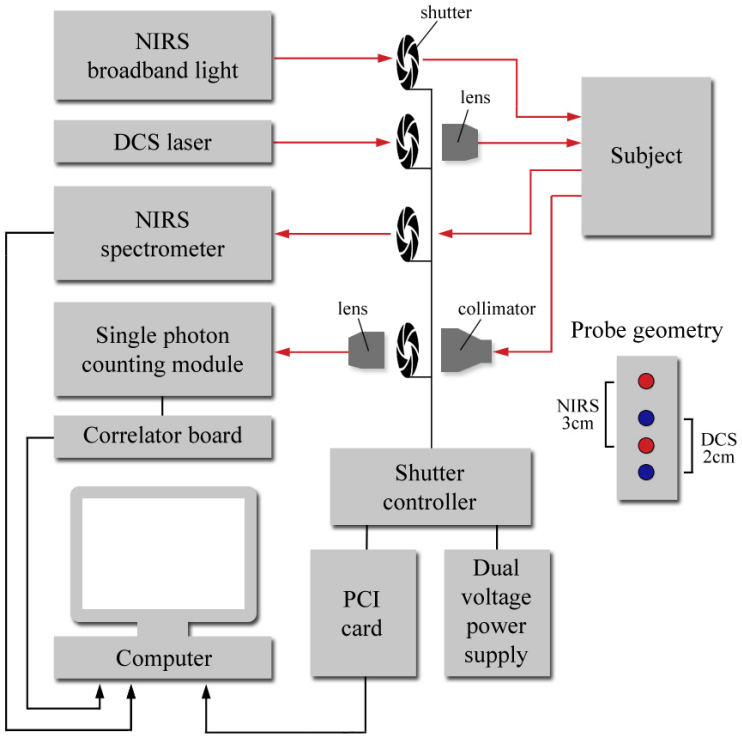

Figure 2.1: Simplified schematic of B-NIRS/DCS system with the shutter-based multiplexer. Red dots: B-NIRS emission and detection probes; blue dots: DCS emission and detection fibers.

2.3.2 System demonstration

2.3.2.1 Phantom Experiments

To investigate the potential impact of the B-NIRS light on the DCS measurements, autocorrelation curves were acquired while the broadband light source remained on. Data were collected on a liquid phantom consisting of a mixture of Intralipid and India ink that provided a reduced scattering coefficient of 1.0 mm^{-1} and an absorption coefficient of 0.01 mm^{-1}; values were chosen to mimic tissue based on previous reports [24]. In the first set of measurements, the emission probe of the B-NIRS was positioned 30 mm away from the detection fiber of the DCS system, and the level of light contamination experienced by the DCS was varied by modulating the intensity of the B-NIRS light using its built-in aperture. This test was repeated with a 10-mm distance between the B-NIRS emission probe and DCS detection fiber to further increase the intensity of B-NIRS light collected by the DCS system.

2.3.2.2 Hypoxia-ischemia Model

The ability of the hybrid B-NIRS/DCS device to monitor dynamic changes in CBF and oxCCO was demonstrated in an animal model of hypoxia-ischemia (HI) involving newborn piglets aged 10-40 hours. This model was chosen because it results in rapid changes in blood flow and oxygen supply to the brain [15]. Piglets were anesthetized under 3% isoflurane during preparatory surgery (2% post-surgery), tracheotomized, and mechanically ventilated on an oxygen-medical air mixture. Incisions were made lateral to the trachea and vascular occluders (In Vivo Metric, CA) were placed around the carotid arteries posterior to the clavicle. Catheters were inserted into an ear vein for injections and into a femoral artery to monitor vitals (SurgiVet, Smiths Medical, MN), as well as to collect arterial blood samples for gas and glucose analyses. Arterial oxygen saturation (SaO_2) was measured via a pulse oximeter attached to the piglet's right forelimb. Piglets were placed in the prone position and the B-NIRS and DCS probes were secured to the left side of the head, avoiding the sagittal sinus, using an in-house 3D-printed probe holder.

HI insult was induced by first inflating the occluders around the carotid arteries, followed by reducing the inspired oxygen from 21% to 8%. B-NIRS and DCS data were acquired

continuously throughout the insult, starting 5 minutes prior to carotid clamping to acquire baseline measurements. The real-time DCS blood flow index was used to confirm successful clamping, i.e., an immediate drop in CBF. Following this confirmation, inspired oxygen concentration was reduced and the HI insult was maintained for a minimum duration of 10 minutes once the blood flow index reached its nadir. At the end of the HI insult, recovery was initiated by deflating the carotid occluders and returning oxygen supply to baseline levels. Two control animals experienced identical procedures, excluding inflation of the occluders and reduction in inspired oxygen, to confirm the stability of the optical measurements during the experiment.

The continuous recording of B-NIRS and DCS data were set on a 14-s cycle. That is, 12 B-NIRS spectra were acquired over 3 s, followed by 2 DCS measurements over the following 10 s, with a 0.5-s delay both preceding and following each technique. Data were continuously saved and imported into MATLAB for real-time update of the DCS blood flow index and relative oxCCO. The final step in the experiment was to calibrate the DCS data by measuring absolute CBF with DCE-NIRS following the 90-minute recovery (i.e., post HI insult) period [25]. The DCE-NIRS protocol consisted of a bolus injection of indocyanine green (ICG, 0.1 mg/kg) into a cannulated vein. The passage of ICG through the brain was captured by continuously recording B-NIRS data at a temporal resolution of 400 ms. The time-varying arterial ICG concentration was concomitantly measured by a dye densitometer (DDG 2001, Nihon Kohden, Japan) attached to a front paw.

This study was approved by the Animal Use Subcommittee of the Canadian Council on Animal Care at Western University (London, Ontario).

2.3.3 Data Processing

2.3.3.1 Quantification of Tissue Chromophore Concentrations and StO_2

2.3.3.1.1 Broadband Fitting for Absolute Concentrations

Before the start of each study, the spectrometer was wavelength calibrated using a neon light source and a dark-noise signal was also acquired. Thereafter, a reference spectrum was acquired – using a pinhole attenuator, which provided uniform attenuation while

avoiding detector saturation – to account for the spectral properties of the light source and the spectrometer. A de-noising algorithm was subsequently applied to the data to reduce the measurement noise as described previously [26]. The baseline reflectance spectrum R(λ) was then computed from the spectrum measured on the piglet's head, the dark-noise signal of the spectrometer, and the reference spectrum as follows:

$$R(\lambda) = log_{10}\left(\frac{spectrum_\lambda - dark_\lambda}{reference_\lambda - dark_\lambda}\right) \quad (2.1)$$

The 1st and 2nd derivative of R(λ) was fit to the 1st and 2nd derivatives of the solution to the diffusion approximation for a semi-infinite homogenous medium (i.e., the theoretical model) [10], characterized by the reduced scattering (μ_s') and absorption (μ_a) coefficients, described respectively in equations (2.2) and (2.3) [27]:

$$\mu_s' = \mathrm{A}\left(\frac{\lambda}{800(nm)}\right)^{-\alpha} \quad (2.2)$$

where α is the scattering power, characterizing the wavelength dependence of the μ_s', and A is the μ_s' value at a wavelength λ= 800 nm (in our analysis, but can be any wavelength in the range where Eq. 2.2 is valid).

$$\mu_a(\lambda) = WF \cdot \varepsilon_{H_2O}(\lambda) + Hb^b \cdot \varepsilon_{Hb}(\lambda) + HbO_2^b \cdot \varepsilon_{HbO_2}(\lambda) \quad (2.3)$$

where WF is the tissue water fraction, ε is the extinction coefficient of the corresponding chromophore, and Hb^b and $HbO_2{}^b$ are respectively the baseline concentrations of deoxyhemoglobin and oxyhemoglobin in μM. CCO was not included in the baseline analysis due to its relatively small concentration and lack of features in the derivative spectra.

The baseline reflectance spectrum was analyzed using a three-step, multi-parameter fitting algorithm, based on a constrained least-square minimization algorithm built with a custom MATLAB function (*fminsearchbnd*) [10]. Firstly, the second-derivative of the reflectance spectrum R(λ) was fit to the 2nd derivative of the theoretical model between 815 and 845 nm to obtain the tissue water fraction (WF). Although the fitting yielded estimates for all the parameters listed in Table 2.1, we only consider WF to be reliably estimated from this step because it has been previously shown that the 2nd derivative of the scattering

coefficient and the other tissue chromophores do not have significant contribution in this wavelength range [28]. Using the value of WF obtained in the first step as a known parameter, the 2nd derivative fit was performed from 680 to 800 nm to obtain Hb^b. The WF and Hb^b values were then used as known parameters in the fitting of the first derivative of R(λ) from 680 to 845 nm to determine HbO_2^b, A, and α [10,26,28]. The upper and lower bounds, as well as the initial values of the parameters used in the fitting routine are given in Table 2.1.

Table 2-1: Initial values, lower and upper bounds of the fitting parameters.

Parameter	Initial value	Lower bound	Upper bound
WF	0.8	0.6	0.95
Hb^b*(g/dL)*	10	0	60
HbO_2^b*(g/dL)*	40	0	80
A (mm^{-1})	1	0	1.3
α	2.7	0.6	4.0

Baseline tissue oxygen saturation (StO_2^b) was computed using Hb^b and HbO_2^b:

$$StO_2{}^b = \frac{HbO_2{}^b}{Hb^b + HbO_2{}^b} \tag{2.4}$$

2.3.3.1.2 Derivative Spectroscopy for Differential Concentrations

Once the baseline StO_2 was quantified, a modified Beer-Lambert Law approach was used to analyze the complete set of B-NIRS spectra as it is considerably faster than the derivative fitting which takes 84 ± 17 s per spectrum on an i7-4700MQ 2.40 GHz processor. The UCLn algorithm was used to quantify changes in Hb, HbO_2, and oxCCO concentrations (units: μM) from changes in attenuation across 770-900 nm [29], using a dynamic pathlength calculated by fitting the 2nd derivative of R(λ) to the second derivative of the water absorption spectra [28] and correcting for the wavelength dependence of the pathlength [30]. Tissue oxygen saturation at each time point was determined by combining the relative changes derived from the values obtained with the UCLn algorithm with the absolute baseline values obtained by the derivative fitting approach:

$$StO_2 = \frac{(HbO_2^b + \Delta HbO_2)}{(Hb^b + \Delta Hb) + (HbO_2^b + \Delta HbO_2)} \quad (2.5)$$

where ΔHbO_2 and ΔHb represent the relative changes in oxy/deoxy-hemoglobin.

2.3.3.2 Quantifying CBF

DCS data were analyzed by fitting the measured electric field autocorrelation function to a solution to the diffusion approximation for a semi-infinite homogeneous medium [10]. Fitting was performed using the known source-detector distance (20 mm) and values of μ_a and μ_s' at 785 nm obtained from the B-NIRS analysis. Time varying changes in μ_a were used along with the baseline μ_s' [25] to fit the dynamic data. The fitting of the autocorrelation curves yielded the correlation factor (β) and the blood flow index (BFi) [25].

For the DCE-NIRS analysis, CBF was quantified by relating the time-varying arterial concentration of ICG, $C_a(t)$, to the corresponding brain concentration curve, $C_b(t)$, using the following equation [31]:

$$C_b(t) = CBF \cdot R(t) * C_a(t) \quad (2.6)$$

where R(t) is the impulse residue function and * refers to the convolution operation. The product CBF • R(t) was extracted using a deconvolution algorithm [32], from which CBF was determined by the initial value since R(t) by definition begins at a value of one. The CBF measurement was then used to convert the DCS BFi time series into physiological blood flow units (i.e., ml/100g/min) [25].

2.3.4 Error Analysis

Monte Carlo simulations were conducted to assess the accuracy of the 3-step, multi-parameter fitting approach. Simulated spectra were generated using the semi-infinite solution to the diffusion approximation with values of Hb^b and HbO_2^b that corresponded to an StO_2 = 75.5% (all input parameters are given in Table 2.2). Poisson noise was added at each wavelength, and the fitting routine used to obtain best-fit estimates of the 5 parameters. The same initial values and boundary conditions given in Table 2.1 were used. Simulations were run 500 times to generate a distribution of estimates for each fitting

parameter. As well, the entire analysis was repeated by averaging spectra over 8 to 512 repetitions to estimate the precision of the fitting parameters over a range of SNR.

2.3.5 Statistical Analysis

For the tissue phantom experiments, the influence of the NIRS broadband source on the estimated diffusion coefficients was tested using a Student's t-test.

For the HI experiments, individual CBF time series, from each animal, were normalized to their corresponding baseline values. Thereafter, ten CBF values were extracted by dividing the normalized time series into bins of successive 10% reductions in flow and averaging within these bins. The corresponding oxCCO concentration changes were obtained for each CBF interval. A multivariate ANOVA was conducted to determine which oxCCO values were significantly different from baseline. The same approach was also applied to investigate the relationship between CBF and StO_2 during HI.

2.4 Results

2.4.1 Instrumentation

The experiments conducted with the tissue-mimicking phantoms showed a significant effect of the broadband light source on the autocorrelation curves. Fig. 2.2 presents curves acquired with the B-NIRS emission probe at 10 mm away from the DCS detection, along with the corresponding best fit to the diffusion approximation. Note that a single-mode fiber was used in this test to provide a wide dynamic range for the correlation factor, β. The curves shown in Fig. 2.2 were acquired with the B-NIRS light off (A) or on (B).

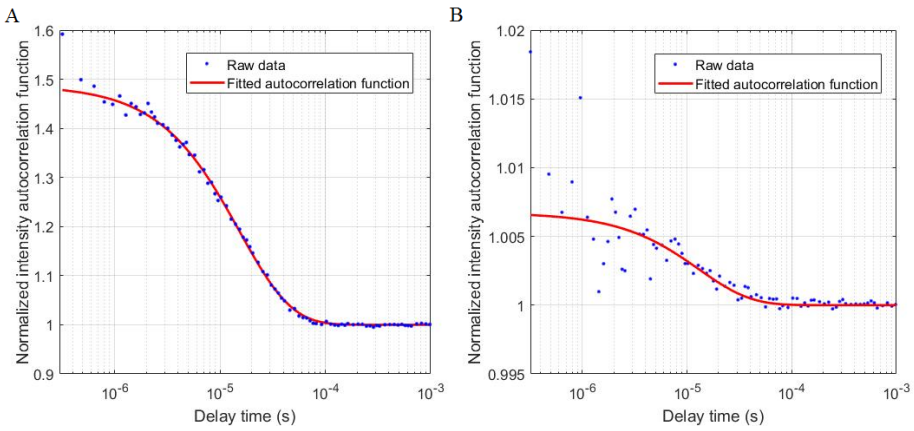

Figure 2.2: Autocorrelation functions (blue symbols) acquired with (a) DCS alone, and (b) DCS in the presence of light from the B-NIRS source (10 mm). The red lines in both figures are the best fit to the diffusion approximation.

As expected at this short distance between the B-NIRS emission and DCS detection, the high intensity of incoherent light from the broadband source significantly reduced the SNR of the acquired autocorrelation functions and the correlation factor β (y-intercept). The use of a few-mode fiber in this test would produce even lower β values, by allowing the propagation of more modes of light. A significant difference in the derived diffusion coefficient was found between the two curves: $1.56 \pm 0.05 \times 10^{-8}$ cm^2/s (DCS alone) and $1.82 \pm 0.30 \times 10^{-8}$ cm^2/s (with broadband light source on) ($p < 0.01$). The broadband light source also affected the estimated β value when using a few-mode fiber with a distance of 30 mm as shown in Fig. 2.3, A. However, in contrast to the data acquired at 10 mm, the broadband light contamination did not significantly affect the values of the derived diffusion coefficient when the B-NIRS emission probe was 30 mm away from DCS detection (Fig. 2.3(B)).

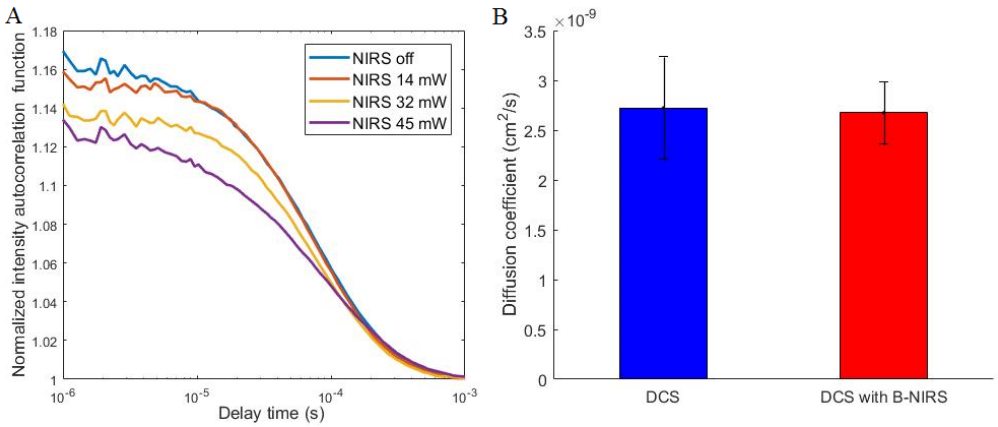

Figure 2.3: (A) DCS autocorrelation curves with B-NIRS light (30 mm from DCS detection) at varying intensities, (B) diffusion coefficient values without (blue) and with (red) the B-NIRS light; data were averaged over 10 acquisitions, error bars represent standard deviation.

To demonstrate the robustness of the B-NIRS multi-parameter fitting, the algorithm described was used to estimate the 5 fitting parameters from spectra of varying SNR (obtained by averaging a varying number of spectra). The parameters obtained by fitting a low SNR spectrum (obtained from one simulated spectrum with added Poisson noise, as described above) and one high SNR spectrum (obtained by averaging 512 spectra low SNR spectra) are displayed in Table 2.2, along with the resulting StO_2 value. Note that the mean and standard deviation displayed in Table 2. 2 were obtained by repeating the simulations 500 times (i.e., Monte Carlo type approach).

Table 2-2: Monte Carlo simulation of B-NIRS fitting algorithm.

Simulation parameter	Input Values	1 acquisition	512 averages
WF	0.8	0.71 ± 0.13	0.80 ± 0.04
$Hb^b(g/dL)$	13	12.0 ± 3.3	12.9 ± 0.6
$HbO_2{}^b(g/dL)$	40	36.2 ± 9.4	39.8 ± 1.7
A (mm^{-1})	0.8	0.93 ± 0.23	0.81 ± 0.04
α	2.6	2.6 ± 0.3	2.6 ± 0.03
StO_2 (%)	75.5	75.0 ± 3.9	75.5 ± 0.2

StO_2 values obtained by using a varying number of averaged spectra are displayed in Fig. 2.4. The error bars represent the standard deviation over 500 simulations.

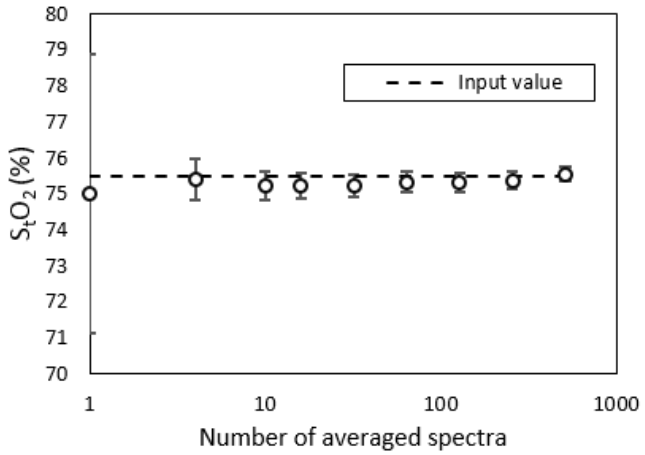

Figure 2.4: Estimation of StO_2 from simulated spectra of varying SNR (obtained by varying the number of averaged spectra). The circles represent the mean and the error bars are the standard deviation over 500 repetitions for each set of averaged spectra.

2.4.2 Hypoxia-ischemia Insult

Experiments were conducted on eight piglets (2 female, mean age = 25 ± 10 h, weight = 1.6 ± 0.3 kg). Of these, control experiments involving no HI insult were conducted on two animals. Table 3 displays the average baseline values across all animals for all 5 fitting parameters, cerebral oxygen saturation, and perfusion.

Table 2-3: Baseline fitting parameters, StO_2, and CBF.

Parameter	Baseline value
WF	0.78 ± 0.02
Hb^b*(g/dL)*	18 ± 3
HbO_2^b*(g/dL)*	35 ± 13
A (mm^{-1})	0.35 ± 0.11
α	3.3 ± 0.5
StO_2 (%)	64 ± 13
CBF (ml/100g/min)	28 ± 7

B-NIRS spectra recorded at baseline and during the peak of HI insult are shown in Fig. 2.5, A). An attenuation difference, calculated as the log of the ratio between these

spectra, is displayed in black in Fig. 2.5 B. The fit of the attenuation by the concentrations recovered from the Beer-Lambert algorithm are shown in blue and red. The blue curve represents the fit of HbO_2 and Hb (2-component model), while the red line represents the fit of HbO_2, Hb, and oxCCO (3-component model). It is clear that the addition of oxCCO to the model improved the fitting; this is further demonstrated in Fig. 5, C which shows residuals between measured and modelled attenuation. The 3-component model has a smaller residual, randomly distributed around 0, whereas, the 2-component model had a residual centered on a peak around 820 nm. This suggests that there is a missing chromophore in the model with a peak at 820 nm, which is very similar to the oxCCO difference spectrum [20].

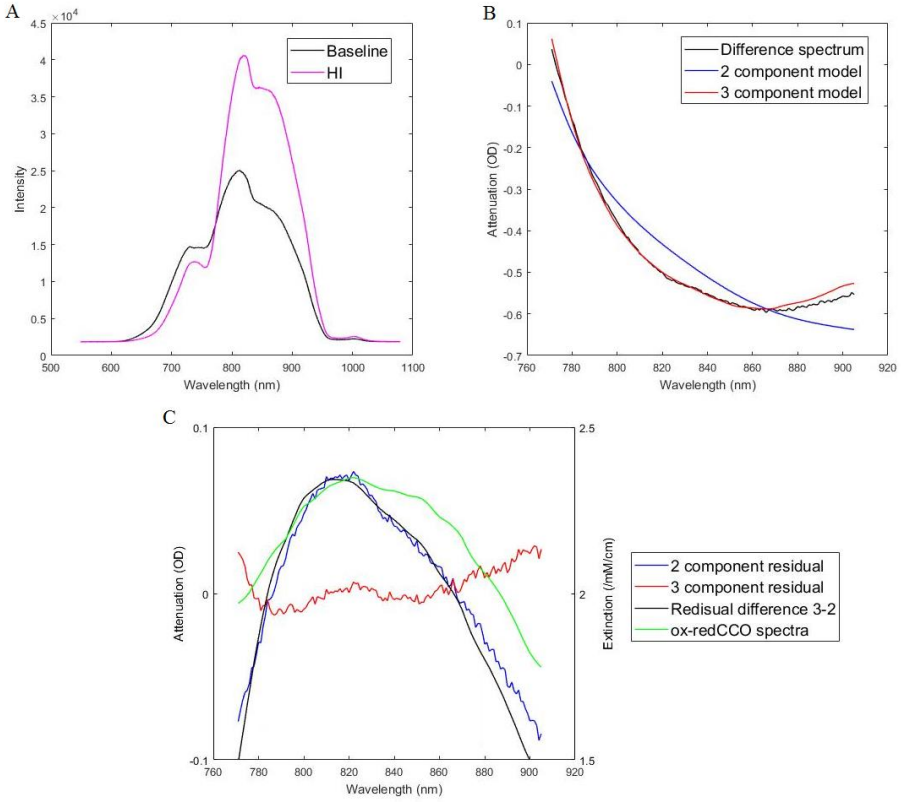

Figure 2.5: Broadband NIRS analysis showing (A) raw intensity measurements at baseline and during HI insult, (B) attenuation and best fit of the 2- (Hb and HbO_2) and 3-component models (Hb, HbO_2, and oxCCO), and (C) and residuals between measured and modelled attenuation, with CCO difference spectrum (ox-redCCO) for comparison.

A 5-s DCS acquisition period provided sufficient SNR with adequate temporal resolution to discern physiological changes caused by HI. Specifically, various DCS acquisition times were tested at baseline, and there was no statistically significant difference between the BFi obtained at 5 and 15 s acquisitions over 30 cycles (difference = 3.2%, p=0.42). DCS autocorrelation curves acquired at baseline, during HI insult, and following recovery are displayed in Fig. 2.6. The CBF values derived by calibrating each BFi were 35.2 ± 0.8 ml/100g/min, 2.6 ± 0.1 ml/100g/min, and 32.5 ± 0.8 ml/100g/min respectively.

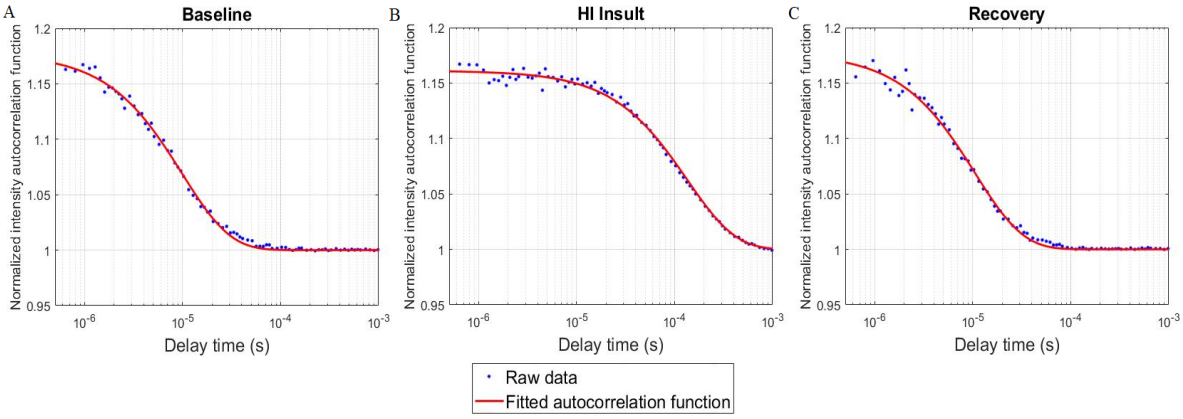

Figure 2.6: DCS autocorrelation curves measured in one piglet during (A) baseline (CBF = 35.2 ± 0.8 ml/100g/min), (B) HI insult (CBF = 2.6 ± 0.1 ml/100g/min), and (C) following insult recovery (CBF = 32.5 ± 0.8 ml/100g/min). The red lines represent best fit to the diffusion approximation.

Fig. 2.7 presents StO_2, CBF, and oxCCO time courses for three HI piglets and one control. Region (i) in each graph corresponds to the brief period between inflating the carotid occluders and reducing the inspired oxygen content. The combination of both components of HI is represented by region (ii). For the controls, no significant changes in the any of the parameters were detected. While StO_2 and CBF responded immediately to occluder inflation, oxCCO displayed a delayed response. As well, a continual reduction in oxCCO persisted after CBF and StO_2 had reached their nadir. This pattern was observable in all HI experiments.

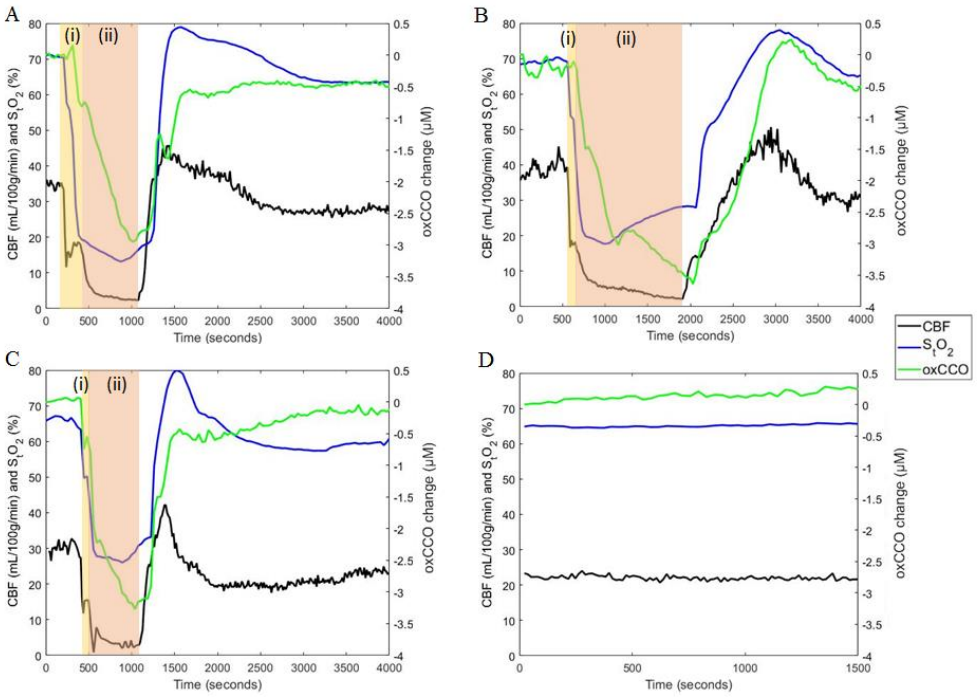

Figure 2.7: Simultaneous monitoring of StO_2, absolute CBF, and oxCCO in 3 hypoxia-ischemia (HI) animals (A, B, C) and a control piglet (D). The HI insult began with clamping the carotid arteries (region (i)), followed by inducing hypoxia by reducing the inspired oxygen fraction to 8% (region (ii)).

To further investigate the temporal relationship between CBF and metabolism during HI, oxCCO and StO_2 were separately correlated to incremental changes in CBF as described in section 2.3.5. Data presented in Fig. 2.8(A) and Fig. 2.8(B) show oxCCO and StO_2, respectively, averaged across all animals and plotted against averaged changes in CBF normalized to baseline values. Due to the rapid and large initial reduction in CBF caused by carotid occlusion, the initial drop in CBF was greater than 40% in some experiments. Consequently, CBF intervals with mean values of 0.62 and 0.76 show only data from two and one animals, respectively.

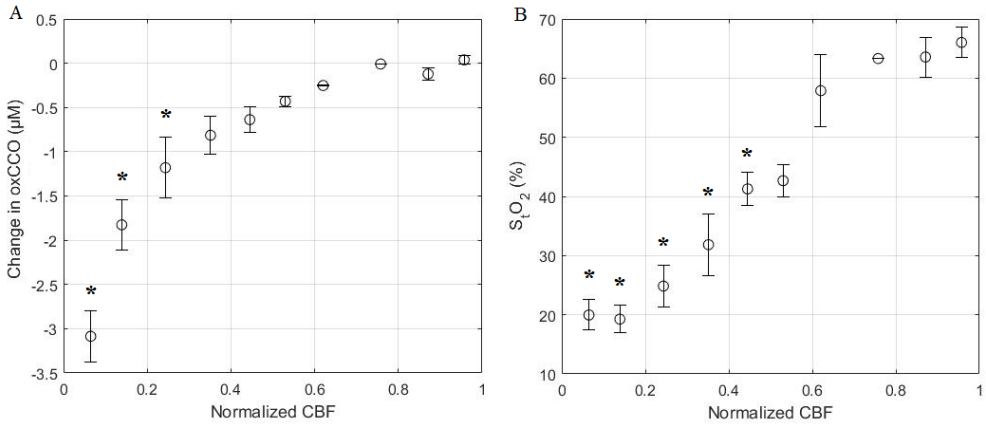

Figure 2.8: Correlation plots of a) oxCCO vs CBF, and b) StO_2 vs CBF; * indicates a significant change in either oxCCO or StO_2 from baseline ($p<0.05$). Error bars represent the standard error of the mean. CBF intervals with mean values of 0.62 and 0.76 show only data from two and one animals, respectively.

2.5 Discussion

In this article, we report on the development of a hybrid diffuse correlation spectroscopy (DCS) and broadband near-infrared spectroscopy (B-NIRS) instrument capable of simultaneous monitoring of cerebral blood flow (CBF) and changes in the oxidation state of cytochrome c oxidase (oxCCO). This was achieved using a simple shutter-based multiplexing method that allowed acquisition of DCS and B-NIRS measurements in quick succession, thereby avoiding crosstalk between the two subsystems.

Although the importance of monitoring both CBF and metabolism has been long recognized, StO_2 is still the most widely used marker of cerebral health in the clinic, despite its limited sensitivity to brain injury [8]. The lower sensitivity of StO_2 is believed to be related, in part, to the inability to separate blood flow and metabolic effects [8,33]. Hemoglobin difference ($\Delta[HbDiff] = \Delta[HbO_2] - \Delta[Hb]$) has been used as a surrogate marker of CBF, but its relationship to flow also depends on oxygen metabolism [33]. Recent advancements have enabled direct CBF monitoring by DCS; however, monitoring CBF alone may not be sufficient to capture the interplay between substrate delivery and demand. To assess clinically significant changes in CBF, which could impact tissue viability, measures of metabolism have been recently investigated. Conversely, monitoring

CBF could help determine if metabolic reductions are due to limited oxygen delivery as opposed to changes in demand.

The multiplexing approach presented here was necessary to avoid crosstalk between the B-NIRS and DCS techniques as the DCS laser would saturate the B-NIRS detector if they are operated simultaneously. As well, when the broadband source is used concurrently with DCS measurements, the autocorrelation curves are altered, particularly at short distances between the B-NIRS emission probe and DCS detection fiber. Even when a single-mode DCS detection fiber was used, to maximize the dynamic range of the correlation factor, we found that with a 10 mm distance between the B-NIRS source and the DCS detection, incoherent light excited additional modes in the DCS fiber. This manifested as a much lower β value in the autocorrelation curves (Fig. 2.2) and resulted in a significantly different diffusion coefficient ($p < 0.01$), warranting the use of shutters. Fig. 2.3 A shows that increasing the B-NIRS light intensity decreases the correlation factor (y-intercept). However, the values of diffusion coefficients obtained by fitting the measured autocorrelation curves in Fig. 2.3 A with the solution to the diffusion equation for a semi-infinite homogeneous medium [34] did not significantly differ, as shown in Fig. 2.3 B. This shows that at larger distances, the B-NIRS light affects the correlation factors of the autocorrelation curves but has no significant effect on the diffusion coefficient.

The SNR can be further increased by reducing the sampling rate; lengthening the shutter cycle times allows for measures to be averaged over more acquisitions, but this would increase the time between successive measurements. In its current configuration, the hybrid B-NIRS/DCS device provided StO_2, CBF, and oxCCO measurements every 14 s. This sampling rate could likely be increased to every 3-5 s using new technologies such as the DCS software correlator [35]. However, the speed of the current system was sufficient to capture the dynamics of the CBF and oxCCO responses to HI, and therefore will likely be sufficient for cerebral monitoring in the NICU.

StO_2 was monitored by a combination of a spectral derivative fitting approach to determine baseline StO_2 and a faster linear algorithm based on the Beer-Lambert law to track subsequent changes in HbO_2 and Hb concentrations. The reproducibility of the baseline

optical properties derived from the former was tested by conducting an error analysis involving Monte Carlo simulations. Fig. 2.4 and Table 2-2 demonstrate the ability of the fitting technique to extract parameter estimates with good precision and accuracy. These estimates were found to be insensitive to the boundary conditions and initial values used by the fitting routine (Table 2-1). Furthermore, the average baseline StO_2 (64±13%) was in good agreement with a previous study (StO_2 = 69±2%) involving the same animal model but using time-resolved NIRS to measure the optical properties [12]. Further validation studies are on-going to assess the accuracy of this technique over a wide range of StO_2 [36]; however, it is important to realize that the computational efficiency of the UCLn algorithm is extremely valuable for real-time monitoring in clinical applications.

Source-detector distances of 3 cm for B-NIRS and 2 cm for DCS were chosen to probe the piglet brain because it has been shown that in reflectance geometry, the penetration depth is approximately the square root of the source-detector distance [37]. Considering that the thickness of the extra-cerebral layers in newborn piglets is 2-3 mm [23], the brain can be reliably probed using a source-detector distance of 2 cm or greater. Note that this approach has been previously validated against CT perfusion measurements in a neonatal piglet model [23]. In addition, the probe geometry depicted in Fig. 2.1 was designed to ensure that DCS and B-NIRS probed overlapping brain regions. It is important to note that the HI model causes global changes in cerebral blood flow and metabolism. Therefore, it is expected that small differences in the tissue volumes interrogated by the two instruments will not alter the relationship between the measured hemodynamic and metabolic changes.

There have been a number of previous studies combining B-NIRS and DCS [38–40]; in particular Lee et al. recently presented a compact device for dual monitoring of tissue flaps. However, the greater source-detector distances required for brain monitoring limits the applicability of many of these approaches. Furthermore, a key novelty of our method is the ability to continuously monitor StO_2, absolute blood flow, and oxCCO, which has not been previously reported. In terms of brain monitoring, a similar concept combining frequency-domain NIRS (FD-NIRS) and DCS [41] was recently reported. This device is capable of simultaneous monitoring of StO_2, CBF, and $CMRO_2$, and has been used to investigate neonatal hemodynamics. Instead of a 785-nm laser, a DCS laser emitting at 850 nm was

used along with optical filters to prevent crosstalk between the two systems. An 850-nm laser is outside of the spectral range used for broadband analysis of hemoglobin concentration (680 to 845 nm), but more critically it is within the range of the CCO feature (780 to 900 nm). Although there are long coherence lasers operating at wavelengths lower than 680 nm, it is noteworthy that they have significantly lower power outputs. As well, above 900 nm, SPCM detectors commonly used in DCS systems have lower quantum efficiencies; both factors would reduce SNR. These limitations of current technology restrict the feasibility of using optical filters for concurrent monitoring of CBF and oxCCO.

The HI piglet model produced rapid and dynamic changes in StO_2, CBF, and oxCCO. More importantly, the experimental results clearly demonstrated the unique individual responses in oxygenation, flow, and metabolism (Fig. 2.7 and 2.8). These differences warrant the inclusion of all three measures in order to understand the broader physiological impact of HI. That is, StO_2 and hemoglobin concentrations allow for monitoring of hypoxia, CBF dynamics indicate ischemia, and changes in oxCCO relate to metabolic stress. Together, these different perspectives describe the hemodynamic and metabolic environment that surrounds and precedes brain injury.

In the 6 animals with HI injury, the decrease of oxCCO was delayed in comparison to CBF and continued to decline even after CBF and StO_2 reached their nadirs. A similar biphasic relationship between oxCCO and HbDiff was found in piglets experiencing anoxia [42]. Group averages of time courses are not shown due to the temporal variability between clamping carotid arteries and reducing oxygen content. The timing of the latter varied because it was only executed once occluders were shown to produce a noticeable decrease in CBF. Nevertheless, time courses across all experiments showed the direct effect of decreased CBF on StO_2 and a delayed oxCCO response. Reduced blood flow is likely met by increased oxygen extraction in order to maintain oxidative metabolism, which is consistent with previous reports between CBF and $CMRO_2$ in piglets [33] and infants [9]. This compensatory mechanism may explain the delayed oxCCO response. However, the relationship between oxidative metabolism and oxCCO is complex. Further investigation into the interrelationship between these values and their physiological significance in predicting brain injury will be the subject of future investigations.

2.6 Conclusion

This article reports on the development of a novel optical system that combines DCS and B-NIRS to enable continuous monitoring of absolute cerebral blood flow and changes in the oxidation state of cytochrome c oxidase – two sensitive biomarkers of brain health. The combination of the two subsystems was achieved through the use of a simple multiplexing approach based on electromechanical shutters and can be easily implemented elsewhere. In addition, the ability to simultaneously monitor CBF and oxCCO has led to a key finding; that is, the response of cerebral oxygen metabolism is delayed in hypoxia-ischemia while the CBF response is instantaneous. We anticipate that real-time monitoring of absolute CBF and oxCCO will provide greater insights into hemodynamic events that precede brain injury and could become valuable for guiding therapeutic interventions. Furthermore, because the hybrid B-NIRS/DCS system is safe and portable, it could be easily deployed in the NICU to monitor cerebral perfusion and metabolism at the bedside in early stages following birth, with the goal of detecting significant hemodynamic events before brain injury occurs.

2.7 Acknowledgements

The authors would like to thank Jennifer Hadway and Lise Desjardins for help in conducting animal experiments, Lynn Keenliside and Lawrence Yip for technical support, and Krisin Lu and Androu Abdalmalak for their help in schematic design and statistical analysis. Funding: Wellcome Trust (104580/Z/14/Z), Canadian Institutes of Health Research (CGP-140171).

2.8 References

1. H. Blencowe, S. Cousens, M. Z. Oestergaard, D. Chou, A. B. Moller, R. Narwal, A. Adler, C. Vera Garcia, S. Rohde, L. Say, and J. E. Lawn, "National, regional, and worldwide estimates of preterm birth rates in the year 2010 with time trends since 1990 for selected countries: A systematic analysis and implications," Lancet 379(9832), 2162–2172 (2012).

2. J. J. Volpe, "Brain injury in premature infants: a complex amalgam of destructive and developmental disturbances Joseph," Lancet 8(1), 110–124 (2009).

3. M. Bracewell and N. Marlow, "Patterns of motor disability in very preterm children," Ment. Retard. Dev. Disabil. Res. Rev. 8(4), 241–248 (2002).

4. H. Bassan, "Intracranial Hemorrhage in the Preterm Infant: Understanding It, Preventing It," Clin. Perinatol. 36(4), 737–762 (2009).

5. R. Bapat, P. A. Narayana, Y. Zhou, and N. A. Parikh, "Magnetic resonance spectroscopy at term-equivalent age in extremely preterm infants: Association with cognitive and language development," Pediatr. Neurol. 51(1), 53–59 (2014).

6. S. Thayyil, M. Chandrasekaran, A. Taylor, A. Bainbridge, E. B. Cady, W. K. K. Chong, S. Murad, R. Z. Omar, and N. J. Robertson, "Cerebral Magnetic Resonance Biomarkers in Neonatal Encephalopathy: A Meta-analysis," Pediatrics 125(2), e382–e395 (2010).

7. F. Groenendaal, R. H. Veenhoven, J. Van Der Grond, G. H. Jansen, T. D. Witkamp, and L. S. De Vries, "Cerebral lactate and N-acetyl-aspartate/choline ratios in asphyxiated full-term neonates demonstrated in vivo using proton magnetic resonance spectroscopy," Pediatr. Res. 35(2), 148–151 (1994).

8. D. A. Boas and M. A. Franceschini, "Haemoglobin oxygen saturation as a biomarker: the problem and a solution," Philos. Trans. R. Soc. A Math. Phys. Eng. Sci. 369(1955), 4407–4424 (2011).

9. R. Arora, M. Ridha, D. S. C. Lee, J. Elliott, H. C. Rosenberg, M. Diop, T.-Y. Lee, and K. St Lawrence, "Preservation of the metabolic rate of oxygen in preterm infants during indomethacin therapy for closure of the ductus arteriosus.," Pediatr. Res. 73(6), 713–8 (2013).

10. M. Diop, J. Kishimoto, V. Toronov, D. S. C. Lee, and K. S. Lawrence, "Development of a combined broadband near-infrared and diffusion correlation system for monitoring cerebral blood flow and oxidative metabolism in preterm infants," Biomed. Opt. Express 6(10), 3907–3918 (2015).

11. T. Durduran and A. G. Yodh, "Diffuse correlation spectroscopy for non-invasive, microvascular cerebral blood flow measurement," Neuro 85(1), 51–63 (2014).

12. K. Verdecchia, M. Diop, T.-Y. Lee, and K. St Lawrence, "Quantifying the cerebral metabolic rate of oxygen by combining diffuse correlation spectroscopy and time-resolved near-infrared spectroscopy.," J. Biomed. Opt. 18(2), 27007 (2013).

13. M. Caldwell, T. Moroz, T. Hapuarachchi, A. Bainbridge, N. J. Robertson, C. E. Cooper, and I. Tachtsidis, "Modelling Blood Flow and Metabolism in the Preclinical Neonatal Brain during and Following Hypoxic-Ischaemia," PLoS One 10(10), e0140171 (2015).

14. P.-Y. Lin, N. Roche-Labarbe, M. Dehaes, S. Carp, A. Fenoglio, B. Barbieri, K. Hagan, P. E. Grant, and M. A. Franceschini, "Non-invasive optical measurement of cerebral metabolism and hemodynamics in infants.," J. Vis. Exp. (73), e4379 (2013).

15. K. M. Tichauer, D. W. Brown, J. Hadway, T.-Y. Lee, K. St Lawrence, K. S. Lawrence, M. Kenneth, Y. Lee, K. St, and L. Near-infrared, "Near-infrared spectroscopy measurements of cerebral blood flow and oxygen consumption following hypoxia-ischemia in newborn piglets.," J. Appl. Physiol. 100, 850–857 (2006).

16. K. M. Tichauer, D. Y. L. Wong, J. A. Hadway, R. J. Rylett, T. Y. Lee, and K. S. Lawrence, "Assessing the severity of perinatal hypoxia-ischemia in piglets using near-infrared spectroscopy to measure the cerebral metabolic rate of oxygen," Pediatr. Res. 65(3), 301–306 (2009).

17. H. M. Watzman, C. D. Kurth, L. M. Montenegro, J. Rome, J. M. Steven, and S. C. Nicolson, "Arterial and venous contributions to near-infrared cerebral oximetry," Anesthesiology 93(4), 947–953 (2000).

18. K. M. Tichauer, J. T. Elliott, J. a Hadway, D. S. Lee, T.-Y. Lee, and K. St Lawrence, "Using near-infrared spectroscopy to measure cerebral metabolic rate of oxygen under multiple levels of arterial oxygenation in piglets.," J. Appl. Physiol. 109(3), 878–85 (2010).

19. M. Sakoh, L. Ostergaard, L. Røhl, D. F. Smith, C. Z. Simonsen, J. C. Sørensen, P. V Poulsen, C. Gyldensted, S. Sakaki, and A. Gjedde, "Relationship between residual cerebral blood flow and oxygen metabolism as predictive of ischemic tissue viability: sequential multitracer positron emission tomography scanning of middle cerebral artery occlusion during the critical first 6 hours after stroke in pigs.," J. Neurosurg. 93(4), 647–57 (2000).

20. G. Bale, C. E. Elwell, and I. Tachtsidis, "From Jöbsis to the present day : a review of clinical near-infrared spectroscopy measurements of cerebral cytochrome-c-oxidase," J. Biomed. Opt. 21(9), (2016).

21. A. Bainbridge, I. Tachtsidis, S. D. Faulkner, D. Price, T. Zhu, E. Baer, K. D. Broad, D. L. Thomas, E. B. Cady, N. J. Robertson, and X. Golay, "Brain mitochondrial oxidative metabolism during and after cerebral hypoxia-ischemia studied by simultaneous phosphorus magnetic-resonance and broadband near-infrared spectroscopy," Neuroimage 102(P1), 173–183 (2014).

22. M. M. Tisdall, I. Tachtsidis, T. S. Leung, C. E. Elwell, and M. Smith, "Increase in cerebral aerobic metabolism by normobaric hyperoxia after traumatic brain injury," J. Neurosurg. 109(3), 424–432 (2008).

23. M. Diop, J. T. Elliott, K. M. Tichauer, T.-Y. Lee, and K. St Lawrence, "A broadband continuous-wave multichannel near-infrared system for measuring regional cerebral blood flow and oxygen consumption in newborn piglets.," Rev. Sci. Instrum. 80(5), 54302 (2009).

24. G. Strangman, M. A. Franceschini, and D. A. Boas, "Factors affecting the accuracy of near-infrared spectroscopy concentration calculations for focal changes in oxygenation parameters," Neuroimage 18(4), 865–879 (2003).

25. M. Diop, K. Verdecchia, T.-Y. Lee, and K. St Lawrence, "Calibration of diffuse correlation spectroscopy with a time-resolved near-infrared technique to yield absolute cerebral blood flow measurements.," Biomed. Opt. Express 2(7), 2068–2081 (2011).

26. H. Z. Yeganeh, V. Toronov, J. T. Elliott, M. Diop, T.-Y. Lee, and K. St Lawrence, "Broadband continuous-wave technique to measure baseline values and changes in the tissue chromophore concentrations.," Biomed. Opt. Express 3(11), 2761–70 (2012).

27. S. L. Jacques, "Optical properties of biological tissues: a review," Phys. Med. Biol. 58(11), R37–R61 (2013).

28. S. J. Matcher, M. Cope, and D. T. Delpy, "Use of the water absorption spectrum to quantify tissue chromophore concentration changes in near-infrared spectroscopy.," Phys. Med. Biol. 39(1), 177–96 (1994).

29. S. J. Matcher, P. J. Kirkpatrick, K. Nahid, M. Cope, and D. T. Delpy, "Absolute quantification methods in tissue near-infrared spectroscopy," Proc. SPIE 2389 (May 1995), 486–495 (1995).

30. M. Essenpreis, M. Cope, C. E. Elwell, S. R. Arridge, P. van der Zee, and D. T. Delpy, "Wavelength dependence of the differential pathlength factor and the log slope in time-resolved tissue spectroscopy.," Adv. Exp. Med. Biol. 333, 9–20 (1993).

31. K. St. Lawrence, K. Verdecchia, J. T. Elliott, and M. Diop, "Measuring Cerebral Hemodynamics and Energy Metabolism by Near-Infrared Spectroscopy," in In: Hirrlinger J., Waagepetersen H. (Eds) Brain Energy Metabolism, Neurometho (Humana Press, 2014), p. Neuromethods, vol 90.

32. D. W. Brown, P. a Picot, J. G. Naeini, R. Springett, D. T. Delpy, and T.-Y. Lee, "Quantitative near infrared spectroscopy measurement of cerebral hemodynamics in newborn piglets.," Pediatr. Res. 51(5), 564–570 (2002).

33. J. A. Cooper, K. M. Tichauer, M. Boulton, J. Elliott, M. Diop, M. Arango, T.-Y. Lee, and K. St Lawrence, "Continuous monitoring of absolute cerebral blood flow by near-infrared spectroscopy during global and focal temporary vessel occlusion.," J. Appl. Physiol. 110(6), 1691–8 (2011).

34. C. Cheung, J. P. Culver, K. Takahashi, J. H. Greenberg, and A. G. Yodh, "In vivo cerebrovascular measurement combining diffuse near-infrared absorption and correlation spectroscopies," Phys. Med. Biol. 46(8), 2053–2065 (2001).

35. D. Wang, A. B. Parthasarathy, W. B. Baker, K. Gannon, V. Kavuri, T. Ko, S. Schenkel, Z. Li, Z. Li, M. T. Mullen, J. A. Detre, and A. G. Yodh, "Fast blood flow monitoring in deep tissues with real-time software correlators," Biomed. Opt. Express 7(3), 776 (2016).

36. M. D. Kewin, D. F. Milej, A. Abdalmalak, A. Rajaram, M. Diop, S. de Ribaupierre, K. St. Lawrence, A. Rajaram, M. Diop, S. de Ribaupierre, and K. St. Lawrence, "Validation of a Hyperspectral NIRS Method for Measuring Oxygen Saturation by Comparison to Time-Resolved NIRS," in Biophotonics Congress: Biomedical Optics Congress 2018 (Microscopy/Translational/Brain/OTS) (OSA, 2018), p. OW4C.4.

37. F. Martelli, T. Binzoni, A. Pifferi, L. Spinelli, A. Farina, and A. Torricelli, "There's plenty of light at the bottom: Statistics of photon penetration depth in random media," Sci. Rep. 6, 1–14 (2016).

38. P. Farzam, J. Johansson, M. Mireles, G. Jiménez-Valerio, M. Martínez-Lozano, R. Choe, O. Casanovas, and T. Durduran, "Pre-clinical longitudinal monitoring of hemodynamic response to anti-vascular chemotherapy by hybrid diffuse optics," Biomed. Opt. Express 8(5), 2563 (2017).

39. S. Y. Lee, J. M. Pakela, M. C. Helton, K. Vishwanath, Y. G. Chung, N. J. Kolodziejski, C. J. Stapels, and D. R. McAdams, "Compact dual-mode diffuse optical system for blood perfusion monitoring in a porcine model of microvascular tissue flaps," J. Biomed. Opt. 22(12), 1 (2017).

40. D. J. Rohrbach, N. Rigual, E. Tracy, A. Kowalczewski, K. L. Keymel, M. T. Cooper, W. Mo, H. Baumann, B. W. Henderson, and U. Sunar, "Interlesion differences in the local photodynamic therapy response of oral cavity lesions assessed by diffuse optical spectroscopies.," Biomed. Opt. Express 3(9), 2142–53 (2012).

41. S. A. Carp, P. Farzam, N. Redes, D. M. Hueber, and M. A. Franceschini, "Combined multi-distance frequency domain and diffuse correlation spectroscopy system with simultaneous data acquisition and real-time analysis," Biomed. Opt. Express 8(9), 3993–4006 (2017).

42. R. Springett, J. Newman, M. Cope, and D. T. Delpy, "Oxygen dependency and precision of cytochrome oxidase signal from full spectral NIRS of the piglet brain.," Am. J. Physiol. - Hear. Circ. Physiol. 279(5), H2202–H2209 (2000).

Chapter 3

3 Perfusion and metabolic neuromonitoring during ventricular taps in infants with post-hemorrhagic ventricular dilatation

This chapter has been adapted from the publication titled "Perfusion and metabolic neuromonitoring during ventricular taps in infants with post-hemorrhagic ventricular dilatation" published in *Brain Sciences* in 2020 by Ajay Rajaram, Lawrence C. M. Yip, Daniel Milej, Marianne Suwalski, Matthew Kewin, Marcus Lo, Jeffrey J. L. Carson, Victor Han, Soume Bhattacharya, Mamadou Diop, Sandrine de Ribaupierre, and Keith St. Lawrence, volume 10, issue 7.

3.1 Abstract

Post-hemorrhagic ventricular dilatation (PHVD) is characterized by a build-up of cerebrospinal fluid (CSF) in the ventricles, which increases intracranial pressure and compresses brain tissue. Clinical interventions (i.e., ventricular taps, VT) work to mitigate these complications through CSF drainage; however, the timing of these procedures remains imprecise. This study presents Neonatal NeuroMonitor (NNeMo), a portable optical device that combines broadband near-infrared spectroscopy (B-NIRS) and diffuse correlation spectroscopy (DCS) to provide simultaneous assessments of cerebral blood flow (CBF), tissue saturation (StO_2), and the oxidation state of cytochrome c oxidase (oxCCO). In this study, NNeMo was used to monitor cerebral hemodynamics and metabolism in PHVD patients selected for a VT. Across multiple VTs in four patients, no significant changes were found in any of the three parameters: CBF increased by 14.6 ± 37.6% ($p = 0.09$), StO_2 by 1.9 ± 4.9% ($p = 0.2$), and oxCCO by 0.4 ± 0.6 µM ($p = 0.09$). However, removing outliers resulted in significant, but small, increases in CBF (6.0 ± 7.7%) and oxCCO (0.1 ± 0.1 µM). The results of this study demonstrate NNeMo's ability to provide safe, non-invasive measurements of cerebral perfusion and metabolism for neuromonitoring applications in the neonatal intensive care unit.

3.2 Introduction

Premature birth, defined as a gestational period less than 37 weeks, occurs in 8% of infants in Canada [1]. Those born with lower birthweights (<1500 g) are at an increased risk of neurological complications, including deficits in cognition and behaviour as well as a higher incidence of major motor disorders (e.g., cerebral palsy) [2]. The largest contributor to preterm brain injury is intraventricular hemorrhaging (IVH). The pathogenesis of IVH involves the combination of an immature cerebral vascular anatomy (i.e., a highly vascularized germinal matrix) and poor cerebral blood flow (CBF) regulation [3,4]. It is believed that IVH elicits an inflammatory response, followed by fibrosis and subsequent obstruction of cerebrospinal fluid (CSF) drainage [5]. This can lead to accumulation of CSF, increased intracranial pressure (ICP), and dilatation of the entire ventricular system, referred to as post-hemorrhagic ventricular dilatation (PHVD).

PHVD is a major complication in severe cases of IVH (Grade III and higher), where more than 50% of the lateral ventricles are experiencing a bleed [6,7]. Due to a progressively increasing ICP, any delay in treatment can result in white matter atrophy and neurologic deterioration [4,8]. Cranial ultrasound (cUS) is the current gold standard in diagnosing and monitoring the progression of PHVD through ventricular measurements such as the ventricular index, anterior horn width, and thalamo-occipital distance [9]. Given these measures, there is still some debate over the timing of clinical intervention [10]. An early approach used by many European centres relies on ventricular measurements before patients are symptomatic. Intervention consists of a variety of techniques to drain CSF, including external ventricular drains (EVD), lumbar punctures (LP), and ventricular taps (VT), among others. [11]. In comparison, many North American centres employ a later approach where treatment is initiated depending on the ventricular index and clinical signs (e.g., increased ICP, head circumference, ventricle size, tense fontanelle, etc.) [12,13]; similar techniques are then implemented to drain CSF.

The discrepancy in the timing of clinical intervention is largely due to a lack of adequate monitoring techniques to quantify PHVD progression and treatment efficacy. Recent work has elucidated the benefits of hemodynamic and metabolic neuromonitoring surrounding the development of PHVD [14,15]. These metrics have shown potential to act as prognostic

markers of PHVD symptoms and could better indicate when to implement CSF drainage strategies. Measurements of CBF by transcranial doppler (TCD) have proven robust in premature infants; however, continuous monitoring is not ideal as TCD is operator-dependent and only measures macrovascular changes in blood flow [16,17]. Biomedical optics instead provide a safe, non-invasive technique ideal for longitudinal brain monitoring at the bedside [3,18–20].

This study presents an in-house built brain monitoring system referred to as NNeMo (Neonatal NeuroMonitor) that is capable of simultaneous measurement of cerebral perfusion, tissue saturation, and oxygen metabolism at the bedside through combining two optical techniques. Broadband near-infrared spectroscopy (B-NIRS) uses near-infrared light to measure absorption properties of tissue that can be used to estimate the concentrations of oxy and deoxyhemoglobin, from which the cerebral tissue saturation (StO_2) can be calculated [21]. B-NIRS can also provide a direct measurement of cerebral metabolism by monitoring absorption changes in the oxidation state of cytochrome c oxidase (oxCCO), which is directly related to mitochondrial ATP production in the electron transport chain [22]. Diffuse correlation spectroscopy (DCS) is an emerging technique that provides continuous monitoring of CBF by analyzing dynamic light scatter from red blood cells [23]. DCS has been validated against multiple modalities, including dynamic contrast-enhanced NIRS, Positron Emission Tomography with oxygen-15 (^{15}O) labelled water, and Arterial spin labelling MRI [24–26]. NNeMo combines B-NIRS and DCS technology to simultaneously monitor CBF, StO_2, and oxCCO.

This study presents the clinical translation of NNeMo to monitor PHVD infants in the neonatal intensive care unit (NICU) undergoing CSF drainage via ventricular taps. Previous work using contrast-enhanced NIRS reported a small increase in CBF after the VT, but with no concurrent change in cerebral energy metabolism [14]. However, only single time-point measurements before and after the procedure were acquired due to the need to inject a contrast agent (indocyanine green). Here, we present continuous bedside monitoring of cerebral perfusion and metabolism in PHVD patients undergoing a VT, with the goal of assessing any potential treatment-related changes in CBF and oxCCO. Based

on the magnitude of CBF changes previously reported [14], it was hypothesized that CSF drainage would lead to a modest increase in CBF, but with minimal impact on oxCCO.

3.3 Materials and Methods

3.3.1 Patient Population

This study was approved by the Western University Health Sciences Research Ethics Board (Project Identification Code: 17828), which adheres to the guidelines of the Canadian Tri-Council Policy Statement: Ethical Conduct for Research Involving Humans. Patients with PHVD were enrolled after obtaining parental consent. The initial IVH was diagnosed by cranial ultrasound (cUS) and graded according to the Papile scale [5]. The decision to perform a ventricular tap was based on standard of care, including clinical evidence (apnea, bradycardia, full fontanelles) and increased ventricle size as measured by cUS.

3.3.2 Study Design

Infants receiving a VT were monitored throughout the procedure with NNeMo (Figure 3.1 a). Prior to surgical setup, optical probes were placed on the infant's scalp above the frontoparietal cortex and held in place by a custom-built probe holder (Figure 3.1b). Two optical probes (one for the B-NIRS and one for the DCS) delivered light to the scalp. Source power levels were maintained within ANSI standards for skin exposure. A common detection fiber bundle was used to collect diffusely reflected light that had propagated through the head. The DCS and B-NIRS systems collected light at source-detector distances (SDD) of 2 and 3 cm, respectively, to ensure adequate brain interrogation (Figure 3.1 c). As an additional precaution, a phototherapy eye shield was employed to avoid exposing the subject's eyes to the light sources.

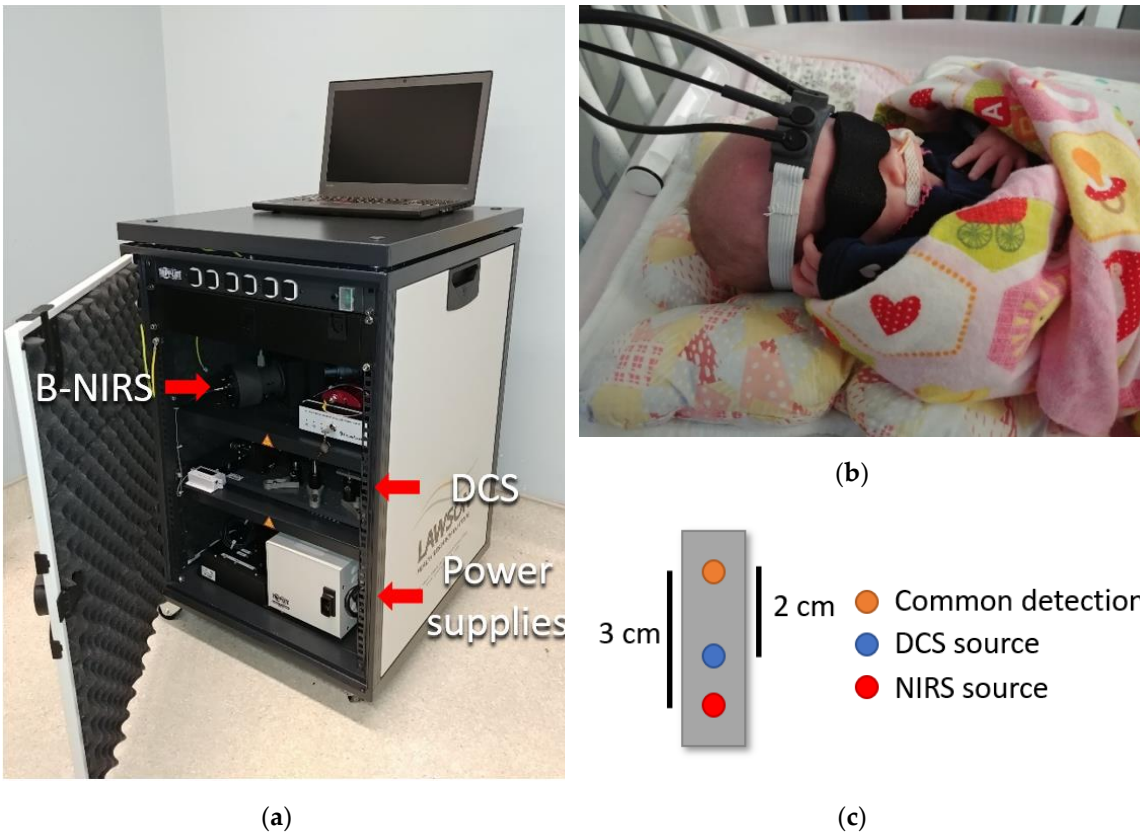

Figure 3.1: (a) Neonatal NeuroMonitor (NNeMo) combining broadband near-infrared spectroscopy (B-NIRS) and diffuse correlation spectroscopy (DCS) techniques. (b) Optical fibers affixed to an infant's head using a 3D-printed probe holder. A phototherapy eye shield was used as a safety precaution. (c) Optical fiber schematic showing two optical sources and a common detection fiber (SDD: DCS 2 cm; B-NIRS 3 cm).

Following sterilization of the surgical site, a VT was performed by a pediatric neurosurgeon. A needle was inserted into the lateral ventricles (Figure 3.2 a) to allow for CSF drainage (Figure 3.2 b). Following sufficient CSF removal, as determined by the clinician, the needle was removed and gentle pressure was applied to the needle insertion site. Optical data were collected throughout the VT, extending a minimum of 10 min prior to and following the procedure. B-NIRS and DCS data were acquired sequentially at a sampling rate of 250 ms and each dataset was averaged to achieve a final temporal resolution of 7 s.

(**a**) (**b**)

Figure 3.2: (a) Pediatric neurosurgeon inserting a needle into the ventricle and (b) draining cerebrospinal fluid (CSF) from the patient. Optical probes were affixed to the patient's head throughout the procedure.

3.3.3 Instrumentation

NNeMo was constructed by combining B-NIRS and DCS modalities using a multiplexing shutter system controlled by custom software developed in LabView (2017 SP1, National Instruments, Austin, TX, USA) and MATLAB (R2018b, MathWorks, Natick, MI, USA) [27]. The acquisition times of both the B-NIRS and DCS were set to 250 ms (4 Hz). The shutter system cycled between the two subsystems in 3 s intervals. A total of 12 data points were acquired in each interval and averaged for both B-NIRS and DCS measurements. A 0.5-s delay was added between the intervals to account for shutter transition times and to avoid overlap between the B-NIRS and DCS data.

The B-NIRS light source was a 20-W halogen bulb (Hl-2000-HP, Ocean Optics, Delay Beach, FL, USA) that was filtered from 600 to 1000 nm and coupled into a custom optical fiber bundle (2.4 mm diameter, 30 µM core, 0.55 numerical aperture ((NA), Loptek, Berlin, Germany) that directed the light to the head. Light from the interrogated tissue was collected by 3 fiber bundles (2 mm diameter, 30 µm core, 0.55 NA, Loptek, Berlin, Germany) that were linearly aligned at the entrance of the spectrometer (iDus 420, Andor, Oxford Instruments, Abingdon, UK; 548–1085 nm bandwidth; 1.65 nm resolution; P&P

Optica, Waterloo, ON, Canada). For DCS, light from a long coherence laser (DL785-100s, CrystaLaser, Reno, NV, USA) was coupled into a fiber bundle (4 × 200 µm core diameter, 0.22 NA, Loptek, Berlin, Germany) and directed towards the head. Light was collected by 4 single-mode fibers (8 µm core diameter, 0.12 NA, Loptek, Berlin, Germany) and coupled to a four-channel single photon counting module (SPCM-AQR-15-FC, Excelitas Technologies, Montreal, QC, Canada). The output from each detector was fed into an edge-detecting counter on a PCIe-6612 counter/timer data acquisition board (National Instruments) [28]. Photon counts were recorded and processed using in-house developed software (LabVIEW, MATLAB) [29]. For each detector, the software generated intensity autocorrelation curves at 50 delay times ranging from 1 µs to 1 ms.

For use in the NICU, the optical fibers were designed to be lightweight and flexible, with a 90°bend at the patient end to further minimize weight on the infant. A 3D-printed fiber probe holder (5 × 2 × 1 cm; Flexible Resin, Form 2, Formlabs, Somerville, MA, USA) was designed to secure the three optical probes (2 emission, 1 detection) to the patient's forehead using a soft and flexible base material with a non-abrasive strap (Figure 1 b).

3.3.4 Data processing

3.3.4.1 NIRS Analysis: Quantifying StO_2 and Changes in oxCCO Concentration

Prior to clinical measurements, a reference spectrum was acquired using a pinhole attenuator to characterize the spectral properties of the optical system. In addition, a measurement of the dark noise was acquired to characterize ambient light conditions. For the clinical NIRS data, each reflectance spectrum, R(λ), was corrected for the reference and dark count spectra as follows:

$$R(\lambda) = log_{10}\left(\frac{spectrum_\lambda - dark_\lambda}{reference_\lambda - dark_\lambda}\right) \quad (3.1)$$

where spectrum λ refers to the clinical measurement at wavelength λ.

To quantify chromophore concentrations, while accounting for the contribution of light scatter, a derivative approach was utilized [18,30,31]. First and second derivatives of R(λ) were calculated and fit to the solution of the diffusion approximation for a semi-infinite

homogeneous medium [19]. Light absorption (Equation (3.2)) and scattering (Equation (3.3)) parameters were input into the solution as follows [30]:

$$\mu_a(\lambda) = WF \cdot \varepsilon_{H_2O}(\lambda) + Hb^b \cdot \varepsilon_{Hb}(\lambda) + HbO_2^b \cdot \varepsilon_{HbO_2}(\lambda) \tag{3.2}$$

where WF is the tissue water fraction, Hb^b and HbO_2^b are baseline concentrations of deoxyhemoglobin and oxyhemoglobin in μM, and ε refers to the unique extinction coefficient for each chromophore.

$$\mu_s{}' = \mathrm{A}\left(\frac{\lambda}{800(nm)}\right)^{-\alpha} \tag{3.3}$$

where α is the scattering power and A is the μ_s' value at λ = 800 nm. Reflectance spectra measured at baseline were analyzed with a multi-parameter fitting algorithm based on a constrained least-square minimization using a custom MATLAB function (*fminsearchbnd*). Briefly, second derivative R(λ) spectra were fit by the model between 815 and 845 nm to obtain WF. The WF value was incorporated into the second derivative fit from 680 to 800 nm to determine Hb^b. Lastly, WF and Hb^b were used in the analysis of the first derivative spectrum. The fitting procedure extended from 680 to 845 nm to obtain an estimate of HbO_2^b [30].

Following baseline analysis, a modified Beer–Lambert law based on the UCLn algorithm (Equation (4)) was used to calculate changes in hemoglobin and oxCCO concentrations for the duration of the study [22].

$$\begin{bmatrix} \Delta HbO_2 \\ \Delta Hb \\ \Delta oxCCO \end{bmatrix} = \frac{1}{DP} \begin{bmatrix} \varepsilon_{HbO_2}(\lambda_1) & \varepsilon_{Hb}(\lambda_1) & \varepsilon_{oxCCO}(\lambda_1) \\ \vdots & \vdots & \vdots \\ \varepsilon_{HbO_2}(\lambda_n) & \varepsilon_{Hb}(\lambda_n) & \varepsilon_{oxCCO}(\lambda_n) \end{bmatrix}^{-1} \times \begin{bmatrix} \Delta A(\lambda_1) \\ \vdots \\ \Delta A(\lambda_n) \end{bmatrix} \tag{3.4}$$

where ΔHbO_2, ΔHb, and ΔoxCCO are relative changes from baseline in oxy-hemoglobin, deoxy-hemoglobin, and the oxidation state of cytochrome c oxidase. The differential pathlength (DP) was set to 4.39 based on previous literature [32,33] and corrected for the wavelength dependency of the pathlength [34]. ΔA represents the measured change in attenuation. Relative and baseline measures of hemoglobin were combined to determine the tissue saturation as follows [27]:

$$S_tO_2 = \frac{(HbO_2^b + \Delta HbO_2)}{(Hb^b + \Delta Hb) + (HbO_2^b + \Delta HbO_2)} \quad (3.5)$$

3.3.4.2 DCS Analysis: Relative Measure of CBF

Acquired normalized intensity autocorrelation data were converted to electric field autocorrelation data following the Siegert relation [35,36]:

$$g_2(\rho,\tau) = 1 + \beta \frac{|G_1(\rho,\tau)|^2}{\langle I(\rho,\tau)\rangle^2} \quad (3.6)$$

where g2(ρ,τ) is the measured normalized intensity autocorrelation, β is the coherence factor, G1(ρ,τ) is the electric field autocorrelation function, and <I(ρ,τ)> is the averaged detected intensity. The parameter ρ refers to the SDD and τ is the correlation time. G1 was modeled using the solution to the diffusion approximation for a semi-infinite homogenous medium and assuming the motion of light scatterers can be characterized by a pseudo-Brownian motion [35,37,38]. Fitting was conducted for ρ = 2 cm and using the dynamic μa measurements obtained by B-NIRS. A constant value for μ_s' of 8 cm−1 was used in accordance with recent literature [39]. Fitting each autocorrelation curve provided an index of cerebral blood flow (CBFi).

3.3.5 Statistical Analysis

All data are presented as mean ± standard deviation (range) unless otherwise noted. Since the tapping duration varied between procedures, the perfusion, oxygen saturation, and metabolic data collected for each VT were temporally normalized to the average tap duration to obtain mean time courses. For pre- and post-VT statistics, data were limited to two minutes prior to needle insertion and following needle removal to avoid motion artifacts. To assess the overall change in CBFi, StO_2, and oxCCO due to a VT, a one-tailed paired t-test was used to compare pre- and post-VT measurements. Potential outliers were identified as points greater than q3 + w × (q3 − q1) or less than q1 – w × (q3 − q1) in the box plots, where w represents the whisker length and q indicates the quartile number. Statistics were repeated excluding any outliers. A matched pairs power analysis was conducted using the G*Power 3 software (v3.1.9.7, Düsseldorf, Germany) to calculate the

total sample size required to achieve significance [40]. Statistical significance was based on a p-value < 0.05; power was set to 0.8.

3.4 Results

Optical measurements were acquired during 14 ventricular taps across four patients (one female, three males, gestational age 25.0 to 37.6 weeks, mean = 29.2 ± 5.6 weeks). Data from four events were excluded due to excessive patient motion. A further three B-NIRS datasets were excluded due to ambient light contamination. DCS data acquired during these periods were not impacted and remained in the analysis. A total of 10 ventricular taps were analyzed for CBFi, and seven for StO_2 and oxCCO. Clinical parameters are displayed in Table 3.1.

Table 3-1: Clinical parameters for post-hemorrhagic ventricular dilatation (PHDV) patients.

Gestational age at birth (weeks)	29.2 ± 5.6 (25–37 4/7)
Birth weight (g)	1259.0 ± 746.7 (810–2376)
Sex (n)	F = 1, M = 3
Apgar 1 min	3.8 (1–8)
Number of VT performed (n)	7.8 (5–10)
Age at first VT (weeks)	3.8 ± 2.1 (2.3–7)
EVD (n)	2
VP shunt (n)	3
IVH Grade: Bilateral III	2
IVH Grade: III (R)/ IV (L)	1
IVH Grade: Bilateral IV	1

EVD, external ventricular drain; VP ventriculoperitoneal; IVH, intraventricular hemorrhage.

Infants were monitored continuously throughout the ventricular tap, spanning needle insertion and CSF drainage. Ventricular tap duration varied across the interventions with an average duration of 16.1 ± 7.7 min (range: 8.75 to 29.25 min). Average time courses of

CBFi, StO_2, and oxCCO during the tapping procedure are displayed in Figure 3.3.

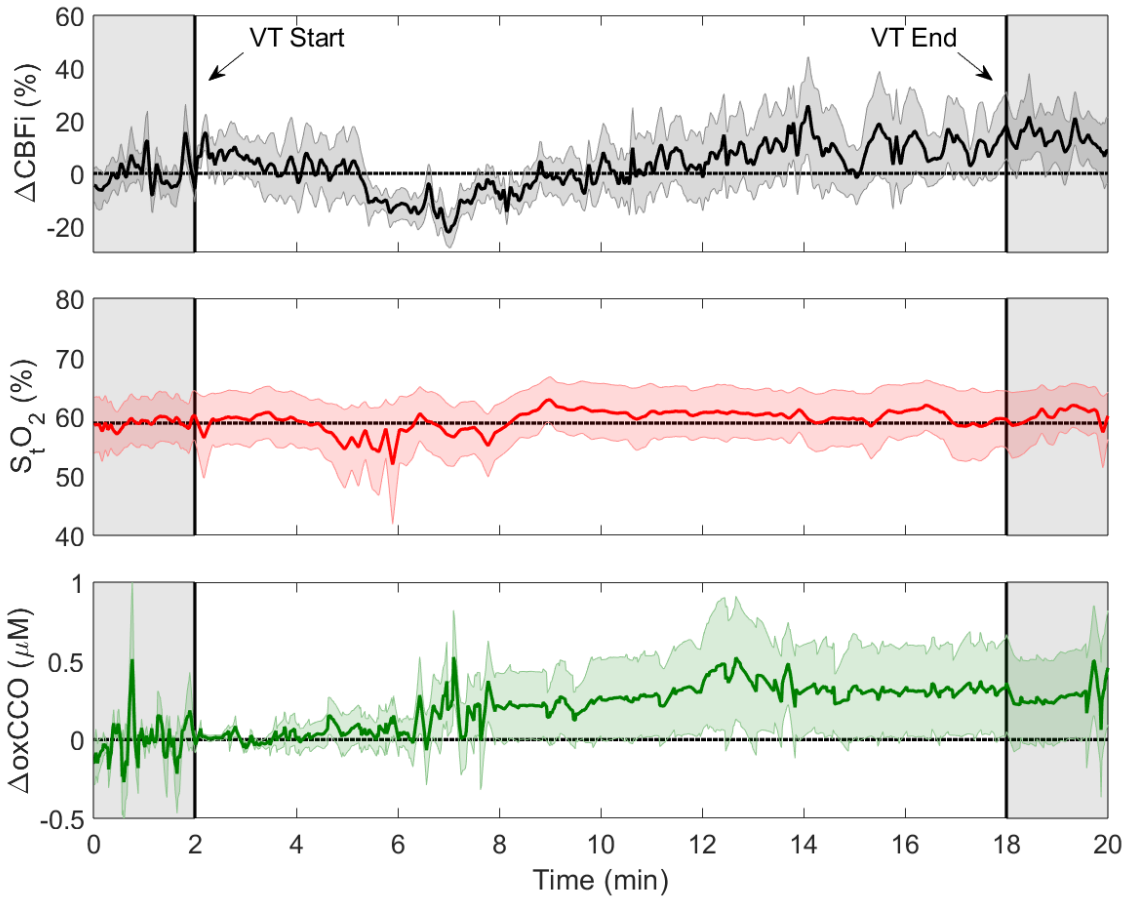

Figure 3.3: Change in cerebral blood flow index (ΔCBFi, n = 10), tissue saturation (StO_2, n = 7), and change in oxidation state of cytochrome c oxidase (ΔoxCCO, n = 7) averaged across multiple trials over the course of ventricular taps (VT). Data were temporally normalized to the averaged tap duration (16 min) and aligned to VT start and end points. Each time course is displayed with its standard error (shaded background).

The grey shaded regions in Figure 3.3 surrounding the CSF drainage period represent the intervals used to calculate average pre- and post-VT values. Figure 3.4 presents the changes in CBFi and oxCCO relative to baseline and pre- and post-VT StO_2 values. The outliers indicated on the plot borders corresponded to ΔCBFi changes of 122.0% and −25.0%, and ΔoxCCO of 1.7 μM. Averaged values are displayed in Table 3-2 along with t-test and power analysis results. Significance was not met for any of the parameters. Power analysis

indicated that sample sizes of 29 and 18 for ΔCBFi and ΔoxCCO, respectively, would be required to achieve significance. A significant increase was found for both ΔCBFi and ΔoxCCO if outliers were excluded.

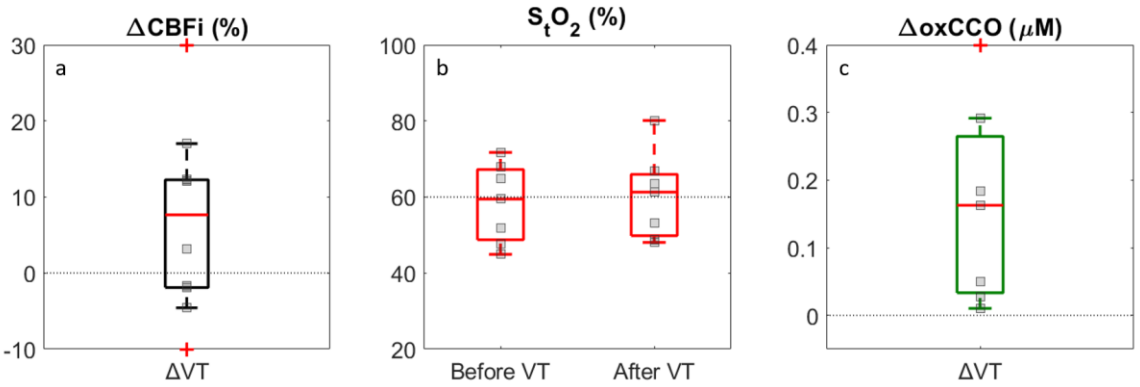

Figure 3.4: Boxplots showing changes in CBFi (a) and oxCCO (c) following ventricular tap and S_tO_2 (b) before and after the tap. Results are based on the difference between pre- and post-VT measurements that were averaged over 2-min periods. Individual data points are displayed; outliers are indicated by the crosses on the borders and represent ΔCBFi values of 122% and −25% and ΔoxCCO of 1.7 μM.

Table 3-2: Average changes following VT relative to baseline, t-test, and power analysis.

Statistical parameter	ΔCBFi (%)	ΔS_tO_2 (%)	ΔoxCCO (μM)
Average change	14.6 ± 37.6	1.9 ± 4.9	0.4 ± 0.6
p-value	0.09	0.20	0.09
Required sample size for significance[1]	29	45	18
Average change excluding outliers	6.0 ± 7.7	-	0.1 ± 0.1
p-value excluding outliers	0.05	-	0.02

3.5 Discussion

The purpose of this study was to implement the recently developed Neonatal NeuroMonitor (NNeMo) to assess cerebral hemodynamics and metabolism during ventricular taps in patients with post-hemorrhagic ventricular dilatation. Compared with commercial NIRS

devices that focus on monitoring StO_2, the goal of implementing NNeMo was to assess the direct impact of a VT on CBF, as measured by DCS, and cerebral oxygen metabolism, as determined by monitoring oxCCO with B-NIRS. Both methods provide continuous recordings, which enabled CBFi and oxCCO to be monitored throughout the tapping procedure (Figure 3.3).

In hydrocephalus, decreases in cerebral perfusion are expected to precede changes in metabolism and clinical symptoms [41]. In agreement with this concept, reductions in CBF have been shown to impact metabolism only when CBF drops below a certain threshold [27,42]. During a VT, as the ventricle volume and ICP decrease, perfusion is expected to improve. The possibility of concurrent changes in metabolism would therefore depend on the extent to which CBF is improved by the VT. A large increase in oxCCO following a VT would suggest that the mitochondria were oxygen-limited prior to the procedure, implying that the intervention could have been performed earlier [43]. In this study, it was anticipated that a VT would improve CBF, but the magnitude of the perfusion increase would likely not be sufficient to have an effect on oxCCO. Following 10 VTs, a non-significant increase was found in ΔCBFi ($14.6 \pm 37.6\%$, $p = 0.09$) and ΔoxCCO (0.4 ± 0.6 μM, $p = 0.09$), while little change was observed in ΔStO_2 ($1.9 \pm 4.9\%$, $p = 0.2$). Power analysis indicated that achieving significance for these relatively small increases would require a sample size of 29 for ΔCBFi and 18 for ΔoxCCO. Removing the outliers in the ΔCBFi ($n = 2$) and ΔoxCCO ($n = 1$) datasets did result in significant increases in both parameters; however, the average changes remained small ($6.0 \pm 7.7\%$ for ΔCBFi and 0.1 ± 0.1 μM for ΔoxCCO).

Several studies have investigated the potential impact of CSF drainage on cerebral hemodynamics in PHVD patients. An increase in CBF velocity was found by Doppler ultrasound across seven patients [44], and stable oxCCO, as measured by NIRS, in 23 infants receiving a VT or lumbar puncture (LP) [45]. In an earlier study, Casaer et al. reported that oxCCO increased in infants with grade 3 or 4 IVH who received an LP if patients had clinical signs of elevated ICP (i.e., increased head circumference, bulged fontanel, $n = 4$), but not if these symptoms were absent ($n = 4$) [46,47]. Similarly, elevated cerebral oxygenation has been reported during cerebrospinal fluid removal, which was

interpreted as evidence of increased CBF [45,48,49]. Previous work by our group measured absolute CBF and the cerebral metabolic rate of oxygen ($CMRO_2$) before and following a VT using dynamic contrast-enhanced NIRS [14]. A significant increase in CBF (15.6%) across 20 VTs was found with no change in $CMRO_2$. In general, evidence of increased CBF following CSF removal has been consistent across studies. The lack of a metabolic response can be explained by the modest perfusion increase, indicating that the reduction in CBF prior to the VT was not sufficient to impede oxygen delivery [18,31]. The results of the current study complement these findings as the average increases in CBFi and oxCCO were small and only reached significance after removing outliers. It is important to note that the technologies used across studies to monitor cerebral perfusion and oxygen metabolism are quite different, yet the findings are similar.

Compared with McLachlan et al. [14], the use of the hybrid B-NIRS/DCS system had the advantages of not requiring an injection of an exogenous contrast agent to assess cerebral perfusion and metabolism and providing continuous monitoring of these parameters throughout the tapping procedure. The combination of B-NIRS and DCS in NNeMo was achieved using a multiplexing shutter system to prevent crosstalk between the two techniques. The intensity of the light from the DCS laser is large enough to easily saturate the B-NIRS spectrometer, which impedes its ability to detect the relatively small spectral features of oxCCO. Conversely, broadband light from the B-NIRS light source is highly incoherent, which can degrade the temporal correlation of dynamic light scattering used by DCS to measure CBFi [50]. These issues can be overcome by cycling data acquisition between the two techniques. In this study, a sample rate of 4 Hz for both systems with an overall cycling time of 7 s was considered sufficient, given the procedure was between 10 to 30 min in duration. It should be noted, however, that the multiplexing shutter system has the flexibility to achieve higher temporal resolutions if required. Both systems are capable of sampling rates up to 10 Hz, which could be used for instance to capture blood flow pulsatility [28]. The minimum cycling time would be on the order of 300 ms, accounting for shutter opening and closing times of less than 50 ms [51]. Alternately, truly simultaneous measurements could be achieved using optical filters to selectively block B-NIRS and DCS light sources from the opposing detectors. Recent works describing hybrid

B-NIRS/DCS and time-resolved NIRS/DCS systems utilizing bandpass and notch filters have been proposed [50,52,53].

In this clinical application, the two major sources of signal contamination were motion artifacts and ambient light. Maintaining adequate probe contact with the scalp was challenging on infants with PHVD as the head is distended due to the enlarged ventricles. As CSF is drained during a VT, head circumference decreases, which can loosen the straps holding the probes to the head. To mitigate this issue, the probes were placed on the forehead above the frontoparietal cortex, where there is minimal change in head circumference. In addition, the elastic property of the strap used to hold the probes in place helped maintain good contact throughout the procedure. To minimize motion artifacts, an NICU nurse gently restrained the patient's head during the VT. Other sources of motion were the repositioning of the infant in the cot for needle insertion and the application of pressure to the head after the needle was retracted (Figure 3.2). As a result, data analysis was limited to 2-min windows immediately prior to and following the VT. This short period prevented monitoring for possible long-term changes after the VT, despite NNeMo's measurement stability over extended durations [27]. In three experiments, subjects were located in an environment with excessive ambient light, as reflected by greater dark count measurements acquired by B-NIRS. Since oxCCO only contributes approximately 10% of the total spectral signal [22], it was necessary to remove B-NIRS datasets in which the dark count was deemed excessive. In contrast, ambient light did not have the same impact on the DCS measurements due to the stronger intensity of the laser and therefore these datasets were included in the analysis.

Another potential source of error with optical neuromonitoring methods is the effect of scalp contamination. The influence of the scalp is considerably less in infants compared with adults, and within this study its effects were mitigated using appropriate source-detector distances for B-NIRS (SDD = 3 cm) and DCS (SDD = 2 cm) [54]. An additional source of signal contamination unique to hydrocephalus is possible light loss in the enlarged ventricle as the cortical mantle becomes increasingly thin. Our group demonstrated that this effect could distort absorption spectra as the thickness of the cortical mantle approaches 1 cm [14]. This likely did not have a significant effect on the CBFi

measurements since the SDD was 2 cm. The NIRS spectra were, however, acquired with SDD = 3 cm, which would increase the chance of light loss in the ventricles. The excellent agreement in mean baseline StO_2 values from the current and previous study – 58.4 ± 9.7% compared to 58.9 ± 2.7% from reference [14] – indicates that cortical thickness did not have a significant effect.

Future work will investigate a potential correlation of hemodynamic changes with subsequent markers of brain injury. Comparison to clinical outcomes has the potential to establish clinical thresholds of perfusion/metabolic change and could aid in describing VT efficacy or in gauging brain injury severity during the progression of PHVD.

3.6 Conclusion

In summary, this feasibility study presents an optical system capable of providing real-time monitoring of cerebral perfusion and oxygen metabolism in the NICU. In this application, cerebral blood flow and metabolic changes monitored throughout VTs were small and only reached significance after removing outliers. These results are in good agreement with previous studies. Considering that the hybrid optical system is portable and completely non-invasive, it is well suited for neuromonitoring in PHVD patients who may be suspected of larger cerebral hemodynamic changes based on clinical symptoms.

3.7 Acknowledgements

The authors would like to acknowledge the newborns and their families who participated in the study and thank Gemma Bale for help in implementing the UCLn algorithm. Funding: Canadian Institutes of Health Research (CGP-14171) and National Scientific and Engineering Research Council (CHRP 478470).

3.8 References

1. Highlights of 2010–2011 Selected Indicators Describing the Birthing Process in Canada. Can. Inst. Heal. Inf. 2012, 1–10. Available online: https://secure.cihi.ca/estore/productSeries.htm?pc=PCC226 (accessed on 10/7/2020).

2. Volpe, J.J. Brain injury in premature infants: A complex amalgam of destructive and developmental disturbances. Lancet Neurol. 2009, 8, 110–124.

3. Lin, P.Y, Hagan, K, Fenoglio, A, Grant, P.E, Franceschini, M.A. Reduced cerebral blood flow and oxygen metabolism in extremely preterm neonates with low-grade germinal matrix- intraventricular hemorrhage. Sci. Rep. 2016, 6, 25903.

4. Bassan, H. Intracranial Hemorrhage in the Preterm Infant: Understanding It, Preventing It. Clin. Perinatol. 2009, 36, 737–762.

5. Cherian, S, Whitelaw, A, Thoresen, M, Love, S. The Pathogenesis of Neonatal Post-hemorrhagic Hydrocephalus. Brain Pathol. 2006

6. Klinger, G, Osovsky, M, Boyko, V, Sokolover, N, Sirota, L, Lerner-Geva, L, Reichman, B. Risk factors associated with post-hemorrhagic hydrocephalus among very low birth weight infants of 24–28 weeks gestation. J. Perinatol. 2016, 36, 557–563.

7. Christian, E.A, Jin, D.L, Attenello, F, Wen, T, Cen, S, Mack, W.J, Krieger, M.D, McComb, J.G. Trends in hospitalization of preterm infants with intraventricular hemorrhage and hydrocephalus in the United States, 2000–2010. J. Neurosurg. Pediatr. 2016, 17, 260–269.

8. Cizmeci, M.N, de Vries, L.S, Ly, L.G, van Haastert, I.C, Groenendaal, F, Kelly, E.N, Traubici, J, Whyte, H.E, Leijser, L.M. Periventricular Hemorrhagic Infarction in Very Preterm Infants: Characteristic Sonographic Findings and Association with Neurodevelopmental Outcome at Age 2 Years. J. Pediatr. 2020, 217, 79–85.

9. Brouwer, M.J, de Vries, L.S, Groenendaal, F, Koopman, C, Pistorius, L.R, Mulder, E.J.H, Benders, M.J.N.L. New Reference Values for the Neonatal Cerebral Ventricles. Radiology 2012, 262.

10. De Vries, L.S, Groenendaal, F, Liem, K.D, Heep, A, Brouwer, A.J, Van'T Verlaat, E, Benavente-Fernández, I, Van Straaten, H.L, Van Wezel-Meijler, G, Smit, B.J, et al. Treatment thresholds for intervention in posthaemorrhagic

ventricular dilation: A randomised controlled trial. Arch. Dis. Child. Fetal Neonatal Ed. 2019, 104(1).

11. Cizmeci, M.N, Khalili, N, Claessens, N.H.P, Groenendaal, F, Liem, K.D, Heep, A, Benavente-Fernández, I, van Straaten, H.L.M, van Wezel-Meijler, G, Steggerda, S.J, et al. Assessment of Brain Injury and Brain Volumes after Posthemorrhagic Ventricular Dilatation: A Nested Substudy of the Randomized Controlled ELVIS Trial. J. Pediatr. 2019, 208, 191-197.

12. Leijser, L.M, Miller, S.P, Van Wezel-Meijler, G, Brouwer, A.J, Traubici, J, Van Haastert, I.C, Whyte, H.E, Groenendaal, F, Kulkarni, A.V, Han, K.S, et al. Posthemorrhagic ventricular dilatation in preterm infants When best to intervene? Neurology 2018, 90(8).

13. Lo, M, Kishimoto, J, Eagleson, R, Bhattacharya, S, de Ribaupierre, S. Does ventricular volume affect the neurodevelopmental outcome in infants with intraventricular hemorrhage? Child's Nerv. Syst. 2020, 36, 569–575.

14. McLachlan, P.J, Kishimoto, J, Diop, M, Milej, D, Lee, D.S.C, de Ribaupierre, S, St. Lawrence, K. Investigating the effects of cerebrospinal fluid removal on cerebral blood flow and oxidative metabolism in infants with post-hemorrhagic ventricular dilatation. Pediatr. Res. 2017, 82, 634–641.

15. Kishimoto, J, Fenster, A, Lee, D.S.C, de Ribaupierre, S. Quantitative 3-D head ultrasound measurements of ventricle volume to determine thresholds for preterm neonates requiring interventional therapies following posthemorrhagic ventricle dilatation. J. Med. Imaging 2018, 5(2).

16. Polito, A, Ricci, Z, Di Chiara, L, Giorni, C, Iacoella, C, Sanders, S.P, Picardo, S. Cerebral blood flow during cardiopulmonary bypass in pediatric cardiac surgery: The role of transcranial Doppler—A systematic review of the literature. Cardiovasc. Ultrasound 2006, 4, 47.

17. Baker, W.B, Balu, R, He, L, Kavuri, V.C, Busch, D.R, Amendolia, O, Quattrone, F, Frangos, S, Maloney-Wilensky, E, Abramson, K, et al. Continuous non-

invasive optical monitoring of cerebral blood flow and oxidative metabolism after acute brain injury. J. Cereb. Blood Flow Metab. 2019, 39(8), 1469-1485.

18. Diop, M, Kishimoto, J, Toronov, V, Lee, D.S.C, St. Lawrence, K. Development of a combined broadband near-infrared and diffusion correlation system for monitoring cerebral blood flow and oxidative metabolism in preterm infants. Biomed. Opt. Express 2015, 6, 3907-3918.

19. Chock, V.Y, Variane, G.F.T, Netto, A, Van Meurs, K.P. NIRS improves hemodynamic monitoring and detection of risk for cerebral injury: Cases in the neonatal intensive care nursery. J. Matern. Neonatal Med. 2020, 33, 1802–1810,.

20. Bale, G, Taylor, N, Mitra, S, Sudakou, A, de Roever, I, Meek, J, Robertson, N, Tachtsidis, I. Near-Infrared Spectroscopy Measured Cerebral Blood Flow from Spontaneous Oxygenation Changes in Neonatal Brain Injury. In Oxygen Transport to Tissue XLI; Ryu, P.-D., LaManna, J.C., Harrison, D.K., Lee, S.-S., Eds, Springer International Publishing: Cham, Switzerland, 2020; pp. 3–9, ISBN 978-3-030-34461-0.

21. Kewin, M, Rajaram, A, Milej, D, Abdalmalak, A, Morrison, L, Diop, M, St Lawrence, K. Evaluation of hyperspectral NIRS for quantitative measurements of tissue oxygen saturation by comparison to time-resolved NIRS. Biomed. Opt. Express 2019, 10, 4789–4802.

22. Bale, G, Elwell, C.E, Tachtsidis, I. From Jöbsis to the present day: A review of clinical near-infrared spectroscopy measurements of cerebral cytochrome-c-oxidase. J. Biomed. Opt. 2016, 21(9).

23. Buckley, E.M, Parthasarathy, A.B, Grant, P.E, Yodh, A.G, Franceschini, M.A. Diffuse correlation spectroscopy for measurement of cerebral blood flow: Future prospects. Neurophotonics 2014, 1(1), 011009.

24. He, L, Baker, W.B, Milej, D, Kavuri, V.C, Mesquita, R.C, Busch, D.R, Abramson, K, Jiang, Y.J, Diop, M, St Lawrence, K, et al. Noninvasive continuous optical monitoring of absolute cerebral blood flow in critically ill adults. Neurophotonics 2018, 5(4), 045006.

25. Pham, T, Tgavalekos, K, Sassaroli, A, Blaney, G, Fantini, S. Quantitative measurements of cerebral blood flow with near-infrared spectroscopy. Biomed. Opt. Express 2019, 10, 2117.

26. Durduran, T, Zhou, C, Buckley, E.M, Kim, M.N, Yu, G, Choe, R, Gaynor, J.W, Spray, T.L, Durning, S.M, Mason, S.E, et al. Optical measurement of cerebral hemodynamics and oxygen metabolism in neonates with congenital heart defects. J. Biomed. Opt. 2010, 15, 037004.

27. Rajaram, A, Bale, G, Kewin, M, Morrison, L.B, Tachtsidis, I, St. Lawrence, K, Diop, M, Lawrence, K. St, Diop, M. Simultaneous monitoring of cerebral perfusion and cytochrome c oxidase by combining broadband near-infrared spectroscopy and diffuse correlation spectroscopy. Biomed. Opt. Express 2018, 9, 2588–2603.

28. Wang, D, Parthasarathy, A.B, Baker, W.B, Gannon, K, Kavuri, V, Ko, T, Schenkel, S, Li, Z, Li, Z, Mullen, M.T, et al. Fast blood flow monitoring in deep tissues with real-time software correlators. Biomed. Opt. Express 2016, 7(3), 776-797.

29. Khalid, M, Milej, D, Rajaram, A, Abdalmalak, A, Morrison, L, Diop, M, St. Lawrence, K. Development of a stand-alone DCS system for monitoring absolute cerebral blood flow. Biomed. Opt. Express 2019, 10(9), 4607-4620.

30. Diop, M, Wright, E, Toronov, V, Lee, T.-Y, St Lawrence, K. Improved light collection and wavelet de-noising enable quantification of cerebral blood flow and oxygen metabolism by a low-cost, off-the-shelf spectrometer. J. Biomed. Opt. 2014, 19, 057007.

31. Arora, R, Ridha, M, Lee, D.S.C, Elliott, J, Rosenberg, H.C, Diop, M, Lee, T.Y, St. Lawrence, K. Preservation of the metabolic rate of oxygen in preterm infants during indomethacin therapy for closure of the ductus arteriosus. Pediatr. Res. 2013, 73, 713–718.

32. Wyatt, J.S, Cope, M, Delpy, D.T, Richardson, C.E, Edwards, A.D, Wray, S, Reynolds, E.O. Quantitation of cerebral blood volume in human infants by near-infrared spectroscopy. J. Appl. Physiol. 1990, 68, 1086–1091.

33. Duncan, A, Meek, J.H, Clemence, M, Elwell, C.E, Tyszczuk, L, Cope, M, Delpy, D. Optical pathlength measurements on adult head, calf and forearm and the head of the newborn infant using phase resolved optical spectroscopy. Phys. Med. Biol. 1995, 40, 295–304.

34. Essenpreis, M, Elwell, C.E, Cope, M, van der Zee, P, Arridge, S.R, Delpy, D.T. Spectral dependence of temporal point spread functions in human tissues. Appl. Opt. 1993, 32, 418.

35. Verdecchia, K, Diop, M, Morrison, L.B, Lee, T.-Y, St. Lawrence, K. Assessment of the best flow model to characterize diffuse correlation spectroscopy data acquired directly on the brain. Biomed. Opt. Express 2015, 6, 4288.

36. Lemieux, P.-A, Durian, D.J. Investigating non-Gaussian scattering processes by using nth -order intensity correlation functions. J. Opt. Soc. Am. A 1999, 16(7), 1651-1664.

37. Cheung, C, Culver, J.P, Takahashi, K, Greenberg, J.H, Yodh, A.G. In vivo cerebrovascular measurement combining diffuse near-infrared absorption and correlation spectroscopies. Phys. Med. Biol. 2001, 46(8), 2053-2065,.

38. Verdecchia, K, Diop, M, Lee, T.-Y, St. Lawrence, K. Quantifying the cerebral metabolic rate of oxygen by combining diffuse correlation spectroscopy and time-resolved near-infrared spectroscopy. J. Biomed. Opt. 2013, 18(2), 27007.

39. Milej, D, He, L, Abdalmalak, A, Baker, W.B, Anazodo, U.C, Diop, M, Dolui, S, Kavuri, V.C, Pavlosky, W, Wang, L, et al. Quantification of cerebral blood flow in adults by contrast-enhanced near-infrared spectroscopy: Validation against MRI. J. Cereb. Blood Flow Metab. 2019, 40(8).

40. Faul, F, Erdfelder, E, Lang, A.-G, Buchner, A. G*Power 3: A flexible statistical power analysis program for the social, behavioral, and biomedical sciences. Behav. Res. Methods 2007, 39, 175–191.

41. Richards, H.K, Bucknall, R.M, Jones, H.C, Pickard, J.D. Uncoupling of LCBF and LCGU in two different models of hydrocephalus: A review. Child's Nerv. Syst. 1995, 11, 288–292.

42. Cooper, J.A, Tichauer, K.M, Boulton, M, Elliott, J, Diop, M, Arango, M, Lee, T.-Y, St Lawrence, K. Continuous monitoring of absolute cerebral blood flow by near-infrared spectroscopy during global and focal temporary vessel occlusion. J. Appl. Physiol. 2011, 110, 1691–1698.

43. Bale, G, Mitra, S, Roever, I. De; Sokolska, M, Price, D, Bainbridge, A, Gunny, R, Uria-avellanal, C, Kendall, G.S, Meek, J, et al. Oxygen dependency of mitochondrial metabolism indicates outcome of newborn brain injury. 2018 39(10), 2035-2047.

44. Hopman, J.C, Klaessens, J.H, Feuth, T, Sengers, R.C, Liem, K.D. Cerebral hemodynamics and oxygenation after serial CSF drainage in infants with PHVD. Brain Dev. 2007, 29, 623–629.

45. Soul, J.S, Eichenwald, E, Walter, G, Volpe, J.J, Du Plessis, A.J. CSF Removal in Infantile Posthemorrhagic Hydrocephalus Results in Significant Improvement in Cerebral Hemodynamics. Pediatr. Res. 2004, 55, 872–876.

46. Casaer, P, Siebenthal, K, van der Vlugt, A, Lagae, L, Devlieger, H. Cytochrome aa3 and Intracranial Pressure in Newborn Infants; A Near Infrared Spectroscopy Study. Neuropediatrics 1992, 23, 111–111.

47. Von Siebenthai, S.K, Van Der Vlugt, A, Devlieger, H, Casaer, P. Effect of Changes in Intracranial Pressure on Cytochrome aa3 (Cytaa3) and haemoglobinvolume (Hbvol): A Near Infrared Spectroscopy (NIRS). Pediatr. Res. 1992, 32, 612.

48. Norooz, F, Urlesberger, B, Giordano, V, Weninger, M, Berger, A, Olischar, M. Decompressing posthaemorrhagic ventricular dilatation significantly improves regional cerebral oxygen saturation in preterm infants. Acta Pædiatrica. 2015, 104, 663–669.

49. Bembich, S, Cont, G, Bua, J, Paviotti, G, Demarini, S. Pediatric Neurology Cerebral Hemodynamics During Neonatal Cerebrospinal Fluid Removal. Pediatr. Neurol. 2019, 94, 70–73,.

50. Rajaram, A, St. Lawrence, K, Diop, M. Development of a hybrid broadband NIRS/diffusion correlation spectroscopy system to monitor preterm brain injury. In Advanced Biomedical and Clinical Diagnostic and Surgical Guidance Systems XV. 2017, SPIE Proceedings Volume 10054.

51. Diop, M, Elliott, J.T, Tichauer, K.M, Lee, T.Y, St. Lawrence, K. A broadband continuous-wave multichannel near-infrared system for measuring regional cerebral blood flow and oxygen consumption in newborn piglets. Rev. Sci. Instrum. 2009, 80, 54302.

52. Milej, D, Shahid, M, Abdalmalak, A, Rajaram, A, Diop, M, St. Lawrence, K. Characterizing Dynamic Cerebral Vascular Reactivity using a Hybrid System Combining Time-Resolved Near-Infrared and Diffuse Correlation Spectroscopy. Biomed. Opt. Express 2020, 11(8), 4571-4585.

53. Giovannella, M, Contini, D, Pagliazzi, M, Pifferi, A, Spinelli, L, Erdmann, R, Donat, R, Rocchetti, I, Rehberger, M, König, N, et al. BabyLux device: A diffuse optical system integrating diffuse correlation spectroscopy and time-resolved near- infrared spectroscopy for the neuromonitoring of the premature newborn brain. Neurophotonics 2019, 6(2).

54. Milej, D, Rajaram, A, Abdalmalak, A, Khalid, M, Shahid, M, Kewin, M, St. Lawrence, K. Assessing Extracerebral Signal Contamination in Optical Measurements of Cerebral Blood Flow and Oxygenation. In Clinical and Preclinical Optical Diagnostics II. 2019, SPIE Proceedings Volume 11074.

Chapter 4

4 Monitoring cerebral hemodynamic, oxygenation and metabolic stability in premature infants following birth using a hybrid broadband NIRS/DCS optical brain monitor

This chapter features unpublished work in preparation for submission by Ajay Rajaram, Daniel Milej, Lilian Kebaya, Matthew Kewin, Lawrence C. M. Yip, Marianne Suwalski, Sandrine de Ribaupierre, Soume Bhattacharya, Mamadou Diop, and Keith St. Lawrence.

4.1 Introduction

As the perinatal period is a time of rapid neurodevelopment, a shortened gestation leaves an immature and fragile cerebrovascular system vulnerable to damage that can lead to long-term cognitive dysfunction or life-long disability [1]. Premature birth is defined as a gestational age (GA) less than 37 weeks and has shown to strongly correlate with the development of adverse neurological outcomes, such as cognitive and behavioural deficits, and more severe disorders, such as cerebral palsy. [2–4]. The duration of gestation and an infant's weight at birth are factors that influence the likelihood of adverse effects. Clinical management (e.g. thermoregulation, respiratory management, etc.) during the first few days following birth have proven critical in improving short and long-term outcome [5,6].

A common brain injury associated with preterm birth is intraventricular hemorrhaging (IVH), which is characterized by bleeding in the germinal matrix and surrounding white matter. IVH has been found to occur in 20-25% of preterms born with very low birth weights (VLBW, <1500 g) and most commonly appears within the first 72 hours following birth [7]. The pathogenesis behind IVH is multifactorial. However, contributing factors include an unstable cerebral blood flow (CBF), resulting from an underdeveloped cerebrovascular system, and having a limited ability to adequately perfuse distal white-matter regions [8]. This is exacerbated by the absence of intact cerebral autoregulation (CA; i.e., the ability to maintain constant CBF during changes in blood pressure). In addition, the premature brain likely has a minimal tolerance to reductions in CBF due to the lower basal values compared to adults [9]. Diagnosis of IVH is achieved through

imaging with cranial ultrasound (cUS) to visually assess and grade cerebral hemorrhages at the bedside. In most centers, standard practice calls for imaging within the first week of life and again within the first month [10]. A major drawback is that cUS is not a prognostic technique as it can only indicate damage that has already occurred.

Recent work has demonstrated the value of optical devices to non-invasively monitor physiological precursors of brain injury. Near-infrared spectroscopy (NIRS) utilizes light in the near-infrared spectral range to determine cerebral tissue saturation (StO_2) by quantifying hemoglobin concentrations. Commercial NIRS devices have been utilized to demonstrate the value of StO_2 as a biomarker of cerebral hemodynamic stability in the premature brain [11–14]. Notably, the SafeBoosC Phase II randomized clinical trial found that neuromonitoring using NIRS within the first 72 hours resulted in a significantly reduced burden of hypoxia [15]. While StO_2 has become an accessible and robust marker of cerebral oxygenation, the development of diffuse correlation spectroscopy (DCS) offers a non-invasive approach to directly monitor CBF [16]. The index of cerebral blood flow (CBFi) obtained by DCS has been validated against numerous gold-standard techniques, such as arterial spin labelling MRI [17–21] and transcranial doppler ultrasound [22], and it has proven useful in monitoring neonatal populations during various developmental stages and clinical interventions. For example, CBF has been monitored in preterm infants during the first six weeks of life and has shown to positively correlate with postmenstrual age [23,24].

A measure of cerebral hemodynamics alone is likely insufficient for describing the risk of injury since sufficient oxygen delivery can be maintained despite fluctuations in CBF due to compensatory changes in the oxygen extraction fraction (OEF) [25,26]. If changes in CBF are significant or persistent enough to exceed this compensatory mechanism, the cerebral energy metabolism will be negatively impacted. Substantial drops in metabolism often lead to cell death and subsequent tissue damage [27]. Recent work using broadband NIRS (B-NIRS) to quantify light absorption over the NIR spectrum has allowed for robust measurements of cytochrome c oxidase (CCO), a direct marker of cerebral oxidative metabolism [28]. CCO is an enzyme in the mitochondria’s electron transport chain vital to cellular energy production through oxidative phosphorylation. In the final step of this

process, CCO becomes oxidized, which contributes to an electrochemical gradient driving energy production. Similar to hemoglobin, changes in light absorption from the oxidation state of CCO (oxCCO) can be quantified by B-NIRS. Changes in oxCCO during anoxia events have shown to correlate severity of injury in animal models [29] and, in term infants with hypoxic-ischemic encephalopathy, oxCCO has shown indicative of outcome [30].

NNeMo (Neonatal NeuroMonitor) is an in-house built hybrid B-NIRS/DCS device capable of continuous bedside monitoring of cerebral perfusion and metabolism, via the marker oxCCO. With a concurrent measure of metabolism, more physiological context can be given to CBF monitoring by describing both oxygen supply and its impact on utilization. This study aims to demonstrate NNeMo's ability to characterize CBF and metabolic stability within the first 72 hours of life in infants with an increased risk of developing IVH (i.e., < 32 weeks GA and/or weighing < 1500 g). It is hypothesized that only significant changes in CBF will impact metabolism. With a simultaneous acquisition of perfusion and metabolism, the interrelationship of these metrics can be investigated and could provide insight on hemodynamic instability during early brain development, the presence/absence of CA, and potential links to the onset of IVH.

4.2 Materials and Methods

4.2.1 Patient Population

This study was approved by the Western University Health Sciences Research Ethics Board, which adheres to the guidelines of the Canadian Tri-Council Policy Statement: Ethical Conduct for Research Involving Humans. Subjects recruitment for this study was conducted in the neonatal intensive care unit at the Children's Hospital, London Health Sciences Center. Following parental consent, infants born less than 32 weeks GA and/or weighing less than 1500 g were enrolled in the study and monitored for two six-hour periods within the first 72-hours of life. The first period was conducted as soon as clinically feasible following birth and resuscitation and the second at 48 hours post-natal age (PNA). During each monitoring period, cUS was performed to diagnose cerebral hemorrhaging, which was graded according to the Papile scale [31].

4.2.2 Study Design

Once transferred to the NICU from the birthing suite, following acquisition of vitals by nursing staff, the optical probes were secured to the scalp above the frontoparietal cortex using a 3-D printed probe holder and adjustable strap (Figure 4.1, A). The optical fibers were bent 90° at the point of contact on the head for ease of use, and the optical prober holder was designed to be light, flexible and non-abrasive (Figure 4.1, B; 5×2×1 cm; Flexible Resin, Form 2, Formlabs, Somerville, MA, USA). The design of the probe holder enabled it to be used with infants requiring ventilation with continuous positive airway pressure (CPAP) as it could be positioned under the CPAP cap and tube. The infant's eyes were shielded using phototherapy eye goggles as a precaution. Two optical fibers (B-NIRS and DCS sources) directed light to the head, while a third (common detection) collected diffusely reflected light. The source-detector distance (SDD) was 3 cm for B-NIRS and 2 cm for DCS. A smaller distance was chosen for DCS as it is inherently more sensitive to the brain [32]. Light source power levels and spot size incident on the scalp were adjusted to meet ANSI standards for skin exposure. Following the monitoring period, the probe holder was removed and the skin immediately under was assessed for redness or irritation. This workflow was repeated for the second day monitoring session.

Figure 4.1: A) Premature infant with optical probes secured to the forehead and phototherapy eye shield, B) schematic of probe holder with NIRS (3-cm SDD) and DCS (2-cm SDD) optical fibers with the common detection fiber shaded; probe holder dimensions: 5×2×1 cm.

4.2.3 Instrumentation

NNeMo is a multimodal optical device that combines B-NIRS and DCS. It incorporates a multiplexing shuttering system to cycle between acquisitions from the two subsystems; the details are described elsewhere [33,34]. For this study, NIRS and DCS data were each acquired at sampling frequency of 4 Hz in consecutive 3-s intervals, resulting in full data sets every 7 s (with a 0.5-s dead-time between techniques). For B-NIRS, a 20-W halogen bulb (Hl-2000-HP, Ocean Optics, Delay Beach, FL, USA), filtered from 600 to 1000 nm, and a spectrometer (iDus 420, Andor, Oxford Instruments, Abingdon, UK; 548–1085 nm bandwidth; 1.65 nm resolution; P&P Optica, Waterloo, ON, Canada) were employed. An optical fiber bundle (2.4 mm diameter, 30 µM core, 0.55 numerical aperture (NA), Loptek, Berlin, Germany) directed light towards the subject, while a second set of fibers (three linearly aligned 2 mm diameter fibers, 30 µm core, 0.55 NA, Loptek, Berlin, Germany) collected light interrogating tissue. The DCS light source was a long-coherence laser (DL785-100s, CrystaLaser, Reno, NV, USA) and a four-channel single-photon counting module (SPCM-AQR-15-FC, Excelitas Technologies, Montreal, QC, Canada) was used for detection. A DCS emission fiber (4 × 200 µm core diameter, 0.22 NA, Loptek, Berlin, Germany) and a single-mode detection fiber (8 µm core diameter, 0.12 NA, Loptek, Berlin, Germany) directed light towards and collected light from the scalp. A PCIe-6612 data acquisition board collected the SPCM output which was processed using in-house developed software (LabVIEW, MATLAB) [35,36].

4.2.4 Data Analysis

4.2.4.1 Quantifying StO_2 and ΔoxCCO by B-NIRS

Each monitoring period began by measuring a dark signal, which was determined by taking a measurement with the emission source turned off. A reference measurement was collected prior to monitoring to characterize the spectral properties of the instrumentation. The reference spectrum and the dark signal measurement were incorporated into the analysis of measured light reflectance spectra. A derivative spectroscopy approach was applied to reflectance spectra to quantify hemoglobin and water concentrations, while accounting for light scatter contributions [26,37]. The first and second derivatives of

reflectance spectra were fit to a solution of the diffusion approximation for a semi-infinite homogeneous medium. A multi-parameter minimization fitting algorithm was utilized to estimate the tissue water fraction, hemoglobin concentrations (oxy-, HbO_2, and deoxy-hemoglobin, Hb), and optical properties [38]. Baseline cerebral tissue oxygen saturation ($StO_2{}^b$) was determined from the corresponding hemoglobin concentrations:

$$StO_2{}^b = \frac{HbO_2{}^b}{Hb^b + HbO_2{}^b} \tag{4.1}$$

A modified Beer-Lambert Law approach based on the UCLn algorithm was utilized to determine time-varying changes in the concentrations of HbO_2, Hb, and oxCCO [28].

$$\begin{bmatrix} \Delta HbO_2(t) \\ \Delta Hb(t) \\ \Delta oxCCO(t) \end{bmatrix} = \frac{1}{DP} \begin{bmatrix} \varepsilon_{HbO_2}(\lambda_1) & \varepsilon_{Hb}(\lambda_1) & \varepsilon_{oxCCO}(\lambda_1) \\ \vdots & \vdots & \vdots \\ \varepsilon_{HbO_2}(\lambda_1) & \varepsilon_{Hb}(\lambda_1) & \varepsilon_{oxCCO}(\lambda_1) \end{bmatrix}^{-1} \times \begin{bmatrix} \Delta A(\lambda_1, t) \\ \vdots \\ \Delta A(\lambda_n, t) \end{bmatrix} \tag{4.2}$$

where Δ denotes a change relative to baseline concentration, DP is the differential pathlength (set to 4.9 based on previous literature [39,40]), ε is the molar extinction coefficient of each chromophore, and A is the measured change in attenuation. Changes in hemoglobin were calibrated using absolute values measured at baseline with the derivative approach to provide continuous quantification of StO_2. Metabolic changes were represented by absolute changes in the concentration of oxCCO.

4.2.4.2 Monitoring CBF by DCS

To determine the cerebral blood flow index (CBFi), measured normalized intensity autocorrelation data were converted to electric field autocorrelation data using the Siegert relation [16,41]:

$$g_2(\rho, \tau) = 1 + \beta \frac{|G_1(\rho,\tau)|^2}{\langle I(\rho,\tau)\rangle^2}, \tag{4.3}$$

where $g_2(\rho,\tau)$ represents the measured normalized intensity autocorrelation as a function of SDD and time (ρ,τ), $G_1(\rho,\tau)$ is the electric field autocorrelation function, $\langle I(\rho,\tau)\rangle$ is the average intensity, and β is the coherence factor. G_1 was fit with the solution to the diffusion approximation for a semi-infinite homogenous medium while assuming pseudo-Brownian motion of light scatterers [42,43]. The fitting was performed by incorporating changes in

the absorption coefficient determined by B-NIRS and a constant scattering coefficient of 8 cm^{-1} [44]. All CBFi estimates were normalized to their respective baseline value to generate a time series of relative changes in CBF.

4.2.5 Data Post-processing and Statistical Analysis

Time courses of StO_2, CBFi, and oxCCO were filtered as a function of frequency using an inverse wavelet transform with a Morlet wavelet (cwt MATLAB function) [45–47]. This approach has been applied for time-frequency analysis of similar patient populations [48,49]. To isolate relevant physiological frequencies, high ($f > 0.01$ Hz) and low ($f < 0.001$ Hz) frequencies were removed. Next, time courses for each parameter were corrected for motion artifacts using an algorithm utilizing a moving standard deviation and spline interpolation [50,51].

Absolute StO_2 measures as well as the standard deviation of CBFi and oxCCO values were compared across day one and day three monitoring periods. The relationship between saturation and perfusion was investigated to assess differences between these metabolic markers. Both StO_2 and CBFi were also compared to oxCCO measures to characterize the impact of hemodynamic changes on metabolism. Comparisons were made by analyzing correlations between CBFi/StO_2, CBFi/oxCCO, and StO_2/oxCCO and calculating coherence and semblance across the frequency range (0.001-0.01 Hz). A measure of coherence characterizes the strength of the relationship between variables, ranging from 0 to 1, while semblance describes the phase difference, ranging from -1 (antiphase) to 1 (in phase) [48]. Coherence and semblance for all three combinations of optical measures were compared across patients for both monitoring periods.

For data displayed in boxplots, statistical outliers were determined as points greater than $q3 + w \times (q3 - q1)$ or less than $q1 - w \times (q3 - q1)$ where q is the quartile number and w is the whisker length. All data are presented as mean ± standard deviation (range) unless otherwise noted. Statistical analyses were conducted using a statistical toolbox (MATLAB) and significance was defined as $p < 0.05$. A paired t-test was used to investigate differences in measurements across days. In addition, regression analysis was conducted to assess the relationships between CBFi, StO_2 and oxCCO within a single day. A one-way repeated-

measures analysis of variance was used to investigate differences in average coherence and semblance values obtained from data measured in each subject across both monitoring periods.

4.3 Results

Optical data were acquired in nine infants on the first and third days of life (6 male, 3 female, GA 28 ± 2 weeks, range: 24 weeks, 5 days to 31 weeks, one day). The first monitoring period began on average at 5.9 ± 6.2 hours after birth (range: 1 to 18 hours) and the second at 53.8 ± 8.2 hours (range: 44.5 to 61 hours). Data from the first subject were excluded due to excessive ambient light that resulted in substantial signal artifacts. For subsequent acquisitions, the optical probes were covered at the site of contact using a thin blanket to reduce signal from ambient light. This was confirmed by quantifying the spectrometer's intensity output with the light source turned off. Data from the remaining eight infants are reported in this work. Optical data acquired during significant patient handling (e.g. vital signs, patient repositioning) or clinical intervention (e.g. x-ray, US imaging) were omitted to avoid motion artifacts. On average, 233 ± 68 minutes (range: 145 to 340 minutes) of data were analyzed on day one and 254 ± 36 minutes (range: 210 to 290 minutes) on day three. Clinical parameters of patients enrolled are displayed in Table 4-1.

Table 4-1: Patient demographics and clinical metrics.

Gestational age at birth (weeks + days)	28 ± 2 (24+5 – 31+1)
Birth weight (g)	1123 ± 344
Sex (n)	5 M; 3 F
Apgar score 5 min	6.4 ± 3.2 (1 – 9)
Apgar score 10 min	8.3 ± 1.0 (7 – 9)
Monitoring start time on day 1 (hours)	5.9 ± 6.2 (1 – 18)
IVH diagnosis (n, grade)	1, Grade II right/Grade I left

Optical parameters (StO_2, ΔCBFi, and ΔoxCCO) were analyzed over the duration of the monitoring period. An example of time courses obtained from one patient are displayed in

Figure 4.2. In this dataset, a clear discrepancy is noted between CBFi values during the first and third day of life. Large fluctuations in ΔCBFi were found during the first monitoring period compared to the second. For StO_2 and ΔoxCCO time courses, smaller differences were observed across days.

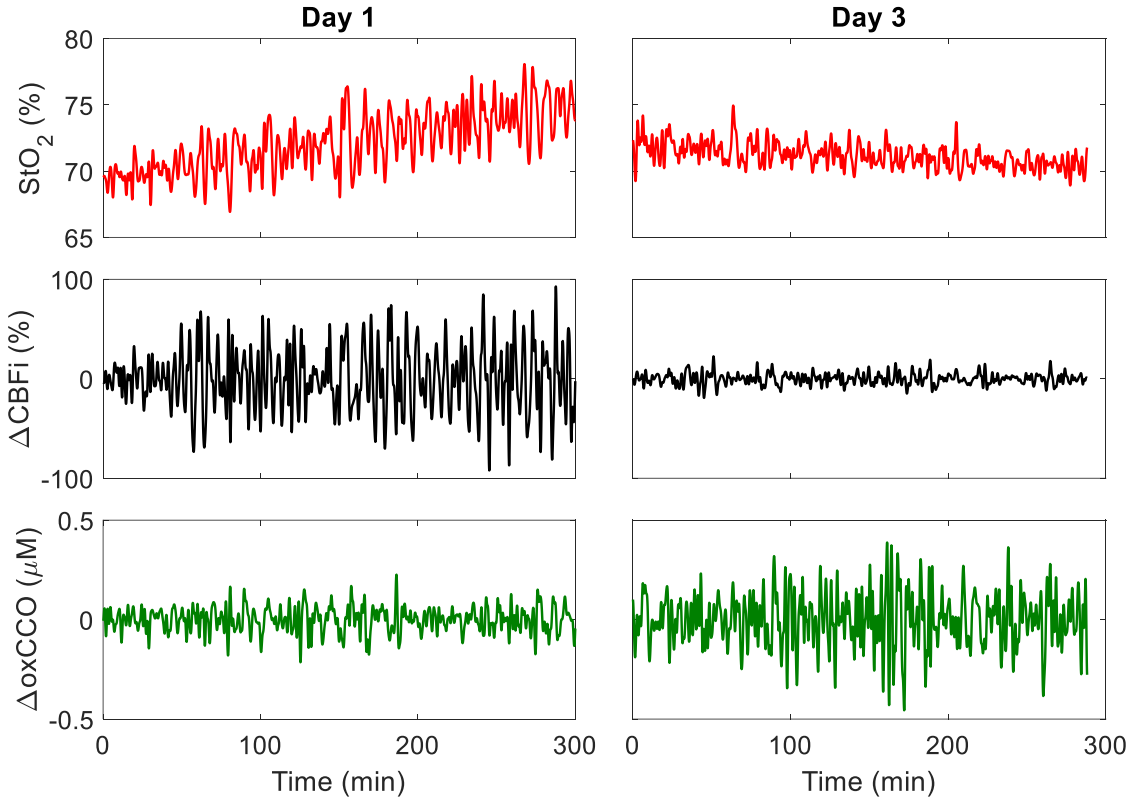

Figure 4.2: Cerebral tissue saturation (StO_2), change in cerebral blood flow index (ΔCBFi), and change in oxidation state of cytochrome c oxidase (ΔoxCCO) of a subject on the first (A) and third (B) day of life.

To illustrate the stability of time courses obtained in all subjects, absolute StO_2 and the standard deviation of ΔCBFi and ΔoxCCO across both days are presented in Figure 4.3. Mean StO_2 was 73.9 ± 11.6% on the first day of life and 79.7 ± 5.9% on the third day. For relative ΔCBFi and ΔoxCCO measures, the standard deviation of time courses across monitoring periods were found to decrease from 11.5 to 7.9% and 0.7 to 0.5 µM, respectively; however, these changes were not statistically significant. While a trend is apparent in StO_2 and σCBFi values across days, much smaller changes were observed in

σoxCCO. As oxCCO is measured as an absolute change, it is necessary to provide context to characterize the extent of these fluctuations.

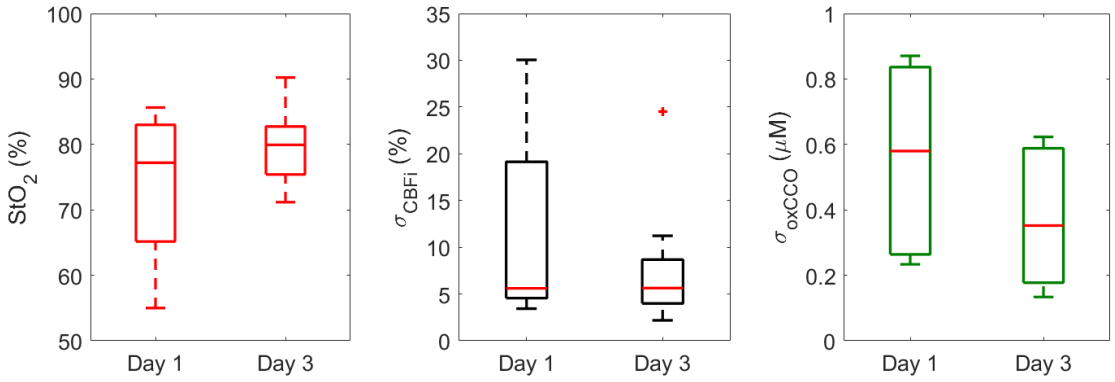

Figure 4.3: StO_2, standard deviation of ΔCBFi , and standard deviation of ΔoxCCO during day 1 and day 3; statistical outliers are indicated by +.

For each subject, time courses of optical metrics were analyzed using an inverse wavelet transform to describe prevalent frequencies over the monitoring period. Figure 4.4 depicts the heat maps for the same infant featured in Figure 4.2. A notable frequency band around 0.004 Hz was apparent in the CBFi data on day 1 and is highlighted for illustration purposes only. By day 3, this oscillation was no longer present. A similar but less pronounced effect was observed in the StO_2 data that also dissipated by day 3. No oscillations were evident in the corresponding oxCCO data.

Figures 4.5 and 4.6 display the coherence and semblance between optical parameters for the same subject featured above. In both cases, there was notable coherence and semblance only in the CBFi/StO_2 relationship on day 1, which was less prominent on day 3.

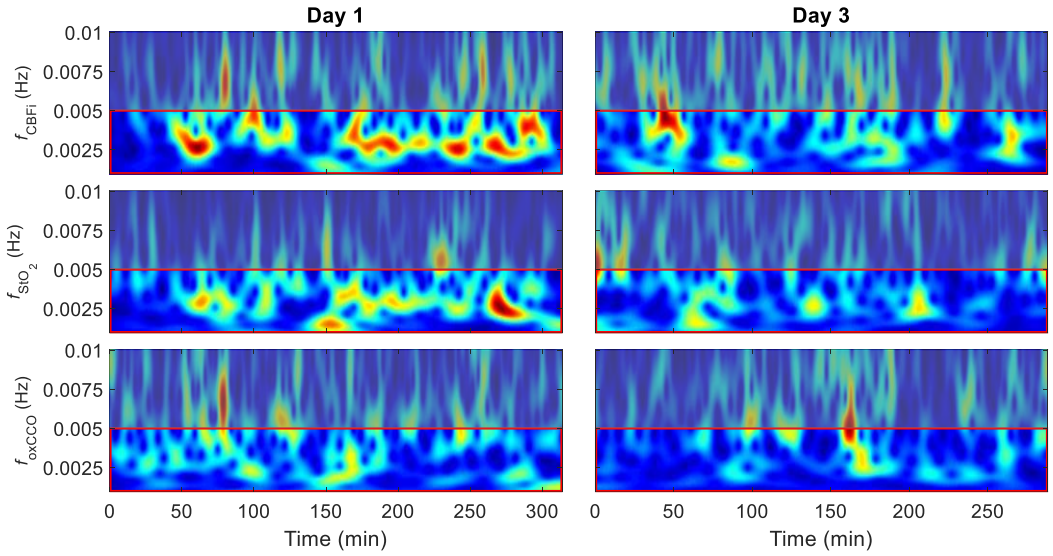

Figure 4.4: Frequency analysis of cerebral tissue saturation (StO_2), cerebral blood flow index (CBFi), and oxidation state of cytochrome c oxidase (oxCCO) on the first (A) and third (B) day of life for one subject. The highlighted region isolates a notable frequency band.

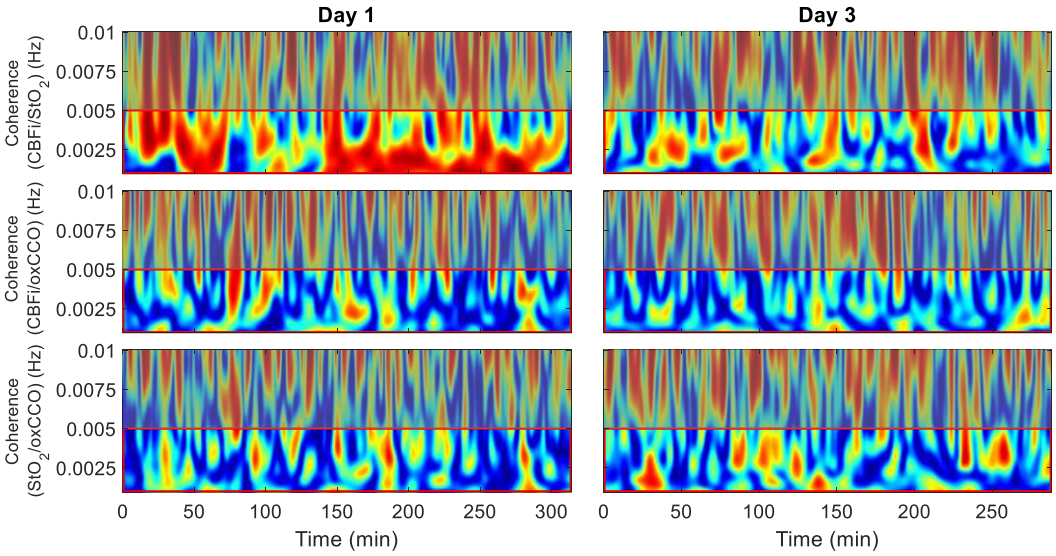

Figure 4.5: Coherence of cerebral tissue saturation (StO_2), cerebral blood flow index (CBFi), and oxidation state of cytochrome c oxidase (oxCCO) on the first (A) and third (B) day of life for one subject.

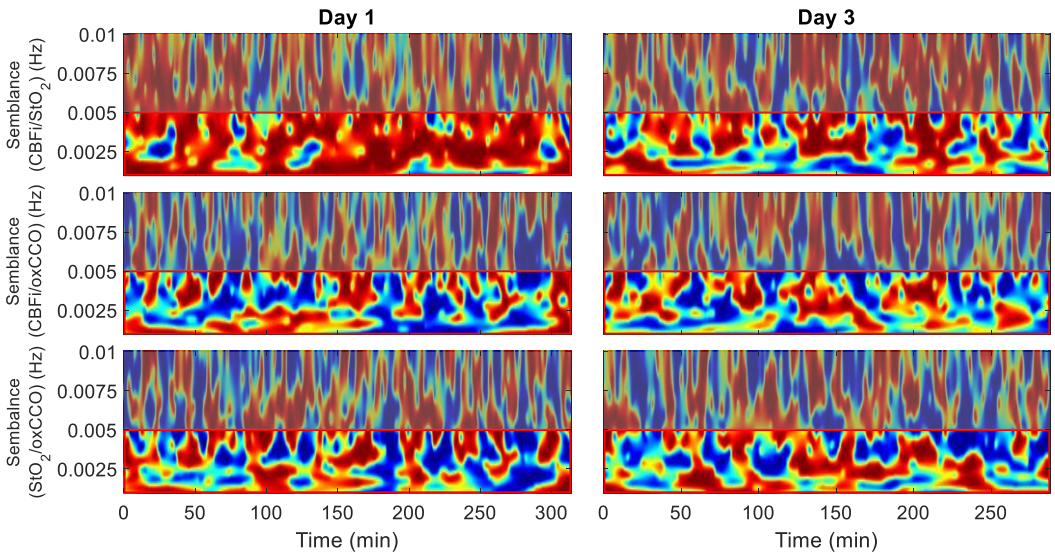

Figure 4.6: Semblance of cerebral tissue saturation (StO_2), cerebral blood flow index (CBFi), and oxidation state of cytochrome c oxidase (oxCCO) on the first (A) and third (B) day of life for one subject.

Coherence and semblance measurements across all subjects are depicted in boxplots in Figure 4.7. A significant difference was found between coherence of CBFi/StO_2 compared to coherence of CBFi/oxCCO on day 1. Semblance of CBFi/StO_2 was significantly different from the two semblances that included the metabolic marker oxCCO (i.e., CBFi/oxCCO and StO_2/oxCCO) on both days.

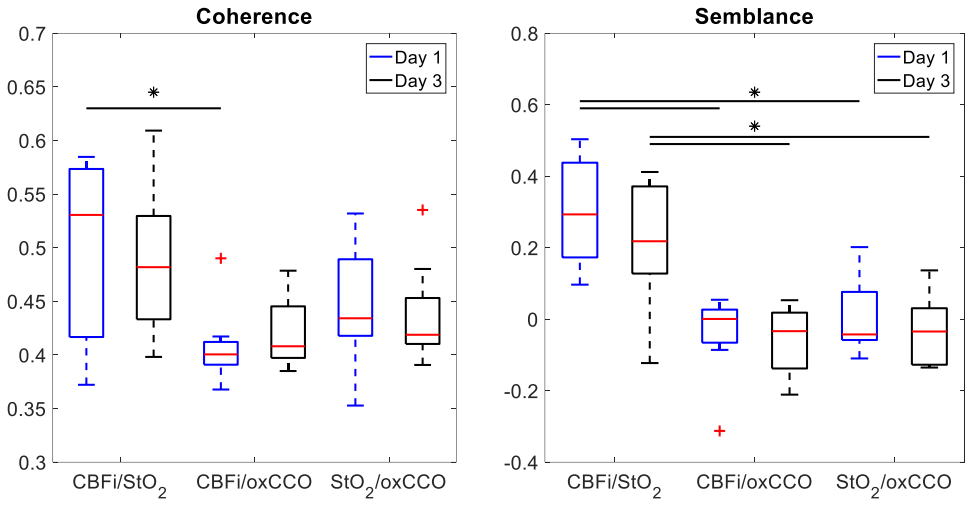

Figure 4.7: Boxplot showing coherence and semblance in all parameters across both measurement days; statistical outliers are indicated by +.

4.4 Discussion

This study demonstrated the ability to monitor cerebral perfusion and metabolism concurrently in preterms infants within the first critical 72 h of life. Numerous practical challenges exist in monitoring premature infants so soon after birth. First, many births that occur at this gestation are sudden or emergencies, which poses a challenge for patient recruitment and obtaining consent. Clinical and research teams must communicate closely to identify potential study participants and commence monitoring. Infants admitted to the NICU are not only at risk of adverse neurological development, many have complications with respiration, circulation, temperature control, or a number of other potential ailments, which all require some form of intervention. As such, the period immediately following birth has many events likely to produce artifacts in optical data from ambient light or motion (e.g. phototherapy, imaging, patient handling). While each infant in this study was monitored for 6 hours at a time, only 65% and 70% of the data sets on average were usable on days one and three, respectively.

NNeMo provided continuous measures of StO_2, CBFi, and oxCCO. These metrics each provide a different perspective in terms of characterizing early brain development. Work by Kissak et al. monitored OEF using NIRS in VLBW infants during the first three post-

natal days and reported significant fluctuations in OEF in infants with IVH [52]. However, NIRS measurements of StO_2 and OEF alone have shown limited use as surrogate markers of cerebral metabolism [53]. For example, a study monitoring premature infants following administration of indomethacin (vasoconstrictor) for treatment of patent ductus arteriosus found statistically significant decreases in CBF and corresponding significant increases in the OEF. Despite these changes, no notable difference in cerebral metabolism was reported [25]. It is therefore more useful to combine NIRS measures of oxygen content with CBF and metabolic information to provide a more wholistic understanding of hemodynamic fluctuations and their impact on energy production. A study by Noori et al monitored StO_2 using NIRS and CBF with Doppler ultrasound in extremely premature infants during the first three days of life [54]. This work reported a lower StO_2 and an increased OEF in infants who developed IVH compared to those who did not. The IVH group also experienced a notable difference in cerebral hemodynamics; a fluctuating CBF was observed and attributed to a hypoperfusion-reperfusion cycle that preceded the onset of hemorrhaging. By adding a measure of metabolism, the impact of these fluctuations in CBF could be further investigated and related to tissue viability and potential injury.

In our study, a large range of StO_2 values as well as an increased standard deviation of CBFi was found during the first day of life compared to the third (Figure 4.3). Much smaller changes were observed in the standard deviation of oxCCO across the monitoring periods. This implies that hemodynamic fluctuations were not significant enough to impede energy metabolism. To place the oxCCO measure in context, animal experiments conducted in adult rats estimate that the absolute concentration of CCO to be between 4.5 and 5.5 µM [27,55]. As metabolism in this animal model is higher than in humans, this value should be considered an upper limit [28]. Furthermore, the total concentration of CCO in neonates is likely less than the adult brain. Compared to the 0.7 µM standard deviation in oxCCO observed on day much larger changes in oxCCO have been observed in animal models prior to hypoxic ischemic injury [34] and following seizures in term infants [56].

Frequency analysis using an inverse wavelet transform was implemented to characterize the stability of optical parameters. Frequencies were limited between 0.001 – 0.01 Hz to

isolate physiologically relevant signals [48,49]. Figure 4.4 illustrates the data from one patient. For this infant, a consistent oscillation in CBFi and StO_2 was observed only on day one. By day three, a change in frequency components in this signal (i.e., a more balanced distribution of fast and slow frequencies) left no disenable pattern. No prevailing frequency was observed for metabolic measures. This observation was made for several subjects in the study, as reflected in Figure 4.3.

To compare the interrelationship between saturation, perfusion, and metabolism, the coherence and semblance for each pair was calculated. Figures 4.5 and 4.6 depict these relationships for the same subject featured in Figure 4.2. Analyzing these metrics over all subjects resulted in a significantly different coherence of CBFi/StO_2 (Figure 4.7, A) from CBFi/oxCCO on day one. Similarly, CBFi/StO_2 semblance was significantly higher than CBFi/oxCCO and StO_2/oxCCO relationships on both monitoring periods (Figure 4.7, B). In the healthy brain, a distinction between CBF and metabolic measures is expected, as metabolism is heavily regulated and is largely independent [57]. A measure of metabolic reactivity therefore has the potential to better characterize the impact of impaired CA on the preterm brain. This relationship was shown to predict outcome in term infants with hypoxic-ischemic encephalopathy as validated by metabolic measures of Lac/NAA levels, using magnetic resonance spectroscopy, and a one-year neurodevelopmental outcome check [48]. Within premature infants, CA is known to be frequently impaired; however, in this work no significant relationship between metabolism and other optical measures was observed, implying sufficient energy production. Fluctuations in StO_2 and CBF had a negligible influence on oxCCO measures.

In this study, only one subject was diagnosed with IVH and this scan took place prior to optical monitoring on day 1. Due to this timing and the small sample size, no distinction could be made between hemodynamic/metabolic instability and the onset of a bleed. In addition, this study is limited in the amount of time monitored. Data from approximately four hours was compared on the first and third day of life. Since CBFi is a relative measure and oxCCO represents a change in concentration, trends in flow and metabolism could not be compared across monitoring periods. Instead, data analysis focused on comparing the standard deviations, as a marker of stability, within each monitoring period. Future work

seeks to monitor changes continuously for the first 72 hours of life to better characterize changes over this entire period. While frequency analysis provided valuable insight to the relationship between hemodynamics and metabolism, a larger cohort is required to determine if changes in oxCCO can be linked to IVH. Furthermore, NNeMo does not provide any spatial resolution, having only a single B-NIRS/DCS interrogation site, and therefore can only infer local changes. The one subject diagnosed with IVH experienced a bilateral bleed (Grade II, right, Grade I, left). With the current system, discerning any difference in hemodynamics across these two sites is not possible. Additional source-detector pairs could allow for hemispheric/regional monitoring.

4.5 Conclusion

This study demonstrates the feasibility of simultaneous bedside monitoring of cerebral perfusion and metabolism following premature birth using a hybrid optical system combining broadband-NIRS and DCS. Perfusion and metabolic stability on the first and third day of life was demonstrated using frequency analysis with an inverse wavelet transform. Prevalent oscillations in StO_2 and ΔCBFi present on day one diminished by day three. No accompanying changes were noted in ΔoxCCO. Coherence and semblance analysis of optical parameters found a notable relationship between CBFi/StO_2 only on the first day while measures of metabolism were independent. Monitoring dynamic changes in cerebral perfusion and its potential influence on metabolism could provide a clearer indication of the impact of autoregulation in the newborn brain, sufficient energy production, and tissue viability. Optical measures have potential as prognostic markers of tissue damage and timely detection of injury could allow for corrective patient management and improved clinical outcome.

4.6 Acknowledgements

The authors would like to acknowledge the bedside nurses and clinicians who aided in patient recruitment and thank the newborns and their families who participated in the study. Funding: Canadian Institutes of Health Research (CGP-14171) and National Scientific and Engineering Research Council (CHRP 478470).

4.7 References

1. E. P. Davis, C. Buss, L. T. Muftuler, K. Head, A. Hasso, D. A. Wing, C. Hobel, and C. A. Sandman, "Children's brain development benefits from longer gestation," Front. Psychol. 2, (2011).

2. C. Nosarti, M. H. S. Al-Asady, S. Frangou, A. L. Stewart, L. Rifkin, and R. M. Murray, "Adolescents who were born very preterm have decreased brain volumes," Brain 125(7), 1616–1623 (2002).

3. A. L. Stewart, R. J. Thorburn, P. L. Hope, M. Goldsmith, A. P. Lipscomb, and E. O. R. Reynolds, "Ultrasound appearance of the brain in very preterm infants and neurodevelopmental outcome at 18 months of age," Arch. Dis. Child. 58(8), 598–604 (1983).

4. J. J. Volpe, "Brain injury in premature infants: a complex amalgam of destructive and developmental disturbances," Lancet 8(1), 110–124 (2009).

5. S. E. W. Croop, S. M. Thoyre, S. Aliaga, M. J. McCaffrey, and S. Peter-Wohl, "The Golden Hour: a quality improvement initiative for extremely premature infants in the neonatal intensive care unit," J. Perinatol. 40(3), 530–539 (2020).

6. D. Sharma, "Golden hour of neonatal life: Need of the hour," Matern. Heal. Neonatol. Perinatol. 3(1), 1–21 (2017).

7. H. Bassan, "Intracranial Hemorrhage in the Preterm Infant: Understanding It, Preventing It," Clin. Perinatol. 36(4), 737–762 (2009).

8. J. J. Volpe, H. C. Kinney, F. E. Jensen, and P. A. Rosenberg, "The developing oligodendrocyte: Key cellular target in brain injury in the premature infant," Int. J. Dev. Neurosci. 29(4), 423–440 (2011).

9. D. I. Altman, W. J. Powers, J. M. Perlman, P. Herscovitch, S. L. Volpe, and J. J. Volpe, "Cerebral blood flow requirement for brain viability in newborn infants is lower than in adults," Ann. Neurol. 24(2), 218–226 (1988).

10. H. J. McCrea and L. R. Ment, "The Diagnosis, Management and Postnatal Prevention of IVH in the Preterm neonate," Clin Perinatol 35(4), (2010).

11. G. Greisen, B. Andresen, A. M. Plomgaard, and S. Hyttel-Sørensen, "Cerebral oximetry in preterm infants: an agenda for research with a clear clinical goal," Neurophotonics 3(3), 031407 (2016).

12. M. Wolf and G. Greisen, "Advances in Near-Infrared Spectroscopy to Study the Brain of the Preterm and Term Neonate," Clin. Perinatol. 36(4), 807–834 (2009).

13. S. Hyttel-Sorensen, G. Greisen, B. Als-Nielsen, and C. Gluud, "Cerebral near-infrared spectroscopy monitoring for prevention of brain injury in very preterm infants," Cochrane Database Syst. Rev. 2017(9), (2017).

14. L. M. L. Dix, F. van Bel, and P. M. A. Lemmers, "Monitoring cerebral oxygenation in neonates: An update," Front. Pediatr. 5(March), 1–9 (2017).

15. A. M. Plomgaard, W. Van Oeveren, T. H. Petersen, T. Alderliesten, T. Austin, F. Van Bel, M. Benders, O. Claris, E. Dempsey, A. Franz, M. Fumagalli, C. Gluud, C. Hagmann, S. Hyttel-Sorensen, P. Lemmers, A. Pellicer, G. Pichler, P. Winkel, and G. Greisen, "The SafeBoosC II randomized trial: Treatment guided by near-infrared spectroscopy reduces cerebral hypoxia without changing early biomarkers of brain injury," Pediatr. Res. 79(4), 528–535 (2016).

16. T. Durduran and A. G. Yodh, "Diffuse correlation spectroscopy for non-invasive, microvascular cerebral blood flow measurement," Neuro 85(1), 51–63 (2014).

17. T. Durduran, R. Choe, W. B. Baker, and A. G. Yodh, "Diffuse optics for tissue monitoring and tomography," Reports Prog. Phys. 73(7), (2010).

18. S. A. Carp, G. P. Dai, D. A. Boas, M. A. Franceschini, and Y. R. Kim, "Validation of diffuse correlation spectroscopy measurements of rodent cerebral blood flow with simultaneous arterial spin labeling MRI; towards MRI-optical continuous cerebral metabolic monitoring," Biomed. Opt. Express 1(2), 553 (2010).

19. G. Yu, T. F. Floyd, T. Durduran, C. Zhou, J. Wang, J. A. Detre, and A. G. Yodh, "Validation of diffuse correlation spectroscopy for muscle blood flow with concurrent arterial spin labeled perfusion MRI," Opt. Express 15(3), 1064–1075 (2007).

20. V. Jain, E. M. Buckley, D. J. Licht, J. M. Lynch, P. J. Schwab, M. Y. Naim, N. A. Lavin, S. C. Nicolson, L. M. Montenegro, A. G. Yodh, and F. W. Wehrli, "Cerebral oxygen metabolism in neonates with congenital heart disease quantified by MRI and optics," J. Cereb. Blood Flow Metab. 34(3), 380–388 (2014).

21. D. A. Goff, E. M. Buckley, T. Durduran, J. Wang, and D. J. Licht, "Noninvasive cerebral perfusion imaging in high-risk neonates," Semin Perinatol. 34(1), 46–56 (2010).

22. E. M. Buckley, N. M. Cook, T. Durduran, M. N. Kim, C. Zhou, R. Choe, G. Yu, S. Schultz, C. M. Sehgal, D. J. Licht, P. H. Arger, M. E. Putt, H. H. Hurt, and A. G. Yodh, "Cerebral hemodynamics in preterm infants during positional intervention measured with diffuse correlation spectroscopy and transcranial Doppler ultrasound.," Opt. Express 17(15), 12571–12581 (2009).

23. N. Roche-labarbe, S. A. Carp, A. Surova, M. Patel, A. David, P. E. Grant, and M. A. Franceschini, "Noninvasive Optical Measures of CBV, StO_2, CBF Index, and rCMRO2 in Human Premature Neonates' Brains in the First Six Weeks of Life," Hum Brain Mapp 31(3), 341–352 (2010).

24. N. Roche-Labarbe, A. Fenoglio, A. Aggarwal, M. Dehaes, S. a. Carp, M. A. Franceschini, and P. E. Grant, "Near-infrared spectroscopy assessment of cerebral

oxygen metabolism in the developing premature brain," J. Cereb. Blood Flow Metab. 32(3), 481–488 (2012).

25. R. Arora, M. Ridha, D. S. C. Lee, J. Elliott, H. C. Rosenberg, M. Diop, T.-Y. Lee, and K. St Lawrence, "Preservation of the metabolic rate of oxygen in preterm infants during indomethacin therapy for closure of the ductus arteriosus.," Pediatr. Res. 73(6), 713–8 (2013).

26. M. Diop, J. Kishimoto, V. Toronov, D. S. C. Lee, and K. S. Lawrence, "Development of a combined broadband near-infrared and diffusion correlation system for monitoring cerebral blood flow and oxidative metabolism in preterm infants," Biomed. Opt. Express 6(10), 3907–3918 (2015).

27. C. E. Cooper, S. J. Matcher, J. S. Wyatt, M. Cope, G. C. Brown, E. M. Nemoto, and D. T. Delpy, "Near-infrared spectroscopy of the brain: Relevance to cytochrome oxidase bioenergetics," Biochem. Soc. Trans. 22(4), 974–980 (1994).

28. G. Bale, C. E. Elwell, and I. Tachtsidis, "From Jöbsis to the present day : a review of clinical near-infrared spectroscopy measurements of cerebral cytochrome-c-oxidase," J. Biomed. Opt. 21(9), (2016).

29. G. Bale, A. Rajaram, M. Kewin, L. Morrison, A. Bainbridge, M. Diop, K. S. Lawrence, and I. Tachtsidis, "Broadband NIRS Cerebral Cytochrome-C-Oxidase Response to Anoxia Before and After Hypoxic-Ischaemic Injury in Piglets," Oxyg. Transp. to Tissue XL 1072, 151–156 (2018).

30. G. Bale, S. Mitra, I. De Roever, M. Sokolska, D. Price, A. Bainbridge, R. Gunny, C. Uria-avellanal, G. S. Kendall, J. Meek, N. J. Robertson, and I. Tachtsidis, "Oxygen dependency of mitochondrial metabolism indicates outcome of newborn brain injury," J. Cereb. Blood Flow Metab. 39(10), 2035–2047 (2018).

31. S. Cherian, A. Whitelaw, M. Thoresen, and S. Love, "The pathogenesis of neonatal post-hemorrhagic hydrocephalus," Brain Pathol. 14(3), 305–311 (2004).

32. J. Selb, D. a. Boas, S.-T. Chan, K. C. Evans, E. M. Buckley, and S. a. Carp, "Sensitivity of near-infrared spectroscopy and diffuse correlation spectroscopy to brain hemodynamics: simulations and experimental findings during hypercapnia.," Neurophotonics 1(1), 015005 (2014).

33. A. Rajaram, L. C. M. Yip, D. Milej, M. Suwalski, M. Kewin, M. Lo, J. J. L. Carson, V. Han, S. Bhattacharya, M. Diop, S. de Ribaupierre, and K. St. Lawrence, "Perfusion and Metabolic Neuromonitoring during Ventricular Taps in Infants with Post-Hemorrhagic Ventricular Dilatation," Brain Sci. 10(7), 452 (2020).

34. A. Rajaram, G. Bale, M. Kewin, L. B. Morrison, I. Tachtsidis, K. St. Lawrence, and M. Diop, "Simultaneous monitoring of cerebral perfusion and cytochrome c oxidase by combining broadband near-infrared spectroscopy and diffuse correlation spectroscopy," Biomed. Opt. Express 9(6), 2588–2603 (2018).

35. M. Khalid, D. Milej, A. Rajaram, A. Abdalmalak, L. Morrison, M. Diop, and K. St. Lawrence, "Development of a stand-alone DCS system for monitoring absolute cerebral blood flow," Biomed. Opt. Express 10(9), 4607–4620 (2019).

36. D. Wang, A. B. Parthasarathy, W. B. Baker, K. Gannon, V. Kavuri, T. Ko, S. Schenkel, Z. Li, Z. Li, M. T. Mullen, J. A. Detre, and A. G. Yodh, "Fast blood flow monitoring in deep tissues with real-time software correlators," Biomed. Opt. Express 7(3), 776–797 (2016).

37. M. Kewin, A. Rajaram, D. Milej, A. Abdalmalak, L. Morrison, M. Diop, and K. St Lawrence, "Evaluation of hyperspectral NIRS for quantitative measurements of tissue oxygen saturation by comparison to time-resolved NIRS," Biomed. Opt. Express 10(9), 4789–4802 (2019).

38. M. Diop, E. Wright, V. Toronov, T.-Y. Lee, and K. St Lawrence, "Improved light collection and wavelet de-noising enable quantification of cerebral blood flow and oxygen metabolism by a low-cost, off-the-shelf spectrometer.," J. Biomed. Opt. 19(5), 057007 (2014).

39. J. S. Wyatt, M. Cope, D. T. Delpy, C. E. Richardson, A. D. Edwards, S. Wray, and E. O. R. Reynolds, "Quantitation of cerebral blood volume in human infants by near-infrared spectroscopy," J. Appl. Physiol. 68(3), 1086–1091 (1990).

40. A. Duncan, J. H. Meek, M. Clemence, C. E. Elwell, L. Tyszczuk, M. Cope, and D. Delpy, "Optical pathlength measurements on adult head, calf and forearm and the head of the newborn infant using phase resolved optical spectroscopy," Phys. Med. Biol. 40(2), 295–304 (1995).

41. P.-A. Lemieux and D. J. Durian, "Investigating non-Gaussian scattering processes by using nth -order intensity correlation functions," J. Opt. Soc. Am. 16(7), 1651–1664 (1999).

42. C. Cheung, J. P. Culver, K. Takahashi, J. H. Greenberg, and A. G. Yodh, "In vivo cerebrovascular measurement combining diffuse near-infrared absorption and correlation spectroscopies," Phys. Med. Biol. 46(8), 2053–2065 (2001).

43. K. Verdecchia, M. Diop, L. B. Morrison, T.-Y. Lee, and K. St. Lawrence, "Assessment of the best flow model to characterize diffuse correlation spectroscopy data acquired directly on the brain," Biomed. Opt. Express 6(11), 4288–4301 (2015).

44. D. Milej, L. He, A. Abdalmalak, W. B. Baker, U. C. Anazodo, M. Diop, S. Dolui, V. C. Kavuri, W. Pavlosky, L. Wang, R. Balu, J. A. Detre, O. Amendolia, F. Quattrone, W. A. Kofke, A. G. Yodh, and K. St Lawrence, "Quantification of cerebral blood flow in adults by contrast-enhanced near-infrared spectroscopy: Validation against MRI," J. Cereb. Blood Flow Metab. 40(8), (2020).

45. A. A. Mendelson, A. Rajaram, D. Bainbridge, K. S. Lawrence, T. Bentall, M. Sharpe, M. Diop, and C. G. Ellis, "Dynamic tracking of microvascular hemoglobin content for continuous perfusion monitoring in the intensive care unit: pilot feasibility study," J. Clin. Monit. Comput. (2020).

46. A. Grinsted, J. C. Moore, and S. Jevrejeva, "Application of the cross wavelet transform and wavelet coherence to geophysical time series," Nonlinear Process. Geophys. 11(5), 561–566 (2004).

47. M. Latka, M. Turalska, M. Glaubic-Latka, W. Kolodziej, D. Latka, and B. J. West, "Phase dynamics in cerebral autoregulation," Am. J. Physiol. - Hear. Circ. Physiol. 289(5), 2272–2279 (2005).

48. S. Mitra, G. Bale, D. Highton, R. Gunny, C. Uria-Avellanal, A. Bainbridge, M. Sokolska, D. Price, A. Huertas-Ceballos, G. S. Kendall, J. Meek, I. Tachtsidis, and N. J. Robertson, "Pressure passivity of cerebral mitochondrial metabolism is associated with poor outcome following perinatal hypoxic ischemic brain injury," J. Cereb. Blood Flow Metab. 39(1), 118–130 (2019).

49. M. D. Papademetriou, I. Tachtsidis, M. J. Elliot, A. Hoskote, and C. E. Elwell, "Multichannel near infrared spectroscopy indicates regional variations in cerebral autoregulation in infants supported on extracorporeal membrane oxygenation," J. Biomed. Opt. 17(6), (2012).

50. F. Scholkmann, S. Spichtig, T. Muehlemann, and M. Wolf, "How to detect and reduce movement artifacts in near-infrared imaging using moving standard deviation and spline interpolation," Physiol. Meas. 31(5), 649–662 (2010).

51. A. J. Metz, M. Wolf, P. Achermann, and F. Scholkmann, "A new approach for automatic removal of movement artifacts in near-infrared spectroscopy time series by means of acceleration data," Algorithms 8(4), 1052–1075 (2015).

52. C. M. Kissack, R. Garr, S. P. Wardle, and A. M. Weindling, "Postnatal changes in cerebral oxygen extraction in the preterm infant are associated with intraventricular hemorrhage and hemorrhagic parenchymal infarction but not periventricular leukomalacia," Pediatr. Res. 56(1), 111–116 (2004).

53. D. A. Boas and M. A. Franceschini, "Haemoglobin oxygen saturation as a biomarker: the problem and a solution," Philos. Trans. R. Soc. A Math. Phys. Eng. Sci. 369, 4407–4424 (2011).

54. S. Noori, M. McCoy, M. P. Anderson, F. Ramji, and I. Seri, "Changes in cardiac function and cerebral blood flow in relation to peri/intraventricular hemorrhage in extremely preterm infants.," J. Pediatr. 164(2), 264–70 (2014).

55. G. C. Brown, M. Crompton, and S. Wray, "Cytochrome oxidase content of rat brain during development," BBA - Bioenerg. 1057(2), 273–275 (1991).

56. S. Mitra, G. Bale, S. Mathieson, C. Uria-Avellanal, J. Meek, I. Tachtsidis, and N. J. Robertson, "Changes in cerebral oxidative metabolism during neonatal seizures following hypoxic-ischemic brain injury," Front. Pediatr. 4(83), (2016).

57. M. E. Raichle, R. L. Grubb, M. H. Gado, J. O. Eichling, and M. M. Ter-Pogossian, "Correlation Between Regional Cerebral Blood Flow and Oxidative Metabolism In Vivo Studies in Man," Arch Neurol. 33(8), 523–526 (1976).

Chapter 5

5 Optical monitoring of cerebral perfusion and metabolism in adults during cardiac surgery with cardiopulmonary bypass

This chapter has been adapted from the publication titled “Optical monitoring of cerebral perfusion and metabolism in adults during cardiac surgery with cardiopulmonary bypass” published in *Biomedical Optics Express* in 2020 by Ajay Rajaram, Daniel Milej, Marianne Suwalski, Lawrence C. M. Yip, Linrui R. Guo, Michael W. A. Chu, Jason Chui, Mamadou Diop, John M. Murkin, and Keith St. Lawrence, volume 11, issue 10.

5.1 Abstract

During cardiac surgery with cardiopulmonary bypass (CPB), adequate maintenance of cerebral blood flow (CBF) is vital in preventing postoperative neurological injury – i.e., stroke, delirium, cognitive impairment. Reductions in CBF large enough to impact cerebral energy metabolism can lead to tissue damage and subsequent brain injury. Current methods for neuromonitoring during surgery are limited. This study presents the clinical translation of a hybrid optical neuromonitor for continuous intraoperative monitoring of cerebral perfusion and metabolism in ten patients undergoing non-emergent cardiac surgery with non-pulsatile CPB. The optical system combines broadband near-infrared spectroscopy (B-NIRS) to measure changes in the oxidation state of cytochrome c oxidase (oxCCO) – a direct marker of cellular energy metabolism – and diffuse correlation spectroscopy (DCS) to provide an index of cerebral blood flow (CBFi). As the heart was arrested and the CPB-pump started, increases in CBFi (88.5 ± 125.7%) and significant decreases in oxCCO (−0.5 ± 0.2 μM) were observed; no changes were noted during transitions off CPB. Fifteen hypoperfusion events, defined as large and sustained reductions in CPB-pump flow rate, were identified across all patients and resulted in significant decreases in perfusion and metabolism when mean arterial pressure dropped to 30 mmHg or below. The maximum reduction in cerebral blood flow preceded the corresponding metabolic reduction by 18.2 ± 15.0 s. Optical neuromonitoring provides a safe and non-invasive approach to

assessing intraoperative perfusion and metabolism and has potential in guiding patient management to prevent adverse clinical outcome.

5.2 Introduction

Cardiopulmonary bypass (CPB) has become a cornerstone of cardiac surgery since its introduction in the 1950s. By taking over the physiological functions of the heart and lungs, CPB provides surgeons with an operating field unobstructed by blood and free of cardiac motion; however, there are numerous postoperative neurological complications associated, including cognitive dysfunction [1–3], delirium, and stroke [4–6]. During CPB, procedural changes in pump flow rate and unplanned fluctuations in cardiac output can produce variations in cerebral blood flow (CBF) [7]. Given the high metabolic demands of the brain and its reliance on a continuous supply of oxygen, changes in CBF that are large enough to impact cerebral metabolism could lead to tissue damage and subsequent brain injury.

There is currently no established method for intraoperative monitoring of CBF and cerebral metabolism during CPB. Traditionally, CBF was measured using Xenon-133, a discontinuous method that requires an invasive injection via the arterial circulation [8]. Transcranial Doppler (TCD) ultrasound has also been used to measure CBF in major cerebral arteries [9]; however, TCD embodies numerous drawbacks, including space limitations when utilizing a large transducer probe, inconsistent acoustic windows due to variations in thickness and porosity of the skull [10], and signal contamination from electrocautery used during surgery [11]. Optical techniques are becoming more prevalent for real-time monitoring due to their safety, low-cost, and ease of implementation [12]. Cerebral oximetry can continuously measure cerebral tissue saturation (StO_2) during surgery and provides valuable insight into cerebral hemodynamics but has proven insufficient for monitoring oxygen utilization [13–15]. More advanced optical methods of neuromonitoring have demonstrated the ability to measure microcirculatory blood flow and cerebral metabolism continuously and noninvasively [16,17]. Broadband near-infrared spectroscopy (B-NIRS) provides a means of directly monitoring cerebral energy metabolism by measuring the oxidation state of cytochrome c oxidase (oxCCO). This enzyme is involved in the electron transport chain and is vital to energy production via oxidative phosphorylation [18]. In addition, diffuse correlation spectroscopy (DCS)

provides continuous CBF monitoring by tracking the temporal correlation of light scatter from red blood cells in the cerebral microvasculature [19–22].

This manuscript reports the clinical translation of a hybrid B-NIRS/DCS optical neuromonitor to provide non-invasive and continuous monitoring of CBF and oxCCO throughout cardiac surgery with CPB. The goal was to assess the system's ability to identify fluctuations in perfusion and metabolism, while determining the efficacy of CPB in maintaining adequate oxygen supply and utilization. It was hypothesized that transitions on and off CPB would impact CBF, based on the CPB-pump flowrate (FR_{CPB}) chosen, but fluctuations in flow would be insufficient to impact cerebral metabolism. It was also expected that significant operational changes in FR_{CPB}, while patients were fully reliant on CPB, would directly influence cerebral hemodynamics, with large and sustained drops leading to metabolic change.

5.3 Methods

5.3.1 Patient Population

This study was approved by the Western University Health Sciences Research Ethics Board, which adheres to the guidelines of the Tri-Council Policy Statement: Ethical Conduct for Research Involving Humans (REB #113650). After obtaining consent, patients admitted to University Hospital's Cardiac Surgical Unit in London, Ontario, were monitored during non-emergent cardiac surgery with the use of non-pulsatile CPB.

5.3.2 Clinical Monitoring

Optical monitoring was conducted throughout surgery with CPB. Vital parameters were recorded with a clinical unit (Intellivue MX800, Philips Healthcare, MA, USA) and exported to the optical system. In accordance with clinical protocol, patients presenting with an increased risk of postoperative cognitive effects were monitored with EEG and a cerebral oximeter (SedLine®, Masimo, CA, USA). The optical probes were placed on the right temporal region of the forehead following anesthetic induction, endotracheal intubation, and placement of arterial and venous lines, but prior to skin incision. The probes were secured using a 3D-printed probe holder (Fig. 5.1a) and medical tape. Two optical

fibers delivered light from the DCS and B-NIRS sources onto the patient's scalp. Diffusely reflected light was collected from a common detection fiber bundle that corresponded to source-detector distances (SDD) of 2 and 3 cm for DCS and B-NIRS, respectively (Fig. 5.1b), to ensure adequate brain interrogation. Prior to monitoring, broadband light spectra were assessed to ensure negligible contamination from ambient light and the Masimo oximeter (< 5% signal contribution). Optical source power levels were maintained within ANSI limits for skin exposure.

B-NIRS and DCS measurements were acquired sequentially in a period of 3 s each. Within each period, the integration time was 250 ms. A transition delay of 0.5 s was incorporated between techniques to account for shutter transition times, achieving a cycle time of 7 s. Data were continuously acquired during the entire surgical procedure, spanning the transition on and off the CPB machine. Prior to and following CPB, DCS data were acquired for a minimum of 10 seconds at an increased sampling rate (20 Hz) to capture pulsatile waveforms.

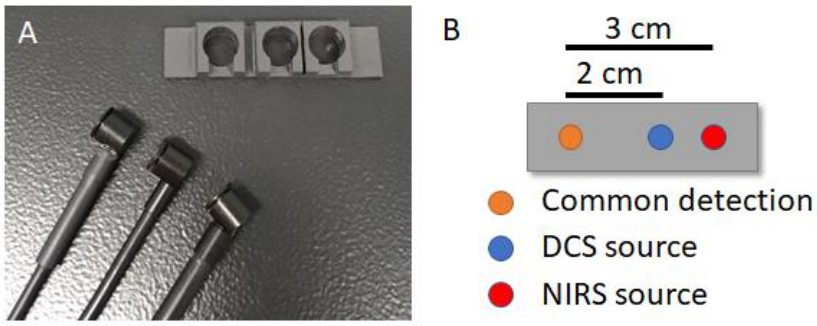

Figure 5.1: A) Optical fiber probes and 3D-printed probe holder (5 × 2 × 1 cm) B) Schematic of the probe holder showing near-infrared spectroscopy (NIRS, 3-cm SDD) and diffuse correlation spectroscopy (DCS, 2-cm SDD) emission probes with a common detection probe

5.3.3 Instrumentation

The development of a hybrid B-NIRS/DCS system has been previously reported and demonstrated continuous monitoring of cerebral blood flow, cerebral oxygen saturation,

and metabolism in both animal models and infants in the neonatal intensive care unit [16-17].

The system was constructed by combining B-NIRS and DCS modalities using a multiplexing shuttering system. The B-NIRS source (Hl-2000-HP, Ocean Optics, FL, USA) was coupled into a custom optical fiber bundle (2.4 mm diameter active area, 30 µM core, 0.55 numerical aperture (NA), Loptek, Germany) to guide light to the subject's head. Light that interrogated the head was collected by a detection fiber bundle (2 mm diameter active area, 30 µm core, 0.55 NA, Loptek, Germany), and led to a custom-made spectrometer (548 to 1085 nm bandwidth; 1.65 nm resolution; P&P Optica, ON, Canada). Light from the DCS laser (DL785-100s, CrystaLaser, NV, USA) was similarly coupled into a fiber bundle (4 × 200 µm core diameter, 0.22 NA, Loptek, Germany) and directed towards the head. Diffusely reflected DCS light was collected with a bundle of four single-mode fibers (8 µm core diameter, 0.12 NA, Loptek, Germany) coupled to a four-channel single-photon counting module (SPCM-AQR-15-FC, Excelitas Technologies, QC, Canada). The output of the detectors was sent to a data acquisition board (PCIe-6612, National Instruments, TX, USA) and processed by in-house developed software (LabVIEW, National Instruments, TX, USA; MATLAB, MathWorks, MI, USA) [23,24]. Intensity autocorrelation curves at 50 delay times, ranging from 1 µs to 1 ms, were generated for each detector.

For use in the operating room, the fibers were shielded to prevent ambient light contamination from the bright surgical environment. The tips of the optical probes, in contact with the scalp, were bent 90 degrees to maintain a low profile and held in placed by a 3D-printed holder constructed from a lightweight, flexible material (5 × 2 × 1 cm; Flexible Resin, Form 2, Formlabs, MA, USA).

5.3.4 Data Processing

5.3.4.1 B-NIRS Quantification of Baseline StO_2

Prior to clinical monitoring, the spectral profile of the optical system was characterized by acquiring a reference measurement. Once the probes were positioned on the scalp, a dark count measurement was acquired while the light sources of the optical system were off. A

reflectance measurement R(λ) was determined by correcting for both reference and dark count measures as follows:

$$R(\lambda) = log_{10}\left(\frac{spectrum_{\lambda} - dark_{\lambda}}{reference_{\lambda} - dark_{\lambda}}\right) \quad (5.1)$$

where spectrumλ refers to the measured light intensity at wavelength λ. Reflectance data were analyzed by fitting the first and second derivatives of R(λ) to solutions of the diffusion approximation for a semi-infinite homogeneous medium [12,25,26]. As previously reported, the tissue water fraction, oxy- and deoxy-hemoglobin (HbO_2, Hb) concentrations, and scattering parameters were estimated using a three-step multi-parameter fitting with a constrained minimization algorithm based on the MATLAB function fminsearchbnd [12,16,17]. Baseline tissue oxygen saturation (StO_2^b) was calculated from the estimated hemoglobin concentrations:

$$StO_2{}^b = \frac{HbO_2{}^b}{Hb^b + HbO_2{}^b} \quad (5.2)$$

where the superscript b denotes baseline values.

5.3.4.2 Monitoring StO_2 and Absolute Change in Oxidative State of Cytochrome c oxidase

Following a minimum five-minute baseline measurement, a modified Beer-Lambert Law based on the UCLn algorithm (Equation 3) was used to calculate changes in Hb, HbO_2, and oxCCO concentrations [18].

$$\begin{bmatrix} \Delta HbO_2 \\ \Delta Hb \\ \Delta oxCCO \end{bmatrix} = \frac{1}{DP} \begin{bmatrix} \varepsilon_{HbO_2}(\lambda_1) & \varepsilon_{Hb}(\lambda_1) & \varepsilon_{oxCCO}(\lambda_1) \\ \vdots & \vdots & \vdots \\ \varepsilon_{HbO_2}(\lambda_n) & \varepsilon_{Hb}(\lambda_n) & \varepsilon_{oxCCO}(\lambda_n) \end{bmatrix}^{-1} \times \begin{bmatrix} \Delta A(\lambda_1) \\ \vdots \\ \Delta A(\lambda_n) \end{bmatrix} \quad (5.3)$$

where ΔHbO_2, ΔHb, and ΔoxCCO are the relative changes from baseline in oxy-hemoglobin, deoxy-hemoglobin, and the oxidation state of cytochrome c oxidase, respectively. DP is the differential pathlength and ΔA is the measured change in attenuation. DP was set to 6.26, based on previous literature representing measurements in the adult head [27], and corrected for the wavelength dependency of the pathlength [28]. Relative measures determined by the modified Beer-Lambert approach were utilized in

conjunction with absolute baseline values from the derivative approach. This method provided absolute saturation values at faster computational speeds, allowing for real-time data interpretation. Tissue saturation was determined as follows [17]:

$$S_tO_2 = \frac{(HbO_2^b + \Delta HbO_2)}{(Hb^b + \Delta Hb) + (HbO_2^b + \Delta HbO_2)} \quad (5.4)$$

5.3.4.3 CBF Monitoring

Acquired DCS intensity data were normalized, autocorrelated, and converted to electric field autocorrelation data following the Siegert relation [29,30]. Each autocorrelation function was fit with the solution to the diffusion approximation for a semi-infinite homogenous medium for SDD = 2 cm, dynamic μa measurements obtained by B-NIRS, and a constant value for μ_s' of 8 cm^{-1} [22]. Fitting resulted in an estimate of the cerebral blood flow index (CBFi). CBFi data were normalized to baseline values to represent relative changes [31].

5.3.5 Statistical Analysis

All data are presented as mean ± standard deviation and statistical significance is defined as $p < 0.05$. CPB transition periods were defined as the minimum time to increase the CPB-pump flow rate (FR_{CPB}) from zero to values sustained throughout the procedure, and vice-versa. To characterize this impact, data were averaged over 5-minute periods immediately surrounding CPB transitions and displayed in boxplots. An additional 5-minute period was analyzed 15 minutes into CPB and compared to baseline values. Outliers were defined as points greater than $q3 + w \times (q3 - q1)$ or less than $q1 - w \times (q3 - q1)$, where w represents the whisker length and q indicates quartile number. A two-tailed paired t-test was conducted to determine significance following the onset/end of CPB. Intraoperative hypoperfusion events were identified, defined as sudden and large decreases in FR_{CPB} lasting a minimum of 30 s. Changes in optical parameters during these events were binned into 10-mmHg MAP intervals and plotted. A multivariate ANOVA was used to determine statistical significance in optical parameters compared to baseline values. For each hypoperfusion event, the maximum reductions in CBFi and oxCCO were compared.

5.3.6 Results

Optical measurements were acquired in ten adult patients (nine male, one female, aged 34 to 76 years, mean age = 58.1 ± 13.8 years). Data from the first three patients had to be excluded due to excessive ambient light from the bright surgical environment. Additional shielding, in the form of an optical blackout cloth (Thorlabs, NJ, USA), was implemented following these subjects to minimize artifacts from external light sources (< 5% signal contribution). Data from the fourth and seventh patients were limited to hypoperfusion events due to excessive motion during CPB transitions. The fourth subject experienced the onset of a bleed in the chest cavity resulting in a severely deteriorating condition and ultimately death. Remaining data sets were analyzed for changes in CBFi, StO_2, and oxCCO. Table 5-1 displays patient demographics.

Table 5-1: Demographic and procedural variables.

Sex (n)	F = 1, M= 6
Age (year)	58.1 ± 13.8
Duration of surgery (min)	409.4 ± 191.4
Duration of CPB (min)	191.9 ± 177.3
Procedure (n)	
- CABG	3
- CABG + AVR	1
- Aortic arch repair	1
- Bentall	1
- Bentall + MVR	1
Patient death (n)	1

CABG: Coronary artery bypass graft; AVR: Aortic valve replacement; MVR: Mitral valve replacement. Values are represented as mean ± standard deviation.

Fig. 5.2 displays time courses from one patient during the transition on (Fig. 5.2 A) and off (Fig. 5.2 B) CPB; the FR_{CPB}, mean arterial pressure (MAP), and optical measurements – ΔCBFi, StO_2, and ΔoxCCO – are displayed. The FR_{CPB} was measured by the CPB machine and MAP with the clinical Philips monitor from a radial artery site.

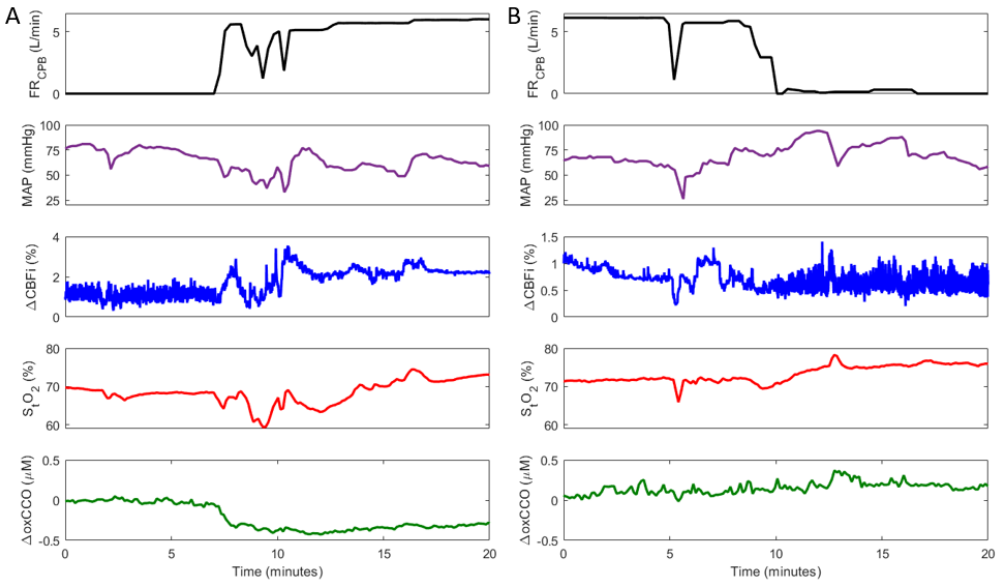

Figure 5.2: Cerebral hemodynamics during transition A) on cardiopulmonary bypass (CPB) and B) off CPB. Figure shows a continuous measure of CPB-pump flowrate (FR_{CPB}), mean arterial pressure (MAP), change in the cerebral blood flow index (ΔCBFi), cerebral tissue saturation (StO_2), and changes in the oxidation state of cytochrome c oxidase (ΔoxCCO). ΔCBFi scales are adjusted across plots for data visualization.

As each patient was transitioned onto CPB, as indicated by the increase in the FR_{CPB}, and the heart was arrested using a potassium solution, blood flow changed from a pulsatile to non-pulsatile state. This is apparent in the standard deviation of CBFi; pulsatile flow produced a larger range of values (Fig. 5.2 A < 8 min) compared to on-pump flow. The reverse effect was evident during the transition off CPB (Fig. 5.2 B > 10 min) as the heart was restarted. Averaged values across all subjects during pre-, on-, and post-CPB periods are displayed in Table 5-2. Data represented as a change (Δ) were acquired for 5-minute intervals immediately surrounding the transition on CPB, 15 minutes into CPB, and immediately surrounding the transition off CPB. CPB transitions are represented in boxplots in Fig. 5.3. The average transition time on CPB was 202 ± 111 s, and off CPB was 230 ± 160 s. During the on-CPB transition, subjects showed a notable increase in CBFi and a statistically significant decrease in MAP and ΔoxCCO. No significant change

persisted 15 minutes into CPB. Following CPB, MAP increased, while CBFi and ΔoxCCO displayed no significant change. StO_2 remained stable throughout the procedure.

Table 5-2: Hemodynamic parameters throughout cardiopulmonary bypass (CPB).

Parameter	Pre-CPB	On-CPB	Post-CPB
tHb (g/L)	112.6 ± 20.8	85.0 ± 13.0*	111.8 ± 42.8
pH	7.41 ± 0.06	7.33 ± 0.02*	7.38 ± 0.03
$PaCO_2$ (mmHg)	41.1 ± 3.9	35.3 ± 6.2	38.8 ± 1.5
Temperature (ºC)	35.6 ± 0.4	33.6 ± 2.4	36.3 ± 0.5
Parameter	Transition on CPB	Mid-CPB	Transition off CPB
ΔMAP (mmHg)	-18.8 ± 11.3*	-6.0 ± 9.5	11.0 ± 21.8
ΔCBFi (%)	88.5 ± 125.7	51.9 ± 91.4	-3.3 ± 17.2
ΔStO_2 (%)	1.2 ± 5.2	-2.8 ± 5.7	1.4 ± 3.1
ΔoxCCO (μM)	-0.5 ± 0.2*	-0.3 ± 0.5	0.2 ± 0.3

tHb: total Hemoglobin, $PaCO_2$: partial pressure of carbon dioxide. ‘Transition on CPB’ data were acquired as a change immediately surrounding CPB onset; ‘Mid CPB’ data were acquired 15 min following CPB onset and compared to pre-CPB data; ‘Transition off CPB’ data were acquired as a change immediately surrounding the end of CPB. Data were averaged over 5-minute intervals; * indicates statistical significance ($p < 0.05$).

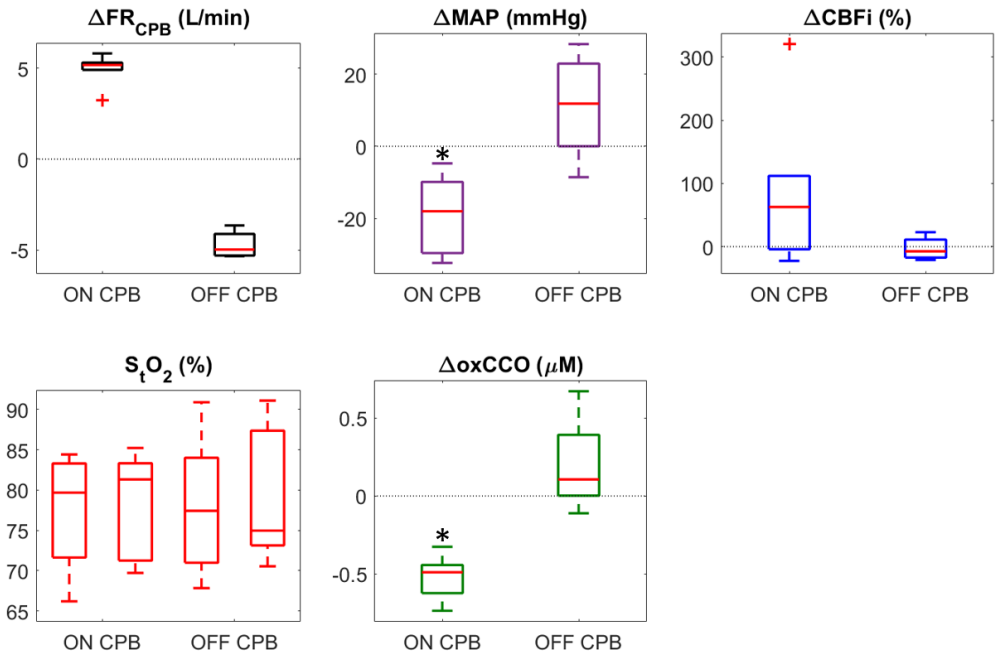

Figure 5.3: Box plots showing average change across subjects during transitions onto the CPB pump (ON CPB) and off of the pump (OFF CPB). Absolute StO_2 values are shown for periods immediately before and after each transition. Data were averaged for 5-minute durations immediately surrounding the transition period; + indicates statistical outliers and * indicates a statistically significant difference across the transition. Average transition time on CPB was 202 ± 111 s, and off CPB was 230 ± 160 s.

CBFi data were also acquired at increased acquisition rate (20 Hz) prior to and following CPB. Fig. 5.4 depicts fast blood flow monitoring in an aortic valve replacement (AVR) patient before (Fig. 5.4 A) and following (Fig. 5.4 B) replacement of the defective valve. The increased sampling rate allowed for depiction of pulsatile waveforms within the CBFi measure. Following AVR, the range of CBFi values increased for each ejection and a change in the shape of the secondary peak – which represents a change in pressure due to vascular elastic recoil following AV closure – became apparent, indicating a potential improvement in flow and pressure dynamics within the heart [23,32].

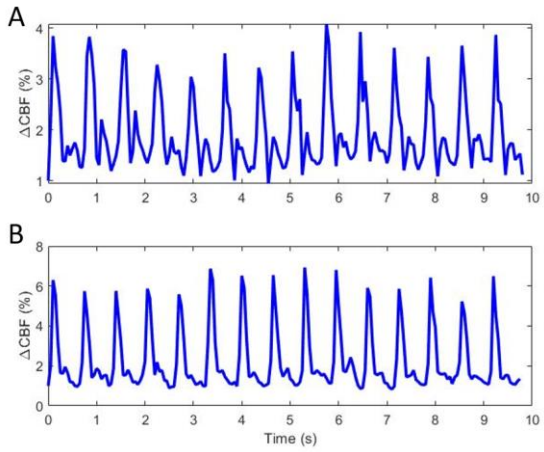

Figure 5.4: Pulsatile waveforms observed in cerebral microcirculation measured at 20 Hz A) pre and B) post aortic valve replacement.

Across the seven patient data sets, 15 hypoperfusion events, defined as large decreases in FR_{CPB} (mean change 2.8 ± 1.4 L/min, 70.6 ± 28.8%) and lasting a minimum of 30 seconds in duration (mean duration 93.9 ± 52.5 s), were observed. Fig. 5.5 displays data acquired in subject four during a stable period (Fig. 5.5 A) and when experiencing successive drops in FR_{CPB} (Fig. 5.5 B). With a stable FR_{CPB}, no significant changes were detected in the optical parameters. In Fig. 5.5 B, the drop in ΔCBFi (~2.5-minute mark) coincides with the onset of a significant bleed during surgery. This event prompted immediate reductions in FR_{CPB} to allow for surgical correction. MAP and optical measures were found to mirror changes in FR_{CPB}, with StO_2 and ΔoxCCO displaying a delayed response compared to ΔCBFi.

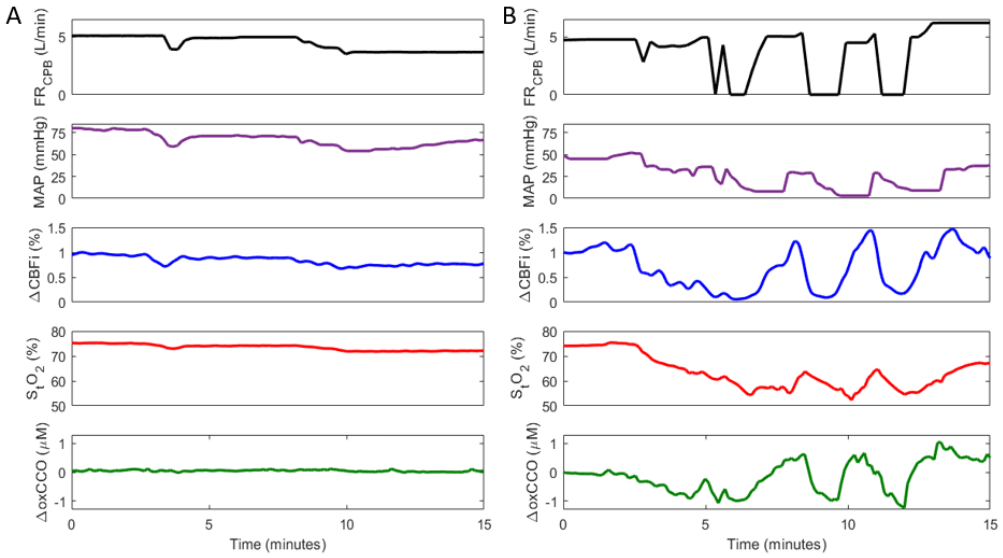

Figure 5.5: Cerebral hemodynamics in subject 4 during A) a stable period and B) successive FR_{CPB}-driven hypoperfusion events. Each graph includes a continuous measure of CPB-pump flow rate (FR_{CPB}), mean arterial pressure (MAP), change in cerebral blood flow (ΔCBFi), cerebral tissue saturation (StO_2), and changes in the oxidation state of cytochrome c oxidase (ΔoxCCO). Data were temporally averaged (7-s window) for visualization.

Correlation plots of hypoperfusion events, showing changes in optical parameters as a function of MAP, are displayed in Fig. 5.6; statistical outliers are depicted by red crosses. Statistically significant changes in ΔCBFi occurred below MAP values of 30 mmHg, in StO_2 below 20 mmHg, and in ΔoxCCO between 30 to 20 mmHg and below 10 mmHg.

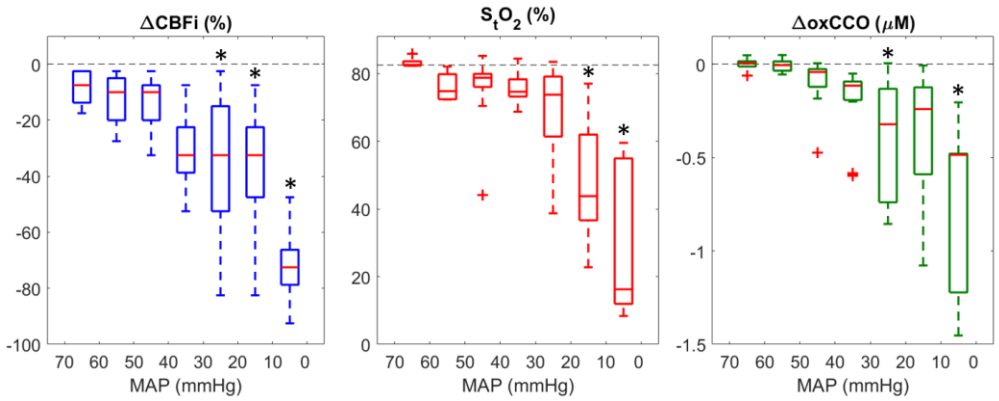

Figure 5.6: Correlation boxplots of ΔCBF, StO_2, and ΔoxCCO as a function of MAP; + indicates statistical outliers and * indicates a statistically significant difference from baseline values.

The maximum changes in oxCCO during each hypoperfusion event were plotted against the maximum change in CBFi in Fig. 5.7. A temporal delay of 18.2 ± 15.0 s was found between nadirs of ΔCBFi and ΔoxCCO. A delayed metabolic response in relation to flow has been previously reported [16,17,33,34]. Changes in CBFi greater than 70% resulted in large decreases in oxCCO.

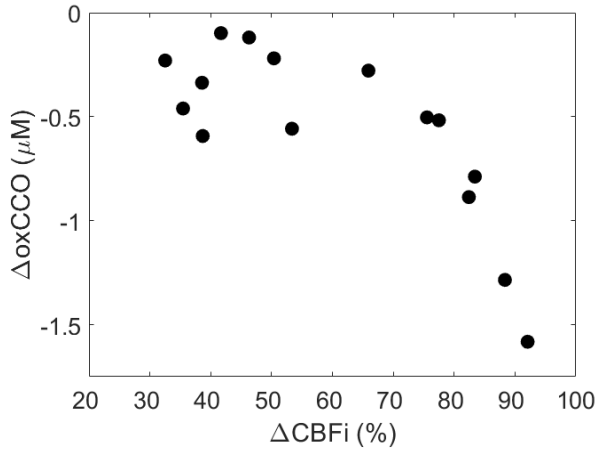

Figure 5.7: Correlation plot showing the relationship between the maximum reductions in ΔCBFi and ΔoxCCO. On average, the ΔoxCCO nadir occurred 18.2 ± 15.0 s after the corresponding ΔCBFi nadir.

5.4 Discussion

For patients undergoing cardiac surgery with the use of CPB, current clinical standards are either completely absent of brain specific monitoring or reliant on commercial oximetry devices to provide regional cerebral oxygen saturation measurements. While oximetry has advanced to provide robust continuous measures, saturation alone has proven insufficient in describing metabolism and predicting neurological outcome [15,35]. The goal of this study was to test the feasibility of a newly developed optical brain monitor to provide intraoperative measurements of cerebral hemodynamics and metabolism during CPB.

In seven patients undergoing cardiac surgery with CPB, the hybrid optical device provided continuous monitoring of cerebral blood flow based on the DCS blood flow index (CBFi) and metabolism using B-NIRS to measure changes in the oxidation state of cytochrome c oxidase (ΔoxCCO). During transitions onto CPB (Fig. 5.2 A), the FR_{CPB} was increased to provide adequate perfusion as the heart was arrested. The CPB pump was initially filled with a crystalloid solution in its reserve; when the pump was started, the first cycle was devoid of blood. As it continued, the crystalloid solution and blood mixed, resulting in a hemodilution effect that gradually diminished. From the perspective of the B-NIRS acquisition, there was a sudden change in the optical properties which may have contributed to the observed change in oxCCO. While Fig. 5.3 shows a statistically significant drop in ΔoxCCO, implying inadequate oxygen utilization across the on-CPB transition, the influence of hemodilution during this transition phase must be considered. It is also noteworthy that a significant increase in MAP was observed across this period and that no significant change in oxCCO persisted 15 minutes into CPB. Studies by Lassnigg et al. and Talpahewa et al. both reported similar changes in oxCCO following CPB-onset while noting contributions from hemodilution effects [36,37]. While hemodilution also results in a reduced number of moving light scatterers (e.g., red blood cells), it did not appear to have the same impact on DCS, since the CBFi measure relies on the temporal correlation of dynamic light scatter. Instead, CBFi was influenced to a greater extent by the FR_{CPB}. The clinically chosen FR_{CPB} was generally within a limited range from 2.0 to 2.5 L/min/m^2, using an estimated surface area for each patient [38–40]. Fig. 5.3 displays a large range of ΔCBFi following CPB onset, with an average increase of

88.5 ± 125.7%. This shows that pump-flow rates were consistently overestimated, in relation to baseline values. While this ensures sufficient perfusion, intraoperative blood flow monitoring has potential in allowing for patient specific flow rates. Following the procedure, no significant changes were observed coming off CPB, suggesting no loss of oxygen supply or utilization when restarting the heart. Similarly, no change in StO_2 was observed across either transition. Patients also experienced significant drops in total hemoglobin and pH during CPB, while no significant changes in temperature and $PaCO_2$ were observed.

Fig. 5.4 demonstrates the system's ability to capture pulsatile waveforms in the cerebral microcirculation. A patient presented with a bicuspid aortic valve (Fig. 5.4 A), which was replaced with an artificial valve (Fig. 5.4 B). In the pulse pressure waveform, the first and largest peak represents the systolic phase, corresponding to the aortic valve opening and left ventricular ejection. The second peak visualized represents the vascular elastic recoil following aortic valve closure [32]. After valve replacement, alterations in the height of the curve and shape of the secondary peak were observed. These changes could represent improvements in stroke volume and aortic pressure from cardiac pathologies (e.g., the progressive decrease in aortic pressure due to aortic stenosis) or surgical repairs (e.g. valve integrity) and could provide more insight on the impact of cardiac output on CBF. CPB produces a non-pulsatile blood flow while the heart is arrested. Pulsatile flow has been shown to significantly enhance organ perfusion (i.e., in kidneys) prior to transplant [41], and recent studies investigating non-pulsatile versus pulsatile CPB in major cerebral arteries suggest the potential benefit of cerebral pulsatility [42]; however, there is currently insufficient evidence to necessitate the clinical implementation of pulsatile CPB. Continuous monitoring of CBF and oxCCO could be used to assess the effects of pulsatile versus non-pulsatile CPB on cerebral health.

Throughout surgery, numerous hypoperfusion events caused by large and sustained drops in FR_{CPB} were observed. While on CPB, oxygen supply is solely dependent on the CPB-pump flow rate; reducing FR_{CPB} therefore directly impacts cerebral perfusion and could lead to adverse neurological outcome. Fig. 5.5 displays an example dataset acquired from a patient during a stable period (Fig. 5.5 A, no notable changes in FR_{CPB}) and during

multiple successive drops in FR_{CPB}. Optical metrics during 15 hypoperfusion events (mean drop in FR_{CPB} of 70.6 ± 28.8% for 93.9 ± 52.5 s) are summarized in Fig. 5.6 as a function of MAP. As MAP decreased with reduced FR_{CPB}, correlation plots show a consistent decrease in cerebral perfusion, saturation, and metabolism. Statistically significant differences were found for MAP values below 30 mmHg. ΔCBFi showed the earliest response with delayed responses in StO_2 and ΔoxCCO. For each event, the maximum change in oxCCO was plotted as a function of the corresponding largest change in CBFi (Fig. 5.7). Mild-to-moderate reductions in CBFi (< 70%) resulted in small decreases in oxCCO; similar reductions were reported in patients undergoing transaortic valve replacements [43], and in healthy volunteers undergoing hypoxia and hypocapnia challenges [44,45]. Reductions in CBFi > 70% instigated larger changes in metabolism comparable to reductions observed in infants with brain injury [46]. The adult brain is assumed to have a total CCO concentration of approximately 5.5 μM [18]. The largest observed drop (−1.5 μM) represents an approximate 27% change in oxCCO within the brain. Furthermore, an 18.2 ± 15.0-s delay was observed between metabolic and flow nadirs. Previous studies have shown similar delays in piglets [17,47] and infants [16,33]. Reductions in CBF are likely met by increases in oxygen extraction to maintain stable metabolic levels. Following large and sustained drops in CBF, this compensatory mechanism could become overwhelmed and metabolism impacted. The variability in oxCCO is therefore influenced by the duration of hypoperfusion events observed. While shorter events can elicit similar CBF responses, they may not last long enough to cause the maximum reduction in oxCCO. Further investigations are required to establish clinical thresholds for changes in CBFi and oxCCO in order to understand when values become clinically relevant. Previous work has utilized continuous CBF monitoring to determine a patient-specific lower limit of autoregulation (LLA) [11]. Future work will look to determine the relationship of the LLA with changes in cerebral metabolism.

When translating the optical system to the cardiac operating room, the bright ambient light in the surgical suite was initially a significant source of signal contamination. In this environment, additional shielding in the form of an optical blackout cloth was essential. Further, frequent bed motion and patient repositioning/intervention (i.e., head-cooling with ice, manipulating the transesophageal echocardiography probe) during surgical procedures

necessitated strong contact between the optical probes and the surface of the skin. This was achieved by anchoring the optical fibers at a point above the patient, minimizing weight and providing leeway for motion. An additional challenge of the current set-up is the inherent depth sensitivity of the optical technology. The SDDs chosen for B-NIRS and DCS have proven sufficient to interrogate the brain in adult populations [43,48,49]; however, previous work has shown the large contribution from the scalp for NIRS measures [50–52]. While StO_2 is susceptible to this effect, oxCCO is less impacted since CCO concentrations are considerably higher in the brain than in extracerebral tissues [18]. To further address depth sensitivity, future work will implement multi-distance measurements to simultaneously acquire scalp perfusion and metabolism and correct for their influence. Previous reports have elaborated on the benefits of measuring extracerebral layers in discerning this contribution [43,49,53,54]. Another future direction will be to modify the system to enable measurements from multiple vascular territories. A limitation with the current system was that the single probe only afforded monitoring in one brain region. In this study, a patient had an intraoperative ischemic stroke in the M1 branch of the right middle cerebral artery, which was not detected by the probes placed on the right side of the forehead. With advancements in lower-cost detector technology, implementing multiple source-detection pairs would enable monitoring across multiple vascular territories [12,55].

5.5 Conclusion

This study presents the clinical translation and feasibility of an optical neuromonitor capable of continuous measurement of cerebral perfusion and metabolism during cardiac surgery with CPB. Temporal resolution was sufficient to capture physiological responses to transitions on and off the CPB pump and intraoperative hypoperfusion events. Increases in CBFi and significant decreases in MAP and oxCCO were noted during transitions on CPB, with no change during transitions off. Large reductions in CPB-pump flowrate resulted in significant drops in CBFi and oxCCO when MAP decreased below 30 mmHg. The findings regarding metabolic change are supported by previous literature using similar methodologies. The optical system described provides a safe and non-invasive approach for real-time assessment of cerebral hemodynamics and metabolism. More studies are

required to determine if direct intraoperative monitoring of CBFi and oxCCO could aid clinicians in patient management and possibly provide insight into the impact of CPB on postoperative cognitive decline and brain injury.

5.6 Acknowledgements

The authors would like to acknowledge the patients who participated in this study. Funding: Natural Sciences and Engineering Research Council of Canada (CHRP 478470); Canadian Institutes of Health Research (CGP-14171); Academic Medical Organization of Southwestern Ontario (INN19-001).

5.7 References

1. D. Van Dijk, M. Spoor, R. Hijman, H. M. Nathoe, C. Borst, E. W. L. Jansen, D. E. Grobbee, P. P. T. De Jaegere, and C. J. Kalkman, “Cognitive and cardiac outcomes 5 years after off-pump vs on-pump coronary artery bypass graft surgery,” J. Am. Med. Assoc., 297(7), 701–708, (2007).

2. T. Xu, L. Bo, J. Wang, Z. Zhao, Z. Xu, X. Deng, and W. Zhu, “Risk factors for early postoperative cognitive dysfunction after non-coronary bypass surgery in Chinese population,” J. Cardiothorac. Surg., 8(1), 1–6, (2013).

3. S. Glumac, G. Kardum, and N. Karanovic, “Postoperative cognitive decline after cardiac surgery: A narrative review of current knowledge in 2019,” Med. Sci. Monit., 25, 3262–3270, (2019).

4. G. H. Almassi, T. Sommers, T. E. Moritz, A. L. W. Shroyer, M. J. London, W. G. Henderson, G. K. Sethi, F. L. Grover, and K. E. Hammermeister, “Stroke in cardiac surgical patients: Determinants and outcome,” Ann. Thorac. Surg., 68(2), 391–397, (1999).

5. J. D. Salazar, R. J. Wityk, M. A. Grega, L. M. Borowicz, J. R. Doty, J. A. Petrofski, and W. A. Baumgartner, “Stroke after cardiac surgery: Short- and long-term outcomes,” Ann. Thorac. Surg., 72(4), 1195–1201, (2001).

6. J. P. Gold, M. E. Charlson, P. Williams-Russo, T. P. Szatrowski, J. C. Peterson, P. A. Pirraglia, G. S. Hartman, F. S. F. Yao, J. P. Hollenberg, D. Barbut, J. G. Hayes,

S. J. Thomas, M. H. Purcell, S. Mattis, L. Gorkin, M. Post, K. H. Krieger, and O. W. Isom, “Improvement of outcomes after coronary artery bypass: A randomized trial comparing intraoperative high versus low mean arterial pressure,” J. Thorac. Cardiovasc. Surg., 110(5), 1302–1314, (1995).

7. J. M. Murkin, J. K. Farrar, W. A. Tweed, F. N. McKenzie, and G. Guiraudon, “Cerebral autoregulation and flow/metabolism coupling during cardiopulmonary bypass: The influence of $PaCO_2$,” Anesth. Analg., 66(9), 825–832, (1987).

8. U. H. Trivedi, R. L. Patel, M. R. J. Turtle, G. E. Venn, and D. J. Chambers, “Relative changes in cerebral blood flow during cardiac operations using xenon-133 clearance versus transcranial Doppler sonography,” Ann. Thorac. Surg., 63(1), 167–174, (1997).

9. D. Hori, Y. Nomura, M. Ono, B. Joshi, K. Mandal, D. Cameron, M. Kocherginsky, and C. W. Hogue, “Optimal blood pressure during cardiopulmonary bypass defined by cerebral autoregulation monitoring,” J. Thorac. Cardiovasc. Surg., 154(5), 1590-1598.e2, (2017).

10. S. Purkayastha and F. Sorond, “Transcranial doppler ultrasound: Technique and application,” Semin. Neurol., 32(4), 411–420, (2012).

11. J. M. Murkin, M. Kamar, Z. Silman, M. Balberg, and S. J. Adams, “Intraoperative Cerebral Autoregulation Assessment Using Ultrasound-Tagged Near-Infrared-Based Cerebral Blood Flow in Comparison to Transcranial Doppler Cerebral Flow Velocity: A Pilot Study,” J. Cardiothorac. Vasc. Anesth., 29(5), 1187–1193, (2015).

12. M. Diop, E. Wright, V. Toronov, T.-Y. Lee, and K. St Lawrence, “Improved light collection and wavelet de-noising enable quantification of cerebral blood flow and oxygen metabolism by a low-cost, off-the-shelf spectrometer.,” J. Biomed. Opt., 19(5), 057007, (2014).

13. A. Casati, G. Fanelli, P. Pietropaoli, R. Proietti, R. Tufano, G. Danelli, G. Fierro, G. De Cosmo, G. Servillo, M. Nuzzi, F. Mentegazzi, A. Fanelli, C. Martani, E. Spreafico, F. Pugliese, P. Aceto, and F. Monaco, “Continuous monitoring of

cerebral oxygen saturation in elderly patients undergoing major abdominal surgery minimizes brain exposure to potential hypoxia," Anesth. Analg., 101(3), 740–747, (2005).

14. J. M. Murkin, S. J. Adams, R. J. Novick, M. Quantz, D. Bainbridge, I. Iglesias, A. Cleland, B. Schaefer, B. Irwin, and S. Fox, "Monitoring brain oxygen saturation during coronary bypass surgery: A randomized, prospective study," Anesth. Analg., 104(1), 51–58, (2007).

15. D. A. Boas and M. A. Franceschini, "Haemoglobin oxygen saturation as a biomarker: the problem and a solution," Philos. Trans. R. Soc., 369, 4407–4424, (2011).

16. A. Rajaram, L. C. M. Yip, D. Milej, M. Suwalski, M. Kewin, M. Lo, J. J. L. Carson, V. Han, S. Bhattacharya, M. Diop, S. de Ribaupierre, and K. St. Lawrence, "Perfusion and Metabolic Neuromonitoring during Ventricular Taps in Infants with Post-Hemorrhagic Ventricular Dilatation," Brain Sci., 10(7), 452, (2020).

17. A. Rajaram, G. Bale, M. Kewin, L. B. Morrison, I. Tachtsidis, K. St. Lawrence, M. Diop, K. St. Lawrence, and M. Diop, "Simultaneous monitoring of cerebral perfusion and cytochrome c oxidase by combining broadband near-infrared spectroscopy and diffuse correlation spectroscopy," Biomed. Opt. Express, 9(6), 2588–2603, (2018).

18. G. Bale, C. E. Elwell, and I. Tachtsidis, "From Jöbsis to the present day : a review of clinical near-infrared spectroscopy measurements of cerebral cytochrome-c-oxidase," J. Biomed. Opt., 21(9), (2016).

19. L. He, W. B. Baker, D. Milej, V. C. Kavuri, R. C. Mesquita, D. R. Busch, K. Abramson, Y. J. Jiang, M. Diop, K. St Lawrence, O. Amendolia, F. Quattrone, R. Balu, W. A. Kofke, and A. G. Yodh, "Noninvasive continuous optical monitoring of absolute cerebral blood flow in critically ill adults," Neurophotonics, 5(04), 1, (2018).

20. T. Pham, K. Tgavalekos, A. Sassaroli, G. Blaney, and S. Fantini, “Quantitative measurements of cerebral blood flow with near-infrared spectroscopy,” Biomed. Opt. Express, 10(4), 2117, (2019).

21. T. Durduran, C. Zhou, E. M. Buckley, M. N. Kim, G. Yu, R. Choe, J. W. Gaynor, T. L. Spray, S. M. Durning, S. E. Mason, L. M. Montenegro, S. C. Nicolson, R. A. Zimmerman, M. E. Putt, J. Wang, J. H. Greenberg, J. A. Detre, A. G. Yodh, and D. J. Licht, “Optical measurement of cerebral hemodynamics and oxygen metabolism in neonates with congenital heart defects,” J. Biomed. Opt., 15(3), 037004, (2010).

22. D. Milej, L. He, A. Abdalmalak, W. B. Baker, U. C. Anazodo, M. Diop, S. Dolui, V. C. Kavuri, W. Pavlosky, L. Wang, R. Balu, J. A. Detre, O. Amendolia, F. Quattrone, W. A. Kofke, A. G. Yodh, and K. St Lawrence, “Quantification of cerebral blood flow in adults by contrast-enhanced near-infrared spectroscopy: Validation against MRI,” J. Cereb. Blood Flow Metab., 40(8), 1672–1684, (2020).

23. D. Wang, A. B. Parthasarathy, W. B. Baker, K. Gannon, V. Kavuri, T. Ko, S. Schenkel, Z. Li, Z. Li, M. T. Mullen, J. A. Detre, and A. G. Yodh, “Fast blood flow monitoring in deep tissues with real-time software correlators,” Biomed. Opt. Express, 7(3), 776, (2016).

24. M. Khalid, D. Milej, A. Rajaram, A. Abdalmalak, L. Morrison, M. Diop, and K. St. Lawrence, “Development of a stand-alone DCS system for monitoring absolute cerebral blood flow,” Biomed. Opt. Express, 10(9), 4607, (2019).

25. M. Diop, J. Kishimoto, V. Toronov, D. S. C. Lee, and K. St. Lawrence, “Development of a combined broadband near-infrared and diffusion correlation system for monitoring cerebral blood flow and oxidative metabolism in preterm infants,” Biomed. Opt. Express, 6(10), 3907, (2015).

26. M. Kewin, A. Rajaram, D. Milej, A. Abdalmalak, L. Morrison, M. Diop, and K. St Lawrence, “Evaluation of hyperspectral NIRS for quantitative measurements of

tissue oxygen saturation by comparison to time-resolved NIRS," Biomed. Opt. Express, 10(9), 4789, (2019).

27. A. Duncan, J. H. Meek, M. Clemencet, C. E. Elwellt, and L. Tyszczuk, "Optical pathlength measurements on adult head , calf and forearm and the head of the newborn infant using phase resolved optical spectroscopy," Phys. Med. Biol., 40, 295–304, (1995).

28. M. Essenpreis, C. E. Elwell, M. Cope, P. van der Zee, S. R. Arridge, and D. T. Delpy, "Spectral dependence of temporal point spread functions in human tissues," Appl. Opt., 32(4), 418, (1993).

29. K. Verdecchia, M. Diop, L. B. Morrison, T.-Y. Lee, and K. St. Lawrence, "Assessment of the best flow model to characterize diffuse correlation spectroscopy data acquired directly on the brain," Biomed. Opt. Express, 6(11), 4288, (2015).

30. P. Lemieux and D. J. Durian, "Investigating non-Gaussian scattering processes by using n th-order intensity correlation functions," 16(7), 1651–1664, (1999).

31. M. Diop, K. Verdecchia, T.-Y. Lee, and K. St Lawrence, "Calibration of diffuse correlation spectroscopy with a time-resolved near-infrared technique to yield absolute cerebral blood flow measurements," Biomed. Opt. Express, 2(7), 2068, (2011).

32. D. M. MacCanon, F. Arevalo, and E. C. Meyer, "Direct Detection and Timing of Aortic Valve Closure," Circ. Res., 14(5), 387–391, (1964).

33. R. Arora, M. Ridha, D. S. C. Lee, J. Elliott, H. C. Rosenberg, M. Diop, T. Y. Lee, and K. St. Lawrence, "Preservation of the metabolic rate of oxygen in preterm infants during indomethacin therapy for closure of the ductus arteriosus," Pediatr. Res., 73(6), 713–718, (2013).

34. G. Bale, A. Rajaram, M. Kewin, L. Morrison, A. Bainbridge, M. Diop, K. S. Lawrence, and I. Tachtsidis, "Broadband NIRS Cerebral Cytochrome-C-Oxidase Response to Anoxia Before and After Hypoxic-Ischaemic Injury in Piglets," Oxyg. Transp. to Tissue XL, 1072, 151–156, (2018).

35. M. Taillefer and A. Y. Denault, “Cerebral near-infrared spectroscopy in adult heart surgery: systematic review of its clinical efficacy,” Cardiothorac. Anesth. Respir. Airw., 79–87, (2005).

36. A. Lassnigg, M. Hiesmayr, P. Keznickl, T. Müllner, M. Ehrlich, and G. Grubhofer, “Cerebral oxygenation during cardiopulmonary bypass measured by near- infrared spectroscopy: Effects of hemodilution, temperature, and flow,” J. Cardiothorac. Vasc. Anesth., 13(5), 544–548, (1999).

37. S. P. Talpahewa, A. T. Lovell, G. D. Angelini, and R. Ascione, “Effect of cardiopulmonary bypass on cortical cerebral oxygenation during coronary artery bypass grafting,” Eur. J. Cardio-thoracic Surg., 26(4), 676–681, (2004).

38. G. W. Fischer, H. M. Lin, M. Krol, M. F. Galati, G. Di Luozzo, R. B. Griepp, and D. L. Reich, “Noninvasive cerebral oxygenation may predict outcome in patients undergoing aortic arch surgery,” J. Thorac. Cardiovasc. Surg., 141(3), 815–821, (2011).

39. G. S. Murphy, E. A. Hessel, and R. C. Groom, “Optimal perfusion during cardiopulmonary bypass: An evidence-based approach,” Anesth. Analg., 108(5), 1394–1417, (2009).

40. A. Wahba, M. Milojevic, C. Boer, F. M. J. J. De Somer, T. Gudbjartsson, J. Van Den Goor, T. J. Jones, V. Lomivorotov, F. Merkle, M. Ranucci, G. Kunst, L. Puis, P. Alston, D. Fitzgerald, A. Nikolic, F. Onorati, B. Steen Rasmussen, and S. Svenmarker, “2019 EACTS/EACTA/EBCP guidelines on cardiopulmonary bypass in adult cardiac surgery”, European Journal of Cardio-thoracic Surgery 57(2). (2020).

41. C. von Horn and T. Minor, “Isolated kidney perfusion: the influence of pulsatile flow,” Scand. J. Clin. Lab. Invest., 78(1–2), 131–135, (2018).

42. M. P. O. Neil, R. Alie, L. R. Guo, M. Myers, J. M. Murkin, and C. G. Ellis, “Microvascular Responsiveness to Pulsatile and Nonpulsatile Flow During Cardiopulmonary Bypass,” Ann. Thorac. Surg., 105(6), 1745–1753, (2019).

43. T. N. Nguyen, W. Wu, E. Woldemichael, V. Toronov, and S. Lin, “Hyperspectral near-infrared spectroscopy assessment of the brain during hypoperfusion,” J. Biomed. Opt., 24(03), 1, (2019).

44. M. Tisdall, M. Smith, I. Tachtsidis, and C. E. Elwell, “Changes in concentrations of oxidised cytochrome oxidase measured using both broadband and four wavelength near infrared spectroscopy reflect changes in oxygen delivery during hypoxaemia in healthy volunteers,” in Optical Society of America conference proceedings, (2006), ME66.

45. L. Holper, J. J. Mann, L. Holper, and J. J. Mann, “Test – retest reliability of brain mitochondrial cytochrome-c-oxidase assessed by functional near-infrared spectroscopy,” J. Biomed. Opt., 23(5), (2018).

46. G. Bale, S. Mitra, I. de Roever, M. Sokolska, D. Price, A. Bainbridge, R. Gunny, C. Uria-Avellanal, G. S. Kendall, J. Meek, N. J. Robertson, and I. Tachtsidis, “Oxygen dependency of mitochondrial metabolism indicates outcome of newborn brain injury,” J. Cereb. Blood Flow Metab., 39(10), 2035–2047, (2019).

47. J. A. Cooper, K. M. Tichauer, M. Boulton, J. Elliott, M. Diop, M. Arango, T.-Y. Lee, and K. St Lawrence, “Continuous monitoring of absolute cerebral blood flow by near-infrared spectroscopy during global and focal temporary vessel occlusion.,” J. Appl. Physiol., 110(6), 1691–8, (2011).

48. D. Milej, M. Shahid, A. Abdalmalak, A. Rajaram, M. Diop, and K. St. Lawrence, “Characterizing dynamic cerebral vascular reactivity using a hybrid system combining time-resolved near-infrared and diffuse correlation spectroscopy,” Biomed. Opt. Express, 11(8), 4571-4585, (2020).

49. K. Verdecchia, M. Diop, A. Lee, L. B. Morrison, T.-Y. Lee, and K. St. Lawrence, “Assessment of a multi-layered diffuse correlation spectroscopy method for monitoring cerebral blood flow in adults,” Biomed. Opt. Express, 7(9), 3659, (2016).

50. J. Selb, D. A. Boas, S.-T. Chan, K. C. Evans, E. M. Buckley, and S. A. Carp, “Sensitivity of near-infrared spectroscopy and diffuse correlation spectroscopy to

brain hemodynamics: simulations and experimental findings during hypercapnia," Neurophotonics, 1(1), 015005, (2014).

51. D. Milej, A. Abdalmalak, A. Rajaram, and K. St Lawrence, "Direct Assessment of Extracerebral Signal Contamination on Optical Measurements of Cerebral Blood Flow, Oxygenation, and Metabolism," Neurophotonics, (2020).

52. D. Milej, A. Rajaram, A. Abdalmalak, M. Khalid, M. Shahid, M. Kewin, and K. St. Lawrence, "Assessing extracerebral signal contamination in optical measurements of cerebral blood flow and oxygenation," SPIE proceedings 11074, Diffuse Optical Spectroscopy and Imaging VII, 90 (2019).

53. T. Sato, I. Nambu, K. Takeda, T. Aihara, O. Yamashita, Y. Isogaya, Y. Inoue, Y. Otaka, Y. Wada, M. Kawato, M. Sato, and R. Osu, "Reduction of global interference of scalp-hemodynamics in functional near-infrared spectroscopy using short distance probes," Neuroimage, 141, 120–132, (2016).

54. A. Gerega, D. Milej, W. Weigl, M. Kacprzak, and A. Liebert, "Multiwavelength time-resolved near-infrared spectroscopy of the adult head: assessment of intracerebral and extracerebral absorption changes," Biomed. Opt. Express, 9(7), 2974, (2018).

55. P. Kaynezhad, S. Mitra, G. Bale, C. Bauer, I. Lingam, C. Meehan, A. Avdic-Belltheus, K. A. Martinello, A. Bainbridge, N. J. Robertson, and I. Tachtsidis, "Quantification of the severity of hypoxic-ischemic brain injury in a neonatal preclinical model using measurements of cytochrome-c-oxidase from a miniature broadband-near-infrared spectroscopy system," Neurophotonics, 6(04), 1, (2019).

Chapter 6

6 Conclusion and Future Directions

This section revisits the overarching aims of this dissertation and summarizes findings from each chapter. Limitations are discussed to address notable drawbacks within this work along with potential solutions and future directions in this field.

6.1 Research Objectives

Infants born prematurely (i.e., a gestational period fewer than 37 weeks) have an increased risk of adverse neurological outcome. The shorter the gestation, and the less infants weigh at birth, the higher the risk of developing a brain injury. For example, 25-50% of very low birth weight infants (< 1500 g) experience cognitive/behaviour deficits, and 5-10% develop major disorders such as cerebral palsy [1]. A common brain injury among this population is intraventricular hemorrhaging (IVH), which describes bleeding in the germinal matrix and surrounding white matter. Due to an underdeveloped vascular bed in this region, infants are particularly susceptible to hemorrhaging, particularly within the first 48 hours after birth [2]. Severe bleeding can trigger an inflammatory response and subsequent fibrosis, which can prevent drainage of cerebrospinal fluid (CSF) from the brain's ventricles. Significant build-up of CSF can cause increases in intracranial pressure and result in ventricle enlargement; this is referred to as post-hemorrhagic ventricle dilatation (PHVD) [3,4]. PHVD is a common complication in high-grade IVH, both of which place infants at a higher risk of developing brain damage and long-term cognitive deficits.

Currently, diagnosis of IVH and PHVD is conducted using cranial ultrasound (cUS) to visually grade/assess hemorrhages and ventricular dilatation [4,5]. Ultrasound is limited in its ability to longitudinally monitor and acquired images can only be used to assess damage that has already occurred. Advancements in optical technologies have shown potential in providing non-invasive monitoring of physiological markers of brain injury. Broadband near-infrared spectroscopy (B-NIRS) exploits light absorption properties of tissue constituents, such as hemoglobin, to quantify their concentrations [6]. This technique can therefore provide continuous monitoring of cerebral tissue saturation (StO_2). Due to the

wide range of wavelengths implemented using B-NIRS, a measure of cytochrome c oxidase (CCO) can also be acquired. CCO is an enzyme in the mitochondria vital to oxidative phosphorylation (i.e., cellular energy production). Through monitoring CCO's oxidation state (oxCCO), B-NIRS can provide a direct measure of metabolism [7]. Diffuse correlation spectroscopy (DCS) is a relatively newer optical technique that can provide continuously monitoring of cerebral blood flow (CBF). Whereas B-NIRS can quantify StO2 through measuring light absorption, DCS can provide a measure of blood flow by analyzing light scattered off of red blood cells (RBC) [8,9]. As RBC are the primary moving scatterers in tissue, changes in light scatter reflect RBC motion [10]. Using a stable long-coherence laser, DCS can directly monitoring CBF in the microvasculature.

The overarching goal of this dissertation was to develop an optical system combining B-NIRS and DCS techniques to provide a simultaneous acquisition of CBF and oxCCO. Bedside monitoring of perfusion and metabolism could act as a prognostic tool to provide insight into physiological precursors of brain injury before significant damage occurs. This thesis sought to achieve this through the following aims:

1. Develop and validate a hybrid B-NIRS and DCS neuromonitor to simultaneously acquire CBF and oxCCO at the bedside (Chapter 2).
2. Assess system feasibility in PHVD infants in the neonatal intensive care unit (Chapter 3).
3. Investigate cerebral perfusion and metabolic stability during early brain development in premature infants soon after birth (Chapter 4).
4. Investigate the impact of significant changes in CBF on cerebral energy metabolism (Chapter 5).

6.2 Summary of Individual Chapters

6.2.1 Development of a hybrid broadband NIRS and DCS device for concurrent measurements of cerebral perfusion and cytochrome c oxidase

Chapter 2 presented a novel optical system combining B-NIRS, to monitor cerebral tissue saturation and oxidative metabolism (via the marker cytochrome c oxidase), with DCS to

provide measures of blood flow in the cerebral microvasculature. Though implementing a multiplexing shuttering system, B-NIRS and DCS techniques were acquired in quick succession while avoiding system crosstalk as demonstrated in a phantom model. Dynamic measurements of StO_2, CBF, and oxCCO were reported in a piglet model of neonatal hypoxia-ischemia, achieved through clamping carotid arteries and reducing oxygen content. StO_2 and CBF were found to react immediately to the onset of injury, while a delay in metabolism was observed. The hybrid system presented showed potential for real-time bedside monitoring of hemodynamics and metabolism as a prognostic tool to indicate injury.

6.2.2 Monitoring changes in cerebral blood flow and metabolism in infants with post-hemorrhagic ventricular dilatation during ventricular taps

Chapter 3 describes the clinical translation of NNeMo (Neonatal NeuroMonitor), a hybrid B-NIRS/DCS device for bedside characterization of cerebral perfusion and metabolism. In this work, StO_2, CBF, and oxCCO were monitored in term infants with post-hemorrhagic ventricular dilatation while receiving ventricular taps to drain excessive cerebrospinal fluid and alleviate intracranial pressure. The minimal optical fiber and probe holder design allowed for convenient longitudinal monitoring. Across 14 ventricular taps, an approximately 15% increase in CBF was reported following the procedure, which was supported by previous investigations. Much smaller changes in metabolism were noted over this same period. NNeMo's ability to provide bedside monitoring of perfusion and metabolism showed potential for numerous neuromonitoring applications in the neonatal intensive care unit.

6.2.3 Monitoring cerebral hemodynamic, oxygenation and metabolic stability in premature infants following birth using a hybrid broadband NIRS/DCS optical brain monitor

Chapter 4 reports the clinical translation of NNeMo to monitor the brains of eight premature infants soon after birth. Perfusion and metabolic stability were demonstrated on the first and third days of life. No significant differences in measurement stability was reported between days. Continuous wavelet transforms were applied to perform frequency

analysis and characterize prevailing oscillations during these monitoring periods. Apparent oscillations were found in StO_2 and CBF markers on day 1, which diminished by day 3. Coherence and semblance were calculated to determine the relationship between optical measures of StO_2, CBF, and oxCCO. The semblance of CBF/StO_2 was found to significantly differ from relationships with oxCCO, suggesting that persistent fluctuations in CBF and StO_2 did not influence the metabolism.

6.2.4 Changes in cerebral blood flow and metabolism in response to hypoperfusion events in adults during surgery with cardiopulmonary bypass

Chapter 5 demonstrates similar perfusion and metabolic measures in seven adults during cardiac surgery with cardiopulmonary bypass. This patient population experiences large intraoperative fluctuations in perfusion, as dictated by the bypass pump, to allow for surgical intervention. During the transition on bypass CBF increased by an average of approximately 89%. During this same period, a statistically significant drop in oxCCO was noted (0.5 μM), which was in part due to a hemodilution effect as the pump was turned on. Across all subjects, fifteen hypoperfusion events characterized by large and sustained drops in CBF were identified. During these periods, significant reductions in CBF and oxCCO were reported when mean arterial pressure dropped below 30 mmHg. Changes in CBF were found to precede metabolic response during these events. Optical neuromonitoring showed strong potential to aid in assessing hemodynamics intraoperatively, determining the presence of autoregulation, and in guiding patient management.

6.3 Limitations

This section describes limitations with respect to each chapter. General limitations common to all of the work discussed in addition to study specific limitations. A more detailed discussion of limitations for each body of work is presented within each chapter.

6.3.1 General Limitations

In the work presented, NNeMo utilizes a single source-detector pair for both B-NIRS and DCS techniques. This geometry limits data acquired to represent local changes in hemodynamics and metabolism as a representation of the global environment. In neonatal

studies, this prevented characterizing hemispheric differences which are often prevalent. For example, in chapter 3, the one subject who experienced IVH was diagnosed with a Grade II on the right and Grade I on the left. While hemorrhaging will likely affect the brain globally, a single acquisition site prevents characterizing the differences between these bleeds. Similarly, in the cardiac operating room, a patient in our study experienced an intraoperative ischemic stroke away from the site of monitoring. Due to the single source-detector pair, any influence on perfusion/metabolism from this event would be indistinguishable from global changes. NNeMo also utilizes only a single source-detector distance for B-NIRS and DCS measures, which limits depth sensitivity. While, in neonatal studies, signal contamination from extracerebral layers is minimal, increased depth sensitivity could aid in capturing changes in deeper brain regions where IVH originates.

6.3.2 Study Specific Limitations

Chapter 2: The work in this section describes the first combination of B-NIRS and DCS using a multiplexing shuttering system to avoid signal cross talk. Shutters were implemented, opposed to optical filters, since the DCS emission source (785 nm) overlaps with HbO_2's (680-845 nm) and oxCCO's (780-900 nm) broad absorption spectra. Therefore, this acquisition was not truly simultaneous with each technique acquired in quick succession. As such, the system was limited in its temporal resolution, only achieving a full data set once every 14 seconds. The piglet model of hypoxia-ischemia involved clamping carotid arteries and reducing oxygen content to produce injury. When piglets were initially occluded, sudden and extreme changes in CBF resulted. The temporal resolution of the system limited the ability to resolve changes during this initial drop and compare metabolic response to moderate changes in CBF, opposed to the large changes that the occluders ultimately produced.

Chapter 3: Subjects in this study underwent ventricular taps to drain cerebrospinal fluid directly from the brain's ventricles. Due to sterilization of the site of interest prior to the procedure, and patient repositioning following, motion artifacts were prevalent surrounding the immediate monitoring period. As a result, data analysis was limited to 2-mintute windows before needle insertion and removal. Changes in hemodynamics and metabolism therefore only represented the immediate effects of the ventricular tap, while

further changes likely persisted in the hours or days following. Data in this work were also prone to signal contamination from ambient light sources due to the increased lighting to aid surgeons in inserting the needle and the proximity of the optical probes to the site of insertion.

Chapter 4: This section describes optical neuromonitoring with NNeMo soon after premature birth and analyzed an average of approximately 4 hours of data from each 6-hour period of data acquired. This discrepancy was largely due to the abundance of patient handling and medical intervention during this early time frame, leading to excessive motion artifacts. The relative nature of CBF and oxCCO measures, prevented direct comparison of perfusion and metabolism between the first and third day of life. Instead, analysis was limited to signal stability (i.e., standard deviation), frequency analysis, and comparison between optical measures acquired concurrently. The small number of subjects monitored in this investigation also prevented correlation of measurement stability/prevailing frequencies to the onset of IVH, as only a single subject experienced a bleed.

Chapter 5: This study demonstrated the translation of NNeMo to monitor adults during cardiac surgery with cardiopulmonary bypass. The data presented in this work was also quite susceptible to ambient light and motion artifacts. The former produced by the extremely bright environment in the operating suite and the latter from frequent bed motion, patient repositioning, movement of the transesophageal echocardiography probe, etc. Data collected as patients were transitioned onto bypass was influenced by a hemodilution effect, caused by the ‘first pass’ of the bypass pump which was initially filled with a crystalloid solution. This apparent decrease in hemoglobin concentration contributed in part to the significant drop in metabolism reported. Compared to previous work in piglets and neonates, the data presented in this study was limited in terms of depth sensitivity and had a larger influenced by scalp contribution. This likely impacted StO_2 to the greatest extent since oxCCO is naturally more abundant in cerebral tissue due to higher metabolic demands [7] and CBF has an inherent greater depth sensitivity than NIRS measures [11].

6.4 Future Work

To address the limitations discussed, future work seeks to modify NNeMo to allow for both multi-distance and regional measurements. For the former, the addition of a shorter source-detector separation for B-NIRS would provide an estimate of extracerebral tissue saturation. This approach is well established for commercial NIRS devices to control for scalp effects. For the B-NIRS measure of metabolism this similarly useful, although to a lesser extent. Work by Nguyen et al. utilizing multi-distance measures of oxCCO in cardiac arrest patients showed a discrepancy in oxCCO response over 1-cm and 3-cm SDDs, supporting oxCCO's inherent depth sensitivity. Multi-distant DCS measures have shown strong potential in separating flow responses from the brain and scalp [12], and have been utilized to quantify optical properties, allowing for DCE measurements and quantitative measures of CBF [13].

Regional measurements can be achieved by bifurcating optical fibers for emission sources and employing additional detectors. Alternatively, by utilizing optical shutters, light interrogating different regions can be collected and sent to the same detector in succession. This will allow for analysis from both regions without additional components but with a trade-off in a decreased temporal resolution. For B-NIRS detection, a spectrometer's detection plane can be digitally sectioned and light incident on different regions can be separately analyzed. This requires an optical fiber detection bundle which spatially separates light from different regions when entering the spectrometer. An area of dead space between different sources is needed to avoid signal crosstalk; this approach allows for simultaneous B-NIRS acquisition and analysis from different sites. In neonatal populations, regional measurements have reported significant differences in cerebral saturation, flow, and metabolism across hemispheres, with the right hemisphere consistently reporting greater values [14]. Monitoring regional changes has potential to indicate local hemorrhaging or stroke.

The recent development of supercontinuum lasers has allowed for combined B-NIRS and TR-NIRS techniques using a single source [15]. This approach is able to collect time-of-flight information, through a temporal point spread function, for photons across a wide wavelength range. This would allow for TR-NIRS acquisition of the broad oxCCO spectra.

By isolating later arriving photons, an increased depth sensitivity can also be achieved compared to traditional B-NIRS approaches. Similarly, time-resolved DCS technology has proven capable of acquiring time-of-flight information in addition to measuring the autocorrelation function [16]. This allows for CBF monitoring with increased depth sensitivity by differentiating between photon pathlengths.

Chapter 2 describes the development of the hybrid B-NIRS/DCS system using optical shutters. This approach was chosen since the wavelength of the DCS laser implemented overlapped with the absorption spectra of HbO_2 and oxCCO. Recent work by Carp et al. has demonstrated DCS acquisition using an emission source at 1064 nm [17]. Using this approach, high/low-pass optical filters could be implemented to shield detectors from opposing sources, allowing for a truly simultaneous acquisition, significantly improving temporal solution. A similar approach has been demonstrated when combining TR-NIRS and DCS techniques [18].

Chapter 3 describes hemodynamics and metabolism during ventricular taps in PHVD infants. Future investigation seeks to monitor infants at risk of CSF accumulation in the days and weeks preceding potential intervention with the aim of assessing perfusion and metabolism as prognostic markers. This will be achieved through correlating fluctuations and longitudinal changes in CBF and oxCCO to changes in ventricle volume and intracranial pressure prior to and following CSF drainage. Current practice relies on measurements of head circumference, and in some centers ventricular volume, to dictate intervention. Optical monitoring could provide a clearer indication of the when to intervene and/or how much CSF to drain in order to maintain sufficient cerebral metabolism and avoid tissue damage.

Chapter 4 similarly discusses fluctuations in perfusion and metabolism as potential prognostic markers of IVH in premature infants. Firstly, a larger patient cohort will allow for stratification of subjects without prevailing injury and those with mild to severe IVH. Infants with IVH upon birth, as diagnosed by a day-one cranial ultrasound scan, can be further separated from infants who initially present without a bleed and subsequently experience hemorrhaging. The goal of this work will be to establish clinical thresholds of

perfusion and metabolic change that are indicative of subsequent injury. This will be achieved by monitoring infants continuously over the first few days of life and correlating optical measures to clinical outcome.

Chapter 5 demonstrates CBF and oxCCO measures in adults undergoing surgery with cardiopulmonary bypass. Numerous large reductions in CBF were noted within this small patient cohort and were found to impact cerebral metabolism at low mean arterial pressures. Similar to chapter 4, fluctuations in optical measures will be utilized to establish clinical thresholds of neurological injury. In this study, patient specific thresholds can be achieved by determining a real-time measure of cerebral autoregulation. This is possible with an accompanying measure of MAP, which is absent in most neonatal populations. In addition, regional measurements of optical parameters will allow for an increased spatial resolution which has potential to identify local hemodynamic events such as strokes.

6.5 Conclusion

In conclusion, this dissertation provides a fundamental understanding of optical techniques and their applications in neuromonitoring, with a particular focus on the neonatal brain. NNeMo, a novel optical brain monitor, is presented combining B-NIRS and DCS technology to simultaneously characterize cerebral perfusion and metabolism at the bedside. The studies described in this thesis show potential for optical measures of flow and metabolism to act as prognostic markers of brain injury in both the NICU and cardiac operating room. Real-time monitoring of cerebral hemodynamics and energy production has potential to aid clinicians in patient management, mitigate adverse neurological injury, and ultimately improve long-term clinical outcome.

6.6 References

1. J. J. Volpe, "Brain injury in premature infants: a complex amalgam of destructive and developmental disturbances," Lancet 8(1), 110–124 (2009).

2. P. Ballabh, "Intraventricular hemorrhage in premature infants: Mechanism of disease," Pediatr. Res. 67(1), 1–8 (2010).

3. S. Cherian, A. Whitelaw, M. Thoresen, and S. Love, "The pathogenesis of neonatal post-hemorrhagic hydrocephalus," Brain Pathol. 14(3), 305–311 (2004).

4. A. Whitelaw, "Intraventricular haemorrhage and posthaemorrhagic hydrocephalus: Pathogenesis, prevention and future interventions," Semin. Neonatol. 6(2), 135–146 (2001).

5. M. Hinojosa-Rodríguez, T. Harmony, C. Carrillo-Prado, J. D. Van Horn, A. Irimia, C. Torgerson, and Z. Jacokes, "Clinical neuroimaging in the preterm infant: Diagnosis and prognosis," NeuroImage Clin. 16(August), 355–368 (2017).

6. M. Diop, J. Kishimoto, V. Toronov, D. S. C. Lee, and K. S. Lawrence, "Development of a combined broadband near-infrared and diffusion correlation system for monitoring cerebral blood flow and oxidative metabolism in preterm infants," Biomed. Opt. Express 6(10), 3907–3918 (2015).

7. G. Bale, C. E. Elwell, and I. Tachtsidis, "From Jöbsis to the present day : a review of clinical near-infrared spectroscopy measurements of cerebral cytochrome-c-oxidase," J. Biomed. Opt. 21(9), (2016).

8. D. A. Boas, L. E. Campbell, and A. G. Yodh, "Scattering and Imaging with Diffusing Temporal Field Correlations," Phys. Rev. Lett. 75(9), 1855–1859 (1995).

9. D. A. Boas and A. G. Yodh, "Spatially varying dynamical properties of turbid media probed with diffusing temporal light correlation," J. Opt. Soc. Am. A 14(1), 192–215 (1997).

10. R. Bonner and R. Nossal, "Model for laser Doppler measurements of blood flow in tissue," Appl. Opt. 20(12), 2097–2107 (1981).

11. J. Selb, D. a. Boas, S.-T. Chan, K. C. Evans, E. M. Buckley, and S. a. Carp, "Sensitivity of near-infrared spectroscopy and diffuse correlation spectroscopy to brain hemodynamics: simulations and experimental findings during hypercapnia.," Neurophotonics 1(1), 015005 (2014).

12. D. Milej, A. Abdalmalak, A. Rajaram, and K. St. Lawrence, "Direct assessment of extracerebral signal contamination on optical measurements of cerebral blood flow, oxygenation, and metabolism," Neurophotonics 7(04), 1–17 (2020).

13. M. Khalid, D. Milej, A. Rajaram, A. Abdalmalak, L. Morrison, M. Diop, and K. St. Lawrence, "Development of a stand-alone DCS system for monitoring absolute cerebral blood flow," Biomed. Opt. Express 10(9), 4607–4620 (2019).

14. P. Y. Lin, N. Roche-Labarbe, M. Dehaes, A. Fenoglio, P. E. Grant, and M. A. Franceschini, "Regional and hemispheric asymmetries of cerebral hemodynamic and oxygen metabolism in newborns," Cereb. Cortex 23(2), 339–348 (2013).

15. D. J. F. Cohen and M. Diop, "Late-photons hyperspectral near-infrared spectroscopy improves the sensitivity to cerebral oxygenation in adults," OSA 2020 Proc. Opt. InfoBase Conf. Pap. BTh3C.2, (2020).

16. J. Sutin, B. Zimmerman, D. Tyulmankov, D. Tamborini, K. C. Wu, J. Selb, A. Gulinatti, I. Rech, A. Tosi, D. A. Boas, and M. A. Franceschini, "Time-domain diffuse correlation spectroscopy," Optica 3(9), 1006 (2016).

17. S. A. Carp, D. Tamborini, D. Mazumder, K.-C. (Tony) Wu, M. R. Robinson, K. A. Stephens, O. Shatrovoy, N. Lue, N. Ozana, M. H. Blackwell, and M. A. Franceschini, "Diffuse correlation spectroscopy measurements of blood flow using 1064 nm light," J. Biomed. Opt. 25(09), 1–15 (2020).

18. D. Milej, M. Shahid, A. Abdalmalak, A. Rajaram, M. Diop, and K. St. Lawrence, "Characterizing dynamic cerebral vascular reactivity using a hybrid system combining time-resolved near-infrared and diffuse correlation spectroscopy," Biomed. Opt. Express 11(8), 4571-4585 (2020).

Appendices

Appendix A: Health Science Research Ethics Board Approval Letters

Western

2015-077:4:

AUP Number: 2015-077
AUP Title: Impaired Cerebral Oxygen Consumption Is An Early Predictor of Brain Damage Following Hypoxia-Ischemia
Yearly Renewal Date: 05/01/2020

The YEARLY RENEWAL to Animal Use Protocol (AUP) 2015-077 has been approved by the Animal Care Committee (ACC), and will be approved through to the above review date.

Please at this time review your AUP with your research team to ensure full understanding by everyone listed within this AUP.

As per your declaration within this approved AUP, you are obligated to ensure that:

1) Animals used in this research project will be cared for in alignment with:
   a) Western's Senate MAPPs 7.12, 7.10, and 7.15
   http://www.uwo.ca/univsec/policies_procedures/research.html
   b) University Council on Animal Care Policies and related Animal Care Committee procedures
   http://uwo.ca/research/services/animalethics/animal_care_and_use_policies.html
2) As per UCAC's Animal Use Protocols Policy,
   a) this AUP accurately represents intended animal use;
   b) external approvals associated with this AUP, including permits and scientific/departmental peer approvals, are complete and accurate;
   c) any divergence from this AUP will not be undertaken until the related Protocol Modification is approved by the ACC; and
   d) AUP form submissions - Annual Protocol Renewals and Full AUP Renewals - will be submitted and attended to within timeframes outlined by the ACC. http://uwo.ca/research/services/animalethics/animal_use_protocols.html
3) As per MAPP 7.10 all individuals listed within this AUP as having any hands-on animal contact will
   a) be made familiar with and have direct access to this AUP;
   b) complete all required CCAC mandatory training (training@uwo.ca); and
   c) be overseen by me to ensure appropriate care and use of animals.
4) As per MAPP 7.15,
   a) Practice will align with approved AUP elements;
   b) Unrestricted access to all animal areas will be given to ACVS Veterinarians and ACC Leaders;
   c) UCAC policies and related ACC procedures will be followed, including but not limited to:
      i) Research Animal Procurement
      ii) Animal Care and Use Records
      iii) Sick Animal Response
      iv) Continuing Care Visits
5) As per institutional OH&S policies, all individuals listed within this AUP who will be using or potentially exposed to hazardous materials will have completed in advance the appropriate institutional OH&S training, facility-level training, and reviewed related (M)SDS Sheets, http://www.uwo.ca/hr/learning/required/index.html

Submitted by: Copeman, Laura
on behalf of the Animal Care Committee
University Council on Animal Care

Western Research

Date: 30 March 2020

To: Dr. Sandrine de Ribaupierre

Project ID: 100315

Study Title: New technologies in the management of post-hemorrhagic hydrocephalus in preterm infants (REB #17827)

Application Type: Continuing Ethics Review (CER) Form

Review Type: Delegated

REB Meeting Date: 07/Apr/2020

Date Approval Issued: 30/Mar/2020

REB Approval Expiry Date: 05/Apr/2021

Dear Dr. Sandrine de Ribaupierre,

The Western University Research Ethics Board has reviewed the application. This study, including all currently approved documents, has been re-approved until the expiry date noted above.

REB members involved in the research project do not participate in the review, discussion or decision.

Western University REB operates in compliance with, and is constituted in accordance with, the requirements of the TriCouncil Policy Statement: Ethical Conduct for Research Involving Humans (TCPS 2); the International Conference on Harmonisation Good Clinical Practice Consolidated Guideline (ICH GCP); Part C, Division 5 of the Food and Drug Regulations; Part 4 of the Natural Health Products Regulations; Part 3 of the Medical Devices Regulations and the provisions of the Ontario Personal Health Information Protection Act (PHIPA 2004) and its applicable regulations. The REB is registered with the U.S. Department of Health & Human Services under the IRB registration number IRB 00000940.

Please do not hesitate to contact us if you have any questions.

Sincerely,

Daniel Wyzynski, Research Ethics Coordinator, on behalf of Dr. Joseph Gilbert, HSREB Chair

Note: This correspondence includes an electronic signature (validation and approval via an online system that is compliant with all regulations).

Western Research

Date: 3 June 2020

To: Dr Soume Bhattacharya

Project ID: 111168

Study Title: Feasibility and Utility of Cerebral and Cardiac Function Monitoring in Premature Neonates in the First 72 Hours of Life

Application Type: Continuing Ethics Review (CER) Form

Review Type: Delegated

REB Meeting Date: 16June2020

Date Approval Issued: 03/Jun/2020 18:43

REB Approval Expiry Date: 22/Jun/2021

Dear Dr Soume Bhattacharya,

The Western University Research Ethics Board has reviewed the application. This study, including all currently approved documents, has been re-approved until the expiry date noted above.

REB members involved in the research project do not participate in the review, discussion or decision.

Western University REB operates in compliance with, and is constituted in accordance with, the requirements of the TriCouncil Policy Statement: Ethical Conduct for Research Involving Humans (TCPS 2); the International Conference on Harmonisation Good Clinical Practice Consolidated Guideline (ICH GCP); Part C, Division 5 of the Food and Drug Regulations; Part 4 of the Natural Health Products Regulations; Part 3 of the Medical Devices Regulations and the provisions of the Ontario Personal Health Information Protection Act (PHIPA 2004) and its applicable regulations. The REB is registered with the U.S. Department of Health & Human Services under the IRB registration number IRB 00000940.

Please do not hesitate to contact us if you have any questions.

Sincerely,

Daniel Wyzynski, Research Ethics Coordinator, on behalf of Dr. Joseph Gilbert, HSREB Chair

Note: This correspondence includes an electronic signature (validation and approval via an online system that is compliant with all regulations).

Western Research

Date: 22 April 2019

To: Dr. Jason Chui

Project ID: 113650

Study Title: A clinical observational study of brain oxidation metabolism and brain tissue oxygen saturation under general anesthesia

Application Type: HSREB Initial Application

Review Type: Full Board

Meeting Date: 12/Mar/2019

Date Approval Issued: 22/Apr/2019 10:41

REB Approval Expiry Date: 22/Apr/2020

Dear Dr. Jason Chui

The Western University Health Science Research Ethics Board (HSREB) has reviewed and approved the above mentioned study as described in the WREM application form, as of the HSREB Initial Approval Date noted above. This research study is to be conducted by the investigator noted above. All other required institutional approvals must also be obtained prior to the conduct of the study.

Documents Approved:

Document Name	Document Type	Document Date	Document Version
CLEAN-CCO-2019-03-29-JC	Protocol	29/Mar/2019	
ContinuousNonInvasiveMonitorin	Online Survey	29/Mar/2019	
LOI-NIRS-2019-04-15	Written Consent/Assent	15/Apr/2019	

No deviations from, or changes to, the protocol or WREM application should be initiated without prior written approval of an appropriate amendment from Western HSREB , except when necessary to eliminate immediate hazard(s) to study participants or when the change(s) involves only administrative or logistical aspects of the trial.

REB members involved in the research project do not participate in the review, discussion or decision.

The Western University HSREB operates in compliance with, and is constituted in accordance with, the requirements of the TriCouncil Policy Statement: Ethical Conduct for Research Involving Humans (TCPS 2); the International Conference on Harmonisation Good Clinical Practice Consolidated Guideline (ICH GCP); Part C, Division 5 of the Food and Drug Regulations; Part 4 of the Natural Health Products Regulations; Part 3 of the Medical Devices Regulations and the provisions of the Ontario Personal Health Information Protection Act (PHIPA 2004) and its applicable regulations. The HSREB is registered with the U.S. Department of Health & Human Services under the IRB registration number IRB 00000940.

Please do not hesitate to contact us if you have any questions.

Sincerely,

Karen Gopaul, Ethics Officer on behalf of Dr. Joseph Gilbert, HSREB Chair

Note: This correspondence includes an electronic signature (validation and approval via an online system that is compliant with all regulations).

Appendix B: Permission for Reproduction of Scientific Articles

Copyright Agreement for the Journal of *Biomedical Optics Express* (Chapter 2 & 5)

From: …
Sent: Jan 22nd, 2021
To: …
Subject: RE: Permission to Use Copyrighted Material in a Doctoral Thesis

Dear Ajay Rajaram,

Thank you for contacting The Optical Society (OSA).

For the use of material from Ajay Rajaram, Gemma Bale, Matthew Kewin, Laura B. Morrison, Ilias Tachtsidis, Keith St. Lawrence, and Mamadou Diop, "Simultaneous monitoring of cerebral perfusion and cytochrome c oxidase by combining broadband near-infrared spectroscopy and diffuse correlation spectroscopy," Biomed. Opt. Express 9, 2588-2603 (2018) and Ajay Rajaram, Daniel Milej, Marianne Suwalski, Lawrence C. M. Yip, Linrui R. Guo, Michael W. A. Chu, Jason Chui, Mamadou Diop, John M. Murkin, and Keith St. Lawrence, "Optical monitoring of cerebral perfusion and metabolism in adults during cardiac surgery with cardiopulmonary bypass," Biomed. Opt. Express 11, 5967-5981 (2020)

> Because you are the author of the source paper from which you wish to reproduce material, OSA considers your requested use of its copyrighted materials to be permissible within the author rights granted in the Copyright Transfer Agreement submitted by the requester on acceptance for publication of his/her manuscript. It is requested that a complete citation of the original material be included in any publication. This permission assumes that the material was not reproduced from another source when published in the original publication.
>
> If the entire article is being included, it is permissible to use the **version of record**.

While your publisher should be able to provide additional guidance, OSA prefers the below citation formats:

> For citations in figure captions:
> [Reprinted/Adapted] with permission from [ref #] © The Optical Society. (Please include the full citation in your reference list)
>
> For images without captions:
> Journal Vol. #, first page (year published) An example: Opt. Express 19, 2720 (2011)

Please let me know if you have any questions.

Kind Regards,
Hannah Greenwood
January 26, 2021
Authorized Agent, The Optical Society

The Optical Society (OSA)
2010 Massachusetts Ave., NW
Washington, DC 20036 USA
www.osa.org

From: …
Sent: Jan 19th, 2021
To: …
Subject: Permission to Use Copyrighted Material in a Doctoral Thesis

Hello,

I am a University of Western Ontario graduate student completing my Doctoral thesis in Medical Biophysics. My thesis will be available in full-text on the internet for reference, study and/or copy. Except in situations where a thesis is under embargo or restriction, the electronic version will be accessible through the Western Libraries web pages, the Library's web catalogue, and also through web search engines. I will also be granting Library and Archives Canada and ProQuest/UMI a non-exclusive license to reproduce, loan, distribute, or sell single copies of my thesis by any means and in any form or format. These rights will in no way restrict republication of the material in any other form by you or by others authorized by you.

I would like permission to allow inclusion of the following material in my thesis:

1. A. Rajaram, G. Bale, M. Kewin, L. B. Morrison, I. Tachtsidis, K. St. Lawrence, and M. Diop, "Simultaneous monitoring of cerebral perfusion and cytochrome c oxidase by combining broadband near-infrared spectroscopy and diffuse correlation spectroscopy," Biomed. Opt. Express 9(6), 2588–2603 (2018). https://doi.org/10.1364/BOE.9.002588

2. A. Rajaram, D. Milej, M. Suwalski, L. C. M. Yip, L. R. Guo, M. W. A. Chu, J. Chui, M. Diop, J. M. Murkin, and K. St. Lawrence, "Optical monitoring of cerebral perfusion and metabolism in adults during cardiac surgery with cardiopulmonary bypass," Biomed. Opt. Express 11(10), 5967-5981 (2020). https://doi.org/10.1364/BOE.404101

The material will be attributed through a citation.
Please confirm in writing or by email that these arrangements meet with your approval.

Thank you!

Ajay Rajaram

Copyright Agreement for the Journal of *Biomedical Optics Express* (Chapter 3)

From: …
Sent: Jan 19th, 2021
To: …
Subject: RE: Permission to Use Copyrighted Material in a Doctoral Thesis

Dear Ajay Rajaram,

Thank you for your message. Please feel free to use the published material in your paper with a proper citation. We are an open access journal, the copyright of the published material is retained by the author.

Kind regards,
Amanda

Ms. Amanda Zhang
Managing Editor
Brain Sciences (http://www.mdpi.com/journal/brainsci/)
Twitter: @BrainSci_MDPI

MDPI
Postfach, CH-4020 Basel, Switzerland
Office: St. Alban-Anlage 66, 4052 Basel
E-Mail: brainsci@mdpi.com

From: …
Sent: Jan 19th, 2021
To: …
Subject: Permission to Use Copyrighted Material in a Doctoral Thesis

Hello,

I am a University of Western Ontario graduate student completing my Doctoral thesis in Medical Biophysics. My thesis will be available in full-text on the internet for reference, study and/or copy. Except in situations where a thesis is under embargo or restriction, the electronic version will be accessible through the Western Libraries web pages, the Library's web catalogue, and also through web search engines. I will also be granting Library and Archives Canada and ProQuest/UMI a non-exclusive license to reproduce, loan, distribute, or sell single copies of my thesis by any means and in any form or format. These rights will in no way restrict republication of the material in any other form by you or by others authorized by you.

I would like permission to allow inclusion of the following material in my thesis:

A. Rajaram, L. C. M. Yip, D. Milej, M. Suwalski, M. Kewin, M. Lo, J. J. L. Carson, V. Han, S. Bhattacharya, M. Diop, S. de Ribaupierre, and K. St. Lawrence, "Perfusion and

Metabolic Neuromonitoring during Ventricular Taps in Infants with Post-Hemorrhagic Ventricular Dilatation," Brain Sci. 10(7), 452 (2020).
https://doi.org/10.3390/brainsci10070452

The material will be attributed through a citation.
Please confirm in writing or by email that these arrangements meet with your approval.

Thank you!

Ajay Rajaram

Curriculum Vitae

EDUCATION

2015-2021 Doctor of Philosophy in Medical Biophysics
Department of Medical Biophysics
Western University, London, Ontario, Canada
Supervisors: Dr. Keith St. Lawrence & Dr. Mamadou Diop
Thesis: Optical neuromonitoring to prevent brain injury

2010-2015 Honours Bachelor of Science
Co-operative Medical and Health Physics
McMaster University, Hamilton, Ontario, Canada
Thesis: Dosimetric measurements of an orthovoltage unit using radiochromic film

HONOURS AND AWARDS

2021 **Debbie Comuzzi CHRI Trainee of the Year Award (2020)**
Children's Health Research Institute, London, Ontario
Awarded for significant contributions to the field of children's health research from 2018-2020
Local ($1,000)

2021 **Alfred Jay Award for Translational Research**
Department of Medical Biophysics, Western University
Awarded for innovation in the development of a clinical diagnostic or therapeutic procedure, showing significant progress on bench to bedside translation
Institutional ($2,000)

2019-2021 **Alexander Graham Bell Canadian Graduate Scholarship**
Natural Sciences and Engineering Research Council (NSERC)
Awarded to high-caliber doctoral students based on academic merit and research productivity
National ($70,000)

2020 **Nellie Farthing Fellowship in Medical Sciences**
Schulich School of Medicine and Dentistry, Western University
Awarded to graduate students based on research excellence
Institutional ($3,000)

2020 **1st place clinical talk – Child Health Research Day**
London Health Sciences
Awarded for the best clinical talk
Institutional ($200)

2020 **Doctoral Excellence Research Award**
Department of Medical Biophysics, Western University
Recognized for having a tri-agency doctoral scholarship (NSERC)
Institutional ($3,000)

2020 **Western Graduate Research Scholarship**
Department of Medical Biophysics, Western University
Awarded to graduate students who maintain an average of 80% or more
Institutional ($4,500)

2019 **Alan C Groom Seminar Award**
Department of Medical Biophysics, Western University
Awarded for the best departmental seminar presentation
Institutional ($1,000)

2019 **Queen Elizabeth II Graduate Scholarship in Science and Technology**
Government of Ontario
Merit based scholarship awarded for academic achievement and research excellence
Provincial ($15,000) *declined*

2018 **3rd place oral presentation – ImNO conference**
Imaging Network Ontario, London, Ontario
Awarded for scientific presentation
Provincial ($200)

2019 **Doctoral Excellence Research Award**
Department of Medical Biophysics, Western University
Recognized for having a tri-agency doctoral scholarship (NSERC)
Institutional ($3,000)

2019 **Western Graduate Research Scholarship**
Department of Medical Biophysics, Western University
Awarded to graduate students who maintain an average of 80% or more
Institutional ($4,500)

2018 **Ontario Graduate Scholarship (OGS)**
Government of Ontario
Merit based scholarship awarded for academic achievement and research excellence
Provincial ($15,000)

2018 **2nd place poster – Lawson Imaging Discovery Day**
London Health Sciences
Awarded for scientific poster presentation
Institutional

2018 **Western Graduate Research Scholarship**
Department of Medical Biophysics, Western University
Awarded to graduate students who maintain an average of 80% or more
Institutional ($4,500)

2017 **Ontario Graduate Scholarship (OGS)**
Government of Ontario
Merit based scholarship awarded for academic achievement and research excellence
Provincial ($15,000)

2017 **CIHR Travel Award,**
Canadian Institutes of Health Research (CIHR)
Awarded based on research proposal and scientific merit
National ($1,000)

2017 **MexNIRS Travel Award,**
Mexican Symposium on Neuroimaging, Mexico
Awarded based on research abstract
International ($900)

2017 **1st place poster – Newborn Brain conference**
Brain monitoring and Neuroprotection in the Newborn, Ireland
Awarded based on scientific poster presentation
International ($375)

2017 **Western Graduate Research Scholarship**
Department of Medical Biophysics, Western University
Awarded to graduate students who maintain an average of 80% or more
Institutional ($4,500)

2016 **Ontario Graduate Scholarship (OGS)**
Government of Ontario
Merit based scholarship awarded for academic achievement and research excellence
Provincial ($15,000)

2016 **2nd place 3-Minute Thesis Competition**
Western University
Awarded for delivering a concise and engaging lay research presentation
Institutional ($500)

2016 **Western Graduate Research Scholarship**
Department of Medical Biophysics, Western University
Awarded to graduate students who maintain an average of 80% or more
Institutional ($4,500)

2015 **Western Graduate Research Scholarship**
Department of Medical Biophysics, Western University
Awarded to graduate students who maintain an average of 80% or more
Institutional ($4,500)

2014 **Harold E. John's Medical Physics Studentship Award**
Cancer Care Ontario
Cancer Center of Southeastern Ontario, Kingston, Ontario
Awarded based on academic achievement, funding a co-operative placement at a cancer center in Ontario
Institutional ($9,600)

2014 **Harold E. John's Medical Physics Studentship Award**
Cancer Care Ontario
Juravinski Cancer Center, Hamilton, Ontario
Awarded based on academic achievement, funding a co-operative placement at a cancer center in Ontario
Institutional ($9,600)

2013-2015 **Dean's Honour List**
McMaster University
Awarded for academic achievement
Institutional

ACADEMIC AND RESEARCH POSITIONS

2018-2020 **Teaching Assistant Graduate Biophysics Communications**
(4 terms) BIOPHYS 9513/9514, Western University, London, Ontario
Lectured MSc and PhD candidates on scientific presentations and assessed student work
Supervisor: Dr. Matthew Teeter

2016-2017 (2 terms)
Teaching Assistant Undergraduate Physics
PHYS 1028/1029, Western University, London, Ontario
Led physics laboratory sessions for first year undergraduates and assessed student work
Supervisor: Dr. Kanthi Kaluarachchi

2015
Research Assistant
Lawson Health Research Institute, London, Ontario
Supervisors: Dr. Keith St. Lawrence & Dr. Mamadou Diop
Project: Optical monitoring of hemodynamics and inflammation in an animal model of rheumatoid arthritis

2014
Research Assistant
Cancer Center of Southeastern Ontario, Kingston, Ontario
Supervisors: Dr. John Schreiner
Project: Development of a radiochromic film dosimetry imaging system

2014
Research Assistant
Juravinski Cancer Center, Hamilton, Ontario
Supervisors: Dr. Gordon Chan
Project: Orthovoltage dosimetric measurements using radiochromic film

2013
Research Assistant
Grand River Regional Cancer Center, Waterloo, Ontario
Supervisors: Dr. Runqing Jiang
Project: Linear accelerator quality assurance; Radiation deposition in whole breast radiotherapy versus accelerated partial breast irradiation

COMMITTEE PARTICIPATION

2020
National Scholarship Ranking Committee
Western University
Assessed scholarship for incoming undergraduate students

2016-2020
Medical Biophysics Graduate Recruitment Committee
Department of Medical Biophysics, Western University
Presented at graduate fairs and recruitment nights

2013-2015
President - McMaster Medical Physics Undergraduate Society
McMaster University
Led executive team in organizing academic and recreational events

INVITED LECTURES

2021	**AC Burton Day** Department of Medical Biophysics, Western University Institutional
2020	**Fetal Neonatal Neuroimaging Developmental Science Center Lecture Series** Harvard Medical School, Boston Children's Hospital International
2019	**Talks on Friday** **Lawson Health Research Institute Lecture Series** St Joseph Hospital, London, Ontario Institutional
2019	**AC Burton Day** Department of Medical Biophysics, Western University Institutional
2018	**Illuminating Innovation – Children's Hospital Philanthropic Event** Victoria Hospital, London, Ontario Local
2018	**Neonatology Grand Rounds** Victoria Hospital, London, Ontario Local
2018	**Talks on Friday** **Lawson Health Research Institute Lecture Series** St Joseph Hospital, London, Ontario Institutional
2017	**Talks on Friday** **Lawson Health Research Institute Lecture Series** St Joseph Hospital, London, Ontario Institutional
2016	**Neonatology Grand Rounds** Victoria Hospital, London, Ontario Local

ACADEMIC REVIEWING ACTIVITES

Scientific Reports

Biomedical Optics Express

Neurophotonics

Neuroscience Methods

University of Western Ontario Medical Journal

CONFERENCE JUDGING

2019 Imaging Network Ontario (Platform & Posters)
London, Ontario

2019 London Health Research Day (Posters)
London, Ontario

2017-2019 Thames Valley Science and Engineering Fair (Posters)
London, Ontario

PUBLICATIONS AND PRESENTATIONS

Peer-reviewed Journal Manuscripts:
(11 published/in-press; 1 in review; 4 first-author)

1. **A. Rajaram**, D. Milej, M. Suwalski, L. Yip, L. Guo, M. Chu, J. Chui, M. Diop, J. Murkin, K. St. Lawrence. *"Optical monitoring of cerebral perfusion and metabolism in adults during cardiac surgery with cardiopulmonary bypass"* Biomed. Optics Exp., 11(10), 5967-5981 (2020) DOI:10.1364/BOE.404101

2. A. Mendleson, **A. Rajaram,** D. Bainbridge, K. St. Lawrence, T. Bentall, M. Sharpe, M. Diop, C. Ellis *"Dynamic tracking of microvascular hemoglobin content for continuous perfusion monitoring in the intensive care unit: a pilot study."* Journal of Clinical Monitoring and Computing (2020) DOI:10.1007/s10877-020-00611-x

3. D. Milej, A. Abdalmalak, **A. Rajaram**, K. St. Lawrence *"Direct Assessment of Extracerebral Signal Contamination on Optical Measurements of Cerebral Blood Flow, Oxygenation, and Metabolism"* Neurophotonics, 7(4) 045002 (2020) DOI:10.1117/1.NPh.7.4.045002

4. **A. Rajaram**, L. Yip, D. Milej, M. Suwalski, M. Kewin, M. Lo, J. Carson, V. Han, S. Bhattacharya, M. Diop, S. de Ribaupierre, K. St. Lawrence *"Perfusion and Metabolic Neuromonitoring during Ventricular Taps in Infants with Post-hemorrhagic Ventricular Dilatation"* Brain Sci., 10(7) (2020) DOI:10.3390/brainsci10070452

5. D. Milej, M. Shahid, A. Abdalmalak, **A. Rajaram**, M. Diop, K. St. Lawrence *"Characterizing Dynamic Cerebral Vascular Reactivity using a Hybrid System Combining Time-Resolved Near-Infrared and Diffuse Correlation Spectroscopy"* Biomed. Optics Exp. 11(8), 4571-4585 (2020) DOI:10.1364/BOE.392113

6. G. Bale, **A. Rajaram**, M. Kewin, L. Morrison, A. Bainbridge, L. Liu, U. Anazodo, M. Diop, K. St. Lawrence, I. Tachtsidis. *"Multimodal measurements of brain tissue metabolism and perfusion in a neonatal model of hypoxic-ischaemic injury"* Accepted for publication in Oxygen Transport to Tissue XLII, Springer International Publishing (2020)

7. M. Kewin, **A. Rajaram**, D. Milej, A. Abdalmalak, L. Morrison, M. Diop, K. St Lawrence *"Evaluation of hyperspectral NIRS for quantitative measurements of tissue oxygen saturation by comparison to time-resolved NIRS"* Biomed. Optics Exp., 10(9), 4789-4802 (2019) DOI:10.1364/BOE.10.004789

8. M. Khalid, D. Milej, **A. Rajaram**, A. Abdalmalak, L. Morrison, M. Diop, K. St. Lawrence *"Development of a stand-alone DCS system for monitoring absolute cerebral blood flow"* Biomed. Optics Exp., 10(9), 4607-4620 (2019) DOI:10.1364/BOE.10.004607

9. **A. Rajaram**, G. Bale, M. Kewin, L. Morrison, I. Tachtsidis, K. St. Lawrence, M. Diop *"Simultaneous monitoring of cerebral perfusion and cytochrome c oxidase by combining broadband near-infrared spectroscopy and diffuse correlation spectroscopy"* Biomed. Optics Exp. 9(6), 2588-2603 (2018) DOI:10.1364/BOE.9.002588

10. G. Bale, **A. Rajaram**, M. Kewin, L. Morrison, A. Bainbridge, M. Diop, K. St Lawrence, I. Tachtsidis *"Broadband NIRS cerebral cytochrome-c-oxidase response to anoxia before and after neonatal hypoxic-ischemic injury in piglets."* Oxygen Transport to Tissue XL, O. Thews, J.C. LaManna, and D.K. Harrison, eds. Springer International Publishing, 151-156 (2018) DOI: 10.1007/978-3-319-91287-5_24

11. **A. Rajaram**, S. Ioussoufovitch, L. Morrison, K. St Lawrence, T.Y. Lee, Y. Bureau, M. Diop *"Joint blood flow is more sensitive to inflammatory arthritis than oxyhemoglobin, deoxyhemoglobin, and oxygen saturation."* Biomed. Optics Exp 7(10), 3843-3845 (2016) DOI: 10.1364/BOE.7.003843

***In review*:**

12. D. Milej, A. Abdalmalak, **A. Rajaram**, A. Jhajj, A. Owen, K. St. Lawrence *"Using regression analysis to improve the reconstruction of cerebral hemodynamic responses acquired by time-resolved near-infrared spectroscopy"* Submitted to Journal of Biomedical Optics (JBO 210070), Mar 2021

***In preparation*:**

1. **A. Rajaram**, D. Milej, M. Suwalski, L. Kebaya, M. Kewin, L. C. M. Yip, , S. de Ribaupierre, S. Bhattacharya, M. Diop, and K. St. Lawrence *"Monitoring cerebral hemodynamic, oxygenation and metabolic stability in premature infants following birth using a hybrid broadband NIRS/DCS optical brain monitor"*

Peer-reviewed Conference Proceedings & Published Abstracts:
(12 published; 4 first-author)

1. D. Milej*, A. Abdalmalak, **A. Rajaram**, K. St. Lawrence. *"Assessing the ability to monitor cerebral blood flow and oxygen consumption by combining time-resolved near-infrared and diffuse correlation spectroscopy"* SPIE Proceedings vol 11639 Optical Tomography and Spectroscopy of Tissue XIV; 1163918 SPIE BiOS, (Online, 2021) DOI:10.1117/12.2577933

2. D. Milej*, A. Abdalmalak, **A. Rajaram**, M. Suwalski, K. St. Lawrence. *"Combining time-resolved near-infrared spectroscopy with regression analysis to improve the reconstruction of cerebral hemodynamic responses"* SPIE Proceedings vol 11639 Optical Tomography and Spectroscopy of Tissue XIV; 116390R SPIE BiOS, (Online, 2021) DOI:10.1117/12.2577237

3. L. Mawdsley*, **A. Rajaram**, L. Yip, N. Abayomi, S. Milkovich, K. St. Lawrence, J. Carson, C. Ellis, M. Diop. *"Using near infrared spectroscopy and diffuse correlation spectroscopy to determine the microvascular effects of phenylephrine in vivo"* SPIE Proceedings vol 11639 Optical Tomography and Spectroscopy of Tissue XIV; 116390Z SPIE BiOS, (Online, 2021) DOI:10.1117/12.2577237

4. L. Mawdsley*, **A. Rajaram**, L. Yip, C. Ellis, M. Diop. *"Using near infrared spectroscopy, diffuse correlation spectroscopy, and intravital video microscopy to monitor skeletomuscular and cerebral microcirculation"* Experimental Biology 2020 Proceedings FASEB Journal 34 (S1), 1-1 (San Diego, CA, 2020) DOI:10.1096/fasebj.2020.34.s1.02980

5. **A. Rajaram***, L. Yip, M. Kewin, L. Morrison, M. Diop, K. St. Lawrence. *"Development of a neonatal neuromonitor for concurrent measurements of cytochrome c oxidase and $CMRO_2$"* Brain & Brain PET Proceedings PB01-D04 (Yokohama, Japan, 2019) DOI:10.1177/0271678X19851020

6. G. Bale*, **A. Rajaram**, M. Kewin, L. Morrison, A. Bainbridge, M. Diop, K. St. Lawrence, I. Tachtsidis. *"Multimodal measurements of brain tissue metabolism and perfusion in a neonatal model of hypoxic-ischaemic injury"* European Conference on Biomedical Engineering Proceedings 11074_38 (Munich, Germany, 2019) DOI:10.1117/12.2526729

7. D. Milej, **A. Rajaram**, A. Abdalmalak, M. Khalid, M. Shahid, M. Kewin, K. St. Lawrence*. *"Assessing extracerebral signal contamination in optical measurements of cerebral blood flow and oxygenation"* European Conference on Biomedical Engineering Proceedings 11074_90 (Munich, Germany, 2019) DOI:10.1117/12.2527150

8. **A. Rajaram**, G. Bale, M. Kewin, I. Tachtsidis, K. St. Lawrence, M. Diop*. "*Hybrid broadband NIRS/Diffuse correlation spectroscopy system for simultaneous monitoring of cerebral perfusion and cytochrome c oxidase*." Optical Society of America Proceedings JW3A.50 (Hollywood, FL, 2018) DOI:10.1364/TRANSLATIONAL.2018.JW3A.50

9. M. Kewin*, D. F Milej, A. Abdalmalak, **A. Rajaram**, M. Diop, S. de Ribaupierre, K. St Lawrence. "*Validation of a Hyperspectral NIRS Method for Measuring Oxygen Saturation by Comparison to Time-Resolved NIRS*." Optical Society of America Proceedings OW4C.4 (Hollywood, FL, 2018) DOI:10.1364/OTS.2018.OW4C.4

10. M. Khalid*, D. F Milej, **A. Rajaram**, A. Abdalmalak, M. Diop, K. St Lawrence. "*Self-calibrated DCS for monitoring absolute cerebral blood flow*." Optical Society of America Proceedings JTu3A.63 (Hollywood, FL, 2018) DOI:10.1364/TRANSLATIONAL.2018.JTu3A.63

11. **A. Rajaram***, K. St. Lawrence, M. Diop. "*Development of a hybrid broadband NIRS/diffusion correlation spectroscopy system for real-time monitoring of cerebral perfusion and oxygenation in preterm brain injury*." SPIE BiOS Photonics West Proceedings 100540T (San Francisco, CA, 2017) DOI:10.1117/12.2253358

12. **A. Rajaram**, K. St. Lawrence, M. Diop*. "*Monitoring vascular markers of joint inflammation in a rabbit model of rheumatoid arthritis with time-resolved near-infrared spectroscopy*." Optical Society of America & Proceedings JTu3A.30 (Ft. Lauderdale, FL, 2016) DOI:10.1364/CANCER.2016.JTu3A.30

Peer-reviewed Conference Abstracts/Presentations:
(50 total; 20 first-author; 26 oral presentations; 24 international conferences)
* indicates presenting author

1. SPIE BiOS Photonics West: International/Online Oral presentation
   A. Rajaram*, L. Yip, M. Suwalski, D. Milej, L. Kebaya, M. Kewin, M. Diop, S. de Ribaupierre, S. Bhattacharya, K. St. Lawrence. *"NNeMo (Neonatal NeuroMonitor): A non-invasive brain monitor for continuous acquisition of cerebral blood flow and cytochrome c oxidase in the premature brain"* (Online, 2021)

2. SPIE BiOS Photonics West: International/Online Oral presentation
   A. Rajaram*, M. Suwalski, D. Milej, L. Yip, L. Guo, M. Chu, J. Chui, M. Diop, J. Murkin, K. St. Lawrence. *"Cerebral perfusion and metabolic neuromonitoring during cardiopulmonary bypass"* (Online, 2021)

3. SPIE BiOS Photonics West: International/Online Oral presentation
   D. Milej*, A. Abdalmalak, **A. Rajaram**, M. Suwalski, K. St. Lawrence. *"Combining time-resolved near-infrared spectroscopy with regression analysis to improve the reconstruction of cerebral hemodynamic responses"* (Online, 2021)
4. SPIE BiOS Photonics West: International/Online Oral presentation
   D. Milej*, A. Abdalmalak, **A. Rajaram**, K. St. Lawrence. *"Assessing the ability to monitor cerebral blood flow and oxygen consumption by combining time-resolved near-infrared and diffuse correlation spectroscopy"* (Online, 2021)

5. SPIE BiOS Photonics West: International/Online Oral presentation
   L. Mawdsley, N. Abayomi, **A. Rajaram**, L. Yip, S. Milkovich, C. Ellis, M. Diop. *"Using Hyperspectral Near Infrared Spectroscopy and Diffuse Correlation Spectroscopy to Monitor the Microvascular Effects of Phenylephrine in vivo"* (Online, 2021)

6. Experimental Biology: International/Online Oral presentation
   L. Mawdsley*, **A. Rajaram**, L. Yip, N. Adayomi, N. Li, S. Milkovich, J. Carson, K. St. Lawrence, C. Ellis, M. Diop. "*Simultaneous Monitoring of the Cerebral and Skeletomuscular Microcirculation using Hyperspectral Near Infrared Spectroscopy and Intravital Video Microscopy*" (Online, 2021)

7. Children's Health Research Day: Local/Online Oral Presentation
   A. Rajaram*, D. Milej, M. Kewin, L. Kebaya, L. Yip, M. Lo, M. Suwalski, M. Diop, S. De Ribaupierre, S. Bhattacharya, K. St. Lawrence. *"Cerebral blood flow and metabolic neuromonitoring immediately following premature birth"* (Online, 2020)

8. Canadian Anesthesiologists' Society: National/Online Poster Presentation
   J. Murkin*, J. Chui, **A. Rajaram**, D. Milej, M. Chu, R. Guo, J. Morriseau, M. Diop, K. St. Lawrence. *"Non-invasive Monitoring of CBF and Brain Oxidative Metabolism During Cardiopulmonary Bypass: A Novel Feasibility Study"* (Online, 2020)

9. Optical Society of America: International/Online Poster Presentation
   Z. Fang, M. O'Neil, **A. Rajaram**, A. Mendelson, K. St. Lawrence, C. Ellis, M. Diop*. *"Real-Time Monitoring of Muscle Blood Flow Regulation in Cardiac Surgery Patients with Near-Infrared Spectroscopy"* (Online, 2020)

10. Experimental Biology 2020: International/Online Oral Presentation
    L. Mawdsley*, **A. Rajaram**, L. Yip, C. Ellis, M. Diop. *"Using near infrared spectroscopy, diffuse correlation spectroscopy, and intravital video microscopy to monitor skeletomuscular and cerebral microcirculation"* (Online, 2020)

11. Brain & Brain PET: International/Oral Presentation
    A. Rajaram*, L. Yip, M. Kewin, L. Morrison, M. Diop, K. St. Lawrence. *"Development of a neonatal neuromonitor for concurrent measurements of cytochrome c oxidase and $CMRO_2$"* (Yokohama, Japan, 2019) doi:10.1177/0271678X19851020

12. Lawson Imaging Discovery Day: Local/Oral Presentation
    M. Shahid*, D. Milej, A. Abdalmalak, **A. Rajaram**, M. Khalid, M. Diop, K. St. Lawrence. *"Developing an optical device for simultaneous monitoring of oxygenation and blood flow dynamics in the adult brain"* (London, ON, 2019)

13. London Health Research Day: Local/Oral Presentation
    A. Rajaram*, L. Yip, M. Kewin, L. Morrison, M. Diop, K. St. Lawrence. *"Optical neuromonitoring for continuous quantification of cerebral blood flow and energy metabolism in the developing brain"* (London, ON, 2019)

14. London Health Research Day: Local/Poster Presentation
    M. Shahid*, D. Milej, A. Abdalmalak, **A. Rajaram**, M. Khalid, M. Diop, K. St. Lawrence. *"Developing a non-invasive optical system for monitoring oxygenation and blood flow dynamics in the adult brain"* (London, ON, 2019)

15. London Health Research Day: Local/Poster Presentation
    L. Mawdsley*, **A. Rajaram**, M. Diop, C. Ellis *"The effect of sepsis on skeletomuscular and cerebral microvascular blood flow"* (London, ON, 2019)

16. European Conference on Biomedical Engineering: International/Oral Presentation
    G. Bale*, **A. Rajaram**, M. Kewin, L. Morrison, A. Bainbridge, M. Diop, K. St. Lawrence, I. Tachtsidis. *"Multimodal measurements of brain tissue metabolism and perfusion in a neonatal model of hypoxic-ischaemic injury"* (Munich, Germany, 2019)

17. European Conference on Biomedical Engineering: International/Poster Presentation
    D. Milej, **A. Rajaram**, A. Abdalmalak, M. Khalid, M. Shahid, M. Kewin, K. St. Lawrence*. *"Assessing extracerebral signal contamination in optical measurements of cerebral blood flow and oxygenation"* (Munich, Germany, 2019)

18. Imaging Network Ontario: Provincial/Oral Presentation
A. Rajaram*, L. Yip, M. Kewin, L. Kebaya, V. Han, S. Bhattacharya, M. Diop, K. St. Lawrence. *"NNeMo (Neonatal NeuroMonitor): A non-invasive optical device for assessing the coupling of cerebral blood flow and energy metabolism in the developing brain"* (London, ON, 2019)

19. Imaging Network Ontario: Provincial/Poster Presentation
M. Kewin*, **A. Rajaram**, D. Milej, M. Diop, S. de Ribaupierre, K. St. Lawrence *"Confirmation of a Derivative Hyperspectral NIRS Method to Measure Oxygen Saturation"* (London, ON, 2019)

20. Imaging Network Ontario: Provincial/Poster Presentation
D. Milej*, **A. Rajaram**, A. Abdalmalak, M. Khalid, M. Shahid, M. Kewin, K. St. Lawrence *"Characterization of scalp signal contamination for noninvasive optical brain monitoring"* (London, ON, 2019)

21. Imaging Network Ontario: Provincial/Poster Presentation
M. Shahid*, D. Milej, A. Abdalmalak, **A. Rajaram**, M. Khalid, M. Diop, K. St. Lawrence. "*Developing a Time-Resolved Near-Infrared/Diffuse Correlation Spectroscopy System for Monitoring Oxygenation and Blood Flow Dynamics in the Adult Brain*" (London, ON, 2019)

22. SPIE BiOS Photonics West: International/Oral Presentation
M. Shahid*, D. Milej, A. Abdalmalak, **A. Rajaram**, M. Khalid, M. Diop, K. St. Lawrence. "*Development of a hybrid optical system to study dynamic blood flow/oxygenation regulation in the human brain.*" (San Francisco, CA, 2019)

23. Critical Care Canada Forum: National/Oral Presentation
A. Mendelson*, **A. Rajaram**, D. Bainbridge, K. St. Lawrence, T. Bentall, M. Sharpe, M. Diop, C. Ellis. *"Dynamic tracking of microvascular hemoglobin content in skeletal muscle of ICU patients with a custom near-infrared spectroscopy system,"* (Toronto, ON, 2018)

24. Critical Care Canada Forum: National/Poster Presentation
L. Mawdsley*, **A. Rajaram**, M. Diop, C. Ellis *"The effect of sepsis on skeletomuscular and cerebral microvascular blood flow"* (London, ON, 2019) (Toronto, ON, 2018)

25. Functional-NIRS Tokyo: International/Poster Presentation
D. Milej*, A. Abdalmalak, M. Khalid, M. Shahid, **A. Rajaram**, M. Kewin, M. Diop, K. St. Lawrence. *"Assessing extracerebral signal contamination in NIRS and DCS"* (Toyko, Japan, 2018)

26. Lawson Imaging Discovery Day: Local/Oral Presentation
A. Rajaram*, G. Bale, M. Kewin, L. Morrison, I. Tachtsidis, K. St. Lawrence, M. Diop. "*A bedside optical neuromonitor for quantification of cerebral perfusion and metabolism in preterm brain injury.*" (London, ON, 2018)

27. Lawson Imaging Discovery Day: Local/Oral Presentation
M. Shahid*, D. Milej, **A. Rajaram**, A. Abdalmalak, M. Diop, K. St. Lawrence. "*Development of a hybrid optical system to study dynamic regulation of blood flow/metabolism in the human brain.*" (London, ON, 2018)

28. London Health Research Day: Local/Poster Presentation
A. Rajaram*, G. Bale, M. Kewin, I. Tachtsidis, K. St. Lawrence, M. Diop. "*A novel optical neuromonitor for simultaneous quantification of cerebral perfusion and metabolism in preterm brain injury.*" (London, ON, 2018)

29. London Health Research Day: Local/Oral Presentation
M. Shahid*, A. Abdalmalak, **A. Rajaram**, M. Diop, K. St. Lawrence. "*Development of a hybrid optical system for studying the dynamic regulation of blood flow/metabolism in the human brain.*" (London, ON, 2018)

30. London Health Research Day: Local/Poster Presentation
M. Kewin*, D. Milej, A. Abdalmalak, **A. Rajaram**, M. Diop, S. de Ribaupierre, K. St Lawrence. "*Confirmation of a Derivative Hyperspectral NIRS Method for Measuring Oxygen Saturation by Comparison to Time-Resolved NIRS.*" (London, ON, 2018)

31. London Health Research Day: Local/Poster Presentation
M. Khalid*, D. F Milej, **A. Rajaram**, A. Abdalmalak, M. Diop, K. St Lawrence. "*Monitoring absolute cerebral blood flow using a self-calibrated software-based DCS system.*" (London, ON, 2018)

32. London Health Research Day: Local/Poster Presentation
K. Selvan*, A. Mendelson, **A. Rajaram**, K. St. Lawrence, C. Ellis, M. Diop. *"Monitoring Tissue Oxygenation in ICY patients using Hyperspectral NIRS"* (London, ON, 2018)

33. Imaging Network Ontario: Provincial/Oral Presentation
A. Rajaram*, G. Bale, M. Kewin, I. Tachtsidis, K. St. Lawrence, M. Diop. "*A novel optical neuromonitor for simultaneous and real-time quantification of cerebral saturation, perfusion, and metabolism at the bedside*." (Toronto, ON, 2018)

34. Imaging Network Ontario: Provincial/Poster Presentation
M. Kewin*, D. F Milej, A. Abdalmalak, **A. Rajaram**, M. Diop, S. de Ribaupierre, K. St Lawrence. "*Confirmation of a Derivative Hyperspectral NIRS Method for Measuring Oxygen Saturation by Comparison to Time-Resolved NIRS.*" (Toronto, ON, 2018)

35. Imaging Network Ontario: Provincial/Poster Presentation
M. Khalid*, D. Milej, **A. Rajaram**, A. Abdalmalak, M. Diop, K. St Lawrence. "*Development of a self-calibrated DCS for tracking absolute cerebral blood flow.*" (Toronto, ON, 2018)

36. Optical Society of America: International/Poster presentation
A. Rajaram, G. Bale, M. Kewin, I. Tachtsidis, K. St. Lawrence, M. Diop*. "*Hybrid broadband NIRS/Diffuse correlation spectroscopy system for simultaneous monitoring of cerebral perfusion and cytochrome c oxidase*." (Hollywood, FL, 2018)

37. Optical Society of America: International/Oral presentation
M. Kewin*, D. F Milej, A. Abdalmalak, **A. Rajaram**, M. Diop, S. de Ribaupierre, K. St Lawrence. "*Validation of a Hyperspectral NIRS Method for Measuring Oxygen Saturation by Comparison to Time-Resolved NIRS.*" (Hollywood, FL, 2018)

38. Optical Society of America: International/Poster presentation
M. Khalid*, D. F Milej, **A. Rajaram**, A. Abdalmalak, M. Diop, K. St Lawrence. "*Self-calibrated DCS for monitoring absolute cerebral blood flow.*" (Hollywood, FL, 2018)

39. Mexican Symposium on Neuroimaging: International/Oral presentation
A. Rajaram*, G. Bale, M. Kewin, I. Tachtsidis, K. St. Lawrence, M. Diop. "*A novel hybrid broadband near-infrared/diffuse correlation spectroscopy neuromonitor for simultaneous and real-time quantification of cerebral saturation, perfusion, and metabolism at the bedside.*" (Puebla, Mexico, 2017)

40. Brain Monitoring, Neuroprotection in the Newborn: International/Poster presentation
A. Rajaram*, G. Bale, M. Kewin, I. Tachtsidis, M. Diop, K. St. Lawrence. "*A bedside optical neuromonitor for real-time monitoring of cerebral perfusion/oxidative metabolism."* (Killarney, Ireland, 2017)

41. Functional-NIRS UK: International/Poster presentation
A. Rajaram, G. Bale*, M. Kewin, I. Tachtsidis, K. St. Lawrence, M. Diop. "*Development of a hybrid broadband NIRS/diffuse correlation spectroscopy system for simultaneous monitoring of cytochrome c oxidase and cerebral perfusion.*" (London, United Kingdom, 2017)

42. Internat. Society on Oxygen Transport to Tissue: International/Poster Presentation
A. Rajaram, G. Bale*, M. Kewin, I. Tachtsidis, K. St. Lawrence, M. Diop. "*A novel bedside optical neuromonitor for real-time measurements of cerebral perfusion/metabolism.*" (Halle, Germany, 2017)

43. Internat. Society on Oxygen Transport to Tissue: International/Oral presentation
G. Bale*, **A. Rajaram**, M. Kewin, L. Morrison, K. St. Lawrence, M. Diop, I. Tachtsidis. "*Broadband NIRS cerebral cytochrome-c-oxidase response to anoxia before and after neonatal hypoxic-ischemic injury.*" (Halle, Germany, 2017)

44. SPIE BiOS Photonics West: International/Oral Presentation
A. Rajaram*, K. St. Lawrence, M. Diop. "*Development of a hybrid broadband NIRS/diffusion correlation spectroscopy system for real-time monitoring of cerebral perfusion and oxygenation in preterm brain injury.*" (San Francisco, CA, 2017)

45. London Health Research Day: Local/Poster Presentation
A. Rajaram*, D. Lee, K. St. Lawrence, M. Diop. "*Development of a hybrid broadband NIRS/diffusion correlation spectroscopy system for real-time monitoring of cerebral perfusion and oxygenation in preterm brain injury.*" (London, ON, 2017)

46. Imaging Network Ontario: Provincial/Poster presentation
A. Rajaram*, D. Lee, K. St. Lawrence, M. Diop. "*Development of a hybrid broadband NIRS/diffusion correlation spectroscopy system for real-time monitoring of cerebral perfusion and oxygenation in preterm brain injury*." (London, ON, 2017)

47. Canadian Bone and Joint Conference: National/Oral Presentation
A. Rajaram*, L. Morrison, K. St. Lawrence, T.Y. Lee, M. Diop. "*Monitoring vascular markers of joint inflammation in a rabbit model of rheumatoid arthritis with time-resolved NIRS.*" (London, ON, 2016)
48. Optical Society of America: International/Poster presentation
A. Rajaram, K. St. Lawrence, M. Diop*. "*Monitoring vascular markers of joint inflammation in a rabbit model of rheumatoid arthritis with time-resolved near-infrared spectroscopy.*" (Ft. Lauderdale, FL, 2016)

49. London Health Research Day: Local/Oral Presentation
A. Rajaram*, L. Morrison, K. St. Lawrence, T.Y. Lee, M. Diop. "*Monitoring vascular markers of joint inflammation in a rabbit model of rheumatoid arthritis with time-resolved near-infrared spectroscopy*." (London, ON, 2016)

50. IUPESM World Congress: International/Oral Presentation
K. Alexander*, **A. Rajaram**, J. Schreiner. "*Development of a Radiochromic Film Dosimetry Imaging System*" (Toronto, ON, 2015)